Deposit & Copying of Dissertation Declaration

UNIVERSITY OF CAMBRIDGE

Board of Graduate Studies

Please note that you will also need to bind a copy of this Declaration into your final, hardbound copy of thesis - this has to be the very first page of the hardbound thesis.

1 Surname (Family Name)	Forenames(s)	Title
Hill	Ciaran Scott	Dr

2 Title of Dissertation as approved by the Degree Committee

Experimental Modelling and Molecular Mechanisms of Wallerian Degeneration in Traumatic Axonal Injury

In accordance with the University Regulations in *Statutes and Ordinances* for the PhD, MSc and MLitt Degrees, I agree to deposit one print copy of my dissertation entitled above and one print copy of the summary with the Secretary of the Board of Graduate Studies who shall deposit the dissertation and summary in the University Library under the following terms and conditions:

1. Dissertation Author Declaration

I am the author of this dissertation and hereby give the University the right to make my dissertation available in print form as described in 2. below.

My dissertation is my original work and a product of my own research endeavours and includes nothing which is the outcome of work done in collaboration with others except as declared in the Preface and specified in the text. I hereby assert my moral right to be identified as the author of the dissertation.

The deposit and dissemination of my dissertation by the University does not constitute a breach of any other agreement, publishing or otherwise, including any confidentiality or publication restriction provisions in sponsorship or collaboration agreements governing my research or work at the University or elsewhere.

2. Access to Dissertation

I understand that one print copy of my dissertation will be deposited in the University Library for archival and preservation purposes, and that, unless upon my application restricted access to my dissertation for a specified period of time has been granted by the Board of Graduate Studies prior to this deposit, the dissertation will be made available by the University Library for consultation by readers in accordance with University Library Regulations and copies of my dissertation may be provided to readers in accordance with applicable legislation.

3 Signature	Date

Corresponding Regulation

Before being admitted to a degree, a student shall deposit with the Secretary of the Board one copy of his or her hard-bound dissertation and one copy of the summary (bearing student's name and thesis title), both the dissertation and the summary in a form approved by the Board. The Secretary shall deposit the copy of the dissertation together with the copy of the summary in the University Library where, subject to restricted access to the dissertation for a specified period of time having been granted by the Board of Graduate Studies, they shall be made available for consultation by readers in accordance with University Library Regulations and copies of the dissertation provided to readers in accordance with applicable legislation.

Experimental Modelling and Molecular Mechanisms of Wallerian Degeneration in Traumatic Axonal Injury

Ciaran Scott Hill

Jesus College

University of Cambridge

This dissertation is submitted for the degree of Doctor of Philosophy

May 2018

Abstract

Traumatic brain injury (TBI) is a common event that can lead to profound consequences for the individual involved, and a considerable socio-economic cost. The initial injury event triggers a series of secondary brain injury mechanisms that lead to further mortality and contribute to morbidity. One classical injury pathology is termed traumatic axonal injury (TAI), which in clinical settings produces the picture of diffuse axonal injury. TAI occurs both as a primary insult, and as a consequence of secondary mechanisms. One secondary injury mechanism that worsens TAI may be Wallerian degeneration (WD), a cell-autonomous axonal death pathway. The relationship between traumatic axonal injury and WD is poorly characterised. This thesis explores the basic mechanisms by which a physical axonal trauma can lead to WD, and how modulation of the WD pathway can affect the cellular responses to a traumatic injury. This involves the development and characterisation of *in vitro* and *in vivo* models of traumatic axonal injury. These models are then used to explore the response of cellular cultures to injury when treated with pharmacological and genetic modulators of WD. Using a primary neuronal stretch-injury system we demonstrate that rates of neurite degeneration are altered by modulators of the WD pathway but that a purported neuroprotective compound 'P7C3-A20' did not protect primary cultures *in vivo* and did not act via a WD dependent mechanism. An organotypic hippocampal slice stretch injury model was then used to demonstrate genetic rescue of cellular death, and used to assess amyloidogenic responses to injury. Next we established a TBI model using *Drosophila Melanogaster*, and demonstrated that a loss of function mutation in a key WD gene '*highwire*' which controls NMNAT levels, was capable of rescuing premature death and a range of behavioral deficits after a high impact trauma. The injury caused dopaminergic neuronal loss and this was rescued by *highwire* mutation. Furthermore, this dopaminergic neuronal protection extended to a genetic *PINK1* model of Parkinsonism. Together these results help establish WD as an important secondary injury mechanism in TBI, and provide evidence that modulation of the WD pathways can improve outcomes in various model systems. This provides a foundation for future translational research into the fields of WD and TBI.

Supervisors

Michael P. Coleman

David K. Menon

Declaration and statement of length

This dissertation is the result of my own work and includes nothing which is the outcome of work done in collaboration except as declared in the preface and specified in the text. It is not substantially the same as any that I have submitted, or, is being concurrently submitted for a degree or diploma or other qualification at the University of Cambridge or any other University or similar institution except as declared in the preface and specified in the text. I further state that no substantial part of my dissertation has already been submitted, or, is being concurrently submitted for any such degree, diploma or other qualification at the University of Cambridge or any other University of similar institution except as declared in the preface and specified in the text. It does not exceed the prescribed word limit for the Biology Degree Committee.

Ciaran S. Hill

May 2018
Cambridge

Acknowledgements

I would like to thank my supervisors David Menon and Michael Coleman for their support, guidance and inspiration, members of the laboratories I have worked in for advice, ideas, and practical assistance, scientific colleagues outside Cambridge for useful discussions, the Wellcome Trust and their donors for their generous support, and my family and friends for indefatigable patience.

Contents

List of figures

List of tables

Abbreviations

AAD	Acute axon degeneration
Aβ	Amyloid beta peptide
AD	Alzheimer's disease
AICD	Amyloid beta intracellular domain
ALS	Amyotrophic lateral sclerosis
ANOVA	Analysis of variance
APOE	Apolipoprotein E
APP	Amyloid precursor protein
ATP	Adenosine triphosphate
Axed	Axundead
BACE1	Beta secretase 1
BACE1i	Beta secretase 1 inhibitor
βAPP-CTF	Beta secretase carboxyl-terminal fragment of amyloid beta precursor protein
BSA	Bovine serum albumin
CCI	Cortical contusion injury
CNS	Central nervous system
CS	Canton S
CTE	Chronic traumatic encephalopathy
DAI	Diffuse axonal injury
DAPI	4',6 diamidino-2-phenylindole
DCP-1	Death caspase 1
DiI	1,1'-Dioctadecyl-3,3,3',3'-Tetramethylindocarbocyanine perchlorate
DIV	Days in vitro
DLK	Dual leucine zipper-bearing kinase
DMEM	Dulbecco's Modified Eagle Medium
DMSO	Dimethyl sulfoxide
DNA	Deoxyribonucleic acid
dNMNAT	Drosophila nicotinamide mononucleotide adenylyltransferase
DRG	Dorsal root ganglion
dSARM	Drosophila SARM
DSHB	Developmental studies hybridoma bank
DWI	Diffusion weighted imaging
EBSS	Earle's balanced salt solution
ECL	Enhanced chemoluminescence
ECM	Extracellular matrix
ELISA	Enzyme linked immunosorbent assay
EMS	Ethyl methanesulfonate
EUCOMM	European conditional mouse mutagenesis programme
FBS	Fetal bovine serum
FPI	Fluid percussion injury
FTD	Fronto-temporal dementia
GABA	Gamma amino butyric acid

GFAP	Glial fibrillary astrocytic protein
GFP	Green fluorescent protein
GOF	Gain of function
HA	Human influenza haemagglutin
H&E	Haematoxylin and eosin
HD	Huntington's disease
HEPES	4,2 hydroxyethel-1-piperazineethanesulfonic acid
Hiw	Highwire
HIT	High impact trauma
HPLC	High performance liquid chromatography
HSP	Hereditary spastic paraplegia
huAPP	Human amyloid precursor protein
hiPSCN	Human induced pluripotent stem cell-derived neurons
IBF	Intestinal barrier function
IL-1β	Interleukin 1 beta
IL-1βRA	Interleukin 1 beta receptor antagonist
JNK	c-Jun N-terminal kinase
LOF	Loss of function
LPS	Lipopolysaccharide
MAPK	Mitogen activated protein kinase
MAPKK	Mitogen activated protein kinase kinase
MAPKKK	Mitogen activated protein kinase kinase kinase
MARCM	Mosaic analysis with a repressible cell marker
MART	Mono-ADP-ribosyl transferase
MEM	Modified Eagle's medium
mGluR	Metabotropic glutamate receptors
MLKL	Mixed lineage kinase domain-like
MND	Motor neurone disease
mPTP	Mitochondrial permeability transition pore
MRI	Magnetic resonance imaging
mRNA	Messenger ribonucleic acid
MS	Multiple sclerosis
Myc	Mycooncogene
NA	Nicotinic acid
NaAD	Nicotinic acid phosphoribosyl transferase
NAD	Nicotinamide adenine dinucleotide
NAM	Nicotinamide
NaMN	Nicotinic acid mononucleotide
NAMPT	Nicotinamide phosphoribosyltransferase
NaPRT	Nicotinc acid phosphoribosyltransferase
NFL	Neurofilament heavy chain
NFH	Neurofilament light chain
NGF	Nerve growth factor
NMJ	Neuromuscular junction
NMN	Nicotinamide mononucleotide

NMNAT	Nicotinamide mononucleotide adenylyltransferase
NR	Nicotinamide riboside
NRK	Nicotinamide riboside kinase
OBS	Organotypic brain slice
OHS	Organotypic hippocampal slice/s
PAM	Protein associate with c-myc
PARPs	poly-ADP-ribose polymerases
PBS	Phosphate buffered saline
PBS-T	Phosphate buffered saline with Tween 20
PCN	Primary cortical neurons
PCNd	Primary cortical neuron dissociated culture
PD	Parkinson's disease
PDL	Poly-D-lysine
PDMS	Polydimethylsiloxane
PET	Positron emission tomography
PFA	Paraformaldahyde
PHR1	Phosphate starvation response 1
PI	Propidium Iodide
PINK1	Phosphate and tensin homology induced putative kinase 1
PLL	Poly-L-lysine
PNS	Peripheral nervous system
PO	Poly-ornithine
PTFE	Polytetrafluoroethylene
RFP	Red fluorescent protein
RIP3	Receptor interacting protein kinase 3
RING	Rapid iterative negative geotaxis
RNA	Ribonucleic acid
RNAi	Ribonucleic acid interference
ROS	Reactive oxygen species
Rpm-1	Regulator of presynaptic morphology 1
sAPPβ	soluble peptide amyloid precursor protein beta
SARM1	Sterile alpha and TIR motif-containing protein 1
SCG	Superior cervical ganglion
SCGe	Superior cervical ganglion explant
SCGd	Superior cervical ganglion dissociated culture
SCG10	Superior cervical ganglion 10
SCI	Spinal cord injury
SD	Standard deviation
SEM	Standard error of the mean
ShRNA	Short hairpin ribonucleic acids
SiRNA	Short interfering ribonucleic acids
SIRTs	Sirtuins
TAI	Traumatic axonal injury
TBI	Traumatic brain injury
TBS	Tris-buffered salin

TDP43	Transactive response DNA-binding protein 43 kDa
TH	Tyrosine hydroxylase
TIR	Toll interleukin receptor homology domain
TNFα	Tumour necrosis factor
TSC	Tuberous sclerosis protein
U2OS	Human bone osteosarcoma epithelial
UPS	Ubiquitin proteasome system
WB	Western blot
WD	Wallerian degeneration
WLD^s	Wallerian degeneration slow
Wnd	Wallenda
YFP	Yellow fluorescent protein

Chapter 1

Overview and aims

Traumatic brain injury (TBI) is an alteration in brain function, or other evidence of brain pathology, caused by an external force[1]. It is a common cause of death and disability, and each year in Europe alone around 2.5 million people will experience TBI, 1 million will be admitted to hospital, and 75000 will die[2].

TBI is a heterogenous insult that can be broadly classified into diffuse or focal injuries. Diffuse axonal injury (DAI) is a severe multifocal injury classically associated with high-energy acceleration-deceleration forces. Clinically, it is characterised by an immediate loss of consciousness, persistent coma and disability following a typical injury mechanism involving transmission of high-energy forces[3]. The National Institute of Neurological Disorders common data elements define DAI radiologically as "*more than three separate foci of signal abnormality"*, with theses abnormalities demonstrating *"a pattern consistent with scattered, small hemorrhagic and/or non-hemorrhagic lesions which have been shown historically to correlate with pathologic findings of relatively widespread injury to white matter axons, typically due to mechanical strain related to rotational acceleration/deceleration forces*"[4]. Pathologically, it was defined by Adams *et al* as diffuse damage to axons in the cerebral hemispheres, in the corpus callosum, in the brain stem and sometimes also in the cerebellum resulting from a head injury, and characterized by the presence of axonal bulbs seen in sections stained by hematoxylin and eosin, silver impregnation techniques, or by immunocytological techniques for neurofilaments[5].

The term DAI is sometimes used synonymously with traumatic axonal injury (TAI), although the latter is more commonly used to refer to animal models of TBI that share some pathological features with a human DAI. This inconsistency in terminology pervades the literature and therefore, for clarity, throughout this thesis I shall use the term TAI to refer to any *in vitro* or *in vivo* model that is focussed on a traumatic axonal injury of the brain, and reserve the term DAI for the human injury.

A DAI can be subdivided into a primary and secondary brain injury. Primary injury refers to the damage sustained at the moment of initial trauma. This includes primary axotomy where there is a traumatic disconnection of the distal axon from a proximal segment including the cell body. Deleterious processes that occur after the primary traumatic injury are termed

secondary brain injury. Various secondary injury cascades follow the initial primary insult and lead to ongoing axonal and neuronal loss. The secondary injury response is complex and multifaceted, and comprises a number of facets including axon degeneration[6]. One of the principal mechanisms of axon degeneration is the process of Wallerian degeneration (WD). WD is an active, cell-autonomous pathway that leads to degeneration of the distal axonal segment following transection. WD is now recognised as a discrete axonal death pathway, and research has identified a range of mechanistic steps and molecular players that control this process. Wallerian-like degeneration is axon degeneration that occurs by the same or a related molecular mechanism as classical WD but in the absence of a physical complete transection injury[7]. To avoid confusion, I will refer to axonal degeneration that is dependent upon these common molecular elements as WD regardless of whether it was induced by transection or another trigger, only drawing a distinction where required. In some neuronal subtypes or situations, WD may lead to a progressive dying back of the axon proximal to an injury site, causing death of the neuronal cell body and therefore linking axonal disconnection with neuronal cell loss[8].

Following DAI there is ongoing degeneration of axons in the brain, characterised by time-dependent white-matter volume loss. These processes take place from hours to years after the initial injury, and thus provides a potential opportunity for therapeutic intervention[9]. The extent to which WD contributes this secondary axonal degeneration during this period is not fully known[6]. While primary axotomy is considered an infrequent event in DAI, it has been proposed that there may be a burden of sub-axotomy level injuries that may still be sufficient to induce WD[10,11]. If the WD process could be modulated in this subpopulation of neurons then there may be an opportunity to prevent axonal degeneration until such time as the neuron recovers from the effects of the acute insult, and degeneration is no longer inevitable. Understanding of biology in model systems is fundamental to developing clinical therapies. In order to explore the role of WD in DAI, and develop potential therapeutic solutions, it is crucial to be able to meaningfully model DAI and depending on the particular aspect of DAI that we wish to interrogate, different models will be required [12,13].

Aims

Consequently, the overall aims of the thesis were to:

- Establish model systems capable of interrogating molecular mechanisms involved in TAI
- Establish the relationship between TAI and WD in these systems
- Explore potential therapeutic modulators of TAI in the WD pathway using genetic and pharmacological approaches

The structure of this thesis along with chapter by chapter aims and summaries are presented below (figure 1).

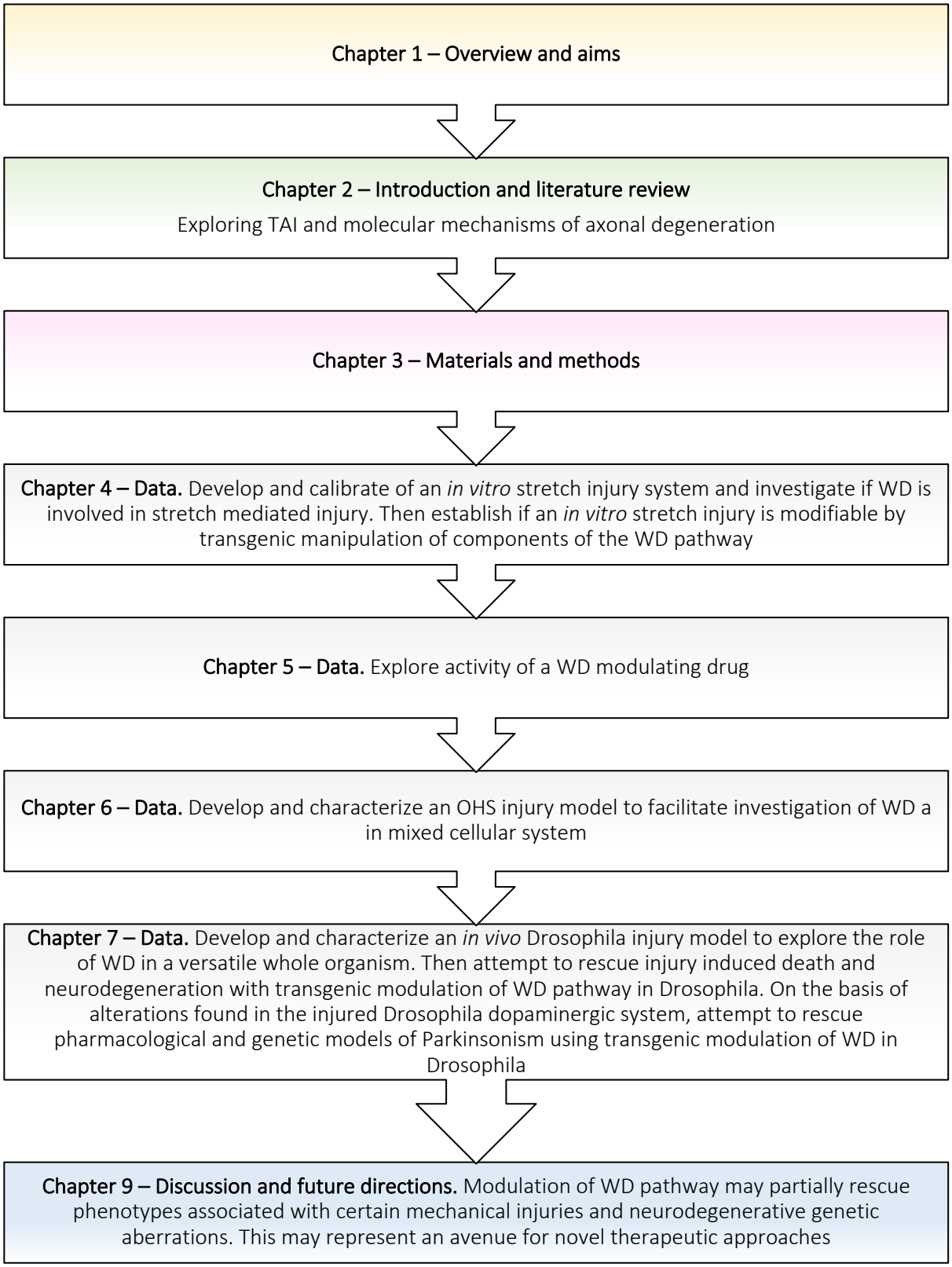

Figure 1. Summary of thesis - key steps and overall direction

WD, Wallerian degeneration. OHS, organotypic hippocampal slice.

Chapter 2 provides an introduction and literature review of the main areas explored in this thesis. The subject of TBI is discussed, with particular focus on its epidemiology, economic and social costs. Different classifications of TBI are presented and primary and secondary injury mechanisms are outlined. The diagnostic criteria of DAI and the concept of TAI are introduced. This gives way to a review of the biomechanics of DAI, with an introduction into the pertinent forces involved, injury thresholds and critical strain. The biological effects of a stretch injury are discussed along with the molecular mechanisms involved in TAI. An overview of the stages of axonal degeneration is presented, then a more detailed discussion is made of the molecular control of WD including the Nicotinamide adenine dinucleotide (NAD) synthetic pathway and key players in WD initiation and control. Potential mechanistic links between WD and TAI are discussed with an introduction to *in vitro* and *in vivo* models that have been used to explore these associations.

Chapter 3 contains core materials and methodology for the subsequent data chapters including details of the *in vitro* and transgenic animals used, culture methods and conditions, various assays and imaging modalities including neurite degeneration, histology/immunohistochemistry, protein analysis, flow cytometry, and *in vivo* behavioral measures.

The aims of **chapter 4** were to design, develop and calibrate an *in vitro* stretch system to allow interrogation of biological responses to mechanically induced axonal stretch injuries. The chapter contains details of the design and calibration of a stretch injury device including the calculation of strain and strain-rates with the system. This is followed by details of the optimization of primary neuronal culture methods on deformable silicone membranes. Optimal parameters are established for a sub-transection level force. Then effects of stretch injury on neurite degeneration in wild-type cultures is presented including induction of length dependent neurite degeneration. Preliminary attempt to explore axonal transport for alterations in injury states is included. The stretch injury model was then used to investigate the effects of various modulators of WD on the axonal response to a stretch injury. This aimed to establish whether WD was responsible for the degenerative effects of stretch and therefore is WD mechanisms provide a potential therapeutic target. Genetic and pharmacological

approaches were used to induce WD protective/vulnerable phenotypes in *in vitro* primary neuronal cultures.

The aims of **chapter 5** were to explore the effects of a specific drug, P7C3-A20, on TAI in order to establish if pharmacological manipulation of WD could be protective in a stretch injury model. P7C3-A20 has been suggested as an agent that is neuroprotective and exerts its protective action through NAD synthetic action, a component of the WD pathway, and this was investigated as a means of rescuing axonal degeneration.

The aims of **chapter 6** were to modify the stretch injury system developed in chapter 4 to characterize the response of a mammalian organotypic hippocampal brain slice (OHS) model to a stretch injury and explore interactions between WD and other neurodegenerative pathology *in vivo*. This was in order to allow the interrogation of WD in an *in vitro* system containing neurons and glia, and with some preservation of tissue architecture.

The aims of **chapter 7** were to characterize an *in vivo* TBI model using *Drosophila melanogaster*. The Drosophila TBI model was established and the response to the inflicted injury was characterized in terms of effect on lifespan and a range of behavioral measures. The aim of these experiments was to recapitulate the effects of TBI in a versatile model organism, opening up the possibility to explore a plethora of genetic mutations in TAI. The model was then used to explore the effects of a *highwire* (*hiw*) genetic mutation that delays WD responses to injury. Then, following on from the finding of selective dopaminergic neuron vulnerability to injury, and the recognized association between TAI and dopaminergic neuron loss and Parkinsonism, we then explore the ability of the *highwire* mutant to rescue the effects of a pharmacological toxin (rotenone) and genetic modification (*PINK1*^{B9}) associated with dopaminergic neuron degeneration.

Chapter 9 provides an integrated critical discussion of the findings from data chapters 4-8 and expands on the theme of WD in TAI, using this as a basis to propose future studies.

Chapter 2

Introduction and literature review

1. The scope and classification of traumatic brain injuries

a. Epidemiology of traumatic brain injury

TBI is a common and potentially devastating event. It can lead to profound consequences for the individual involved and their community, and deliver a high socio-economic cost. An estimated 10 million people per year experience a TBI and it is one of the leading causes of death in many parts of the world[14]. In the United States in 2010 a brain injury directly affected 2.5 million people and cost approximately 76.5 billion dollars, while in Europe around 2.5 million people will experience TBI each year, 1 million will be admitted to hospital, and 75000 will die[2,15]. In the UK the cost to the economy is around 15 billion pounds per year[16]. Over half of survivors from serious head trauma have a moderate or severe disability at one year, and in the UK there are an estimated 1.3 million people living with a TBI-related disability[16,17]. TBI has a propensity to occur in the young but can affect persons of all ages, it can render them unable to work, or dependent upon extensive health and social care. After decades of relative underfunding the field of TBI is now beginning to garner more attention from the research community, with large North American and European comparative effectiveness research studies enrolling several thousands of patients and looking at a broad range of research priorities[2,18,19].

b. Definition and classification of traumatic brain injury

Definition of traumatic brain injury

TBI is defined as "*an alteration in brain function, or other evidence of brain pathology, caused by an external force*"[1]. This definition encompasses a wide range of heterogeneous injuries with a variety of differing injury mechanisms, pathophysiology, and outcomes.

Classification of traumatic brain injuries

At its simplest, sub-classification can be made based on whether the injury is focal or diffuse, and then further categorized based on anatomico-pathological characteristics (Figure 2).

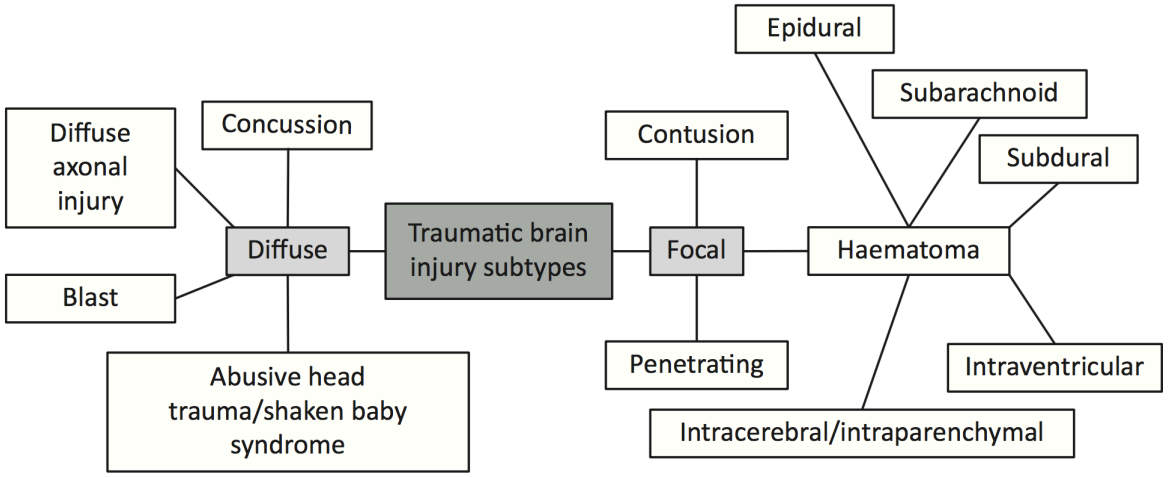

Figure 2. Traumatic brain injury classification

TBI can be classified as a diffuse or focal injury, with further stratification based on anatomicopathological findings. Injuries tend to be heterogeneous and there may have overlap between subtypes (from Hill *et al*[6]).

It should be noted that these injury subtypes often co-exist and overlap. In so far as practicable, the differentiation of these subtypes is important as the pathobiology and optimal therapeutic strategies may differ between them. Further categorization can be provided based on severity as assessed with the Glasgow Coma Scale clinical scoring system[20,21]. TBIs can be classified as 'isolated' if there are no associated extra-cranial injuries, or part of a polytrauma if associated with other injuries. They can also be complicated by other non-traumatic brain injuries including hypoxic-ischemic insults[6].

Primary and secondary brain injuries

An important distinction in any brain injury is between primary and secondary events. Primary brain injuries occur at the moment of trauma. They are instantaneous and result directly from the transfer of force to the brain tissue. Primary brain injuries include macroscopic damage such as brain laceration or contusion, and microscopic injury such as microhaemorrhage, or primary axotomy of axonal fibers. The primary injury sets in motion a cascade of processes that if unopposed can cause further damage and degeneration termed 'secondary brain injury'. Secondary brain injuries are the detrimental processes that follow as a result of the primary injury (Figure 3). They can occur over minutes to years, and lead to ongoing development of the injury including bleeding, hypoxia, excitotoxicity, cytotoxicity,

neuroinflammation– driven by both blood derived and CNS resident systems, oedema and programmed cell death pathways. Later changes including chronic proteinopathies and neurodegeneration manifest years after the initial insult can be separately designated as a 'tertiary brain injury'.

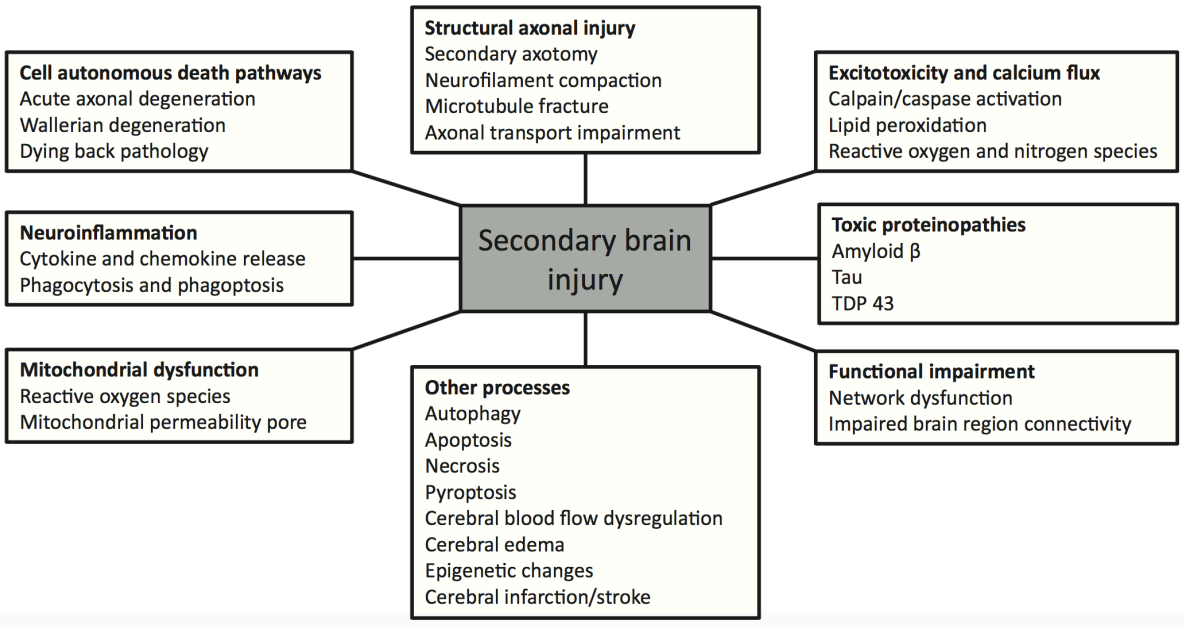

Figure 3. Processes involved in secondary brain injury following trauma

Secondary brain injury occurs after a TBI and involves a series of cellular processes that contribute to ongoing neuronal dysfunction and death. These provide many of the potential therapeutic targets in TBI(from Hill *et al*[6]).

Prevention of primary brain injury is challenging as it occurs at the moment of the triggering event. Thus, interventions are limited to prophylactic measures to reduce the incidence and severity of the initial injury, this includes preventative public health policy and safety legislation, and anticipatory neuroprotective agents[22]. In contrast, secondary brain injury develops over time. Therefore, depending on the expediency of care, these processes offer a window of opportunity to target secondary brain injury mechanisms in order to modify the outcome[6].

c. Diagnostic criteria of diffuse axonal injury

In 1956 Sabina Strich reported a series of patients who initially survived a closed head injury who, despite no focal intracranial mass lesion or signs of raised intracranial pressure,

remained minimally responsive from the time of injury. At post-mortem, all were subsequently noted to have diffuse degeneration and volume loss of white matter tracts including the corpus callosum and posterior brainstem[23]. Initially termed 'dementia following head injury', similar injuries were later referred to as 'diffuse axonal injuries'. Severe DAI typically manifests as an immediate and persistent loss of consciousness following head trauma, that may later progress to a persistent vegetative state or death[11].

Clinical diagnosis of diffuse axonal injury

Diffuse axonal injury (DAI) is a severe multifocal injury classically associated with high-energy acceleration-deceleration forces. Clinically, it is characterised by an immediate loss of consciousness, persistent coma and disability following a typical injury mechanism involving transmission of high-energy forces[3].

Radiological diagnosis of diffuse axonal injury

The National Institute of Neurological Disorders common data elements define DAI radiologically as "*more than three separate foci of signal abnormality*", with these abnormalities demonstrating *"a pattern consistent with scattered, small hemorrhagic and/or non-hemorrhagic lesions which have been shown historically to correlate with pathologic findings of relatively widespread injury to white matter axons, typically due to mechanical strain related to rotational acceleration/deceleration forces*"[4]. MRI has markedly improved diagnostic sensitivity compared to conventional radiology with CT. Advanced MRI techniques including susceptibility-weighted imaging are particularly sensitive for microhaemorrhages[24]. Diffusion tensor based imaging and tractography provide non-invasive information of axonal tract integrity through measurement of net diffusion. These techniques are becoming more common in clinical care but their validation as diagnostic tools remains incomplete[25–29].

Pathological diagnosis of diffuse axonal injury

Pathological diagnosis requires tissue from multiple brain regions and is therefore limited to post-mortem examinations. The most widely accepted definition of DAI of the brain is a histological diagnosis and was provided by Adams *et al.* This diagnosis is based on diffuse damage to axons in the cerebral hemispheres, in the corpus callosum, and/or the brain stem following TBI. It can sometimes also be found in the cerebellum. Injury is characterized by the

presence of axonal bulbs seen in sections stained by hematoxylin and eosin, silver impregnation techniques, or by immunocytological techniques for neurofilaments[5,30,31]. Immunohistochemical analysis for neuronal APP accumulation in a typical pattern including periodic varicosities and axonal retraction bulbs, is currently the most robust method of diagnosis. Currently, staining of axons with the transmembrane glycoprotein beta-amyloid precursor protein (APP) is the gold-standard in routine clinical and experimental use[32,33]. These diagnostic criteria are summarized in table 1.

Clinical	Mechanism – high velocity acceleration-deceleration traumatic injury Presentation – immediate profound loss of consciousness, persistent cognitive dysfunction +/- signs of upper motor neuron dysfunction
Radiological	Microhaemorrhages in multiple brain regions, particularly the corpus callosum and rostral brainstem
Pathological	Neuronal retraction bulbs and varicosities

Table 1. Diagnostic features of diffuse axonal injury

The pathological grading of DAI describes diffuse histological lesions as Grade 1, the additional presence of focal corpus callosum lesions as Grade 2, and the addition of focal brain stem lesions as Grade 3[5]. The frequency of DAI as a subtype of severe head injury is not accurately known but it is likely to constitute a significant proportion of the total[34].

Terminology of diffuse and traumatic axonal injuries

The term DAI is sometimes used synonymously with traumatic axonal injury (TAI), although the later is more commonly used to refer to animal models of TBI that share some pathological features with a human DAI. This inconsistency in terminology pervades the literature and confuses discussions of the disease. Therefore, for clarity this thesis will reserve the term DAI specifically for a human injury that conforms to the diagnostic features in table 1. The term TAI will be used to refer to any traumatic injuries where axonal damage is the dominant component in a model system, regardless of whether this involves animal models, or an *in vitro* system. In cases where this injury involves the PNS, or PNS tissue, as opposed to the CNS this will be highlighted.

2. The biomechanics of traumatic brain injuries

a. Biomechanical forces

Core terminology

Any attempt to understand the human condition of DAI requires an appreciation of the specific type of tissue deformation that takes place in the human brain during an injury that is sufficiently severe to produce DAI. The forces the brain experiences vary depending on many factors including the injury mechanism and the specific brain region we are focused on. Therefore, it is challenging to define the characteristic force seen in a DAI as the pathology may encompass injuries with substantial heterogeneity. However, from a mechanical perspective there are a limited number of forces that act on a human head during an injury process. Some commonly used biomechanical terms along with formal mechanical definitions and examples are found in table 2[35–37].

Biomechanical term	Definition
Acceleration	Rate at which an object changes speed. A changing velocity
Bulk modulus	A measure of a substances resistance to compression. It is high in the brain
Compression	The stress state where forces oppose each other and are balanced inwards. Compressive forces can act in a single direction (uniaxial) or in multiple directions (biaxial)
Deceleration	Negative acceleration
Deformation	Change in shape of an object undergoing a force
Elasticity	The property of an object or material that allows it to resist a distorting force, and to return to its original shape when the force is removed
Elastic modulus (Young's modulus)	A constant describing the ratio of stress to strain, that is a material's elastic resistance to deformation
Extension	The stress state that leads to increasing length of a material in the direction of pull
Force	Something that causes acceleration of a body, or when resisted causes deformation
Linear force	Force exerted on an object with a constant acceleration and a linear trajectory
Moment	Effect of force acting on a lever arm. Can cause bending or torque
Shear	Deformation as a result of unaligned forces in which parallel internal surfaces slide past one another. A plastic shear is irreversible, and an elastic shear is reversible
Shear modulus	A measure of a substances resistance to shear forces. It is the ratio of shear stress to shear strain. It is low in the brain
Strain	The relative change in size or shape of an object due to externally applied forces. It is the ratio of extension to original length and so is dimensionless. Strains can be *normal* (aligned forces) or *shear* (unaligned). Strain can be mathematically represented in several forms including as Lagrangian. The SI

	unit of strain rate is the reciprocal of time in seconds (s^{-1}) so $50s^{-1}$ is equivalent to 20ms
Stress	Force per unit area. Types of stress include shear, extension, compression
Stretch	Elongation of an elastic material
Tensile strength	The maximal tensile force that a material can resist before failure/breaking
Tension	A pulling force
Torque/rotary force	Rotational force that is the cross product of the vector where the force's application point is offset relative to a fixed suspension point. It tends to produce rotational motion. The magnitude of torque depends on the force applied, the length of the lever arm, and the angle between the force vector and the lever arm
Translational motion	The movement of an object from one place to another
Viscosity	Magnitude of internal friction of a fluid. Resistance of a fluid to stress i.e. force per unit area resisting shear and tensile strains
Yield stress	Maximum stress that can be applied before a sample ruptures

Table 2. Key biomechanical terms

Source: [35–37]

TBI can be as a result of direct contact loading (focal impact) or inertial loading where there is no direct impact of the head with an external object. Acceleration can occur in any direction and be linear, rotational, or a combination of the two. Movements will depend on whether the head is fixed or free. The maximum acceleration will depend on the mechanism of injury, the mass of the head/brain, and any restraining forces[36,38]. Despite the limited range of forces that can be applied to the head, the motions that can be produced are highly variable and make every TBI unique. Therefore, to make meaningful use of models we must generalize and try to understand what are the 'typical' forces, or limits of forces, that generates a DAI. If these forces can be extrapolated to cellular levels then it should be possible to mimic the cellular biomechanics required to model injury, regardless of the system used.

Forces involved in a diffuse axonal injury

To address the question of what forces are evident in a severe brain injury like DAI we must first understand the mechanisms of injury that typically causes DAI. In Sabina Strich's original 1956 description of 'diffuse degeneration of cerebral white matter following head injury', which would later come to be known as DAI, there were five cases; which included individuals knocked down by a bicycle, motorcycle, car, and truck. The fifth was involved in an unspecified 'road accident'. She describes two cases from other authors in her monograph, one was a fall

by a tightrope walker, and one from boy who sustained damage from a gun explosion. Modern authors generally cite high energy trauma as the primary cause, with road traffic accidents being the most common. Other causes include falls from significant height, high-energy assaults, and work injury[30,39–44]. The common causes of DAI may vary by geographical location, and is likely to evolve with time as our environments modify[45]. As road traffic accidents are the most common cause of DAI it is logical to look to that group to try and identify the 'archetypal' DAI, and hence forces needed to provoke it. There is a wealth of literature investigating the mechanical properties of road traffic collisions in relation to the brain. Most of this data is derived from correlation of post-mortem data with accident reports, or modeling in the form of organisms, phantoms, or computationally. The term 'road traffic accident/collision' is a blanket term that includes all manner of vehicle interactions that may or may not include pedestrians. DAI can be caused in a pedestrian struck by a vehicle, or to a vehicle occupant when a vehicle collides with an object[46].

Non-contact loading

One important consideration is whether DAI is induced primarily by the acceleration changes due to inertial non-contact loading, or whether head impact is required. Gennerali's classic primate experiments generated DAI like pathology and clinical responses including coma using purely non-contact forces. A review of 67 cases of human DAI where data was coded in the Crash Injury Research Engineering Network (CIREN) database showed over 90% of cases had evidence of contact-loading, with the majority of impacts causing DAI being from a lateral direction, and particularly near-side lateral impacts[47]. This supports earlier proposals that sufficient forces to generate DAI in the majority of motor vehicle accident would require contact loading[48–50]. As CIREN coded impacts as either frontal, rear, or lateral (nearside or farside), and did not take account of passenger position or restraint this is clearly a simplification of force orientation[47]. Some impacts causing DAI may be oblique in nature, giving rise to a combination of rotational and linear head kinematics[51].The necessity of a large gyrencephalic brain to generate sufficient inertial forces to mimic human TBI has been one of the driving factors in the return to use of large animal models. Rodents have smaller lissencephalic brains, less white matter, and different cranial and responses to intracranial pressure changes[52,53].

Rotational forces

There are two broad concepts describing how rotational forces can cause axonal injury in the human condition. Firstly, the mobility of the brain within the cranial vault is variable in different regions, hence there are focal points of shear stresses and strains. Secondly, brain tissue will shear at zones of different brain density[54,55]. Finite element modeling (FEM) is a mathematical computerized modeling technique that predicts how a product reacts to real-world forces. It involves creating a virtual 'mesh' of small elements that can be analyzed individually, and built up to represent the whole brain[56,57]. Several FEM studies have supported the view that rotational acceleration is more liable to result in strain and shearing of the brain than with a linear translation[58–62]. The vulnerability of the brain to rotational forces may vary between species depending on tract orientation[63].

Threshold forces

Tolerance criterion and injury thresholds

Tolerance criterion/injury thresholds are the forces required to induce DAI in humans. They can be estimated through a combination of animal experiments, computational or physical simulations, and isolated tissue tests[49]. Input during the injury can be classified by velocity, mass, location and vector. The output, or cellular response, can be quantified as deformation of brain tissue, rate of strain, and stress force. Input and output can be complicated by variations in brain and skull geometry, and individual properties including age. Therefore, we must recognize that any tolerance curve is a simplification and may not fully represent that of any given individual. Tolerances may also vary between different types of brain tissue[64]. Injury thresholds can be represented for rotation as the rate of change of angular velocity i.e. angular acceleration (rad/s^2), and for linear forces as units of acceleration (msec^2) or acceleration due to gravity (g). A review by Post *et al* in 2012 summarized the literature and found the threshold for mild TBI was ~80-140g, or 3000-16000rad/s^2 depending on lesion type, with DAI injuries being induced at the higher end of the spectrum[65]. Most loading event that cause injury are single as opposed to cyclical, and extremely rapid; in the order 50ms or less[66]. Translating forces in this region of magnitude into comparative insults in *in vitro* or *in vivo* systems, is an ongoing challenge. Relevant injury forces in humans need to be scaled for animal models[65,67]. One approach is to focus upon applying input forces that generate comparable clinical and

pathological outputs including behavior deficits, neuroimaging findings, or brain pathology, regardless of the actual input force[68].

A direct linear acceleration force to the human head typically results in a focal brain injury, for example, a parenchymal contusion or a damaged blood vessel causing a haemorrhagic lesion. The human brain has a bulk modulus that is five to six times higher than the shear modulus, this means that deformation following rapid acceleration-deceleration forces is likely to be predominantly shear in nature[51,69,70]. Most axonal injury in human DAI is thought to occur as a result of mixture of shearing and elongation forces between regions of the brain with different densities, classically at the gray-white matter junction, in regions of long crossing axons like the corpus callosum and near blood vessels[10,71,72]. Brain regions that contain highly anisotropic axons such as the corpus callosum and the brainstem are more vulnerable to axonal stretch injuries. Injury typically occurs where axons change direction or there is density difference, for example the grey-white mater junction[72,73]. During an injury the strain rates can vary in different brain regions as a result of differences in axon orientation and local cellular features, including the stiffness of adjacent tissue, maximum diversion angle and internal neuronal cytostructure. This inherent variability contributes to the internal heterogeneity of any injury[72]. Modeling these forces accurately in a useful manner has been a major preoccupation of the TBI research field.

Critical strain

Central to understanding the external forces that the brain experiences is the concept of critical strain. This is defined as "*a threshold level of tissue deformation which results in axonal injury*"[74]. Direct measures of axonal injury are not always available or easily made, so other measures of tissue tolerance can be used in lieu. Neuronal tissue tolerance can be inferred from the work of Bain and Meaney who stretched guinea pig optic nerves and found functional impairment assessed by evoked potentials at 0.18 Lagrangian strain, and morphological damage assessed with neurofilaments antibody at 0.21[75]. In a hippocampal slice stretch model a similar minimum tissue tolerance of 0.20 Lagrangian strain was suggested based of propidium iodide staining found at strain rates of 10-50s^{-1}. Higher strain rates caused greater injury. This may in part be explained by the viscoelastic properties of axons and brain tissue[76–80]. Abnormal accumulation of APP similar to that seen in DAI was found with injuries at 0.5

Lagrangian strain at rates of 20-50s^{-1} [64,81]. An alternative method of quantifying an injury, primarily used *in vitro*, is to look for non-specific increases in plasma permeability[73,82].

b. Biological effects of stretch injury

Shear deformation is predicted to be the dominant mode of tissue loading in inertia injuries, and in two-dimensional space this may be represented as a stretch[70,83–85]. Stretch forces can tear axons (primary axotomy) or partially damage them, triggering a variety of molecular pathways that in severe cases lead to axon degeneration (secondary axotomy)[31,86–88].

In vitro models have provided a wealth of data regarding axonal responses to mechanical injury. The most extensively characterized *in vitro* insult is mechanical stretch. The responses to an applied *in vitro* axonal and brain tissue stretch have been observed through the use of model systems. Selected examples are summarized in table 3 and figure 4.

Response	Summary of stretch effects	Reference
Calcium dysregulation	Acute release of intracellular calcium, followed by persistent calcium elevation.	82,89,90
Neurofilament alterations	Neurofilament alterations vary depending on stretch severity, and include delayed compaction	86
Microtubule failure	Microtubule structure fails and impairs axonal transport leading to varicosities	78,79
Necrotic and apoptotic death	Calpain and caspase-3 activation causes α-spectrin proteolysis, and loss of neuronal-dendritic MAP2. Necrotic death was also induced.	91
Differential gene expression	Differential expression of genes involved in cell death/survival correlate with injury parameters.	77,92
Neuroprotective gene modulation	Induction of neuroprotective preconditioning response	80
Enhanced NMDA vulnerability	Induction of heightened vulnerability to L-glutamate or NMDA	93
Altered action potentials and network activity	Hyperexcitability in neurons adjacent to regions of stretch	94
Inflammation	Pro-inflammatory mediators are upregulated and released	95
Unmyelinated axonal vulnerability	Unmyelinated axons are more vulnerable to axonal injury compared to myelinated axons	96
Astrocyte signalling	Astrocyte signaling resulting in widespread purinergic receptor activation and excitotoxicity	97
Mitochondrial dysfunction	Mitochondrial dysfunction and production of reactive oxygen species	98,99

Table 3. Cellular/molecular mechanisms influenced by axonal or brain tissue stretch

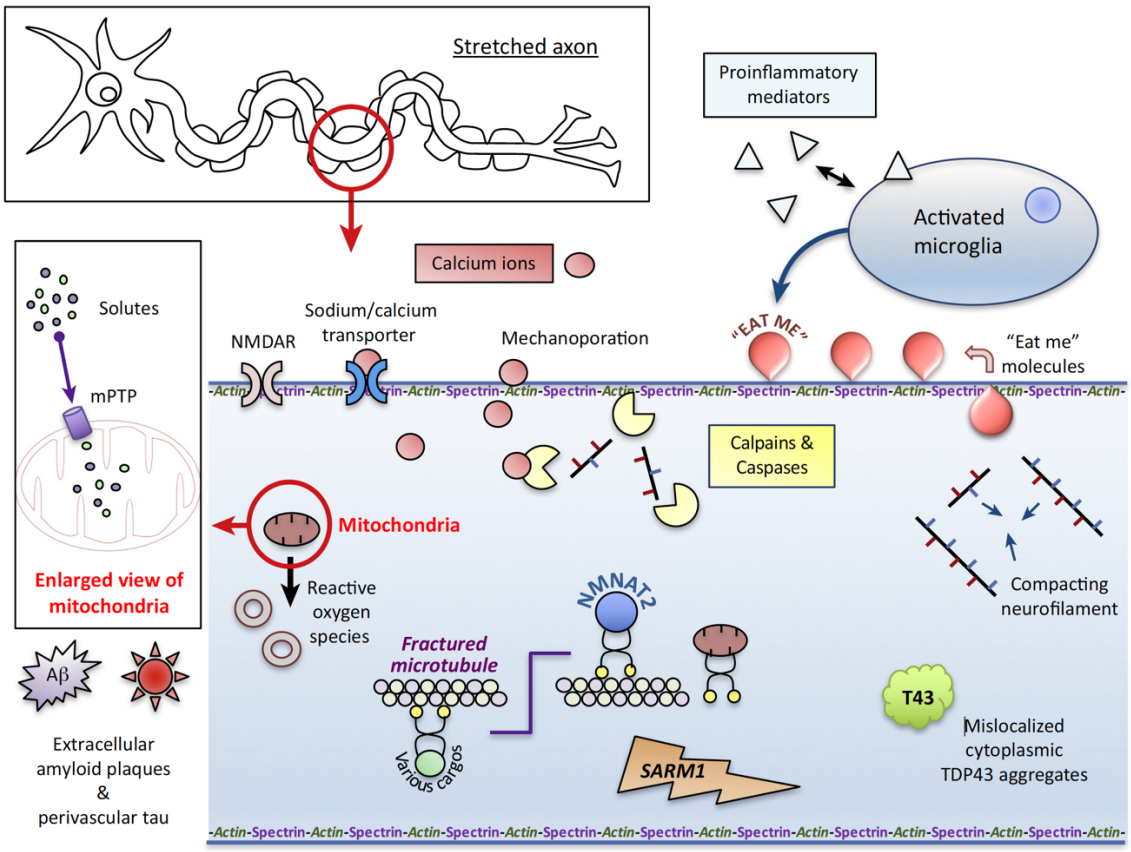

Figure 4. Molecular mechanisms and therapeutic targets in traumatic axonal injury

Mechanical stretch leads to undulation of the axon and activation of various injury pathways. Direct membrane mechanoporation and opening of exchange channels leads to calcium influx. This activates calpains, which degrade structural proteins. Proinflammatory cytokines have broad effects including initiation of caspase mediated proteolysis and microglia recruitment. Calcium influx also triggers generation of the mPTP, with subsequent solute influx and mitochondrial dysfunction/death. Reactive oxygen species are generated and result in oxidative damage. Neurofilaments compact and aberrant proteins including TDP43 and amyloid fibrils accumulate. Microtubules are fractured; this leads to impairment of axonal transport with failure to deliver NMNAT2 and subsequent Wallerian degeneration. Eat-me signals including phosphatidylserine are externalized and may initiate phagoptosis of stressed neurons by microglia. Note that although NMDA channels are shown on the axon for simplicity, most are localised on dendrites and dendritic spines, and axonally based channels are in a minority. Figure taken from Hill *et al*[6].

3. Mechanisms of axon degeneration

a. Stages of axon degeneration after injury

Axons are long neuronal projections that interconnect neurons and facilitate flow of information. They can be ten thousand times the volume of the neuronal cell body but with a far more elongated structure. An axon contains longitudinal tracks of microtubules that span the length of the neuron, acting as structural supports and polarized tracks for motor proteins. These anterograde and retrograde motors deliver cargos back and forth from the soma and the distal axon and synapses. Microtubules are constantly in a state of dynamic flux, characterized by polymerization assembly, static periods, and depolymerization disassembly[100]. Neurofilaments within the axon provide tensile strength and their radial charges determine axonal diameter. Additional longitudinal actin filaments are present and super-resolution imaging has demonstrated a regular repeating ring-like actin structure that runs around the circumference of axons with spectrin links and adductin caps[101,102].

TAI is intimately related to the process of axonal degeneration. Axon degeneration is an active, largely self-regulated series of converging cellular death pathways including acute axon degeneration (AAD), WD and apoptosis. Neuronal cell bodies have additional, independent death pathways that can be co-activated, creating challenges with interpretation of experimental findings[103–106]. The relative activity of each pathway may differ with injury type and also with time from the injury. Indeed, even within the same injury model different subtypes of axon injury are not unusual[107]. Following a transection injury there are four stages of axonal death; AAD, a latent period, WD, and debris clearance[7].

Acute axon degeneration

AAD refers to first stage of axonal death following transection. AAD in the region of injury occurs rapidly following a traumatic lesion and may be mediated by calcium flux, calpain activation, neurofilament compaction, transport failure, mitochondrial fragmentation and autophagy[108–111]. It is mechanistically independent of subsequent death of the remainder of the distal axon. AAD occurs in minutes to hours after an injury and mainly affects around 200-400µm of the axon proximal to the lesion site[112].

Latent period

WD with granular fragmentation of the axon distal to injury site, typically occurs rapidly but only after a latent period during which detached axons remain morphologically intact and electrically active. The duration of the latent period varies by species. In mice it persists for 24 to 48 hours following injury when modelled *in vivo,* or 4-8 hours *in vitro*[7,113–115]. In primates and humans it can last several days[116,117].

Wallerian degeneration

A rapid disintegration of the axon generally occurs within 2 hours of the end of the latent period, this disintegration of the distal axonal segment is WD[114,115]. WD was first described by Augustus Waller in 1850 as a process of curdling, coagulation, and eventual fragmentation of the distal portion of a nerve after transection[118]. WD is an active, cell-autonomous and evolutionarily conserved death pathway. Although a transected axons show positive Annexin V staining near the lesion site, the degeneration is distinct to other death mechanisms including apoptosis[103–106]. This is exemplified by the lack of caspase activation seen in WD, and the failure of caspase knockout, or apoptosis inhibition to prevent degeneration[119–123]. Likewise, treatment with necroptosis inhibitors, or genetic inhibition of signaling molecules in the necroptosis pathway including RIP3 and MLKL do not protect axons[124–126]. When an axon undergoes WD the axon rapidly swells and becomes varicose, it then fragments and the myelin sheath retracts forming dense contractions of myelin ovoid. Breakdown of the axon structure is mediated by calcium dependent proteases called calpains, which trigger cytoskeletal disassembly and a granular disintegration of the distal axon[127–132].

Wallerian-like degeneration

Whereas the original term ‘Wallerian degeneration’ referred to the degeneration of the distal portion of an axon following transection, we now recognize there are various additional factors, such as a transport block and certain chemicals that can lead to active axonal degeneration that is morphologically similar to WD[133–135]. Historically the term ‘Wallerian-like degeneration’ was used to describe axonal degeneration that was morphologically similar to classic WD but did not involve a transection injury. The discovery of mutants that modulate the WD pathway– discussed later– allow us to narrow this definition to axon degenerative processes that share aspects of their molecular mechanism with WD, as opposed to their

morphological reaction. Hence, a disease or intervention that induces axon degeneration but that can be delayed by a slow WD mutation, particularly WLD^s or sterile alpha and TIR motif-containing protein 1 (SARM1) loss of function mutation, can now be classified as a Wallerian-like degeneration dependent process[7]. Given the inconsistencies in the use of terminology in the literature, we will refer to all traumatically-induced WD, and Wallerian-like degeneration, simply as WD regardless of whether the injury is a transection or not. However, where possible we will distinguish this from non-Wallerian causes of axonal degeneration and neuronal death.

In human DAI it is unclear how much WD occurs. Although white-matter degeneration is recognised and can be quantified using neuroimaging and post-mortem analysis, it is unknown how much occurs due to WD and how much is due to other processes or death mechanisms. While primary axotomy– as a transection injury– can be considered definite evidence of WD, it is considered an infrequent event in DAI. The extent to which WD contributes to secondary axonal degeneration during a DAI is not fully known[6]. It has been proposed that there may be a burden of sub-axotomy level injuries that may still be sufficient to induce secondary axon degeneration[10,11]. If this subpopulation of axons exists, and the WD process could be modulated in these neurons then there may be an opportunity to prevent axonal degeneration until such time as the neuron recovers from the effects of the acute insult, and degeneration is no longer inevitable.

Debris clearance

After WD induced axon fragmentation, clearance is mediated by macrophages and Schwann cells in the PNS, and oligodendrocytes and microglia in the CNS[136–141].This response has been demonstrated in brain slice preparations and after a controlled cortical impact (CCI)[142,143]. Temporally, the numbers of microglia appear to follow a multiphasic pattern with early and late peaks in numbers[143]. Beyond the acute inflammatory phase of DAI there is triggering of a chronic microglial activation that can persist for months or years. This has been shown in murine models up to a year following experimental brain injury and also in imaging of human subjects with PET ligand [11C](R)PK11195(PK)[144–146]. Histological examination of the brains of historically injured patients has demonstrated ongoing activation many years and even decades after the original insult, and this finding has been associated with regions of substantial white matter volume loss[9]. More recently the concept of *phagoptosis* has

emerged. This is when a neuron that is not terminally injured, but rather in a stressed but viable state is phagocytosed. Severing of neurites or traumatic injury causes surface expression of phosphatidylserine residues translocated from the inner plasma membrane. This is one of several 'eat me' signals recognized by microglia and which result in phagocytosis of the injured neuron[147–150]. Whether 'eat me' signals are displayed in response to a DAI, and if they play a role in secondary brain injury or long-term neurodegeneration, is currently an open question.

b. Molecular control of Wallerian degeneration

NMNAT and the NAD synthetic pathway

An understanding of the NAD synthetic pathway is a prerequisite for understanding the control of the molecular pathway involved in executing WD. The pathway is summarized in figure 5.

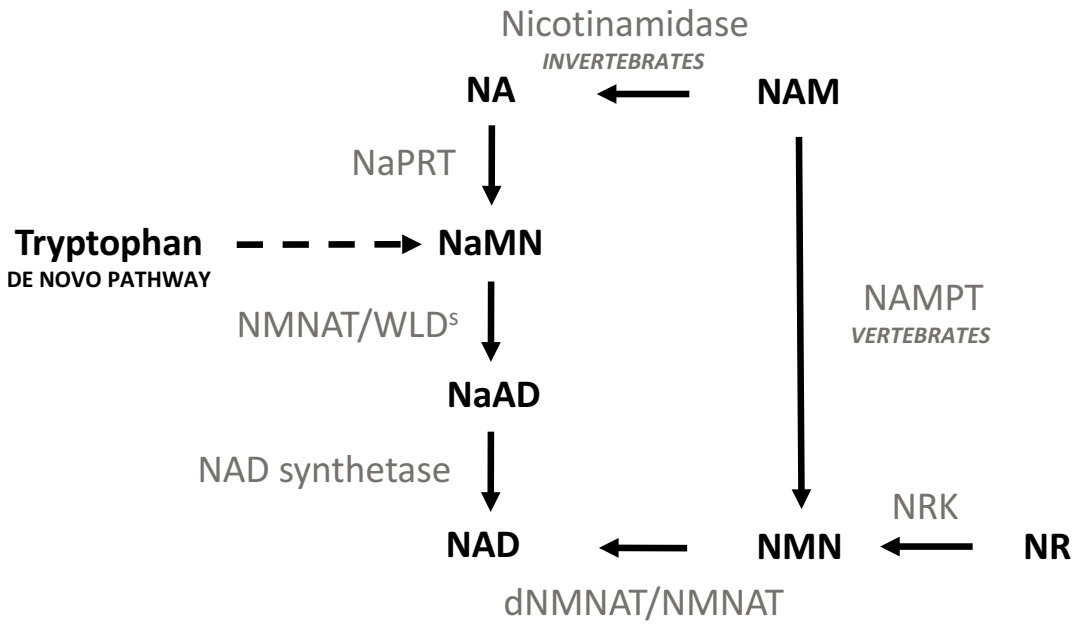

Figure 5. The NAD synthesis pathway

The *de novo* NAD synthesis pathway generates NAD from the essential aromatic amino acid tryptophan. Nicotinic acid mononucleotide (NaMN) is converted to nicotinic acid adenine dinucleotide (NaAD) by nicotinamide mononucleotide adenylyltransferase (NMNAT). NaAD is then converted to NAD by NAD synthetase. There are three additional thee salvage pathways. Nicotinamide mononucleotide (NMN) is produced by nicotinamide phosphoribosyltransferase (NAMPT) from nicotinamide (NAM), and by nicotinamide riboside kinase (NRK) from nicotinamide riboside (NR). NMN is then converted to NAD by NMNAT. Alternatively NAM is converted to nicotinic acid (NA) by nicotinamidase, and then NA is converted to NaMN by nicotinc acid phosphoribosyltransferase (NaPRT)[151–161].

There are three intersecting salvage pathways utilizing nicotinic acid mononucleotide (NAM), nicotinic acid (NA) or nicotinamide riboside (NR), and a single de novo NAD synthesis pathway derived from the dietary essential amino acid tryptophan[151–161]. In mammals nicotinamide mononucleotide (NMN) is a product of NAD hydrolysis by poly-ADP-ribose polymerases (PARPs), mono-ADP-ribosyl transferase (MARTs), sirtuins (SIRTs) and ADP-ribosyl cyclases, and these salvage pathways provide the main NAD supply, the de novo pathway alone being inadequate to maintain health[153,154,159,162,163]. NAD is a critical co-enzyme required for cellular redox reactions and cellular bioenergetics including generation of mitochondrial and glycolytic ATP genesis[164]. It also has functions in calcium signaling and post-translational protein modification[165,166].

The NMNAT enzyme

The nicotinamide mononucleotide adenylyltransferase (NMNAT) enzymes are vital components of the NAD genesis pathways. They are bidirectional enzymes that catalyze conversion of NMN to NAD, and nicotinic acid to adenine dinucleotide (NaMN) to nicotinic acid phosphoribosyl transferase (NaAD)[154,167]. There are three mammalian isoforms of NMNAT, each with individual subcellular localization and tissue expression. NMNAT2 is highly expressed in brain tissue, and to a lesser degree, in cardiac and in skeletal muscle, and the pancreas. In contrast NMNAT1 is expressed similarly in all tissue types, but NMNAT 3 is mainly found in the liver and erythrocytes[168]. The three isoforms are generally regarded as having different subcellular localization based on their differing isoform-specific targeting and interaction domains. NMNAT1 is localized to the nucleus, NMNAT2 is associated with golgi-derived vesicles, and localized to cytoplasm and axons, and NMNAT3 is localized to mitochondria[7,169–171]. Unlike mammals, Drosophila have a single NMNAT gene (dNMNAT) with preserved NAD synthetic function, that undergoes alternative splicing into two neuroprotective variants[172,173]. The NMNAT enzymes are key molecules in the NAD synthetic pathway, they convert NMN to NAD[174].

NMNAT2

NMNAT2 is a critical axon survival factor, it is a labile protein with a half-life of less than one hour that requires constant delivery to axons from the cell body in order to maintain axonal

survival. NMNAT2 transport is via palmitoylation-dependent attachment to Golgi derived vesicles, and turnover is by the ubiquitin-proteasome system[175–177]. If delivery is prevented by inhibition of protein synthesis or targeted Short interfering ribonucleic acids (siRNA) knock-down of NMNAT2 then axon degeneration occurs[134,176,178,179].

There may also be additional roles for NMNATs in axon survival that are independent of the NAD synthetic enzymatic activity. Enzymatically inactive dNMNAT is able to protect against some forms of axonal injury including those causes by Ataxin-1, human tau expression, proteotoxic stress, and crush injuries[180–183]. The mechanism of these protective actions may be related to a chaperone-like function, where NMNAT binds to proteins and prevent stress induced unfolding responses, independent of its enzymatic function[180,182,184–187].

Reduced NMNAT in models

A reduction in NMNAT2 levels in mice, established by gene trap mutagenesis, manifests as severe developmental abnormalities of the central and peripheral nervous system, including reduced axonal growth and innervation patterns, and perinatal lethality. Primary neuronal cultures with homozygous null alleles for NMNAT2 fail to develop normal length axons[178,179]. NMNAT2 levels fall in wild-type neurites following transection and prior to degeneration in a time-dependent manner, acting to trigger WD[134,179]. Reduction of NMNAT2 by siRNA mediated depletion is sufficient to trigger axon degeneration[178,188].

Reduced NMNAT in humans

The only monogenetic human disease that currently has a published association with NMNAT protein abnormalities is Leber's congenital amaurosis. This retinal dystrophy can be caused by numerous homozygous or compound heterozygous mutations in NMNAT1[189–193]. Pre-publication data from our group and collaborators (Peter Huppke & Michael Coleman, personal communication) describes the first known monogenetic disease causing NMNAT2 mutation. In the homozygous state this substitution (c.281C>T, p.T94M) is associated with the painful neuropathic disease– primary erythromyalgia.

Endogenous expression of NMNAT may influence the vulnerability of neurons to various insults that act via the WD pathway including common neurodegenerative disorders[187,194,195].

Up to 50 fold variation in NMNAT2 levels are found in the existing human population, and variations have been correlated with measures of cognitive function and pathological features of neurodegenerative diseases including Alzheimer's disease (AD), Parkinson's disease (PD) and Huntington's disease(HD)[187,196–198]. The extent to which individual variation in NMNAT2 expression might affect outcomes following TBI is unknown.

Other key players in WD control

Wallerian degeneration control

Understanding of the control mechanisms involved in the WD pathway remain incomplete, but there have been several important advances in the last two decades. The presiding view is that a core step in WD is the failure to deliver the essential survival factor NMNAT2 from the neuronal soma to the distal axon. Following an axonal injury, either due to interrupted transport or a transection, the delivery of NMNAT2 from the neuronal cell body to the distal axon is compromised, and NMNAT2 levels fall as it is degraded[134,178,174,199]. Loss of NMNAT2 beyond the site of injury, leads to a functional block in the NAD synthesis pathways with reduction in the ubiquitous coenzyme NAD and an increase in its precursor NMN. It has been proposed that it is NMN that may ultimately lead to triggering of Wallerian degeneration[174,200–202]. Other possibilities include a direct effect of NAD depletion or some combination of both initiating an axon degeneration programme[174,203]. The downstream effect of NMNAT2 depletion is an activation of the SARM1 molecule[179,203–205].

SARM1

The *dSarm* gene was discovered by a forward genetic screen in *Drosophila* to identify gene targets that delay WD. The mammalian ortholog also goes by the name SARM1, while the *Caenorhabditis elegans* ortholog is called TIR-1[204,206]. SARM1 is one of five intracellular adaptors for Toll-like receptor signaling. These receptors are important in the innate immune system where they recognize pathogen associated molecular pattern signals that ultimately activate inflammation or cell death. NMNAT2 depletion leads to SARM1 dimerization, and subsequent axonal fragmentation}[179,203–205]. The exact mechanism by which SARM1 mediates rapid fragmentation of severed axons is unclear, but may relate to active depletion of NAD levels, possibly through NADase activity[203,207–209]. When the SARM1 gene is knocked out, axons show a robust delayed degeneration phenotype comparable to WT axons[125,174,179,203].

SARM1$^{-/-}$ completely rescues NMNAT2$^{-/-}$ lethality and hence can be placed downstream of NMNAT2 in a linear pathway, or alongside it in a convergent pathway (figure 6)[7,179,210].

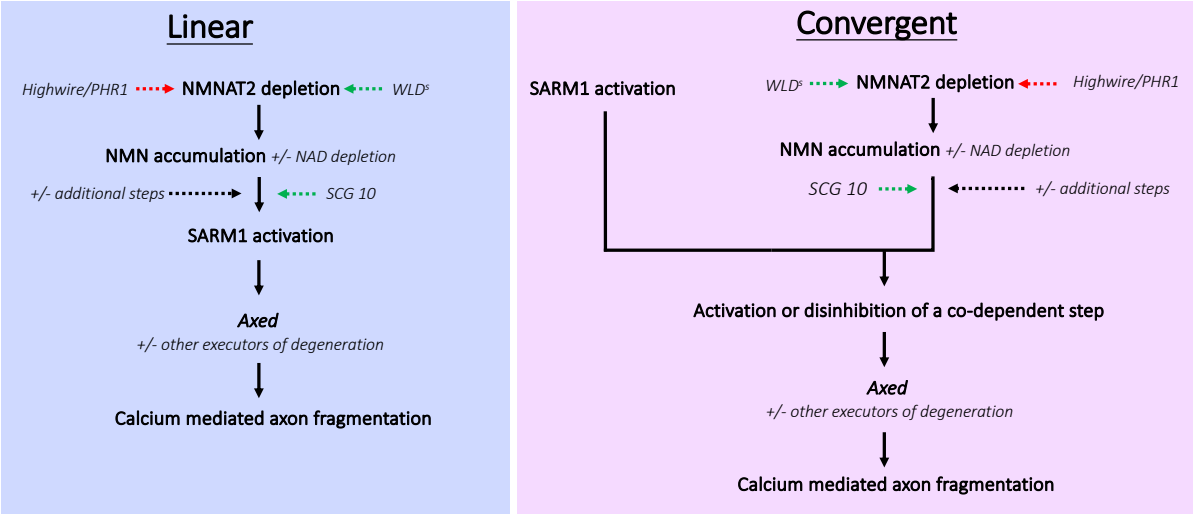

Figure 6. Molecular control pathways of Wallerian degeneration

Experimental evidence has thus far not been able to definitively differentiate between the possibilities of a linear or a convergent Wallerian degeneration pathway. Steps in WD include NMNAT2 depletion, NMN accumulation, prodegenerative SARM1 activation with subsequent Axed activation (in Drosophila), and finally calcium mediated axon dismantling. SARM1 activation may be a linear downstream consequence of NMN accumulation/a changing ratio of NMN/NAD, or SARM1 may function in parallel with a NMNAT2 depletion dependent process to converge on a co-dependent step. Black arrows signify the core pathway, red arrows signify pro-degenerative modulating factors, while green arrows represent factors that delay Wallerian degeneration. It is likely that this picture is incomplete and additional steps will be elucidated in the future. Adapted from Conforti *et al* 2014 & Gilley *et al* 2015[7,179].

The slow Wallerian degeneration mutant (WLDˢ)

Many insights into the molecular mechanism of axon degeneration came from the fortuitous discovery of a spontaneous mutant mouse in which WD was delayed tenfold. This phenotype was termed WLDˢ and details of the mutation and the resulting chimeric protein were systematically elucidated[211,212]. The responsible gene was identified as *Wld*^{s} and found to contain a region encoding the NMNAT1 enzyme[213]. WLDˢ is an aberrant fusion protein with critical NMNAT activity but a longer half-life than the native axon localized NMNAT2. WLDˢ exerts its protective phenotype by substituting for NMNAT2 in the axon. As WLDˢ degradation is slower than NMNAT2, it is likely that this accounts for the delay in WD[178]. NMNAT1 with

aberrant cytoplasmic localization can also delay WD, as can NMNAT3 if overexpressed[214–216]. Notably, both NMNAT1 and NMNAT3 have a greater stability than NMNAT2[134].

The PHR family (including highwire and PHR1)

Another major regulator of the WD is the PHR family of proteins, these include *PAM* (*Homo sapiens*), *highwire* (*Drosophila melanogaster*), *esrom* (*Danio rerio*), *Phr-1* (*Mus musculus*), and *rpm-1* (*Caenorhabditis elegans*). The *highwire* gene encodes a large 5233 amino acid protein (566kDa) with a variety of functions including E3 ubiquitin ligase activity, inhibition of adenylate cyclase, modulation of TSC signalling and pteridine synthesis, and interactions with myc and co-SMAD Medea[217–225].

Loss-of-function (LOF) mutations in the *highwire* gene are associated with a lifelong delay in axon degeneration following transection both *in vitro* and *in vivo*[223,224,226,227]. *Highwire* is thought to function to modulate the levels of dNMNAT primarily through its E3 ubiquitin ligase activity that acts to degrade dNMNAT and is capable of depleting ectopically expressed mammalian NMNAT[224]. The physiological functions of *highwire* include axon guidance and restraining synaptic growth[218,223,228,229].

PHR-1 loss strongly delays Wallerian degeneration in mammals[7,225]. PHR-1 depletion in adult mice with a conditional *Phr-1* allele and a tamoxifen-inducible Cre-recombinase led to a substantial delay in WD with 75% of myelinated sciatic nerve axons structurally intact 5 days after transection injury. The primary mechanism for axon protection in PHR-1 loss is thought to be a slowing in NMNAT2 degradation due to loss of ubiquitin ligase activity. Axon protection persisted even after falls of NMNAT2 levels[230]. This suggests that either the mechanism of degeneration in this case is no longer rapidly inducible by NMNAT2 loss, perhaps due to mechanistic differences between a gradual and sudden loss of NMNAT2, the requirement for depletion early after injury to trigger the pro-degenerative programme, or that measurement of NMNAT2 is insufficiently sensitive to detect low levels that remain sufficient to delay WD[176].

MAPK signalling

Wallenda (Wnd)/*Dual leucine zipper-bearing kinase* (DLK) are additional targets of *highwire*/*Phr-1* involved in WD. *Wnd* encodes a mitogen activated protein kinase (MAPK)

homologous to the vertebral DLK. The MAPK are a group of serine/threonine specific protein kinases that act as signal transduction molecules involved in a directing a wide range of cellular processes including gene expression, differentiation, proliferation, and cell death in response to stimuli including inflammation and stress[231].

Wnd is localised to synapses, and acts as a downstream target of *highwire.* Loss of *highwire* function in collaboration with the F-box protein binding partner DFsn leads to increased levels of *Wnd* which acts on c-Jun N-terminal kinase (JNK) and the transcription factor Fos to result in synaptic overgrowth at the neuromuscular junction (NMJ)[218,228,232]. Axonal injury leads to fall in the level of *highwire* and an acute increase in *Wnd* protein. *Wnd* overexpression results in axonal protection from degeneration, this has led to the suggestion that *Wnd* regulates an adaptive response to axonal stress[233,234]. The *Wnd*/JNK/Fos signalling pathway was also required for axon regeneration in the segment proximal to a larval crush injury[233]. Xiong *et al* proposed a model where distal to an axonal injury *highwire* acts to deplete dNMNAT and *Wnd* hence triggering axon degeneration, while in the proximal stump soma-axon transport maintains sufficient levels of dNMNAT and *Wnd* to support axon maintenance and regeneration[234].

DLK, also known as MAP3K12, is a mammalian MAPK kinase kinase (MAPKKK), a member of the MAPK family. DLK activation initiates a signal cascade that results in JNK phosphorylation, and has a physiological function in nervous system development. DLK null mice have defective nervous system maturation including impaired neuronal migration, axonal growth and synaptic development[228,235,236]. Dorsal root ganglion (DRG) cultures and *in vivo* sciatic nerve from DLK deficient mice show a moderate delay in axon degeneration following transection or vincristine injury, and pharmacological inhibition of JNK confers similar levels of axon protection[237]. The axonal protection seen with DLK deficiency or inhibition is weaker than with WLD^{s} or SARM1 mutation, this can be explained by a degree of functional redundancy in the MAPKs. MEKK4 and MLK2 are related MAPKs that activate MKK4 and MKK7 respectively, these then activate JNK 1-3. ShRNA lentiviral knock down of DLK, MEKK4, and MLK2 each result in partial protection against WD, and the combination is additive[125].

The position of MAPK activity in the WD pathway is contentious. According to Yang *et al*, endogenous SARM1 is required for MAPK dependent activation of axon degeneration. MAPK activation occurs rapidly after injury, within 5 minutes as evidenced by phosphorylation of MKK4, but this is abolished along with JNK activation in SARM1$^{-/-}$ mice. Furthermore, fusing a SARM1-TIR domain to FKBP(F36V) allowed an inducible dimerization that lead to a pro-degenerative SARM1 signal. This degeneration was blocked by combinational depletion of MKK4/MKK7 or JNK1-3. Cytoplasmic expression of NMNAT1 also blocked MAPK activation. These findings suggest a position for MAPK activity downstream of NMNAT depletion and SARM1 activation in the in the WD pathway[125,237]. However, SARM1 deletion confers strong protection even if it is only induced several hours after a transection injury. Likewise, transduction of cytoplasmic NMNAT1 or inhibition of NAMPT with FK866, and hence inhibition of NMN due to NMNAT depletion in an injured axon, imparts a strong protection against WD. It is unclear how these findings can be explained in the context of the MAPK activation seen within minutes[125,203]. Additionally, it has been proposed that MAPK's pro-degenerative activity is executed by increasing NMNAT2 and dNMNAT turnover, and therefore act upstream of NMNAT depletion and SARM1 activation[238]. In PHR-1 deficient mice and *highwire* loss-of-function mutant flies the DLK/*Wnd* levels are increased but despite this axon degeneration is still delayed, suggesting that the MAPK pathway acts upstream of the PHR-1/ *highwire* target, or that the protective effect of PHR-1/*highwire* outweighs any degenerative MAPK activation in these mutants[224,230].

SCG10

SCG10, also known as stathmin 2, is a labile protein that has been implicated in the early stages of WD. It is rapidly depleted in axons *in vitro* and *in vivo* distal to an injury site, while rapidly replaced by fast axonal transport in the proximal segment[239,240]. SCG10 degradation is JNK dependant. The axon protective effect of SCG10 is weak compared to other slow WD modulators like SARM1 and WLD^{s}, and artificial preservation of SCG10 levels after injury has a small protective effect on WD. This is thought to be due to maintenance of mitochondrial transport. Depletion of SCG10 in isolation is insufficient to trigger the WD process but contributes to acceleration of degeneration in injured axons[239].

Axundead

Axed is a further molecular step downstream of dSARM that has recently been identified in Drosophila, that is essential for injury-induced axonal degeneration. In Drosophila LOF mutation in *Axed* has a phenotype that is able to fully rescue loss of the Drosophila's single NMNAT. *Axed* inactivation can suppress the axon degenerative effects of gain-of-function dSARM *in vivo* These findings make *Axed* a potential co-dependent modulatory step in a convergent pathway of dSARM and dNMANT. *Axed* has been identified as a BTB and BACK domain protein, the common function of which is usually recruitment of substrates to CRL complexes for ubiquitin tagging and proteasome degradation. However, this relationship has yet to be demonstrated for *Axed* and so the mechanism of axon protection in *Axed* mutants still remains an open question[241].

Other molecular regulators of Wallerian degeneration

Other molecular regulators of WD have been identified, the manipulation of which may accelerate or delay the process of WD. These include AKT, a target of proteasomal degradation by the E3 ubiquitin ligase ZNRF1, and a negative regulator of MKK4. Inhibitor of nuclear factor–κB kinase (IKK) and Glycogen synthase kinase 3 (GSK3) promote axon degeneration following injury, and knockdown of these molecules are capable of moderate axon protection[242,243]. The trypsinlike serine protease inhibitor TLCK, and the chymotrypsin-like serine protease inhibitor TPCK can also delays WD following injury[242,244]. Terminal execution of WD by calcium mediated cytoskeletal breakdown can be delayed by calcium chelation and calpain inhibition[245]. However, for therapeutics this may be too late a stage in the degenerative pathway to modify outcomes.

4. Wallerian degeneration and diffuse axonal injury

a. Mechanistic links between Wallerian degeneration and diffuse axonal injury

The scope of Wallerian degeneration in disease

Axon degeneration occurs in several neurodegenerative disorders including AD, PD, MND, MS, HD, and Glaucoma. It is also the primary pathology in several peripheral neuropathies including HSP[7,246]. The extent to which WD is involved in a human TBI is unclear. WD has been proposed as a component of secondary brain injury but important questions remain regarding the degree to which it influences outcomes, and its suitability as a therapeutic target. It is important to consider how a traumatic multifocal axonal injury, in the absence of infarct, laceration, haemorrhage or other macroscopic anatomical disruption might add to poor outcomes in brain trauma and whether WD may a contributing factor. There are two principal biomechanical mechanisms potentially linking a DAI and WD. The first is a transection injury. The second is a subtransection stretch. Other non-mechanical secondary brain injury consequences including inflammation, lipid peroxidation, excitotoxicity and energy failure, are less clearly linked to WD[6].

Primary axotomy

Primary axotomy, that is a complete break of an axon at the moment of trauma, disconnects the neuronal soma, its associated dendrites, and the proximal axon from the distal axon. The term was first used as a description of degeneration occurring in a subpopulation of small unmyelinated axons in a lateral acceleration injury primate model[247]. Mechanistically, primary axotomy is an axonal disconnection and hence is mechanistically twinned to classical WD as defined by axonal transection. Primary axotomy is generally considered relatively rare in human DAI[10,34,247–249]. This is based upon various layers of evidence including a failure to see cytoskeletal dissolution at early timepoints following TBI via neurofilaments staining[250], resistance of neurons to high degrees of strain *in vitro*[249], and a recognition that historical neuropathological markers of primary axotomy, including axonal swellings and retraction bulbs, may actually be secondary findings that develop over time[32,131,251–253]. Evidence of complete primary axotomy is inconsistently represented in human studies that examine post-mortem tissue from historical TBIs, and accurate quantification of the amount of primary

axotomy in a severe human DAI is lacking[34,248,250]. Therefore, although it cannot be completely excluded that primary axotomy may play a role in certain subtypes of TBI– for example lacerations or focal microhaemorrhages– or be a small component of DAI, its overall relevance as a potential therapeutic target is unproven. Therefore, further questions must be asked about how an axonal stretch injury, even if it is a widespread multifocal one, can lead to such profound clinical deficits. Although widespread white matter loss is well established following severe TBI, the underlying assumption that deficits following TBI relate directly to neuronal loss has not been unequivocally established[9].

Subtransection injuries

A second potential link between axonal injury and clinical deficits may come from subtransection level axonal injuries. It has been proposed that an axonal stretch can fracture microtubules without membrane rupture. Microtubules are viscoelastic in nature and hence are particularly susceptible to breakage because when rapidly stretched they become the stiffest portion of an axon[78,79]. As microtubules are an essential structural component of the axonal transport machinery then their injury disrupts both anterograde and retrograde cargo delivery. These microtubular fractures contribute to the development of axonal undulations, and may accumulated cargos due to impaired transport may explain the development of varicosities seen after injury[78,79]. There are several ways in which an impairment of axonal transport might contribute to WD. The essential axon survival factor NMNAT2 undergoes constant transport from the cell body to the axonal compartment[175,199,254,255]. A disruption in the delivery of NMNAT2 to the axon will initiate the WD pathway as previously described[256,257]. Mitochondrial axonal transport is also important in axonal health and it has been suggested that WLD^{s} may partially confer its protective action by stabilizing mitochondria and preserving their physiological axonal function[258,259]. Therefore, injury-induced impairment of mitochondrial transport may also interact with the WD pathway, although work from our laboratory demonstrate that SARM1$^{-/-}$ mutation preserves axons despite a substantial reduction in mitochondrial movement , suggesting that a maintenance of mitochondrial axonal transport is not essential to rescue WD (Loreto *et al*, unpublished data).

Dying back pathology

'Dying-back' is a process of proximal axonal degeneration and subsequent cell death that has been observed in response to an axonal injury. This varies by neuronal subtype and the distance of the injury from the cell body[260–262]. Some neuronal cell types, such as the retinal ganglion cell seem more vulnerable to a proximal dying-back pathology, with perikaryal injury or death after the initial insult[7,8,260,263]. This is not to be confused with 'dying-back' pathologies where length-dependent degeneration occurs, such as diabetic neuropathy[264–266]. The reason an axonal injury causes dying-back is incompletely understood, but may relate to abnormal signal transduction at the subcellular level or perikaryal membrane permeability changes induces by a remote neurite lesion[263,267]. The extent to which dying-back occurs in the human CNS, or its contribution to clinical outcomes in DAI, has not been established. Even in cases where an axon distal to an injury site degenerates but the soma survives, there may still be deleterious consequences for connectivity and synaptic activity that will conceivably influence overall neuron function even if plastic reorganization ensues[268].

Beyond direct axon transection/subtransection injury, and dying back neuronal pathology, there are other potential mechanistic links between a human DAI and subsequent clinical impairment, these may include synaptic loss, and impairment of connectivity – both on a cellular, and a network scale. However, the relative contributions of these factors remains to be ascertained[6].

b. Evidence for Wallerian degeneration in traumatic brain injury

Evidence from neuroimaging

MRI based neuroimaging modalities, including DWI and tractography, offer the potential opportunity to investigate the relationship between pathology and clinical outcomes in human survivors of injury. Radiological descriptions of WD in DAI exist across various imaging modalities but correlation of advanced technologies such as DWI and tractography with postmortem tissue are lacking. Therefore, it is not possible to be certain that reported neuroradiological markers of axon degeneration truly represent WD as opposed to non-Wallerian mediated cell death and associated axon degeneration[25,29,269,270].

Evidence from biomarkers

Biomarkers are surrogate markers of disease presence and progression/severity. They are often cytoskeletal proteins or other molecules released during neuronal or glial breakdown. An effective biomarker of axonal injury would provide a diagnostic tool, a quantitative measure of injury severity, and an indicator to gauge treatment efficacy. The ideal biomarker would be highly sensitive and specific for TAI, rapidly reflect changes in injury status, and be easily obtained, such as from a peripheral blood sample. Axon degeneration results in the generation of cytoskeletal breakdown products and several of these have been explored as potential biomarkers, including spectrin breakdown products (SBDPs), neurofilament light and heavy chains, phosphorylated neurofilaments, microtubule associated proteins, and several non-skeletal markers including S100-b, neuron-specific enolase, and ubiquitin C-terminal hydrolase (UCH-L1)[271–274]. Despite active research, biomarkers that are definitely due to axonal injury, as opposed to less-specific markers of brain or neuronal injury or disease are lacking. Likewise, there are currently no biomarkers that can differential WD from non-WD neuronal death.

Evidence from genetic modulation of models

One way to establish the contribution of WD to a TBI is to block WD and examine the outcomes compared to a normal WD control. In the absence of a pharmacological agent to inhibit WD, it is not possible to explore this in humans. Instead we look to animal models. There have been two studies examining the relationship of TBI and WD in animal models. This first concerns a WLD^{s} expressing mouse that was exposed to a single CCIs. It was found to have less motor and cognitive impairment than uninjured control animals[275]. A second mouse CCI model with a SARM1 loss-of-function mutation showed reduced neuronal loss and cognitive impairment following injury[276]. These studies go some way to suggest that therapeutic modulation of the WD pathway could potentially could improve outcomes from TBI, although further research is required[6].

5. Investigating Wallerian degeneration in models of traumatic axonal injury

Understanding of biology in model systems is fundamental to developing clinical therapies. In order to explore the role of WD in TAI, and develop potential therapeutic solutions, it is crucial to be able to meaningfully model DAI and depending on the particular aspect of DAI that we wish to interrogate, different models will be required[12,13].

TBI models can be broadly categorized into *in vitro* and *in vivo* models [12,13,277,278]. These can then be stratified based on the organism or cell types, and further classification can be made depending on the injury subtype that the model attempts to recapitulate, for example a blast injury, or a contusion. In order to explore the relationship between TAI and WD our focus is mainly on models that focus on producing an axonal injury, and allow manipulation of aspects of WD.

a. *In vivo* models of traumatic axonal injury

Historical development of mammalian models of traumatic axonal injury

The majority of early DAI modeling was undertaken using *in vivo* systems. Insights into the nature of forces that axons undergo during a high-velocity acceleration deceleration injury began in earnest with Gama in 1835 who recognized the selective vulnerability of axons to brain trauma [279]. He embedded black threads in jelly within glass jars, when these were struck oscillations were seen in the threads and he hypothesized that vibration was the mechanical correlate of the ensuing disease. In the 1940s Holbourn took a theoretical approach and suggested that it was rotatory deformation (as opposed to linear) and resultant shear strains were the primary culprit in DAI[280,281]. The evolution of *in vivo* models began when Pudenz and Sheldon 1946 replaced the skull of monkeys with a transparent lucite calvarium and used a compressed air gun to deliver a calibrated blow to the head. They used cinematographic recordings to observe gliding movements of the brain that lagged behind the skull movements, and began to correlate various forces to changes in brain motion[282]. DAI as we now know it was born with the reports of Sabina Strich who described the clinico-pathological features in a series of five patients with prolonged coma following closed head injury, and features of diffuse degeneration of white matter at post-mortem [23]. The characterization of mechanical properties of neural tissue began in earnest with Ommaya's introductory work in 1968 which characterized mechanical properties of human neural tissue[283]. As understanding

of the pathological correlates of TBI developed, Adams *et al* further defined diagnostic and grading criteria, and used the term DAI for the first time[5,30,284,285]. A series of increasingly sophisticated animal models culminated in the 1990s when Gennarelli *et al* correlated rapid angular-acceleration in various planes to neurological sequela in primates[31,286]. Using at 60° arc and acceleration periods of 11-22msec^{-1} they found that lateral injury (with coronal head acceleration) was most predictive of poor outcome, and reproduced characteristic findings in human DAI including coma, and focal lesions in the rostral brainstem and corpus callosum[31]. Meaney *et al* in 1995 analyzed physical models of the skull-brain complex to estimate the relationship between inertial loading and brain deformation using the miniature-pig[287]. In the period from the early 1980s onwards several rodent models of mild to severe brain injury were developed, including controlled-cortical impact (CCI), fluid percussion (FPI), weight drop, and blast[12,53,277,288-291]. These models have allowed progressive understanding of the input–output nature of the DAI in animals.

Drosophila as a novel model of traumatic brain injury

Drosophila are a powerful and versatile model organism with a rich history in elucidating molecular mechanisms of development and control. They share a large degree of genetic homology with humans and have been used extensively as models of human neurodegenerative disease[292–296]. Key molecular steps in the WD pathways show conservation in *Drosophila*, and indeed key control genes were originally identified in *Drosophila* by forward-genetic screening approaches[7,204,256,297]. A *Drosophila* models offers several advantages, it is an *in vivo* system with a complex well-characterised central nervous system, a range of behavioural assays, readily available genetic manipulation, short generation time, rapid aging effects, low cost, easy *en masse* maintenance, and less ethical issues than mammalian systems. A *Drosophila* model of severe TBI was developed in 2013 by Katzenberger *et al,* this was followed by a second model of mild TBI in 2016 by Barekat *et al* 2016[298–300]. They will be considered further in Chapter 7.

b. *In vitro* models of traumatic axonal injury

In vitro models can be pure neuronal, mixed population, or tissue explant including organotypic. Tissues can be derived from cell lines, animal tissues, or human induced pluripotent stem cells[13,301]. In some cases a specific aspect of the injury may be separated from the whole to explore its effect in isolation, for example stretch or oxygen-glucose deprivation[95,249]. The mechanical inputs can be categorized into 6 main groups. Transection, tissue compression, hydrostatic pressure, fluid shear stress, shear strain, and stretch injury[13,36]. These input categories each attempt to reproduce an aspect of the complex 3 dimensional shear strain, tensile and compressive forces seen in human injury. The severity of modelled insults span the spectrum from mild with no obvious structural change, through to subcellular transection and destruction. When injuries are sufficient to induce cellular death it is relatively simple to demonstrate and quantify the injury. However, in cases where injuries are below the threshold of cellular death then other methods of quantification are required [302]. Deciding on valid input forces for *in vitro* models is challenging. As there is a lack of behavioral readouts, then we are limited to assessing biological/cellular outputs and looking for concordance with that seen in human brain injured tissue. Meaningful *in vitro* modeling requires an understanding of the mechanical properties of neural tissue. This issue was explored earlier in this chapter.

Primary cellular culture models

There are a limited number of *in vitro* neuronal stretch injury models that have been used in the literature, particularly with regards to TAI[13]. In 1995 Ellis *et al* published a model of rapid stretch injury with rat astrocytic culture termed a Cell Injury Controller. The stretch being controlled by a rapid positive pressure of air[303]. An updated device with the same operating principles but with greater control of the membrane deforming pressure-pulse was published by Johnson *et al* in 2008 and called an Advanced Cell Deformation System[304]. Systems often use a deformable membrane onto which cells are cultured before being subjected to a uniaxial or biaxial tensile force. Depending on the cell growth this can produce a constrained (e.g. longitudinal) or unconstrained deformation, and may be varied in terms of rate and magnitude. Arundin *et al* 2003 developed a biaxial stretch injury model based upon vacuum deformation of a silastic membrane using a the Flexercell® strain unit, applied to fetal mouse

hippocampal neurons, or mixed cortical cell cultures[93,98]. Simpler axonal stretch systems utilizing direct stretching by pulses of sterile fluid in neuronal cultures derived from embryonic Hooded Wistar rats have also been described[86,90,96,305]. One of the best characterized *in vitro* axonal injury models was developed in 1999 by Smith *et al* who described the development of stretch device that consisted of an air-pulse generating system that stretched a deformable silicone cell-culture substrate within a closed chamber. The system was initially used to injure an N-Tera2 cl/D1 (NT2) cell line that had been differentiated into a device, and a similar variant was later used to explore the effects of stretch on primary cortical neurons derived from E17-E19 Sprague-Dawley rats[78,79,82,306–309].

Mixed cellular culture models

Various model systems have been developed to stretch mixed cellular cultures including OHSs. These include vacuum based systems and those reliant upon physical indentation of a deformable membrane with a rigid probe. Some of the best characterized include those developed by Geddes *et al* and Morrison *et al*[64,77,310–313]. The Morrison device has also been adapted and used by Di Pietro *et al* [80,92]. One model has explored stretch of axons extending in microchannels between two brain slices placed in opposition in PDMS mini-wells[314]. Another model describes a system of displacement control, rather than force , that can produce high strain rates of up to $90s^{-1}$, and was demonstrated in differentiated NG108-15 cells[315]. Stretch injury has also been explored in a high-throughput manner using silicone-based 6, 24 and 96 well plates and embryonic rat cortices, or human induced pluripotent stem cell-derived neurons (hiPSCNs)[301,316].

Organotypic models have been used to demonstrate that stretch injuries in mixed/organotypic cultures could induce pathophysiological changes in the absence of cell death including altered genomic expression [77,80, 82,92,313]. Three dimensional *in vitro* models and organoids are now beginning to open up new frontiers in brain injury modeling[70,73,317–319].

Summary and important outstanding questions in the field

This chapter has reviewed the scope of TBI/DAI and the range of molecular mechanisms triggered by physical axonal injury. It has considered biomechanical aspects of an injury and how these translate into axonal pathology. The molecular mechanisms of axons degeneration

have been reviewed with particular emphasis of WD, and the links between TAI and WD were considered. Lastly, we have reviewed the range of *in vivo* and *in vitro* models of TAI found in the literature.

As can be seen from this literature review there have been great advances in the understanding of DAI and related processes of axon degeneration in the 60 years since Sabina Strich first described the injury. However, there have been limited therapeutic advances. There have been improvements neuroimaging, surgical care, and in general medical management based upon greater understanding of physiology, such as avoidance of hypoxia, hypotension, or dysglucosaemia, but these have not been matched by corresponding advances in hypothesis driven basic science research. TBI is different to many other diseases insofar that it is not caused by a pathogen or due to a genetic trigger. The fact that it is a heterogeneous physical event make it likely that some aspects of the injury, particularly those of the 'primary brain injury', are beyond modification by traditional biological interventions. Hence, focus is primarily on modification of secondary injury mechanisms.

There are a number of important outstanding questions that remain in the field of DAI and TBI in general (table 4).

- *To what degree is primary or secondary axotomy responsible for dysfunction following TAI?*
- *Why is there progressive white matter volume loss following TAI*
- *How much does Wallerian degeneration contribute to axonal death in TAI*
- *Can genetic or pharmacological manipulation of the WD pathway protect in model systems?*
- *Why do different axons degenerate at different rates?*
- *Do degenerating axons trigger death in adjacent axons? If so, how is this mediated?*
- *Can stabilization of the axonal structure protect the axon from injury or reduce the rate of secondary axotomy?*
- *What is the functional significance of axonal varicosities and can they be repaired?*
- *Does TAI lead to significant axonal transport impairment at varicosities and/or more widely and does this contribute to the development of neurodegenerative disease?*
- *Are histological subtypes of axons seen in injury (e.g. APP positive and negative) of mechanistic or prognostic importance?*
- *How much does microglial phagoptosis and contribute to axonal death in TAI*
- *Is increasing total neuron survival the optimal target to improve outcomes in TAI?*
- *How much do factors other than neuronal death contribute to poor outcomes in TAI?*
- *How much does a failure of function and connectivity at the level of the individual cell or large network contribute to the burden of disability following TAI?*
- *How does TBI contribute to the development of neurodegenerative diseases?*
- *Why do proteins including amyloid b and TDP43 increase following TAI and are these detrimental?*
- *Can aspects of the inflammatory (cytokine/chemokine) response be modulated to alter neuronal survival and patient outcomes?*
- *What is the role of autophagy in TAI?*
- *What is the optimal biomarker for TAI?*

Table 4. Important outstanding questions in TAI research

Adapted from Hill *et al* [6]

This thesis aimed to address some of these questions, as outlined in chapter 1, as a step towards increasing the understanding of the role of WD in TAI, and ultimately the development of new therapeutics for this devastating disease.

Chapter 3

Materials and methods

1. Animals

a. Mice

All animal work was carried out in accordance with the Animals 'Scientific Procedures' Act of 1986 under M. Coleman's Project License number 70/7620. All mice were obtained from pre-existing mouse lines at Babraham Institute unless otherwise stated.

Wild type

All wild-type mice refer to C57BL/6JBabr mice that were originally obtained from Harlan UK (Bicester, UK) and maintained as a separate colony at the Babraham Institute.

Nmnat2^{262gtE}

Mice with a targeted disruption of *Nmnat2* were used (Nmnat2^{gt262}). This was originally achieved using a gene-trap allele (Nmnat2$^{gt(EUCE0262a08)Hmgu}$) via the European Conditional Mouse Mutagenesis Programme (EUCOMM). The mice have a conditional-ready gene-trap cassette placed in intron 1 of one allele of the *Nmnat2* gene[178]. This gene trap silences the affected *Nmnat2* allele and hence heterozygotes have around 50% Nmnat2 expression[178,179].

Nmnat2^{gtBay}

Mice with a *Nmnat2* gene-trap were used (Nmnat2^{gtBay}). This was originally derived from gene-trap ES cell close RRF238 (BayGenomics)[320]. This gene trap demonstrates incomplete silencing with expression of Nmnat2 in the brain[178,320].

Nmnat2$^{262gt/gtBay}$

A compound gene trap combination was produced by crossing Nmnat2^{gt262} and Nmnat2^{gtBay} mice. The resulting mice Nmnat2$^{gt262/gtBay}$ are estimated to have an approximately 75% reduction in Nmnat2 expression in the brain compared to wild-type animals. They were viable at birth with no overt malformations[178].

SARM1$^{-/-}$

SARM1$^{-/-}$ mice were original obtained from Professor M. Freeman (University of Massachusetts Medical School, Massachusetts, USA) with permission from Professor A. Ding (Weill Cornell Medical College, New York, New York, USA).

WLD^{s} (C57BL/6OlaHsd-WLD)

WLD^{s} (C57BL/6OlaHsd-WLD) homozygous mice were originally from Harlan-Olac (Bicester, UK) and were rederived into the biological support unit, Babraham Institute.

CRND8

CRND8 mice (Tg(PRNP-APPSweInd)8Dwst) overexpressing huAPP as a result of two mutations, the Swedish (K670N/M671L) and Indiana (V717F) FAD mutations under a Syrian hamster prion promoter[321]. Mice were maintained as heterozygotes on a 62.5:37.5 sv129:C57BL/6 background. Breeding was exclusively from males and transgenic and WT littermate controls were generated.

b. *Drosophila*

Conditions

Newly enclosed flies were collected daily and separated by sex into vials of 20-35 flies for aging and experimental use. All experiments were conducted on flies aged 1-4 days unless otherwise stated. All flies were maintained at a constant 25°C temperature and humidity, in glass vials with standard agar/cornmeal/yeast feed. Flies were exposed to a 12h light-dark cycle. Feed was changed in all vials once every 14 days or as required. All experiments were conducted on male flies only unless otherwise stated.

Stocks

All flies were obtained from in-house stocks courtesy of Jemeen Sreedharan (University of Cambridge), purchased from Bloomington Stock Centre at Indiana University, or generated by standard *Drosophila* crossing schemes (table 5).

Shorthand	Full genotype
Canton S	;;
W^{1118}	w;;
hiw$^{+/+}$	FRT^{19A};;
hiw$^{\Delta N}$	*hiw$^{\Delta N}$, FRT^{19A}*;; (a gift from M. Freeman, University of Massachusetts)
Pink1^{B9}	*Pink1^{B9}*;; (a gift from A. Whitworth, University of Cambridge from J.Park's original line[322])
Pink1^{B9},hiw$^{\Delta N}$	*Pink1^{B9},hiw$^{\Delta N}$*;;
TH-Gal4	w;UAS-mCD8GFP/CyO;TH-Gal4/TM3 (a gift from F. Hirth, Kings's College London)
Marcm clones	tg80,19A/19A;OK,G,a^{2a}/UAS-mCD8GFP

***Table 5. Drosophila* genotypes**

c. Genotyping

For mice genotyping, DNA was extracted from ear and tail tip biopsies using QuickExtract™ DNA extraction solution (#QE09050, Epicentre Biotechnologies). 20µL QuickExtract™ was added to the tissue biopsies in 1ml falcons and heated at 65°C for 15 minutes. Samples were then vortexed briefly and placed at 98°C for 2 minutes before being used immediately or frozen at -20°C until ready for use. The following was used for each PCR reaction: 1uL DNA sample, 0.5µL forward primer, 0.5µL reverse primer, 10µL redTaq^{R} DNA polymerase (#2523, sigma) and 9µL DNAse free water. Details of the primer sequences and genotyping conditions are listed below (table 6). Samples were run on 2% agarose gel with ethidium bromide before viewing by ultraviolet light.

Gene	Primers 5' to 3'	Denaturing temperature	Annealing temperature	Extension temperature
tgCRND8	Fwd: GCCTTTGAATTGAGTCCATCACG Rev: ACAAACGCCAAGCGCCGTGACT	94°C	60°C	72°C
NMNAT^{262gt}	Fwd(1): GCTGGCCTAG GTGGTGATTTGC Fwd(2): ACTGGGATGCACGAGACCCTGC Rev(1): AGTCATAGACACTAGACAATCG	94°C	60°C	68°C
NMNAT^{Baygt}	Fwd(1): CAGTGCGAGAGACCTCATCCC Fwd(2): TCTTCGATTACGCCAGCTGG	94°C	65°C	65°C

Table 6. Genotyping reaction conditions

2. Cell culture

a. Primary cell culture

Superior cervical ganglion explant

SCG were dissected from decapitated 0-2 day old mouse pups in Leibovitz's L-15 media (#11415064, Gibco) as previously described[134]. Explants were cleaned and plated on 35mm Nunc cell culture dish (#174943, ThermoFisher) pre-coated with poly-L-lysine (25µg/ml, #P8920, Sigma) for 12 hours in an incubator, washed three times in cell culture water (#BE17724Q, Lonza), dried and re-coated with Laminin (20µg/ml, #L2020, Sigma) in a 0.5cm^2 central region for 2-4 hours in an incubator. Explants were allowed to attach for 24 hours in the centre of a shallow culture media (625µl in a 35 mm Nunc culture dish) before the well was flooded up to a total of 2 ml with fresh culture media. 1 ml of media was then exchanged every 2-3 days. Typically 2-3 explants are plated per 35mm dish. Unless specified all experiments with SCGe were conducted at 5-7 days *in vitro* (DIV).

Dissociated superior cervical ganglion cells

Dissected SCG from 0-2 day old mouse pups (as described for SCGe) were plated in 0.025% trypsin in phosphate buffered saline (PBS) without $CaCl_2$ and $MgCl_2$ (#59427C, Sigma) at 37°C for 10 minutes. They were then removed and placed in 0.2% type II collagenase (#17101015, Gibco) in PBS and incubated for a further 10 minutes. The SCGs were then transferred into 1.5 ml SCG culture medium, gently triturated using a 1 ml pipette, transferred to a 35 mm Nunc cell culture dish (#174943, ThermoFisher) and incubated for 2 hours as a pre-plating step. The medium containing the neurons was aspirated from the 35 mm dish and spun for 5 minutes at 1,000 rpm. The excess supernatant was discarded. 30 µl media for every dish required was added to the pellet to gently re-suspended it. The dissociated neurons in media were then plated in a 0.5 cm^2 area in the centre of a prepared ibidi µ-dish (Thistle Scientific) at a density of 10,000 cells/cm^2. Once the dSCGs were plated they were allowed to incubate for 2-3 hours, then a further 1 ml of primary neuronal cell culture medium was gently added. Medium was changed the next day and every 2-3 days after that. Unless specified all experiments with dSCGs were conducted at 5-7 DIV.

Dissociated primary neuronal culture

Cortices were dissected from decapitated E16-17 mouse embryos in L-15 medium (#11415064, Gibco). They were cleaned of all meninges and placed in 0.25% trypsin (#59427C, Sigma) for 10 minutes with x3 inversions every 3 minutes. The cortices were washed x3 in PNCd culture media. The trypsinised tissue was then removed and bathed in 0.2 mg/ml DNAse solution (#04716728001, Roche) for 2 minutes before again washing x3 times and re-suspension in culture media. The solution was vortexed x3 times for 3 seconds each time to dissociate the cells. The suspension was gently passed through a 40 µm filter and the resulting solution diluted in culture media to a concentration of 300,000 cells/ml as measured using a haemocytometer. Cell viability of >95% as assessed with trypan blue (#T8154, Sigma) was accepted as sufficient. The cell suspension was plated on pre-prepared steel well (preparation described below). Medium was changed the next day and every 2-3 days after that. Unless specified all experiments in PCNCs were conducted at 10-14 DIV.

b. Organotypic hippocampal slice culture

Whole brains from 6-8 day old mouse pups were harvested after cervical dislocation and decapitation, and placed in ice-cold slice OHS dissection media. The cerebellum was removed with a sterile scalpel and the brain divided with a single midline sagittal cut into its two hemispheres. The hemispheres are then glued (Loctite superglue liquid) onto a horizontal vibratome stage (Leica VT10000S) with the temporal surface facing superiorly. The stage and hemispheres are then submersed in ice-cold OHS dissection media and 350µm thick parasagittal slices are taken until the hippocampus is visible. Hippocampi and associated entorhinal cortex are then separated from surrounding brain slices using sterile dissection and transferred using a wide ended sterile pipette to a 50ml falcon tube containing ice-cold OHS dissection media. Once 8-10 slices from each pup are collected, they are plated for long-term culture. Depending on the culture system used the OHS are plated onto either using the 'interface method' with sterile porous 0.4 µm membrane inserts (#PICM0RG50, Merck) sitting in pre-warmed 1ml culture medium in Nunc 6 well plates, *or* they are plated onto the centre of a silicone sheet fitted within a custom steel well. The silicone is pretreated with poly-L-lysine (25µg/ml, #P8920, Sigma) and laminin (80µg/ml, #L2020, Sigma). After plating the OHS they were incubated for 4 hours to promote adherence before coating in Geltrek extracellular

matrix (#A1413202, ThermoFisher) and incubating for a further 1 hour. After this the well were filled with culture media until the slice was just covered by a think meniscus of fluid. OHS were maintained in an incubator at with media changed every 2-3 days. In the case of the steel & silicone wells the cultures are 'rocked' in an incubator at a rate of 1 cycle/50 seconds throughout their lifespan in order to ensure adequate oxygenation. Unless specified all experiments with OHSs were conducted at 14 DIV. This protocol was adapted from the interface method described by De Simoni and Gogolla[323,324].

c. Cell culture media and conditions

The constituents of cell culture media used are summarized below (table 7).

Medium	Volume as used	Stock concentration	Company
SCGd/SCGe			
DMEM -Glucose: 4500 mg/l -Sodium pyruvate: 110 mg/l	44ml	Neat	Sigma
GlutaMAX	500µl	200mM (100x)	ThermoFisher
Aphidicolin (50µL for first media application only)	25µl	4µg/ml	Calbiochem
7s NGF	50µl	100ng/ml	ThermoFisher
FBS (filtered)	5ml	Neat	ThermoFisher
Penicillin-streptomycin	500µl	10,000U/ml	ThermoFisher
PNCd			
Neurobasal	48ml	Neat	ThermoFisher
B-27	1ml	20ml/l (2%)	ThermoFisher
GlutaMAX	500µl	200mM (100x)	ThermoFisher
Penicillin-streptomycin	500µl	10,000U/ml	ThermoFisher
OHS			
MEM with glutamax-1	25ml	Neat	ThermoFisher
EBSS Magnesium and phenol red free	9ml	Neat	ThermoFisher
EBSS and D-glucose 32.5 g D-glucose in 250 ml EBSS All passed through 0.22µm filter	2.5ml	1M	Sigma
New Zealand Horse serum Filtered and heat inactivated	12.5 ml	Neat	ThermoFisher
Nystatin	30µl	10,000U/ml	ThermoFisher
Penicillin-streptomycin	500µl	10,000U/ml	ThermoFisher
OHS dissection media			
EBSS Magnesium and phenol red free	487.5ml	Neat	ThermoFisher
HEPES and EBSS -71.49g HEPES in 300ml EBSS All passed through 0.22µm filter	12.5 ml (≥99.5%)	1M	ThermoFisher
Imaging medium			
FluoroBrite DMEM media	As required	Neat	Gibco

Table 7. Summary of media preparations for cell culture

SCGd, SCGe, and PCNd media had 100% change 24 hours after plating and then every 3 days. OHS media had 100% media change 6 hours after plating and then a 50% change every 7 days. Unless specified all cultures were kept in standard laboratory incubators maintained at a constant 37°C with 5% CO_2.

d. Stretch culture well preparation

Culture wells with silicone bases are prepared as follows. Custom stainless-steel milled wells were obtained from Professor Douglas Smith (University of Pennsylvania). The metal wells and were soaked in acetone (≥99.5%) for 2 hours, washed in cell culture water (#BE17724Q, Lonza), bathed in 70% ethanol for a further hour then washed three times for 2 minutes in cell culture water (#BE17724Q, Lonza), before drying in a sterile tissue culture hood. The silicone sheeting (40D, 125µM, gloss, Speciality Manufacturing Inc, Michigan) was applied to the base and held in place with a 50mm silicone 'O' ring. The silicone sheet was then biaxially tensioned to a set threshold using a 40mm ink stamp marker, thus pre-tensioning the sheet to a 20% strain. The prepared well was then placed in a glass petri dish (100 mm x 20 mm, Corning) autoclaved at 134°C for 60 minutes. A polydimethylsiloxane (PDMS) inner ring was prepared from Sylgard 184 (Dow Corning) and cut using 6 mm and 8 mm punches. This was cleaned and sterilized along with the micropatterned stamps by boiling in cell culture water (#BE17724Q, Lonza), at 70°C for 30 minutes whilst constantly stirring, soaking in 70% ethanol for 1 hour, drying in a sterile hood, bathing in sodium hydroxide (1N) and then washing x6 with cell culture water (#BE17724Q, Lonza). The PDMS ring with or without the micropatterned stamp were then applied to the completed well before application of PLL (#4707, Sigma) and laminin (#L2020, Sigma).

3. Injury models

a. Transection

Transection injury of SCGes was undertaken by a single linear incision made 2mm from the cell mass with a #10 stainless steel scalpel blade(#0301, Swann-Morton). All incisions were checked under phase-contrast microscopy to ensure neurite cuts were complete.

b. Stretch injury model

Unless otherwise stated all stretch injuries on primary neuronal cultures were conducted with a driving pressure of 60 psi, with the piston set to achieve a vertical deflection of 6mm, equivalent to a strain of ~20% at a strain rate of $7.5s^{-1}$.

c. *Drosophila* assays

High impact trauma

All HIT injuries were standardized. They were performed at 9-12am in standardized light and temperature conditions. Flies were transferred without anaesthesia to a fresh polystyrene vial. This was attached to the HIT device (figure 7), the spring recoiled to the predefined angle of initial deflection, and then released to cause a single HIT. All flies were given 10 minutes to recover before transfer back to a vial with food for ongoing experimentation.

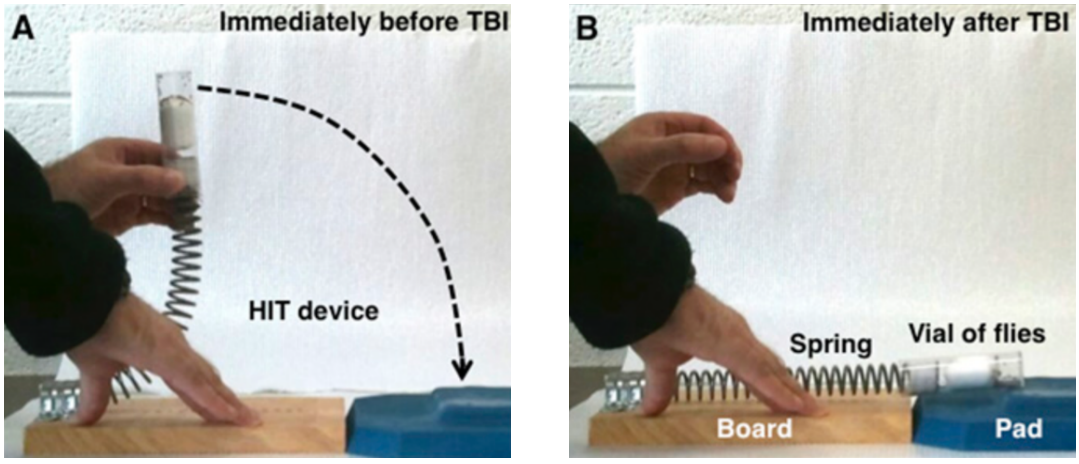

Figure 7. Drosophila high impact trauma device

The *Drosophila* high impact trauma device consists of a vial of *Drosophila* within a polystyrene vial attached to a loaded spring. Upon release this causes a rapid acceleration-deceleration injury with impact. (A) Before TBI. (B) after TBI. *Image from Katzenberger et al*[298].

Incapacitation

Incapacitation rates were recorded by assessing the percentage of flies that failed to show signs of purposeful movement within 20 seconds of HIT.

Early death rate and long-term survival assay

24 hours after HIT the percentage death was recorded. Remaining live flies were transferred to new vials and long-term survival was monitored. A daily count of number of fly deaths was conducted in all vials for the lifetime of all flies. Dead flies were discarded every day. Deaths within the first 24 hours following injury were excluded from the long-term survival analysis.

Rapid iterative negative geotaxis (climbing) assay

A custom made RING device was manufactured and used to measure negative geotaxis/climbing ability as a behavioural measure of motor function (figure 8)[325,326].

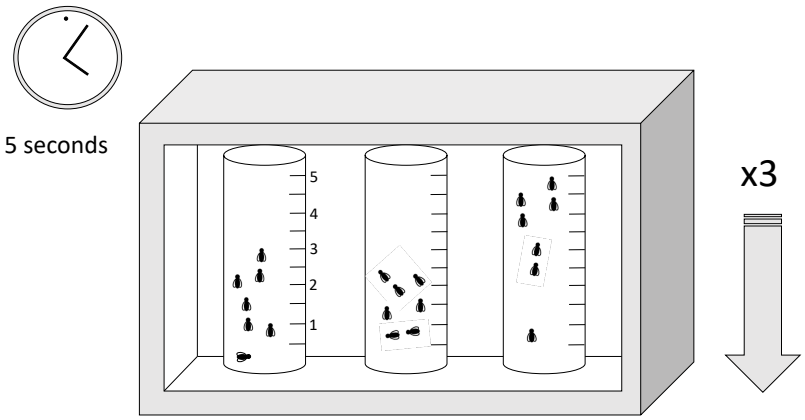

Figure 8. Rapid iterative negative geotaxis (climbing) assay

The rapid iterative negative geotaxis (RING) device measures the climbing ability of flies as a surrogate marker of behavior. It is dependent upon the functioning of multiple systems including central and peripheral nervous system, and the neuromuscular system. In order to perform the assay flies are transferred to food-free fresh polystyrene vials without anesthesia. After a 5 minute adjustment period the device is tapped gently to settle flies at the bottom of the vials. After a 5 second interval a photograph is taken to record the height climbed by flies. The average height climbed is recorded. This is repeated three times at 60 second intervals and the result is averaged.

Flies were gently transferred to fresh empty polystyrene vials without anaesthesia with a maximum density of 25 flies per vial. Groups of up to 6 vials were inserted into the RING device, and after 5 minutes for the flies to adjust to the environmental change the device was

tapped three times to settle flies to the bottom of the vials. Exactly 5 seconds after the last tap a picture was taken to assess the height climbed. The head of the animal was the reference point for the climbing height achieved. Maximum height achieved was graded into 5mm intervals, flies that climbed less than 5mm were scored zero, and any fly that exceeded 50mm was awarded the maximum score was 5cm. The average height achieved for the vial was calculated. This was repeated 3 times at 60 second intervals and an average score given for that vial. The reduction in climbing ability was calculated on a vial by vial basis by subtracting the baseline height climbed preinjury from the final height climbed at 45 days.

Flight assay

Flies were anaesthetised on ice for exactly 5 minutes then the flat of a 30G 1" needle (#Z192368, Sigma) was attached to the anterior notum of a fly just posterior to the neck using clear nail varnish, leaving flight muscles unimpeded. Flies were given 15 minutes to fully recover. Needles were fixed in place under a video microscope. If required then a gentle mouth-blown puff of air was used to stimulate flight and the flying time was recorded for 30 seconds per fly for analysis. This was repeated 3 times per fly and the average of time spent in flight was calculated for each condition. All RING and flight assays were conducted at the same time of day in a quiet room with standardized light and environmental conditions.

Intestinal barrier dysfunction

To evaluate intestinal barrier dysfunction following HIT flies were transferred to feed containing dissolved Brilliant Blue FCF dye (#80717, Sigma). After 24 hours the percentage of flies that had blue food dye dispersed outside of the abdominal cavity and proboscis were counted.

Fertility

To test for male fertility, four newly eclosed male flies of the genotype of interest were placed with four newly hatched wild type (w^{1118}) female flies. Males were scored as sterile if the females failed to produce any larval progeny by 10 days. Each fertility trial was repeated a minimum of 3 times.

4. Imaging based methods

a. DiI staining

The lipophilic membrane dye DiI (1,1'-dioctadecyl-3,3,3',3'-tetramethylindocarbocyanine perchlorate, #D282, ThermoFisher) was used to assess membrane integrity. Cells were fixed with 4% PFA, washed, and stored in PBS. A small crystal of DiI was embedded in the explant cell mass, taking care to ensure that there were no free crystals in solution. The cells were stored at 4% for 2 weeks to allow the dye to diffuse the full length of the explant. DiI staining was then assessed by epi-fluorescent microscopy at x20 magnification.

b. Hematoxylin and eosin

Anaesthetised flies were submerged in cold 1x PBS, the proboscis and rostral trachea were removed, and the amputated heads gently rocked in fresh ice cold 4% paraformaldehyde solution for 45 minutes. The tissue was alcohol dehydrated, xylene washed, and embedded in paraffin for serial sectioning with a microtome (Leica RM2235) at a thickness 7µM. Sections were mounted on poly-L-lysine coated slides (#P0245, Sigma). Wax was removed with a xylene bath then alcohol washes before haematoxylin and eosin staining, and application of coverslips. After blinding, three representative coronal sections were examined from a central brain region that included the medulla using brightfield microscopy. The average number of ≥5µM vacuoles per slice in each brain was calculated.

c. Immunohistochemistry

Mice – Organotypic hippocampal slices

OHS membranes were fixed in 4% paraformaldehyde in 0.1M PBS and washed three times in tris-buffered saline (TBS) then blocked in TBS with 0.5% Triton X-100 and 3% goat serum. The membranes were incubated in 200uL of primary antibody in blocking solution at 4°C. After three TBS washes they were incubated for a further 2 hours at room temperature in the dark with secondary antibody 1:250 (Alexafluor488, Thermofisher). Images were captured. Confocal images were acquired on a Leica microscopy system. Primary antibodies used were APP 1:500 (ab2072), Abcam and BIII tubulin/TUJ1 1:1000 (#18207, Abcam).

Drosophila

Fly brains were dissected in cold 1x PBS, and fixed in 4% paraformaldehyde-PBS for 30 minutes. Samples were washed in 1x PBS with 0.3% Triton X-100 (#T8787, Sigma) and blocked for 1 hour at room temperature in 1x PBS with 0.3% Trition X-100 and 1% BSA (#9647, Sigma). Brains were incubated in primary antibody diluted with blocking solution for 72 hours. After washing and incubating in a fluorescent secondary antibody solution for 4 hours, samples were washed and mounted between two coverslips in ProLong diamond antifade mountant (#P36965, ThermoFisher). Confocal images were acquired on a Leica microscopy system, at z-stack intervals not greater than 0.6µM and blinded for analysis. Primary antibodies used were mouse Tyrosine-Hydroxylase (anti-TH) antibody 1:100 (TH-antibody, #22941, Immunostar Inc.) for the PPL1 cluster, and rabbit anti-cleaved DCP-1 1:200 (#9578, Cell Signalling Technology) for apoptosis. Secondary antibodies were goat anti-mouse IgG (H+L) Alexa Fluor 488 (#A11034, ThermoFisher), and donkey anti-rabbit IgG (H+L) Alexa Fluor 594 (##21207).

d. Neurite degeneration index

The NDI is an established quantitative measure of neurite degeneration[174]. Images of the same (or near same) field of neurites are obtained at different time points or treatment conditions at x20 magnification. The imaged field is typically at a point around 3mm from the explant mass where the density of the neurites allows visualization of morphological change. The NDI is calculated by ImageJ plugin algorithm that is operator independent. The output is a number from 0 to 1 based upon the degree of neurite continuity or fragmentation. Most healthy neurites score around 0.2-0.3 while a profoundly degenerated field would be in the range of 0.6-0.9. In the case of complete degeneration or pathological fragmentation to the point of detachment a score of 1 is assigned.

e. Axonal transport

Axonal transport was measured as per methods described by Hung *et al*[255]. In brief, SCGe cultures were incubated with MitoTracker™ Green to label mitochondria (#M7514, ThermoFisher) for 1 hour prior to imaging with a Andor wide-field/TIRF imaging system (Nikon Ti-E microscope with 100x1.49 TIRF objective). Time-lapse images were captured from a 10 seconds with a 250ms time lapse interval. Temperature was kept constant at 37° throughout. Analysis of particle velocity was calculated using Image J plugin.

5. Non-imaging based methods

a. ELISA

Quantification of protein levels including $A\beta_{1-40}$, $A\beta_{1-42}$, and NFL were carried out using commercially available ELISA kits ($A\beta_{1-40}$ #KMB3481, Invitrogen; $A\beta_{1-42}$ #3442, Invitrogen; NFH #NS170, Merck). The NFL elisa kit was a gift from Andreas Jeromin developed by Quanterix™, and it is not commercial available. ELISAs were used as per manufacturer's instructions. Briefly, samples were diluted in standard diluent buffer and with detection antibody and incubated at room temperature, allowing simultaneous binding to capture antibody on the well and binding of the detection antibody to the protein in the sample. After washing the wells thoroughly, the wells are incubated with HRP-conjugated anti-rabbit IgG at room temperature. After a final wash, the wells are incubated with stabilized chromogen in the dark. The depth of the colour produced directly corresponds to the concentration of target protein in the original sample. After adding a stop solution to prevent the reaction developing further, colour intensity is read using a PHERAstar FS plate reader and standardized against a chromogen blank and a standard curve to yield an accurate concentration readout.

b. Western blotting

Whole *Drosophila* were rapidly frozen using either liquid nitrogen or dry-ice, and placed in a 1ml falcon tube. They were then vortexed for 30 seconds which produced spontaneous separation of the drosophila heads from the bodies. The heads were separated from other body parts on a plastic tray, while continually kept frozen on dry-ice. Heads were retained and bodies discarded. Each sample consisted of 10 pooled heads. The heads were homogenized in 5µL per head of x2 Laemmli lysis buffer (#161-0737, BioRad), centrifuged for 2 minutes at 13,000rpm, and supernatant transferred to a fresh falcon tube. This was done 3 times. The sample was then heated to 100˚C for 5 minutes twice, with a short vortex in-between, and placed on ice. Samples were diluted in Laemmli buffer as required and loaded into 4-20% mini protean TGX precast gels along with a ladder (#4561083, BioRad). The gel was run in Tis/Glycine/SHS gel running buffer at 190v, 400mA until the protein samples were appropriately separated. The protein transfer was undertaken to a Immobilon-P membrane (#IPVH00005, Millipore) at 100v and 400mA in transfer buffer using the Bio-Rad Mini-Protean III wet transfer system. The membrane was blocked for 60 minutes at room temperature in

1xPBS-T with 5% BSA (#A1933, Sigma) on a rocker. The membrane was subsequently incubated in primary antibody overnight in a 4˚C cold room. The membrane was washed 3 times in 1xPBS-T then incubated in the dark with secondary antibody in a 5% BSA blocking solution. Three further 5 minute PBS-T washes were undertaken followed by a final 5 minute PBS wash. In preparation for imaging, the membrane was placed on a Sarogold foil (#9068.1, Carl Roth) and saturated in Supersignal West Dura Extended Duration Chemoluminescent Substrate (#34075, ThermoFisher). Imaging was undertaken with an Alliance Chroma 9.7 chemoluminescence imaging system with Alliance Unitex software. Samples were individually checked for adequate exposure without saturation. Image analysis was undertaken with Image J software (v1.51n)

Primary antibodies				
Antigen	Concentration	Species	Property	Supplier(#)
Bruchpilot (Dmel/BRP, nc82)	1:1000	Mouse	Monoclonal	DSHB
Actin	1:5000	Mouse	Monoclonal	Covance (MMS-435P-250)
Fascicilin II (34B3)	1:3000	Mouse	Monoclonal	DSHB
Highwire (6H4)	1:1000	Mouse	Monoclonal	DSHB
Secondary antibodies				
Antigen	Concentration	Species	Property	Supplier
Mouse IgG	1:3000	Goat	HPE-conjugated	Bio-Rad (# 172-1011)

Table 8. Antibodies for immunoblotting

c. NAD/NADH bioluminescence assay

Levels of NAD were measured using the NAD/NADH-Glo™ assay (#G9071, Promega). The assay was performed according to the manufacturer's protocol. The assay contains a cycling reductase enzyme that reduces a proluciferin reductase substrate to luciferin in the presence of NADH. Luminescence signals were measured by PHERAstar plate reader.

d. High performance liquid chromatography

Flies were rapidly frozen in liquid nitrogen, heads separated, and stored at -80°C until processed by high performance liquid chromatography (HPLC) measuring levels of NMN and NAD. In brief, nucleotides were extracted via sonication in HClO4 with cAMP as an internal standard. Analysis was then by ion pair C18-HPLC and spectroluorometric analysis post acetophenone derivatization. Levels of nucleotides were corrected with spike recovery, and corrected to total protein levels.

e. Flow cytometry

Five fly brains were dissected in cold 1xPBS solution and transferred to dissection media containing 7.5mls of DMEM (high glucose, HEPES, phenol-red free, #21063029, ThermoFisher), 2.5mls of 10x trypsin (#15400054, ThermoFisher), and 1% BSA (#9647, Sigma). Brains were washed in trypsin free dissection media, gently triturated using a 200µL pipette 30 times, then filtered through a 70µm strainer. The resulting solution was mixed in a 1:1 ratio with Annexin V & dead cell solution (Annexin V & 7-AAD, #MCH100105, Merck), incubated at room temperature for 20 minutes, then processed on the Muse Cell Analyser (Merck) using inbuilt analysis software. Dilutions in trypsin free dissection media we made as required. For positive controls brains were incubated in 200mM of Actinomycin D (#A1410, Sigma) at 37°C for 6 hours before processing. Gating was kept constant for all experiments.

Chapter 4

Development of an *in vitro* model of traumatic axonal injury and investigation of the contribution of WD mechanisms to stretch induced axon degeneration

Introduction

1. The requirement to develop a traumatic axonal injury model

The response of axons to traumatic injuries, in particular DAI, is incompletely characterized. How, when, and why axons die remain open fields of enquiry. In order to investigate TAI, and in particular TAI associated mechanotransmission, that is the study of how cells respond biochemically to a mechanical load, a model system was required[66]. There was a lack of established TBI model systems at the University of Cambridge at the time of writing this thesis, with no *in vivo* or *in vitro* models in use. TAI models are not widely available for purchase with most systems being developed by individual groups as required. Therefore, in order to begin answering questions relating to WD in TAI it was incumbent upon us to develop a model in order to answer the aims of this thesis.

2. Choosing a model of DAI

Modeling of DAI is generally undertaken with the aims of reproducing a characteristic injury in a non-human system in order to explore and better understand mechanical and biological aspects of trauma. Thus, the question arises "what is the best DAI model system?". When this question is probed it becomes evident that there is no ideal model system. The 'best' model depends upon the question that is being asked and the ability of that system to answer the question. Different questions require different systems in order to solve them[12]. However, for practical purposes it is useful to have well-characterized models that allow replication of results, and comparison and integration of research finding. This is necessary to allow the field to share information and progress without the need for constant repetition, and to avoid unnecessary re-invention. Regardless of the question posed, the model system will ideally accurately model at least some aspects of the human condition, otherwise inferences based on the results derived from the system risk being erroneous or lacking any external validity. Comprehensive modeling of brain injuries including DAI is challenging, in part due to the heterogeneity and complexity of the disease, and also because of difficulty in accurately recapitulating mechanical forces on a cellular and small animal scale[327]. Likewise, associated local and systemic responses including raised intracranial pressure, reduced cerebral perfusion, hypoxia, caemia, coagulopathy, inflammation and sepsis may all influence outcome and fail to be captured by a model system[328,329]. Additionally, polytrauma and organ

dysfunction may modulate the brain's response to injury adding further challenges in accurately reproducing an injury[330].

3. Models available for use during this research

To my knowledge, at the time of preparing this thesis there was no *in vitro* stretch or TAI models in use at the University of Cambridge. Perhaps the closest to an in vitro TAI system in use was an axon transection model. This model had been extensively used by the Coleman group in order to examine inter alia modifiers of neurite degeneration, particularly in relation to WD[134]. A version of the Smith stretch device described by Tang-Schomer *et al* had previously been brought to Cambridge but the experimental use of the system had been limited[78,79]. The 'Smith device' consists of a sealed chamber with a gas inlet to increase pressure. There is a 1mm slit in the base of the chamber that a culture membrane can prolapsed out of when pressure increases, hence causing a uniaxial stretch of any attached cells. When I initially attempted to use this device there were a some outstanding issues including a lack of functional driver software and the required gas regulator connection. These issues were resolved during this thesis and the system was prepared for use. After some initial trials of the device I felt that development of a new system would be required in order to answer the experimental questions posed in this thesis. Most notably, I did not feel that the Smith device was not suitable for OHS use. The system can only produce a uni-axial strain along a narrow corridor of tissue, this would limit the degree of stretch in an OHS and create a hetrogenous injury. In a human DAI it is unlikely that axonal stretch would affect a small focal segment of the axon with the rest being uninjured. Therefore, while useful for investigating a focal segment of injury- I felt it was less suitable to represent a more generalized cellular axonal stretch. Stretch produced with this device was also dependent upon increasing the pressure within a closed system that contains cultured cells of interest. Raised pressure has been implicated as a cause of injury in cellular cultures and was therefore a potential confounder in any experiments[331,332]. For these reasons it was felt necessary to design new model system.

4. Design of a new model system

In order to accurately model a human DAI, or a sub-component of it, there are a series of steps that must be navigated. Firstly, we must choose the biological tissue we wish to study, be it *in vivo* whole organisms or some derivative in the form of an *in vitro* system. Secondly, we must understand the biomechanical forces that the brain undergoes in a real-life injury. Thirdly, we must decide which forces we wish to replicate, and how we are going to induce this mechanical input. This will determine both the injury type, and also the degree and uniformity of this injury. Finally, these steps must be brought together into a reliable, functional model system.

In vivo or in vitro system

The choice of *in vitro* or *in vivo* system depends primarily upon the experimental question or hypothesis that is being asked. Each system has relative benefits and drawbacks. When deciding upon a model system, researchers face an inherent conflict between high-fidelity and reductionist approaches[12,333]. In high-fidelity models, such as a large animal TBI and polytrauma, the model may closely resemble the human condition, hence providing the opportunity to study a model that is a highly relevant reproduction. However, the nature of such a complex model makes control of confounders difficult. It also suffers the challenges of expense and difficulty achieving high numbers to establish reproducibility of results[53]. Conversely, a reductionist model, such as a primary neuronal culture transection model, allows simplification and isolation of specific aspects of the injury. Injury and analysis of single cells, or sub-regions of cells are even possible. The reductionist models make control of a greater range of confounders possible, and open the possibility of multiple repeats and improved reproducibility[13]. These two extremes of TBI models highlight some inherent conflicts that affect all model systems.

During the first stage of this thesis it was decided to pursue development of an *in vitro* system. There were several reasons for this. As our primary objective was to develop tools to elucidate WD responses to TAI, a simplified system would reduce confounding variables and allow a direct analysis of the response of axons to injury in live cultures. Generally speaking, *in vitro* models are favoured for elucidation of molecular mechanisms and preliminary work to

establish the effects of pathways modification in disease processes. Furthermore, the development of an *in vivo* system, particularly a mammalian one, has logistic challenges and requires greater time and investment to setup.

Numerous *in vitro* model systems have been developed to explore TAI. These were outlined in Chapter 2. In terms of the tissue types examined these can be broadly divided into pure neuronal cultures and mixed cultures. Both have differing benefits and drawbacks.
In order to allow multiple questions to be interrogated in relation to WD pathways in TBI it was decided to develop a system that allowed injury and interrogation of both pure neuronal cultures and glial or mixed cultures, but with the focus initially on pure cultures.

Biomechanical forces involved in human injury and reproduction *in vitro*

Characteristic forces involved in a DAI of the brain, and how these forces translate to *in vitro* model system, have been explored in Chapter 2. Given the knowledge gaps and assumptions implicit in translating a mechanical force from a human DAI to a cellular culture it might be questioned whether any model system can currently replicate the human brain injury with any high-degree of fidelity. A more modest goal is to model a mechanical input that constitutes one or more aspects of human injury, for example – use a comparable force, or acceleration/deceleration rate, or in the case of cellular injury use a realistic degree of deformation. Then mechanical responses, and/or biological responses to the force input can be interrogated[36]. In keeping with the majority of previous *in vitro* TAI models we focused on the reproduction of was a stretch type injury with injury forces approximating those derived from human injury data. The high velocity mechanisms that typically produce DAI constitute the rapid application of high tensile strain. An elongating stretch of at least 10% that occurs in 100ms or less was previously capable of resulting in a degree of axonal injury, therefore this was an initial goal, with modification to be undertaken based upon the injury responses seen in cellular culture[80,334].

The ideal *in vitro* stretch system

An idealized system capable of interrogating WD mechanisms following a TAI would have a number of attributes as outlined below(table 9).

Mechanics	

	Adjustable degree of stretch, for example range of Langragian strain 0.1 to 0.5
	Adjustable and quantifiable rate of stretch 10-50s^{-1}
	Adjustable and quantifiable rate of elastic recoil (relaxation)
	Uniaxial or biaxial stretch of whole field or various portions
Injury	
	Allow multiple concurrent or sequential injuries
	Avoid a direct pressure pulse on tissue
	Ability to isolate axon from cell body
	If possible, the chamber that the culture-well sit on, or within, should allow a flow of gas (e.g. xenon) constantly through it. This would allow the cells to experience an altered gaseous microenvironment
Imaging	
	Capable of live cell imaging around the time of injury
	Ability to image on a microscope stage during an injury or immediately before/after injury
	Culture wells not >120x85mm width so can fit on microscope stage
	If imaged from below (inverted objective) then require culture membrane that is optically transparent
Reliability	
	Inflict a reproducible stretch injury
	Ability to maintain static pressure would allow calibration of pressure to membrane stretch. This would not be required if there was an alternative way of determining stretch such as high-speed video
	A feedback measure or a deformation sensor in the pressure chamber to confirm the pressure delivered. This can then be used with prior calibration data to determine degree of stretch
Culture	
	Allow long-term cellular culture with safe incubation of culture wells following injury
	System adaptable to multiple cellular culture types (primary neuronal, organotypic etc)
	Removable culture wells so they can be put in incubator
	Multiple culture wells so that they can be kept in incubator with different experimental conditions at the same/overlapping times
	Culture wells must be watertight to media and not made of anything toxic to cells - this includes the well material and also any O-rings
	Membrane would ideally allow good gas exchange without fluid leakage, the requirement for gas exchange depends on the cell type used
	Culture wells allow imaging with a microscope objective from either above or below
Practicalities	
	If stretch is produced by pressurized gas then it should ideally be able to connect to standard cylinders of medical air
	Simple fixation device for removing culture wells to minimize time outside of the incubator
	Well should be manufactured from non-corrosive material and easily cleaned so can be used/reused in humid and warm incubator environment
	The depth of each culture well (containing media) should be around 8-10mm
	Electrically and mechanically safe
	Affordability
	Reproducibility or commercialization potential

Table 9. Features of an idealized system for interrogating Wallerian degeneration mechanisms following a traumatic axonal injury like process

As there are no suitable or well-characterized commercial *in vitro* injury model system available for purchase, and there was no such system in use in Cambridge, it was necessary to design and build a model system for use. The preceding information formed the template for model development.

The design, fabrication and testing of a new stretch device in Cambridge is described in the results section of this chapter. This was preceded by useful discussion with Professor Belli's group in Birmingham, who had past experience of similar approaches to modelling stretch injury.

5. The role of WD in an *in vitro* stretch

There are several approaches that can be taken in order to reveal whether WD is an active process in stretch injury. Elements of the WD pathway that function as WD specific promoting or restricting agents can be modified using genetic or pharmacological approaches. This approach can reveal if axon degeneration following stretch is WD dependent, and if it can be modified.

The key molecular players in WD are considered in detail in chapter 2. In brief, transgenic knockout of SARM1 has been shown to strongly protect against WD in a number of model systems[204,210]. Likewise, WLD^{s} expression has a profound WD inhibiting effect[7]. The compound FK866 is known to delay WD for up to 4 days after its administration by non-competitively inhibiting NAMPT and thus preventing NMN accumulation which seems to be central in initiation of WD[174]. A direct genetic modulation of NMNAT expression levels has been used to create and investigate the effects of 'WD-vulnerable' neuronal cultures[161,178,179].

A further compound, P7C3-A20 has an opposing activity to FK866 and has been investigated as a small-molecular activator of NAMPT[335,336]. It has been suggested that this has neuroprotective effects mediated through increasing NAD via the NAD synthetic pathway[337]. The apparent contradiction between a NAMPT activator and inhibitor both being neuroprotective is yet to be resolved.

If we knockout a WD obligatory gene or molecule before stretch injury, or pharmacologically inhibit a necessary step in the WD pathway, then we may be able to determine if axon degeneration following stretch is WD dependent or not. Similarly, by creating pro-WD conditions, be they genetic or pharmacological, we would expect an increased vulnerability to stretch if it is mediated by a WD process. Answering these questions will help establish whether WD is a suitable target for therapy in stretch injuries.

Aims

In order to investigate the biological effects of a TAI and elucidate mechanisms of secondary injury that may be potential therapeutic targets a model system is required. WD is an important regulator of axon degeneration. Our laboratory has extensively probed this mechanism with a superior ganglion cell culture system based on transection and exogenous triggers of WD. However, we lacked the availability of an existing TAI model and therefore the initial stages of this thesis were based around generation of this model.

Specifically, the aims of this chapter were to:

- Design and manufacture a device capable of inducing a modifiable, and quantifiable stretch injury to primary cultures
- Demonstrate that the device can generate features of DAI pathology
- Conduct mechanical and cellular calibration to ensure the device produces a consistent injury of the scale required to induce secondary injury mechanisms in the neurite compartment
- Explore the effects of WD promoting and inhibiting conditions on stretched axons to determine if stretch injury is a WD dependent process, and if it can be rescued *in vitro*

Results

1. Design and manufacture of the injury device

In collaboration with Dr Ari Ercole (Department of Anaesthesia, University of Cambridge), we designed and built a cellular stretch injury device. This device aimed to fulfil as many of the criteria described in the chapter introduction as practically possible while balancing pragmatic factors such as availability of components and avoidance of an unduly complex system (figure 9).

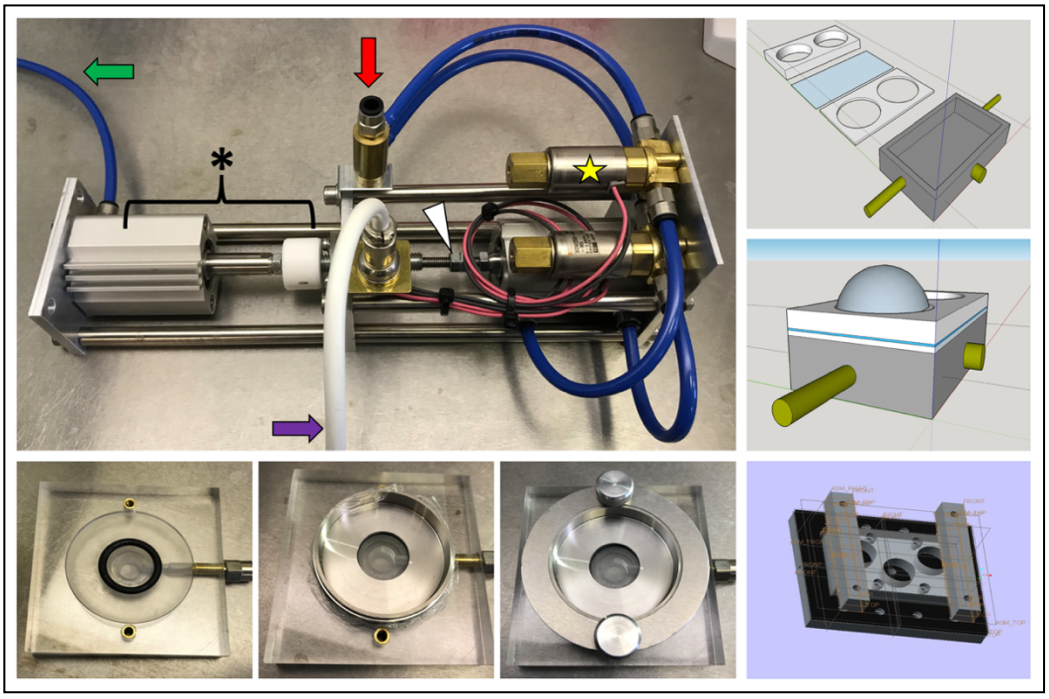

Figure 9. Cellular stretch device injury device

The device produced consists of three main components; a pressure control system composing of solenoid valves (yellow star) with an adjustable pneumatically driven piston and air containment chamber (asterisk), an electronic trigger system (not shown), and a platform for various removable culture wells. Compressed medical air flowed into the system (red arrow), via electronically controlled solenoid valves (yellow star), to drive a piston forward forcing air out of the air containment chamber (asterisk), and out to the platform via an outflow pipe (green arrow). The degree of piston movement, and hence degree of final deformation, was controlled by an adjustable hex-nut block on the piston (white arrowhead). Culture wells, once placed on the platform, could be fixed in place with a screw lock ring before exposure to a stretch injury. Previous iterations included dual and trichamber models (right hand panels).

I produced all initial design specifications and a draft plan of the mechanical function and control of the device. Dr Ari Ercole manufactured the initial prototype based on these specifications with some modifications. After initial testing, further modifications and adjustments were made by an iterative processes.

Compressed medical air from a BOC cylinder passes through a regulator valve that allowed controlled outflow at 0-120 psi. The pressurized air enters the pressure control system and is directed to meet two pneumatic solenoid (electromagnetic) valves, a 'forward' valve and a 'reverse' valve. When the forward solenoid valve is opened by the electronic trigger system then the pressurized air flows through it into a closed piston chamber and drives a piston forward. The distal end of the piston displaces a bolus of air through a closed circuit of piping towards a culture platform. The air pulse flows through the platform and upwards where it deforms the base of an attached culture well. After a programmed period of time the 'reverse' solenoid is activated, this directs another pulse of air into the piston chamber, but on the opposite side of the piston to the first impulse, and so when opened the pressurized air drives the piston back towards its starting position. This returns the pressure within the distal chamber circuit– including the culture platform– to its starting equilibrium and the deformable base of the culture well returns to its original position.

Culture wells

For details of well preparation see materials and methods (Chapter 3). The wells used for all primary culture experiments consisted of a custom stainless-steel milled well– these were obtained from Professor Douglas Smith (University of Pennsylvania), with an attached silicone elastomer base as a deformable cell-culture substrate. The silicone sheeting was chosen for a number of properties that made it appealing as a culture substrate in this system. It has high levels of elasticity and a high elasticity limit, it can be produced in thin, transparent sheets with good optical clarity, and it is resistant to tearing. It is thermally stable and heat resistant, biochemically inert and non-toxic to cell culture. It is also semipermeable to gases, but not liquids[338]. It has been the choice of culture substrate in a number of previous cellular stretch systems[78,92,310,314,334].

2. Mechanical calibration of the stretch device

Controllable variables of the membrane stretch

There are three main variables that that can be adjusted in the system to vary the characteristics of injury. First, the volume of air displaced by the piston movement in either direction is adjustable by hex-nuts (figure 9). This volume corresponds to the extent of deforming force that the cell-culture membrane experiences and hence can alter the total strain/stretch of adherent cells. The deformation and recoil can be independently controlled. Secondly, the pressure outflow from the regulator valve can be adjusted. This controls the velocity at which the piston is driven and thus determines strain rate. Finally, the duration the solenoid gates are open, and the interval between forward and reverse solenoid activation can be adjusted. This allows for an immediate or delayed recoil from the deformed position. Other related variables that do not depend on the system itself include the elastic modulus of the cell culture membrane. This means that calibration was performed separately for each different type of cell-culture membrane used.

Calibration for stretch membrane

All calibration was performed on wells that had been kept in a 37°C incubator for a minimum of one hour to ensure that the silicone membrane were thermally stable and not affected by changes by variations in temperature.

Strain calculation

Strain can be defined as the relative change in size or shape of an object due to externally applied forces. It is a *ratio* of extension to original length and so is generally considered to be dimensionless (without units) but less commonly it can also be presented as the ratio of two unit lengths- for example µM/µM. Strains can be *normal* (aligned forces) or *shear* (unaligned). Strain can be mathematically represented in several forms including as Lagrangian strain which is a simple ratio of extension to original length. *Strain rate* is the reciprocal of time in seconds (s^{-1}) to achieve a certain strain ratio so for example $50s^{-1}$ is equivalent to 20ms.

The degree of strain during a given impulse was estimated from the maximal measured vertical displacement of the culture membrane (figure 10).

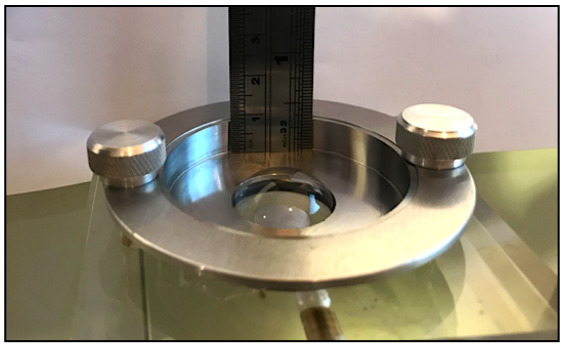

Figure 10. Maximal vertical displacement of the culture membrane can be directly measured to estimate strain for a given pneumatic impulse

---

The piston hex-nuts were adjusted to vary the degree to which the piston could move, and hence the total volume of air moved. This determined membrane deformation and the total vertical displacement of the membrane. The strain experienced by the membrane can be mathematically resolved using the diameter of the culture well and the vertical displacement of the membrane. These variables allow calculation of the radius of the curvature, and hence the arc length of the membrane as a dome. The difference in arc length and diameter is equal to the linear strain.

Radius of curvature (r) = z/2 + dd/8z

Arc length = πr/90 x arcsin (d/2r)

The change in strain with vertical deformations of 0 to 9mm are shown in table 10 & figure 11.

Vertical deformation (mm)	Radius of curvature (mm)	Surface area of dome (mm2)	Change in area (%)	Arc length	Change in arc length (% strain)
0	∞	380.13	0	22 (=d)	0
4	17.13	430.4	13.22	23.89	8.59
5	14.6	458.67	20.66	24.90	13.18
6	13.08	493.23	29.75	26.13	18.78
7	12.14	534.07	40.50	27.53	25.12
8	11.56	581.19	52.89	29.09	32.23
9	11.22	634.6	66.94	30.80	40.0

Table 10. Vertical deformation determines strain

A measure of vertical deformation allows calculation of the radius of curvature, surface area, change in surface area, and changes in arc length that can be represented at a percentage strain

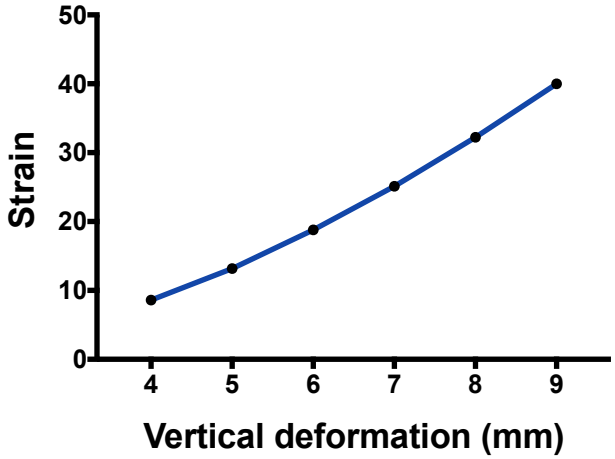

Figure 11. Strain increases with vertical displacement of the culture membrane

Total strain can be controlled by altering the volume of air driven into the culture membrane and hence maximal vertical deformation of the silicone culture membrane

These calculations are dependent upon an assumption that the stretch of the membrane is equal throughout the whole of its surface and that deformation conforms to a standard dome shape. Empirical confirmation of these assumptions involved placing 2 small dots 5mm apart on the membrane, applying a static pressure sufficient to achieve the required vertical deformation, and then measuring the divergence of the points. Measurements were taken with a digital Vernier caliper (#380244, Silverline) with a maximum resolution of 10µm. The divergence of the dots as measured gave an approximate of strain. This caliper method fails to consider vertical elongation (arc length) and so will tend to produce a small underestimation of true strain. However, at each predicted vertical deflection the elongation as measured was within 5% of the predicted value (table 11).

Vertical deformation (mm)	Separation of markers (mm)	Predicted % strain	Measured % horizontal strain
0	5	0	0
4	5.33	8.59	6.60
6	6.08	18.78	21.6
9	6.93	40	38.6

Table 11. Empirical measures of marker separation support predicted strain rates

A mathematical model can be used to predict percentage strain between two markers based on vertical displacement of a membrane that conforms to dome shaped deformation. The measured horizontal strain rates at each of the measured vertical deformations were within 5% of the predicted strain value.

Uniformity of the strain field was assessed throughout the central 15mm of the membrane as this was the entire region within which the membrane would be prepared and cells would be cultured. Elongation of the membrane within the field was assessed with multiple 0.2µm fluorescent carboxylate-modified FluoSpheres™ microspheres (#F8806, ThermoFischer). The separation of microspheres was assessed during membrane relaxation and at maximum deformation using epifluorescent microscopy (x60, NA 1.4). There was no difference in the degree of bead separation throughout the field of interest at strains of 0-40%. This confirms the uniformity of the stretch within the central 15mm of the membrane.

Strain rate

The deformation rate was assessed with high-speed video (240 fps). The solenoid opening duration was set to ~0.3ms. The interval between forward and reverse solenoid activation was <10ms. The rate of membrane deformation was determined by the driving pressure from the compressed air cylinder via a step-down regulator. For driving pressures between 20 and 60 psi there was minimal variation in strain rate. 60 psi was the maximum pressure tolerated by the compressed air attachments without gas leakage. Strain rates at 60psi for silicone based wells are shown in table 12.

Strain (%)	Duration of stretch (ms)	Strain rate (s-1)
8.6	17	5
18.8	25	7.5

Table 12. Empirically determined strain rates vary depending on total strain

3. Optimization of cell culture conditions

A period of cell culture optimization was undertaken in order to establish healthy SCGe cultures, this involved a trial-and-error approach to silicone well preparation, coating, cell explant plating and subsequent culture conditions including cell feeding strategies. The final optimized protocol is described in the material and methods chapter 3.

4. Cellular calibration of the stretch device

In addition to mechanical calibration, the system was also empirically calibrated to cellular response, with titration of strain, and strain-rate from levels which caused clear transection down to sub-transection thresholds. Similar approaches have been employed previously to calibrate *in vitro* stretch systems[98]. At strains above 30% and areas of frank neurite disruption were often seen and distal portion of axons had a propensity to detached from the membrane (figure 12). Between 20% and 30% there was evidence of occasional direct axonal disruption with some primary axotomy and retraction balls (figure 10). At strains below 20% there was no detachment of axons from the membrane or visualization of primary axotomy with brightfield or phase contrast microscopy. At strain and strain-rates where cells remained adherent to the culture membrane, the membrane stretch was considered equivalent to cellular stretch.

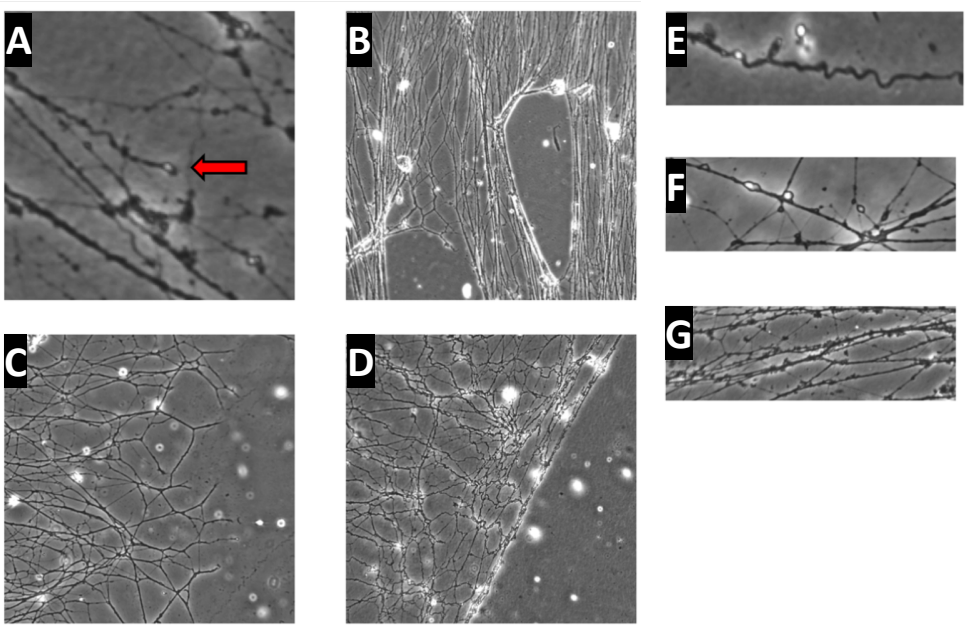

Figure 12. Different injury strains affect the degree of primary axotomy and neurite health

At higher strain rates then retraction bulbs (A) representing primary axotomy, and areas of frank neurite disruption and detachment of neurites from underlying membrane (B) were seen. At lower strain rates distal neurites remain attached and initially appeared healthy with no obvious signs of injury (C), this is contrasted to higher strains where distal neurites detached(D). Undulations were seen at all strains tests but were more prevalent and were larger at higher strains (E). At strain rates of ~20% regions of axons affected by undulations developed small, well-defined varicosities (F) and eventually large diffuse varicosities (G) before frankly degenerating.

In order to exclude the possibility of transections occurring that were not visible under brightfield and phase contrast microscopy wild-type cultures were fixed 30 minutes following application of a stretch insult (60psi, ~20% strain, strain rate 7.5s-1) and the lipophilic membrane stain DiI was applied to the neurite cell mass. This stain diffuses along intact uninterrupted membranes but will not diffuse along a physically transected membrane[339,340]. The DiI stain labelled the whole neurite structure from the explant mass to the periphery of the neurites, demonstrating that at the time of fixation the cell membrane was not transected. A physical cut of the axons with a scalpel was used as a positive control (figure 13).

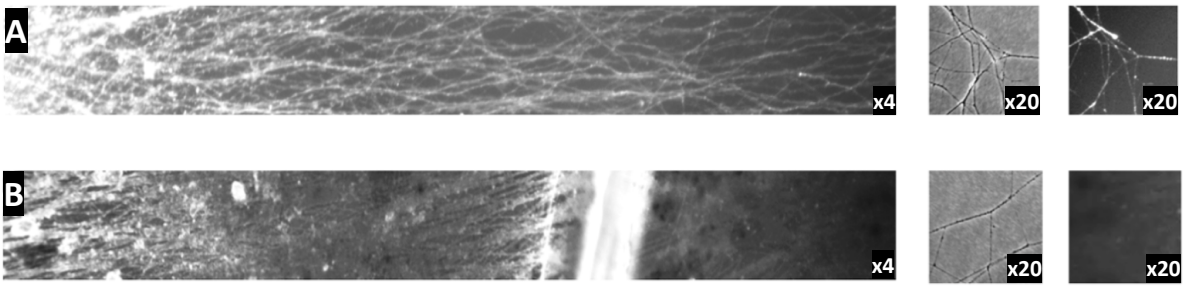

Figure 13. Stretch injury does not cause transection

The lipophilic membrane labelling dye DiI shows staining of distal neurites following stretch injury, but not a transection injury. (A) In a stretch injury DiI administered to the cell bodies diffuses along the intact membrane to the distal neurites. (B) In a transection, the DiI dye cannot diffuse past the lesion site and so distal neurites are not stained (x4 magnification). This can clearly be seen by examining neurites with phase contrast microscopy and comparing them to the same field under fluorescence for DiI staining. In a sub-transection stretch injury the DiI diffusion matches the brightfield neurites, unlike in a transection injury where DiI is unable to reach and stain neurites distal to transection injury (x20 magnification).

At all strains tested (8.6% and above) axonal undulations were seen, this is consistent with findings in previous stretch injury models[78,79]. It has been suggested that undulations seen in brain tissue following a mild central FPI may be artifacts caused by tissue processing as comparative undulations were also seen in control animals[341]. However, these experiments were undertaken in living animals tissue with immediate live-imaging pre and post-injury. Undulations were only ever seen in axons following injury thus the association in this model is convincing (figure 13). In addition, sporadic varicosities were seen with this model. In the first 30-60 minutes following an injury these were occasional and regular in structure. As time passed they became more diffuse and disordered (figure 13).

In order to limit experiments to subtransection effects, all primary culture stretch experiments were conducted with a driving pressure of 60 psi, with the piston set to achieve a vertical deflection of 6mm, equivalent to a strain of ~20% at a strain rate of $7.5s^{-1}$. This was selected as it was the closest achievable to rates used in existing literature that did not cause any detachment from the silicone membrane or primary axotomy. At this strain/strain rate there was no frank change in the architecture of the axons immediately post injury other than occasional areas of axon undulation.

Wild-type SCG cultures were used to examine for progressive changes in neurite degeneration index (NDI) at various timepoints up to 48 hours following stretch injury (figures 14 & 15). The NDI is an established quantitative measure of neurite degeneration that has been used in prior publications[174,207]. Images of a field of neurites are obtained by phase-contrast microscopy x20 magnification. The imaged field is typically at a point around 3mm from an explant mass where the density of the neurites allows visualization of morphological change. The NDI is calculated by an automated ImageJ plugin algorithm that is operator independent. To quantify the axonal degeneration the phase-contrast image is binarized so that the pixel intensity of neurites regions are converted to black (this constitutes the total neurite area) and all other regions are converted to white. Intact, healthy neurites show a continuous tract, whereas degenerated axons are characterized by axonal fragmentation or beading. Degenerated axons were detected by using the particle analyzer module of ImageJ which counts the area of the small fragments or particles of degenerated neurites that are size 20 – 10,000 pixels. The NDI is then calculated as the ratio of fragmented neurite area over total axon area. As it is a ratio it has no unit. The output is a number from 0 to 1 based upon the degree of neurite continuity or fragmentation. Most healthy neurites score around 0.2-0.3 while a profoundly degenerated field would be in the range of 0.6-0.9. In the case of complete degeneration or pathological fragmentation to the point of detachment a score of 1 is assigned.

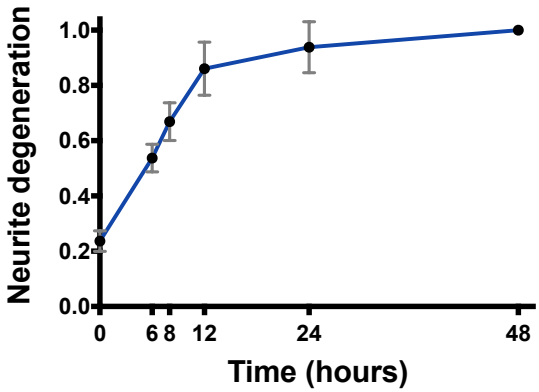

Figure 14. Neurite degeneration in wild-type SCGe is time-dependent following stretch injury

Degeneration is induced in wild-type SCGe by a stretch injury. Degeneration progresses rapidly initially until 12 hours when most degeneration has occurred. The remaining degeneration then occurs at a slower rate up to 48 hours when there is complete fragmentation and detachment of neurites. Neurite degeneration is a ratio and therefore unitless, a higher score indicated more degeneration with 0.2-0.4 representing healthy intact axons, and 0.8 to 1 representing complete degeneration and fragmentation. n = 9 repeats. Error bars = SEM.

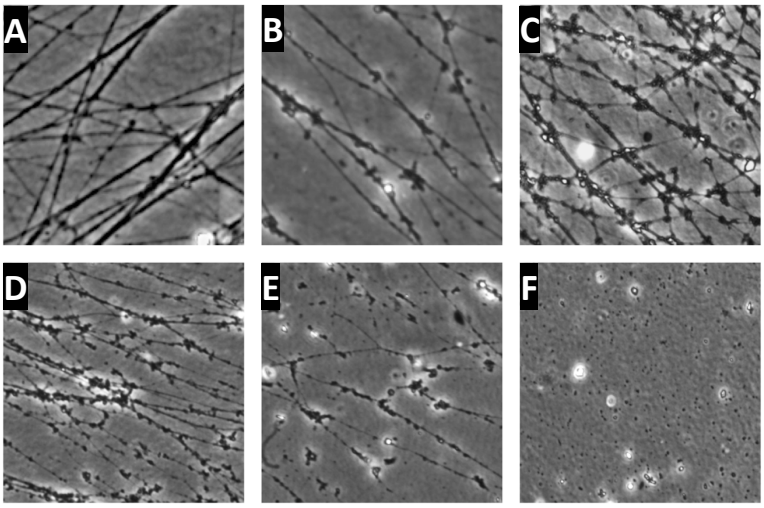

Figure 15. Neurite degeneration occurs progressively following stretch injury in wild type cultures

Following injury or activation of the Wallerian degeneration pathway there is a progressive neurite degeneration. A higher neurite degeneration index (NDI) correlates with increasing deterioration and fragmentation of neurite structure. Panels labelled as follows: A. Healthy neurites (NDI <0.3); B. 6h post-stretch = 0.5 NDI; C. 8h post-stretch = 0.7 NDI; D. 12 hours post-stretch = 0.8 NDI; E. 24 hours post-

stretch = 0.9 NDI; F. 48 hours post-stretch = 1 NDI.

Length dependent degeneration

The neurite degeneration index plugin for Image J is optimized to analyze degeneration in fields with similar density of neurites. Hence, degeneration is measured in the most distal portion of neurites that still lie entirely within the border of the microscope viewfinder [134,174]. Following transection, degeneration occurs in neurites distal to the site of transection. This occurs in a rapid anterograde fashion after a latent phase[112,114,342].

Subsequent to a stretch injury in SCGe culture it was noted that there was length-dependent degeneration with the distal neurites showing evidence of degeneration while proximal neurites, near to the cell bodies in the explant mass, appeared intact (figure 16). The gradient of degeneration is consistent with a length-dependent process.

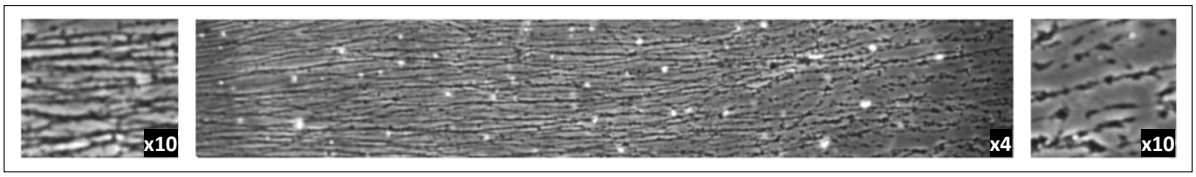

Figure 16. Neurite degeneration is length-dependent following stretch injury

Neurites degenerate in a length-dependent manner following a stretch injury. Distal neurites can be seen to completely fragment at 8 hours following stretch injury while proximal neurites remain apparently healthy and in continuity. Intermediate regions show signs of varicosity development and blebbing that precedes frank disconnection. Central image shows full length of neurites at x4 magnification. Proximal intact field (left), and degenerated distal field (right) are shown at x10 magnification.

5. Axonal transport

The mechanism of neurite degeneration following stretch injury is not fully understood. As one possibility is injury induced failure to transport essential cargos, we directly measured axonal transport in cultures 1 hour following stretch using MitoTracker™ Green to label mitochondria (#M7514, ThermoFisher) but there was a wide degree of baseline variability in transport rates with all cultures (figure 17)[343]. Possible reasons for this are explored in this chapter's discussion.

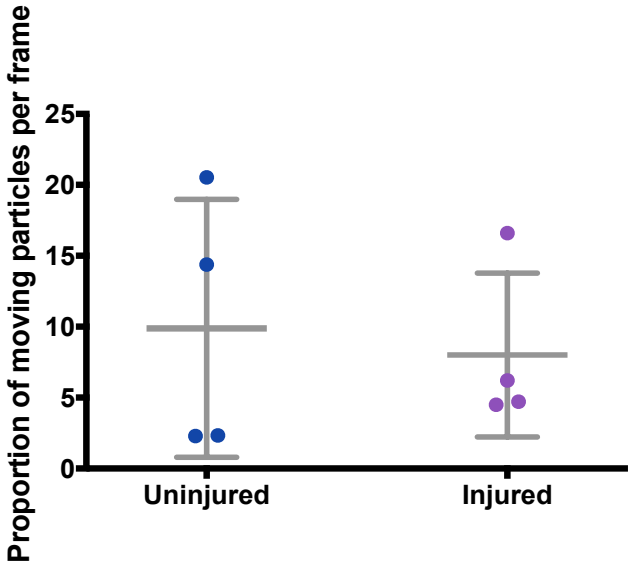

Figure 17. Measurement of axonal transport in stretched cultures

There was a wide variability in overall axonal transport in both uninjured and injured SCG cultures. In this small sample there was no significant difference between the two groups. n = 4 wells per condition. * = p≤ 0.05, ** = p≤ 0.01, *** = p≤ 0.001, **** = p≤ 0.0001, ns = non-significant (p>0.05). Error bars show SD. Statistics: Student's T test.

6. Cortical neuronal cultures

Smith *et al* have previously demonstrated the successful culture of rat PCNds on silicone membranes[78,79]. Through the use of microfabricated PDMS stamps and selective laminin membrane coating it was possible to separate the cell bodies from the neurites, and partially control the direction of growth to isolate parallel bundles of neurites on a silicone membrane (Figure 18).

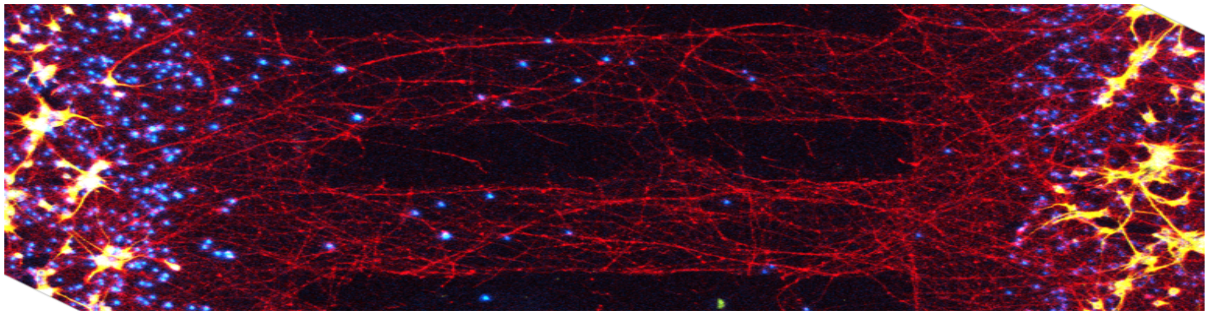

Figure 18. Rat dissociated primary cortical neuron culture grow and neurites on silicone membranes

Rat dissociated primary cortical neurons can be cultured on a silicone membrane. Staining for neurons is with βIII tubulin (red), astrocytes with GFAP (yellow), and nuclei with DAPI (blue). These cultures were prepared and processed with the assistance of the Douglas Smith laboratory in Penn university. Images taken at 7 DIV.

Rat cultures possess some limitations compared to mice including fewer transgenic models and antibodies [344]. Therefore, attempts were made to culture PCNd from mice on the silicone membranes (Figure 19).

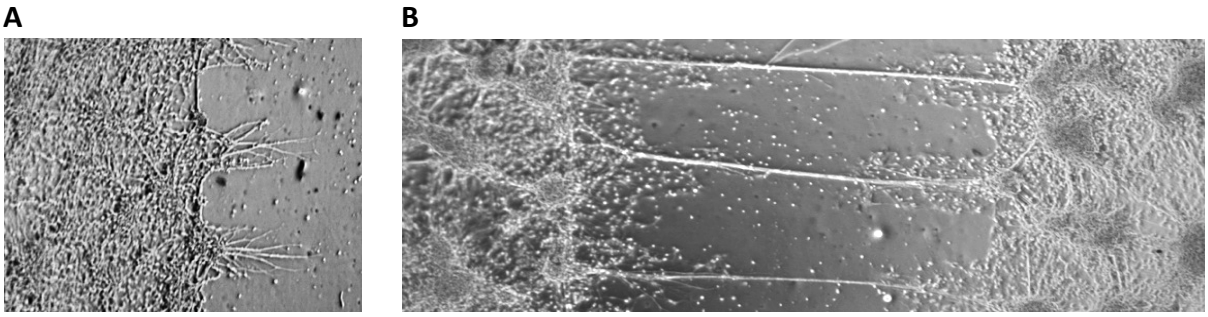

Figure 19. Mouse dissociated primary cortical neuron culture produce sparse neurites on silicone membranes

Mouse dissociated primary cortical neuron culture grow slowly and in thin bundles on silicone membranes. Brightfield images of PCNd from mice. Growth is slower than in rats with only limited outgrowth at 7 DIV (A). At 12DIV the neurites can span a 1mm gap but do so in very fine, limited neurite bundles (B).

While mice cortical culture on the silicone membranes was possible, the cell bodies clumped, did not form such robust neurites bundles, and had a slower growth rate. These limitations were not overcome by adjusting culture conditions including silicone coating and plating density. Axonal growth rate has previously been shown to be lower in cortical neurons than SCGs[178].

Examination of modulators of WD using a stretch based injury system

The development of this new *in vitro* stretch model lays a foundation for further experimentation and characterization of stretch injury in SCGe. It also opens the possibility of investigating molecular aspects axon degeneration, and in particular WD, in this model system. The following section describes a series of experiments investigating the effects of various modulators of WD on SCGe neurite degeneration following a single stretch injury.

7. NMNAT2 levels affect vulnerability to stretch injury

Gilley *et al* generated a Nmnat2^{262gt} gene-trap null for NMNAT2 activity (see chapter 3, materials & methods for details). The Nmnat2^{262gt} gene-trap causes almost complete gene silencing, therefore heterozygous Nmnat2$^{+/262gt}$ mice have ~50% reduction in NMNAT2 activity. They are viable and grow to adulthood[161,178,179]. As these Nmnat2$^{+/262gt}$ cultures have an already reduced steady-state expression of Nmnat2, they could be hypothesized to result in increased vulnerability to axonal injury– with WD occurring at an earlier time point. Therefore, stretch injury was used to test whether SCGe cultures from these animals had any premature neurite degeneration compare to wild-type cultures (figure 20).

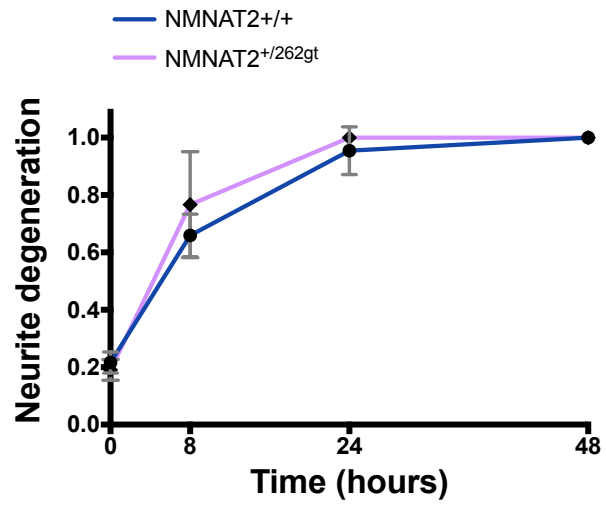

A B

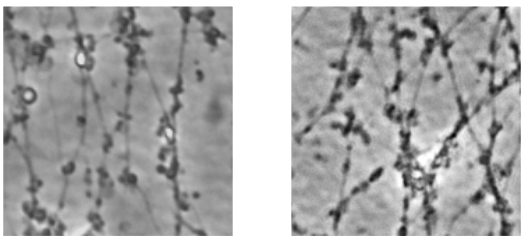

Figure 20. SCGe with reduced expression of NMNAT2 have no significant difference in the rate of neurite degeneration following stretch

The mean rate of degeneration was greater following stretch in Nmnat2$^{+/262gt}$ SCGe cultures compared to Nmnat2$^{+/+}$ controls at 8 and 24 hours, but this was not statistically significant at P≤ 0.05. Representative neurites are shown 8 hours post stretch in the following conditions, Nmnat2$^{+/+}$ (A) and Nmnat2$^{+/262gt}$ (B). n= 9 repeats. * = p≤ 0.05, ** = p≤ 0.01, *** = p≤ 0.001, **** = p≤ 0.0001, ns = non-significant (p>0.05). Error bars show SD. Statistics: 1 way ANOVA.

Following a stretch injury there was no statistically significant additional burden of degeneration in Nmnat2$^{+/262gt}$ cultures. The greatest mean difference was seen at 8 hours post-injury with a mean NDI 66% in Nmnat2$^{+/+}$ v 77% in Nmnat2$^{+/262gt}$.

8. FK866 is a NAMPT inhibitor that delays stretch induced degeneration

The drug FK866 rapidly and non-competitively inhibits the action of NAMPT (also known as visfatin or pre-B cell colony stimulating factor). In the brain NAMPT is primarily expressed in neurons where it blocks the reversible reaction converting NMN to NAD[345,346].The addition of FK866 at the time of neurite transection has previously been shown to rapidly decrease NMN levels in SCG cultures, preserving neurite integrity for at least 72 hours, an effect that has been reversed by co-administration of NMN[174]. These findings contribute to the theory that increased levels of NMN is an important trigger for WD initiation. Over a longer period, in excess of 4 days in SCGe, FK866 induces neurite degeneration even in uncut neurites, possibly due to a critical depletion of NAD[174]. I have also shown this to late degeneration be due to a SARM1 dependent process suggesting that it is a WD dependent mechanism(data not shown).

Therapeutically, FK866 has been proposed as an anti-tumoural agent due to its NAD depleting action[346–348]. It has also been trialed in murine models of acute-lung injury and SCI[349,350]. The results of its use in stroke models have been conflicting[351–353]. There is a paucity of literature examining FK866 in TBI. In 2015 Zhang *et al* examined the effects of FK866 and NMN separately in a murine brain cryoinjury model. They found alleviation of neuronal loss in both cases and concluded that NMN supplementation replenishes NAD levels, while NAMPT inhibits inflammatory cells– specifically the optical density of IbA1 and GFAP positive cells in the lesion core. They present this as evidence of FK866 being protective in TBI[354].

There are two primary reasons to test the effect of FK866 in stretch injury. Firstly, to help determine if degeneration can be prevented by NAMPT inhibition. This would give insight into the mechanism of axon degeneration post-stretch. Also by co-administering NMN it can be determined if the process is NMN dependent. Secondly, to examine FK866 as a potential therapeutic agent, albeit one that has been shown to be capable of also causing degeneration with prolonged exposure[174].

Three conditions were examined. 100nM of FK866 was added at the time of stretch injury, 100nM of FK866 and 1mM of NMN, or DMSO control. NDI was then assessed over the following 48 hours or until complete degeneration had occurred (figure 21).

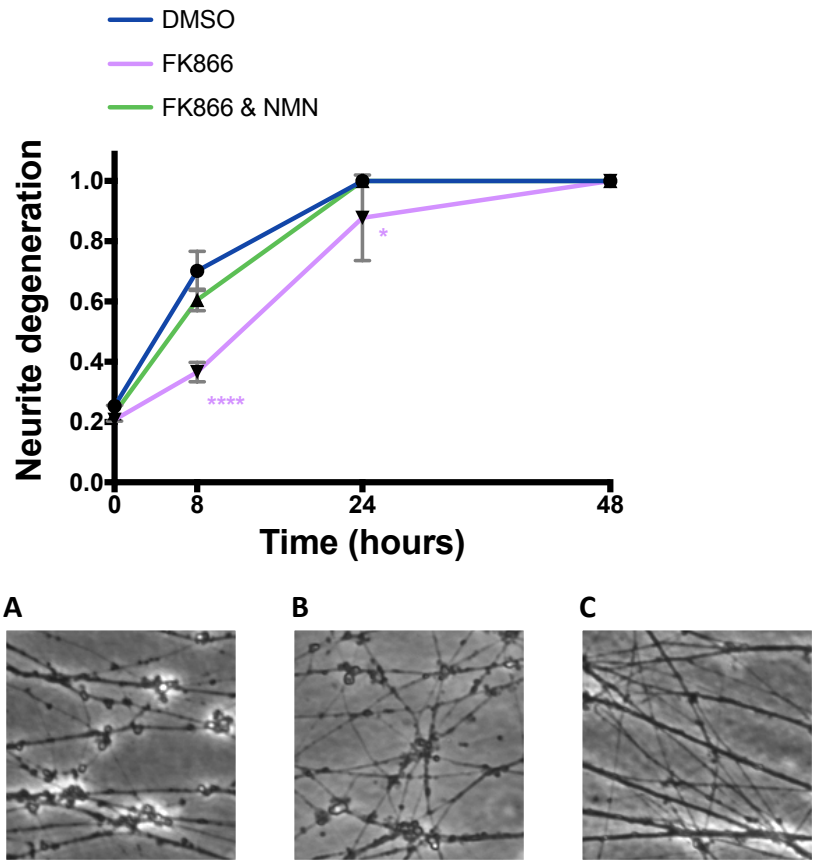

Figure 21. SCGs treated with FK866 have delayed neurite degeneration following stretch that can be abolished by co-administration of NMN

The administration of 100nM of FK866 at the time of stretch resulted in a delay in WD compared to DMSO only wild type controls at 8 and 24 hours, but complete degeneration still occurred by 48 hours. The co-administration of 1mM of NMN at the time of injury abolished the protective effect of 100µM of FK866 with a minimal reduction in degeneration at 8 hours, and full degeneration by 24 hours. Representative neurites are shown 8 hours post stretch in the following conditions, DMSO (A) FK866 plus NMN (B), and FK866 alone (C). n = 9 repeats. * = p≤ 0.05, ** = p≤ 0.01, *** = p≤ 0.001, **** = p≤ 0.0001, ns = non-significant (p>0.05). Error bars show SD. Statistics: 2 way ANOVA.

FK866 resulted in a delay in WD compared to DMSO controls at 8 and 24 hours, but complete degeneration still occurred by 48 hours. The co-administration of 1mM of NMN at the time of injury almost completely abolished the protective effects.

9. SARM1$^{-/-}$ and WLD^{s} delay stretch induced axon degeneration

An alternative approach to elucidate the role of NMANT2 and the WLD pathway activity in a stretch injury is to examine a condition in which NMNAT2 or a substitute, is overexpressed, has enhanced/maintained activity, or the downstream effects of NMNAT depletion are inhibited. WLD^{s} is known to substitute for NMNAT2 and maintain axonal integrity following transection injury through maintenance of NMNAT2-like activity in the distal axon. SARM1 loss of function mutation (SARM1$^{-/-}$) is able to delay WD by stopping the downstream effects of NMNAT depletion in a transected neurite[178,179].

In wild-type mice the distal portion of a transected *in vivo* sciatic nerve degenerates after a latent phase of 24-48 hours, while SCGe that undergo an axotomy degenerate *in vitro* within 8 hours[114,134,204,212]. In WLD^{s} and SARM1$^{-/-}$ mutant mice, degeneration is delayed to at least 10 days in sciatic nerves and 72 hours in SCGs[174,179,204,212,215,355]. WLD^{s} and SARM1$^{-/-}$ have been shown to delay WD in a variety of neuronal subtypes including cultures derived from primary neurons (DRGs and cortical neurons), and optic nerves[356–358]. The ability of WLD^{s} and SARM1$^{-/-}$ to protect also varies depending on the nature of the insult or disease model, with effects varying from no protection, through to long-term or even life-long protection[7].

It was hypothesized that WLD^{s} or SARM1$^{-/-}$ would delay neurite degeneration following stretch via WD pathway effects. This has implications for understanding the mechanism of axonal degeneration following a stretch injury, specifically if it acts via a WD pathway, and also may indicate the potential for a TAI to be amenable to therapeutic modulation of the WD pathway. The results of SARM1$^{-/-}$ and WLD^{s} mutation on NDI after stretch are shown in figure 22.

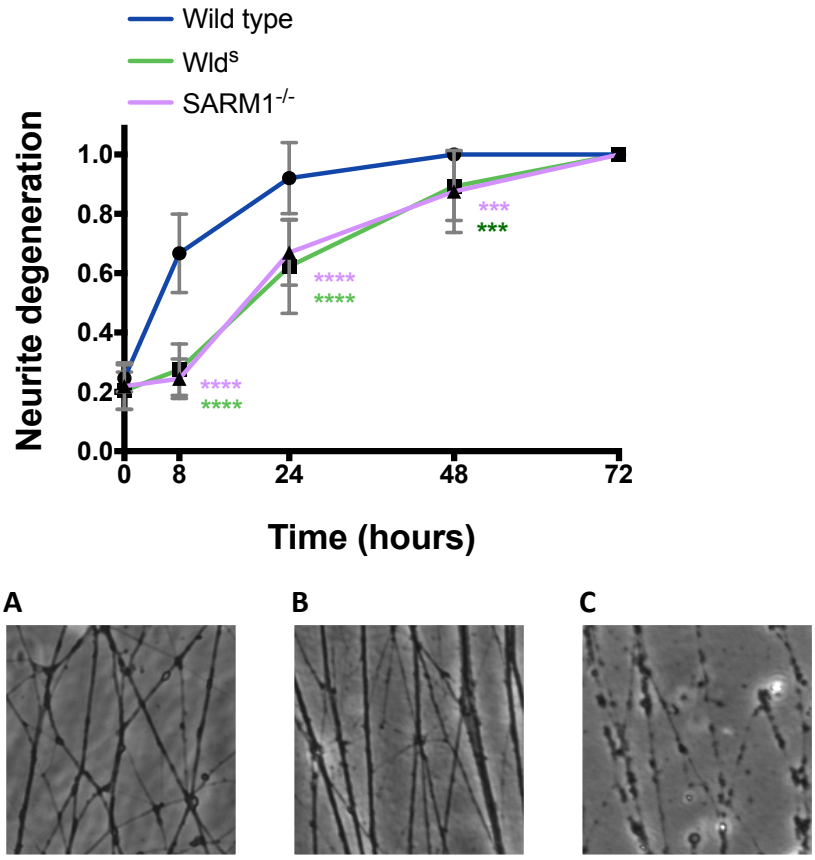

Figure 22. SARM1$^{-/-}$ and WLD^S are associated with delayed neurite degeneration following stretch

In SCGe neurite cultures from mice with SARM1$^{-/-}$, and WLD^S mutation, degeneration was delayed following stretch injury compared to wild-type cultures. At 8 hours a rapid, progressive neurite degeneration was seen in wild-type cultures but not in and SARM1$^{-/-}$ and WLD^S mutants. A delayed degeneration was seen until 72 hours when complete degeneration was seen in all cases. Representative neurites are shown 8 hours post stretch in the following conditions, SARM1$^{-/-}$ (A), WLD^S (B), and wild-type (C). n = 9 repeats. * = p≤ 0.05, ** = p≤ 0.01, *** = p≤ 0.001, **** = p≤ 0.0001, ns = non-significant (p>0.05). Error bars show SD. Statistics: 2 way ANOVA.

Eight hours following a stretch injury there was near complete protection against degeneration in WLD^S and SARM1$^{-/-}$cultures. At 24 and 48 hours degeneration was seen to be progressively occurring in all cultures, but at a slower rate in WLD^S and SARM1$^{-/-}$ compared to wild type. By 72 hours degeneration was complete in all cultures.

Discussion

The use of *in vitro* models of TBI have allowed researchers to interrogate pathobiological mechanisms involved in cellular injury and death due to external effects of physical forces. They have been used to examine molecular events involved in cellular death and dysfunction, and hold the potential to identify and explore therapeutic interventions that may be able to improve outcomes of TBI[13]. Numerous *in vitro* models of TBI are described in the literature, important examples of which were reviewed in chapter 2.

As a platform to investigate mechanisms of traumatic axonal injury this chapter describes the development of a new *in vitro* injury device. As explained in the introduction to this chapter it was decided to attempt development of a stretch based injury as the literature supported this as the most externally-valid method of reproducing the axonal type of injuries seen in DAI. The device design was based on a balance between an idealized injury device and pragmatism. The design was subsequently modified as the device was built by an iterative process. Likewise, a process of optimization was required to establish healthy SCGe culture growth and attachment to the silicone membrane.

The utility of any *in vitro* model is essentially dependent upon its ability to accurately reproduce the elements of interest seen *in vivo*. Regardless of optimisation an *in vitro* system will necessarily remain several steps removed from a human injury due to differences in species, tissue, and to some degree, mechanical differences. Nevertheless, this does not preclude the procurement of useful information from these models, not all aspects of the injury or response need to exactly replicate a human injury. There only needs to be sufficient replication of those aspects of interest. Indeed, some mechanistic information and certain insights into molecular responses of cells to injury may only be possible with such a reductionist set up. This is acceptable so long as we remain cognisance of their limitations and vigilant to over-extrapolation.

There is no consensus of the optimal method of validating a new *in vitro* model of TBI. Several approaches can be taken to establish the fidelity of a model system. As our primary concern was with replication of mechanical forces, and their effects on axon degeneration, this was

the focus of initial calibration efforts. Mathematical modeling and empirical testing was used to establish strain and strain rates in the system. The nature of axonal response to injury has been documented as highly dependent upon the rate and extent of any elongation injury, in part due to the viscoelastic nature of axons[84,249,287,359]. We found that at a strain of 18.8% and a strain rate of $7.5s^{-1}$ subtransection injury was demonstrated using a membrane tracking dye (DiI). As described in chapter 2, this level of strain is thought to be representative of those affecting the brain during a DAI. An alternative method of validation would have been to test the effect on a pharmacological agent with known *in vivo* injury modulating effects and looked for a comparable response *in vitro*. This would give evidence of similar pathway activation. For example, this could have been undertaken by therapeutic targeting of metabotropic glutamate receptors (mGluR) which have been shown to reduce cell death after injury[13]. However, this effect is pathway specific and so while encouraging, alteration of neuronal or axonal survival with a mGluR antagonism, for example with MK-801, would not have informed us about the activation of our pathways of interest, that is WD, with our model[360].

In our case strains were applied to a SCGe culture. SCG cultures were chosen because they have been well-characterised as models of WD with known preservation of the key aspects of the molecular pathway, they also show robust and reliable cellular growth, have clearly identifiable neurites in which we can accurately quantify degeneration, the explants can be taken from transgenic mice to explore genetic modifications, and if needed they can be microinjected/transfected to alter genetic expression. Our laboratory also has extensive experience with this cell type. However, SCGs are not cells derived from the brain. As their name suggest they are derived from the peripheral superior cervical ganglion of mice. These cells are sympathetic neurons from the autonomic nervous system. They are well-characterized and have been used for investigation of axon degeneration and cellular death, neuronal development and differentiation, and signalling mechanisms[179,361–363]. SCGs are an easily accessible source of neurons and have been successfully used to investigate axonal transport, this is facilitated by the clarity of polarity inherent to a system derived from a ganglionic explant[255]. After dissection of the ganglion, removal from a young post-natal mouse pup (see materials and methods, chapter 3), and plating the cells rapidly attach to suitably prepared culture membrane and extend neurites from the mass of cell bodies out in a radial fashion. Within 5 days they grow 5-7mm and allow good visualisation of neurites[364].

To complement the experimental approach using SCG, attempts were made to culture rodent dissociated PCN. These offer some additional research benefits, including the experimental simplicity of a single cell type culture, without the confounding factors implicit in surrogate cell lines or non-CNS/non-cortical neuronal subtypes. Furthermore, although WD mechanisms are generally held to be well preserved in SCG, there may be unidentified differences in mechanisms between different neuronal populations and so using cortical cells is arguably the optimal strategy. We were able to establish healthy rat neuronal cultures, however they possess some important limitations including a reduced availability of transgenic models and antibodies when compared to mice[344]. Therefore, further attempts were made to culture PCNd from mice on the silicone membranes. It was found that mice neurons were generally less robust than their rat counterparts with less neuronal growth capacity. While it was possible to culture PCNd on silicone, the cells tended to clump more and had limited outgrowth capacity compared to rat neurons. When they extended neurites across a gap free from cell bodies they tended to form dense thin bundles. These factors limited the utility of the PCNd from mice in this stretch culture system. Therefore, these cortical cell types technique were not used further. Other cell types including astrocyte derived cell lines are currently being explored with this injury system via collaborators. Also, the opportunity of exploring injury effects in induced neuronal cells derived from the somatic cells of patients now exists, and this opens up an exciting arena of patient specific investigation[365]. For example, assessment of how induced neurons derived from patients with different endogenous NMNAT2 expression levels respond to injury.

Through adjusting the overall strain we were able to titrate injury from zero deformation up to a point of frank axotomy in SCGe. Neurite degeneration was measured using an automated Image J plugin. At subtransection thresholds the rate of neurite degeneration is similar to that seen with SCG following transection injury[134,342]. This is consistent with a WD process but not proof of it.

Neurite degeneration is assessed at a standardized distance from the ganglion cell mass, and in the same neurite field wherever possible. This allows quantification of degeneration in the same culture at different time points. Interestingly, when proximal neurites were examined

there appeared to be a length-dependent degeneration with distal degeneration appearing to be more frankly degenerated at a given time compared to proximal neurites. WD following transection is generally considered to occur rapidly throughout the whole length of the axon at the same time with differences in timing between proximal and distal neurites being negligible. Given the calibration findings of a uniform strain field throughout the membrane and the lack of transection seen with DiI staining this appears to be a stretch specific effect. Length-dependent axon degeneration is well-recognised in certain peripheral neuropathies– where the cause is generally considered to be related to failures in axonal transport[366]. It has not previously been described in stretch injury. Length-dependent axon degeneration is primarily seen in long axons, particularly spinal motor neurons that can reach up to 1m in length. In contrast, axons of the human CNS will typically be spanning much shorter distances, and in this model the SCG neurites are only around 5mm. If axon degeneration were due to impairment of axonal transport as a result of microtubular fracture as suggested by Tang-Schomer *et al* in their stretch injury model of rat cortical neurons then failure to deliver a 'survival factor' to the distal portions might be the cause of the degeneration[78,79]. Failure to deliver NMNAT2 would be a good candidate for this as we know it is axonally transported and interruption of its transport can induce WD of an axon disruption[134,199,255]. Alternatively, the length-dependent degeneration could be due to greater vulnerability of distal neurites to trauma as a result of their sparser density, and tendency to remain as thinner individual neurites, unlike proximally where neurites tend to coalesce into thicker bundles.

Attempts were made to measure axonal transport in cultures following stretch and while transport could be seen there was excessive baseline variability in transport rates with all cultures. This may be due to rapid temperature fluctuations arising from the extremely thin silicone membrane supporting the cultures. The availability of an enclosing temperature chamber for the microscope housing in which cultures could be stabilized would be a possible next step to continue this experiment. We used MitoTracker, a mitochondrial dye, this has been widely used for axonal transport studies. However, it has been criticized as it may alter mitochondrial motility and therefore some groups prefer transgenic cargo labelling[367]. Mitochondrial is also only one of many possible cargos that could be measured[367]. This preliminary investigation of axonal transport showed that while challenging it is at least technically possible to track the migration of cargos in this system. With greater optimization

this might offer an opportunity to directly assess the effect of stretch injury on NMNAT2 transport and its correlation with degeneration.

A series of experiments were then undertaken investigating the effects of various modulators of WD on SCGe neurite degeneration following a single stretch injury. The primary aim of these experiments was to probe the role of the WD system in axonal stretch injury, and explore how known modulators of WD affect the NDI following stretch. In Nmnat2$^{+/262gt}$ cultures there was no statistically significant additional burden of degeneration following stretch compared to wild-type cultures. The reason for the lack of difference in degeneration may be that the rate of degeneration is independent of NMNAT2 levels, as would be expected if degeneration were via a non-WD mechanism, or via an unrelated mechanism that proceeded alongside WD but at a rate that is equal to, or faster than WD. Alternatively, a 50% reduction in NMNAT2 expression may just be is insufficient to manifest as a significantly increased vulnerability to stretch injury. The small non-significant increase in degeneration seen in the Nmnat2$^{+/262gt}$ mice could be a genuine small difference in rates but greater numbers would be required to demonstrate this statistically. An alternative gene-trap is the Nmnat2^{Baygt}, this causes incomplete silencing of the gene and results in around ~50% expression per allele. Therefore, heterozygous Nmnat2$^{+/Baygt}$ mice have around 25% expression of NMNAT2 compared to the 50% reduction seen with heterozygous Nmnat2$^{+/262gt}$ mice. A compound mouse with one copy of each gene-trap, Nmnat2$^{262gt/Baygt}$ therefore has a ~75% reduction in NMNAT2 levels. These mice are overtly normal but repeating this experiment with cultures from the compound heterozygote mice might demonstrate vulnerability to injury not seen with a single gene-trap allele in a heterozygous state[368,369].

The NAMPT inhibitor FK866 resulted in a delay in WD compared to DMSO controls at 8 and 24 hours, with complete degeneration occurring by 48 hours. The co-administration of 1mM of NMN at the time of injury almost completely abolished the protective effects. Firstly, these results indicate that degeneration can be prevented by NAMPT inhibition, at least in the short term. Secondly, we see that normal NAMPT activity is sufficient to initiate degeneration following stretch, and that this can be partially prevented at 8 and 24 hours by FK866 administration. Albeit, the duration of this protection is less than seen with transection injury. The weaker protection suggests that other non-NAMPT/NMN dependent processes may be

taking place. This could include downstream activation of the WD pathway downstream, or activation of a different death pathway. Furthermore, the finding that co-administering NMN along with FK866 is concordant with an NMN dependent process. A finding that is consistent with findings in a transection model[174].

Fox & Faden has shown evidence that WLD^s have improved outcomes following TBI using CCI a murine CCI model[275]. Henninger *et al* 2016, have respectively showed evidence that and $SARM1^{-/-}$ and weight drop models[276].

Henniger *et al* also showed a reduction in axonal β-APP staining, and plasma concentrations of NFH in $SARM1^{-/-}$ compared to wild type mice, which they present as evidence for protection against axonal pathology[276]. However, no study has previously directly assessed the capacity of WLD^s or $SARM1^{-/-}$ to protect against an axonal stretch injury or to directly assess its role in an isolated neuronal population undergoing sub-transection physical injury. WLD^s and $SARM1^{-/-}$cultures demonstrated partial protection against degeneration at 24 and 48 hours. This effect was lost by 72 hours, at which point degeneration was complete in all cultures. This is within the time frame that WLD^s and $SARM1^{-/-}$ usually provide complete protection against degeneration following a complete transection. The ability of WLD^s and $SARM1^{-/-}$ to protect against degeneration at 8 hours suggests that stretch injury can induce a WD that the mutations prevent. However, as with the protection seen with FK866, the delay in degeneration is shorter lasting than seen following a transection injury. Likewise, this could be explained by either activation of the WLD pathway downstream of SARM1, or activation of an additional non-WD pathway during the stretch injury. Specifically, one that leads to degeneration between 8 and 72 hours. The nature of such a process is unknown and requires further investigation, but the time course is consistent with caspase-dependent degeneration secondary to trophic deprivation[106,121,370–373]. Hence, interrogation of the potential mechanism of degeneration with immunohistochemical analysis for activation of apoptotic pathways would a logical next step.

The partial protection of neurites with WLD^s, $SARM1^{-/-}$ and FK866 suggest that at least the initial degeneration is WD mediated. The mechanism of this degeneration may be due to interruption of NMNAT2 delivery due to impaired axonal transport, perhaps due to

microtubule fracture at the site of undulations[78,79,175,199 254]. An investigation of the axonal transport of NMNAT2 following stretch injury could provide direct evidence to support or refute this hypothesis regarding of the mechanism of stretch induced WD.

An alternative approach to establish the contribution of WD to stretch induced axon degeneration would be to assess for a change in a protein marker of WD after injury. For example, NMNAT2 levels in distal neurites following a stretch injury compared to uninjured controls. This is possible using western blots using an NMNAT2 antibody. However, the antibody produces multiple non-specific bands and also requires a large amount of material, and hence cultures, to achieve adequate protein levels for analysis . It is also possible to assess NMN and NAD levels directly using HPLC, but again large amounts of material are required which would have required collection of numerous ganglia.

Summary

In this chapter, we have described the development of a new *in vitro* device capable of producing a quantifiable stretch of a silicone membrane suitable for cellular culture. The mechanics of the stretch force are adjustable and have been mathematically modelled and empirically tested. The model reproduced aspects of DAI *in vitro* in an SCGe culture, including retraction balls, varicosities, and strain dependent primary axotomy. Injury was modified to establish a sub-transection threshold, but progressive neurite degeneration was also seen at these levels. The timing of this degeneration was in keeping with a WD process. Neurite degeneration was demonstrated to be length-dependent with this stretch injury. Attempts to explore axonal transport in this system were challenging due to difficulties controlling baseline variability, however with further optimization this method may still provide insights into mechanisms of stretch injury. As a proof of principle, PCNd were cultured from rats and through the use of micropatterning stamps constrained into bundles of axons. However, mouse PCNd were found to grow shorter and extensively reticular neurites compared to rats with narrow axon bundles that precluded their use. The stretch device was used to explore neurite degeneration in SCGe with a range of variables related to WD modulation. A 50% reduction in NMNAT2 expression levels did not significantly change the rate of WD seen. FK866 delayed axon degeneration in an NMN dependent manner consistent with a WD process. This was supported by delays in degeneration in transgenic WLD^S and $SARM1^{-/-}$ mice. However, the delay in WD was weaker than seen in a transection injury. This suggests that the stretch injury is inducing WD and additional unidentified axon-degenerative mechanisms.

Next steps

In the following chapter we will describe the systematic examination of derivatives of the compound P7C3 which has been proposed as a NAMPT activator capable of preventing or delaying WD induced neuronal damage following TBI[337]. Chapter 5 will explore and characterize its effects *in vitro* with the aim of assessing its efficacy in stretch injury and as a possible therapeutic agent.

Chapter 5

P7C3-A20 fails to protect against Wallerian Degeneration *in vitro*

Introduction

1. Development of pharmacological agents in TBI

As the WD pathway is increasingly understood it may offer new treatment opportunities in DAI and neurodegenerative disease. One example is P7C3 and its analogues P7C3-A20 and P7C3-S243. This aminopropyl carbazole agent was discovered in 2010 using a novel unbiased *in vivo* screening approach [374]. It is structurally related to latrepirdine (dimebon) an antihistamine drug that after initially promising results, ultimately failed to show benefit in phase III trials for Alzheimer's disease[375–377]. In other work P7C3 was found to enhance neuron formation in the sub-granular zone of the dentate gyrus of adult mice, and protect against apoptotic loss of newborn hippocampal neurons in neuronal PAS domain protein 3 knockout mice [374]. P7C3 binds to NAMPT, acting as a small molecule enzyme activator and enhancing its activity. As previously described in chapter 2, NAMPT is the rate-limiting enzyme that converts nicotinamide to NMN and NAD. P7C3-A20 is one of a limited number of known drugs that can act to potentiate or inhibit NAMPT and NMNAT (figure 23).

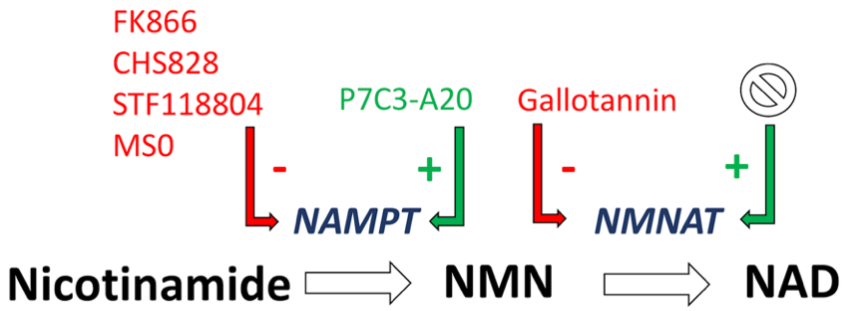

Figure 23. Pharmacological manipulation of the NAMPT pathway

There are a limited number of available pharmacological agents that act directly on NAMPT and NMNAT within the NAD synthetic pathway.

While there are still some questions remaining about P7C3's mechanism of action and how it might interact with WD pathways, reports have suggested that it is proneurogenic and able to reduce apoptosis, possibly related to NAMPT activation[335,374]. It has been shown to protect against doxorubicin toxicity which is due to NAD depletion, supporting NAMPT activation as an important mechanism of its action[336].

Further *in vivo* work in models of visual dysfunction following blast injury and traumatic brain injury have shown neuroprotection and preservation of function with P7C3 derivatives[337,378,379]. While it has not been tested in a classical TAI model, P7C3-S243 has been trialed by Yin *et al* in a blast TBI model, which produces widespread isolated axonal damage in the absence of cell body death or acute inflammation. P7C3-S243 reduced axon degeneration and preserved CA1 stratum radiatum morphology, myelin and mitochondrial structures. It additionally protected against impairment of behaviors, including motor co-ordination, and hippocampal dependent learning and memory loss,[337]. In a separate study P7C3-S243 prevented retinal ganglion cell loss following experimental blast injury in mice[378]. P7C3-A20 administration in a rat fluid-percussion injury model showed a reduction in contusion volume and improved sensorimotor and cognitive function[379].

An active enantiomer of P7C3, called P7C3-A20, differs by the exchange of a fluorine group for a hydroxyl group within the compounds linker region[379]. P7C3-A20 was capable of blocking 1-methyl-4phenyl-1,2,3,4-tetrahydropyridine (MPTP) induced death of dopaminergic substantia nigra cells in an adult mouse model of PD [380]. Protection of spinal motor neurons from cell death was also demonstrated both histologically and functionally in the G93A-SOD1 mouse model of ALS[381]. The fact that it is non-toxic, orally bioavailable and crosses the blood brain barrier, add to its appeal as a potential therapeutic agent.

The *in vivo* phenotypic screen by which the P7C3 compounds were discovered meant that further work was required to elucidate their mode of action. This involved triggering the death of human bone osteosarcoma epithelial (U2OS) cells using eight toxic compounds and testing whether P7C3-A20 could rescue cell death in any of these. In this way, doxorubicin toxicity was found to cause P7C3-A20 sensitive cell death. Doxorubicin is a commonly used chemotherapeutic agent that acts through multiple mechanisms, one of which involves reduction of NAD among other actions. NAD was partially restored in a concentration dependent manner by U2OS cell treatment with P7C3 enantiomers. A photocrosslinking approach followed by click chemistry with Alexa 532 dye then showed that P7C3 bound to NAMPT. Further analysis determined that P7C3 had NAMPT activating activity[336].

There is a conflict in the description of P7C3-A20 as a NAMPT activator, and FK866 as a NAMPT inhibitor, both being axon protective. This conflict has not been resolved. P7C3 derivatives have been demonstrated to be NAMPT activiting. However, additional mechanisms of action have not been explored and the notion that the apparent neuroprotective effects are mediated by this effect is not proven. Furthermore, investigation of P7C3 has been largely limited to *in vivo* murine work and in a U2OS cell line. A fuller understanding of the mechanistic understanding of P7C3 and its enantiomers can only be answered by *in vitro* study.

Aims

This chapters aims to explore whether the pharmacological agent P7C3-A20, can modify outcome following an axonal injury, and whether it functions via the WD pathway. Therefore, the aims of this chapter were to:

- Establish *in vitro* dosing thresholds for P7C3-A20 in various neuronal cultures
- Establish the efficacy of P7C3-A20 in maintaining NAD levels in a pure neuronal culture
- Determine the ability of P7C3-A20 to delay WD in different neuronal populations

Results

1. Establishment of maximum tolerated P7C3-A20 dosing in *in vitro* systems

P7C3-A20 dose finding in superior cervical ganglion explants

In order to select an appropriate concentration of P7C3-A20 (#2850, Biovision) for future *in vitro* experimentation we first assessed for toxicity over a wide concentrations range in SCGe (figure 24).

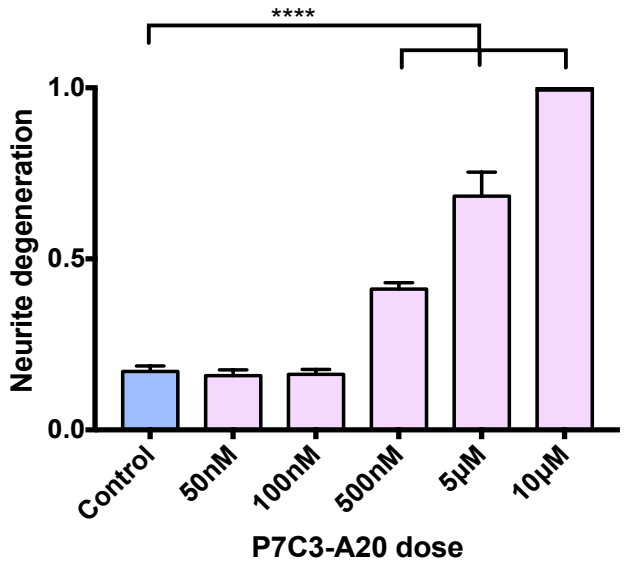

Figure 24. Non-toxic dose finding for P7C3-A20 in superior cervical ganglion explant cultures

Superior cervical ganglion explant cell cultures were exposed to various doses of P7C3-A20 in order to establish the maximum non-toxic dose as assessed by neurite degeneration 6 hours following dosing. n= 12 repeats. * = p≤ 0.05, ** = p≤ 0.01, *** = p≤ 0.001, **** = p≤ 0.0001, ns = non-significant (p>0.05). Error bars show SEM. Statistics: 1 way ANOVA.

Initial dose finding experiments showed no overt phenotypic change in cultures treated with P7C3-A20 at a concentration up to 100nm over a 24 hour period. At higher concentrations there was progressive neurite degeneration, and increased tendency for the neurites to detach from the culture dish. This finding that P7C3-A20 was markedly toxic to SCGe at the dosage range tested was unexpected because P7C3-A20 has been reported as having a wide therapeutic index *in vivo*[337].

Detachment is a relatively uncommon occurrence in carefully handled cultures except in severe, late stage degeneration. For example, it is not commonly seen in transected neurites or in toxic treatments with neurotoxic agents including doxorubicin– see later.

P7C3-A20 degeneration is not due to loss of axonal adhesion

It was unclear whether the levels of neurite degeneration witnessed were due to a direct toxic effect of P7C3-A20, or whether they were due to neurite detachment- as might have been seen with impairment of adhesion molecules. In order to separate these two factors, I developed a method of embedding SCGe ganglion in an extracellular matrix to prevent detachment without affecting degeneration. SCGe were found to be able to grow in a 3-dimensional Geltrex™ (Gibco, Invitrogen) extracellular matrix (ECM). Neurites grew throughout the ECM complex. Untreated SCGe remained healthy and intact in the ECM for over 1 week.

This allowed investigation of neurite degeneration without the confounding factor of detachment (figure 25).

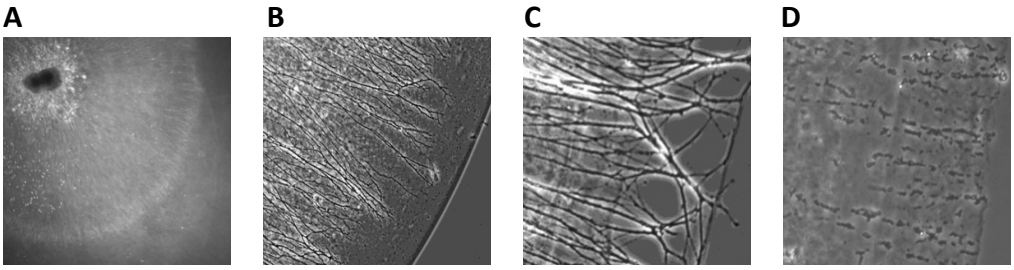

Figure 25. SCGd grow in a 3-dimensional extracellular matrix of Geltrex™ and this reduces detachment without affecting degeneration

Superior cervical ganglion cell explants were plated in 35mm Nunc™ dishes and given 24 hours to attach to a PLL/laminin coating. They were then coated in a Geltrex™ extracellular matrix. The SCGe extended healthy looking neurites throughout the extracellular matrix. Treatment with 10µM of P7C3-A20 caused rapid and complete degeneration within 4 hours. Healthy explant with neurites showing radial outgrowth at x4 magnification (A), x10 magnification (B), and x20 magnification (C). An example of a P7C3-A20 treated neurite that has degenerated but remains embedded in Geltrex™ is shown (D).

A P7C3 dose of 10µM showed rapid degeneration within 4 hours. Neurites were held within the ECM and so could be seen to completely fragment without any detachment.

P7C3-A20 induced degeneration proceeds rapidly in superior cervical ganglion explants

In order to investigate the rate of neurite degeneration due to toxic effects of P7C3-A20 the rate of degeneration was assessed using a treatment dose of 10mM (figure 26).

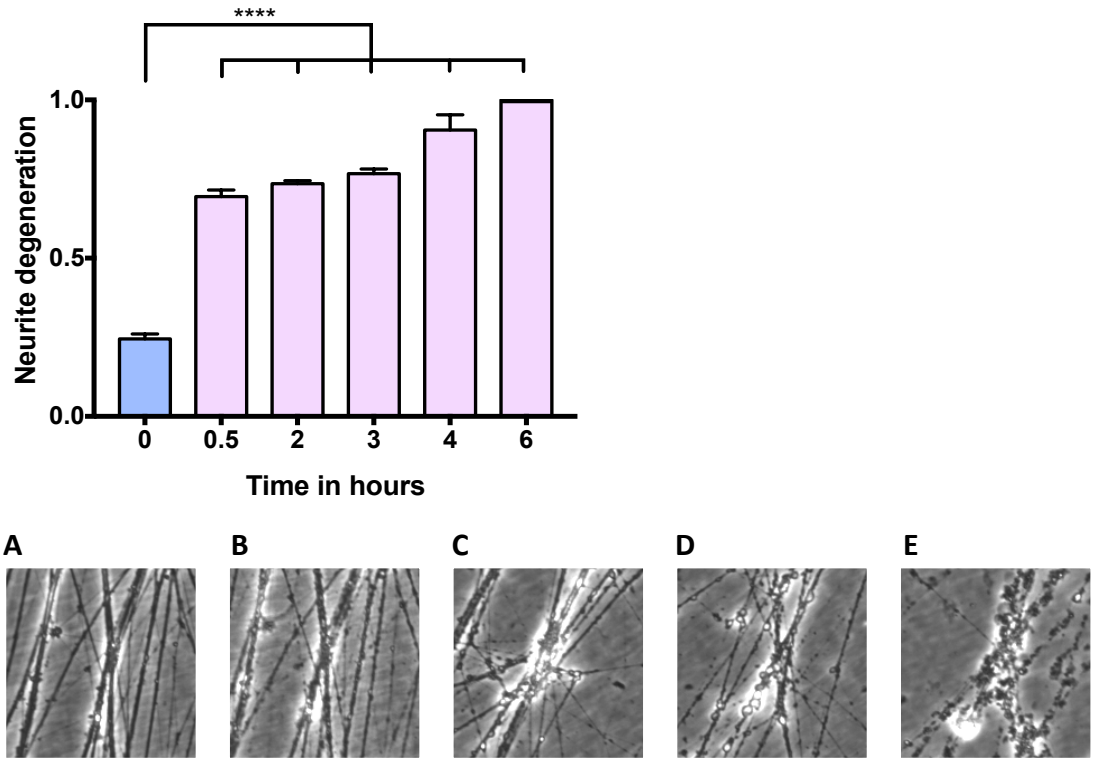

Figure 26. P7C3-A20 treatment of wild type SCGe leads to rapid neurite degeneration at high doses

Superior cervical ganglion cell explant cultures exposed 10µM of P7C3-A20 showed rapid degeneration. Representative images at different time points are shown in bottom panel– 0 hours (A), 30 minutes (B), 2 hours (C), 3 hours (D) and 4 hours (E). At 6 hours degeneration was complete. n= 3 repeats. * = p≤ 0.05, ** = p≤ 0.01, *** = p≤ 0.001, **** = p≤ 0.0001, ns = non-significant (p>0.05). Error bars show SEM. Statistics: 1 way ANOVA.

Within 30 minutes there was strong evidence of degeneration which was nearly complete by 4 hours. The rate of this degeneration was faster than seen with classic WD mediated axon degeneration.

P7C3-A20 dose finding in dissociated superior cervical ganglion cells

The neuronal cell bodies within cultures composed of SCG explants are adherent and closely apposed, and neurites form thick proximal bundles before becoming more segregated in the periphery. This is in contrast to a dissociated SCG culture where the cell bodies are often isolated or in clusters of a few cells, and neurites form an interweaving web. In order to determine whether P7C3-A20 dose finding was altered by these differences, levels of degeneration in response to drug exposure were examined in dissociated SCG cultures (figure 27).

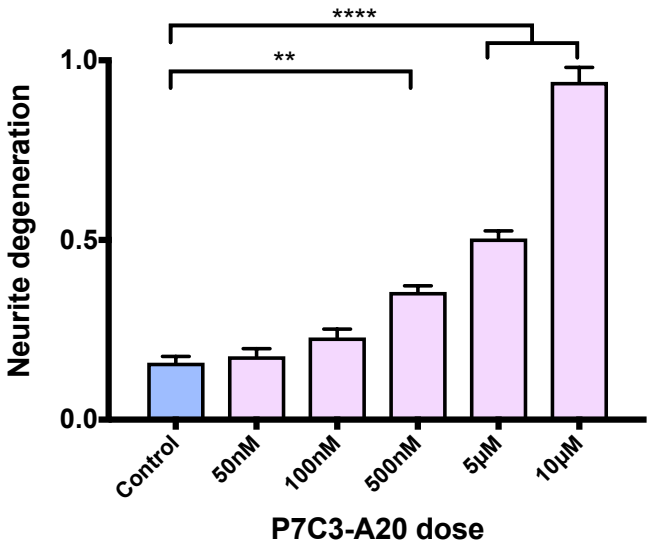

Figure 27. Non-toxic dose finding for P7C3-A20 in dissociated superior cervical ganglion cultures

Dissociated superior cervical ganglion cell cultures were exposed to various doses of P7C3-A20 in order to establish the maximum non-toxic dose as assessed by neurite degeneration 6 hours following dosing. n= 12 repeats. * = p≤ 0.05, ** = p≤ 0.01, *** = p≤ 0.001, **** = p≤ 0.0001, ns = non-significant (p>0.05). Error bars show SEM. Statistics: 1 way ANOVA.

Neurite degeneration was induced in response to various doses of P7C3-A20 at 24 hours in dissociated superior cervical ganglion cells. Toxicity rose at 500nM, a similar level to that seen in SCGe cultures.

P7C3-A20 dose finding in dissociated primary cortical neurons

Further investigation of the dosing range of P7C3-A20 in PCNd was undertaken with assessment made 4 hours following initiation of treatment (figure 28).

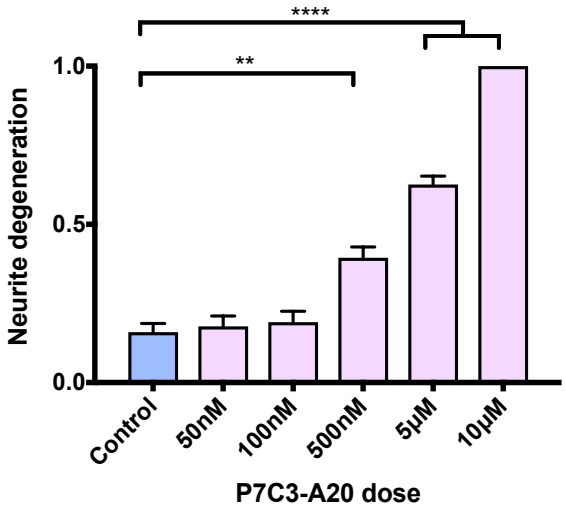

Figure 28. Non-toxic dose finding for P7C3-A20 in primary cortical neuronal cultures

Dissociated primary cortical neuronal cultures were exposed to various doses of P7C3-A20 in order to establish the maximum non-toxic dose as assessed by neurite degeneration 6 hours following dosing. n= 9 repeats. * = p≤ 0.05, ** = p≤ 0.01, *** = p≤ 0.001, **** = p≤ 0.0001, ns = non-significant (p>0.05). Error bars show SEM. Statistics: 1 way ANOVA.

Similarly to findings in SCGe and SCGd, PCNd treated with P7C3-A20 demonstrated a dose-related toxicity with neurite degeneration occurring at concentrations of 500nM and above.

2. P7C3-A20 toxicity is not dependent on the Wallerian degeneration pathway

P7C3-A20 toxicity is not due to NAMPT activation

It was theorized that the rapid profound neurite degeneration seen with P7C3-A20 treatment of 500nM and above might be due to activation of NAMPT driving an increase in NMN to a degree that overwhelms the activity of NMNAT and leads to an accumulation of NMN. The accumulation of NMN has been proposed as the initiating factor in WD. In order to determine if NAMPT over activation was the cause of P7C3-A20 induced neurite degeneration, SCGe were pretreated with either the non-competitive NAMPT inhibitor FK866 (100nM), or the competitive NAMPT inhibitor CHS828, before treating with P7C3-A20 (figure 29). If the degeneration were due the effects of selective NAMPT activation then this might be expected to prevent the degeneration.

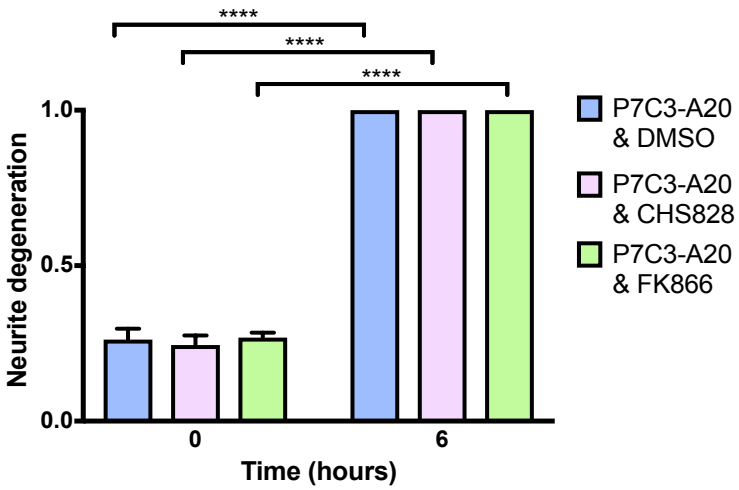

image continued on next page

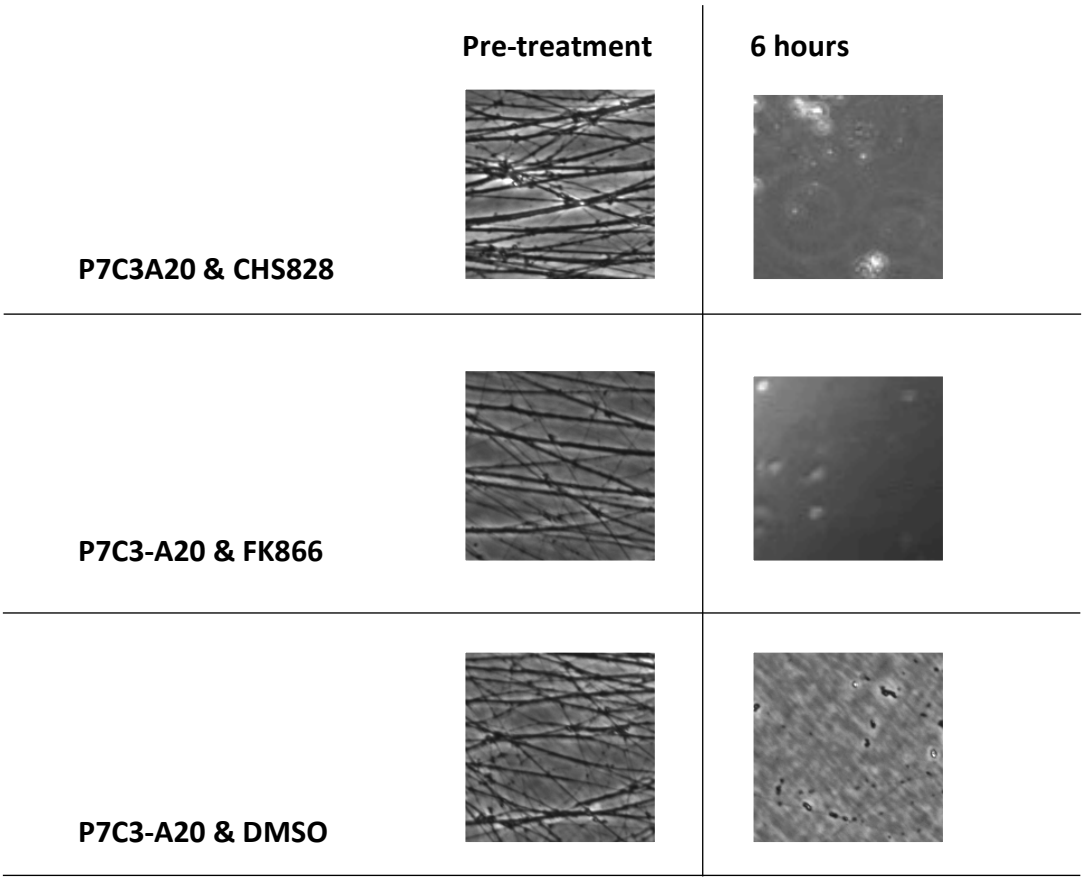

Figure 29. Pre-treatment with FK866 or CHS828 does not protect against P7C3-A20 induced degeneration

Superior cervical ganglion explant cultures were imaged then pretreated with either CHS828 (1µM), FK866 (100nM), or DMSO control for 1 hour before P7C3-A20 (10µM) was added. After 6 hours all conditions demonstrated complete neurite degeneration. Representative neurites before treatment, and 6 hours after pretreatment with CHS828 plus P7C3-A20, FK866 plus P7C3-A20, or DMSO plus P7C3-A20 alone. n= 6 repeats. * = p≤ 0.05, ** = p≤ 0.01, *** = p≤ 0.001, **** = p≤ 0.0001, ns = non-significant (p>0.05). Error bars show SEM. Statistics: 2 way ANOVA.

No protection against P7C3-A20 induced toxicity was seen with either FK866 or CHS828 pretreatment. The failure to protect against high dose P7C3–induced degeneration with a specific NAMPT inhibitor makes an off-target effect of P7C3 more likely in this context. It is also a possible that P7C3-A20 might displace FK866 and CHS 828 and negate their effects.

SARM1$^{-/-}$ mutation or expression of WLD^{s} in dissociated cortical neurons & superior cervical ganglion cultures did not protect against neurite degeneration induced by P7C3-A20

Although the previous experiment demonstrates that P7C3-A20 dosing at 10µM is not due to NAMPT activation it does not exclude that the toxic effects are WD mediated. Therefore, to investigate this possibility we examined the effects of this P7C3-A20 dosing on SARM1$^{-/-}$ and WLD^{s} cultures. These are two separate mutations that both delay WD by altering the normal WD pathway activation sequence. SCGe cultured from wild-type, transgenic SARM1$^{-/-}$, and WLD^{s} mice were treated with 10µM of P7C3-A20 and neurite degeneration measured 6 hours later (figure 30). If the degeneration was due to a WD process then we would expect SARM1$^{-/-}$ and WLD^{s} to protect against this.

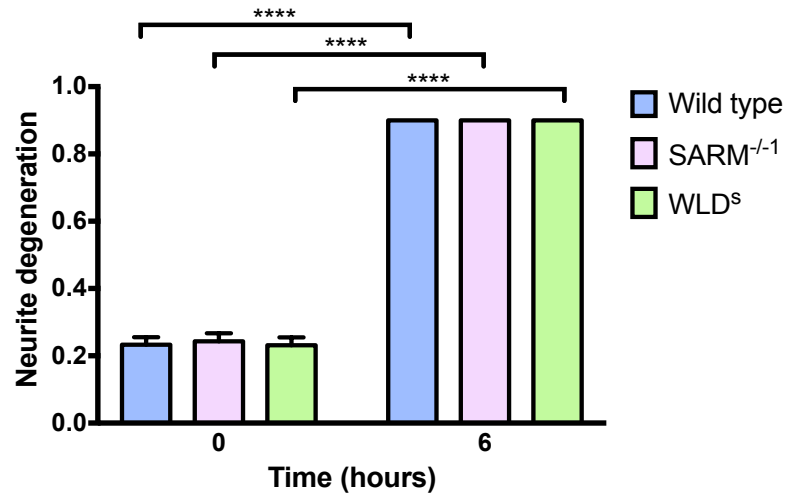

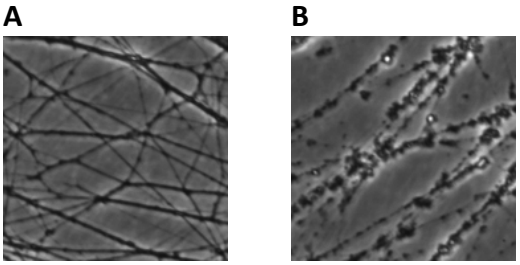

Figure 30. SARM1$^{-/-}$ and WLD^{s} do not delay P7C3-A20 induced degeneration in SCGe

Superior cervical ganglion cell explants were exposed to 10µM of P7C3-A20 at neurites assessed for degeneration 6 hours later in wild type, SARM1$^{-/-}$ and WLD^{s} cultures. A representative image of SARM1$^{-/-}$ neurites are show before P7C3-A20 treatment (A), and 6 hours later (B). n= 9 repeats. * = p≤ 0.05, ** = p≤ 0.01, *** = p≤ 0.001, **** = p≤ 0.0001, ns = non-significant (p>0.05). Error bars show SEM. Statistics: Student T test.

In all conditions there was complete neurite degeneration and subsequent detachment of the cells with no protection afforded by SARM1$^{-/-}$ or WLD^{s} at 6 hours. This suggests that the mechanism of degeneration seen was an off-target effect that was not WD dependent. The mechanism mediating the degeneration is unknown but could be via apoptosis as the time course is rapid and we know that SARM1$^{-/-}$ does not protect against this mechanism of cell death[104].

3. P7C3-A20 has differing NAD synthetic activity in different neuronal populations

Doxorubicin induced NAD suppression is partially rescued in some neuronal subtypes but not others

Previous reports demonstrated that P7C3 was able to rescue NAD depletion caused by doxorubicin toxicity in a U2OS human bone osteosarcoma cell line[336]. In order to establish if this effect was preserved in neuronal subclasses of cells we treated SCGe and PNCd with 0.5µM of doxorubicin, with or without prior pre-incubation with P7C3-A20 for 2 hours. The dose selected for P7C3-A20 was 100nM, this was the maximum that did not cause significant neurite degeneration in earlier dose finding experiments. The dose selected for doxorubicin was 0.5µM, this was based on the toxicity curves produced by Wang *et al* [336]. We then assessed NAD levels 72 hours after the doxorubixin treatment using the Promega NAD/NADH-Glo™ luciferin based NAD assay (figure 31).

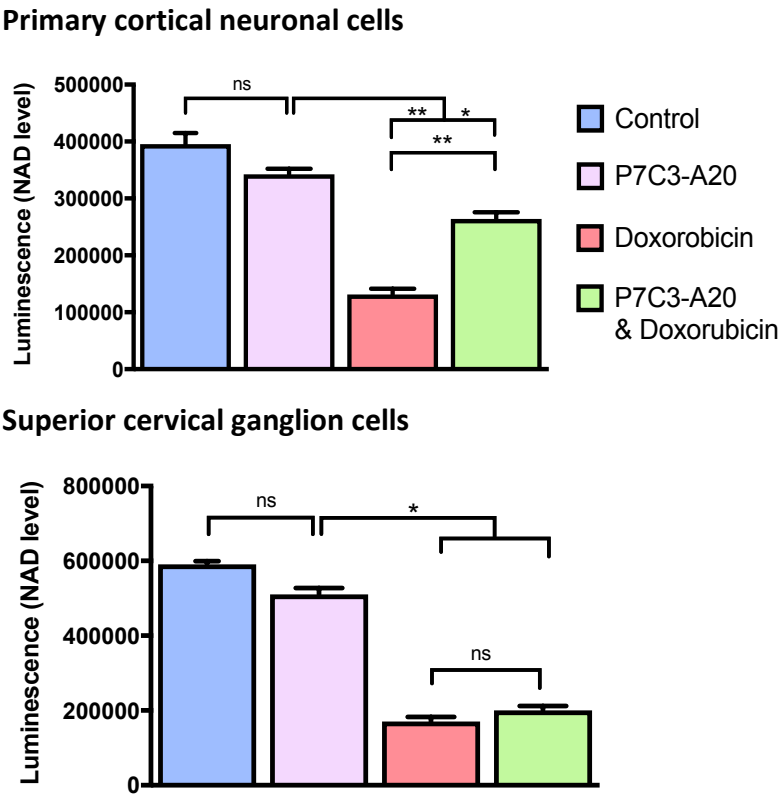

Figure 31. Doxorubicin induces NAD depletion, which is rescued by P7C3-A20 in some primary cortical but not superior cervical neurons

Doxorubicin treatment of dissociated superior cervical ganglion cells and dissociated primary cortical neuronal cells caused a fall in NAD levels in each case. A 2 hour pre-incubation with P7C3-A20 partially

rescued this NAD depletion in the primary cortical neuronal cultures but not the superior cervical ganglion cultures. n= 9 repeats. * = p≤ 0.05, ** = p≤ 0.01, *** = p≤ 0.001, **** = p≤ 0.0001, ns = non-significant (p>0.05). Error bars show SEM. Statistics: 2 way ANOVA.

We tested whether P7C3-A20 was able to rescue doxorubicin induce NAD depletion in a variety of neuronal types as the original report was exclusively performed in U2OS cells[336]. Although these cells convenient because they are fast growing and have high transfection efficiencies, they are a cancer cell like that is not of neuronal origin. Therefore, assumptions about *in vivo* activity based on findings in these cells should be made with caution.

Doxorubicin is a DNA-damaging chemotherapeutic antibiotic agent commonly used to treat several cancers including leukaemias and solid tumours. Doxorubicin at 0.5µM concentration has previously been shown to reduce NAD levels in U2OS cells to less than 35% of baseline with an almost complete cell death at 72 hours. These cells were rescued by addition of an active enantiomer of P7C3 (P7C3-A20) with an increase in cell survival of around 40% following 2 hours of pre-treatment with 5µM concentration of P7C3-A20[336].

Doxorubicin-treated PNC and SCGe cultures showed a significant depletion in NAD levels as measured by Promega NAD/NADH-Glo™ luciferin based NAD assay. When doxorubicin-exposed cells were pre-incubated with P7C3-A20 for 2 hours there was a partial rescue in NAD levels in PCNd cultures. However, there was no rescue the NAD level in SCGd. The failure of P7C3-A20 to rescue the doxorubicin induced NAD depletion in SCGd suggests that its NAMPT activity may not be equally conserved across all neuronal cell types.

Doxorubicin causes neurite degeneration but this is not due to a Wallerian degeneration dependent mechanism

Doxorubicin was used by Wang *et al* as an NAD depleting agent. Their demonstration that NAD levels were rescued in U2OS cells was used as evidence that this was the mechanism of action underlying enhanced neuronal survival in an *in vivo* TBI model [336,337]. However, doxorubicin is a drug with multiple cellular actions [382,383]. NAD depletion is only one of these actions, and given that the effects of P7C3-A20 are not fully characterized it does not follow that any enhanced neuronal survival is necessarily due to NAMPT activation and NAD maintenance. In

order to test whether doxorubicin toxicity at 0.5µM caused WD we firstly assessed if it induced neurite degeneration – an expected consequence of NAD depletion. Then we tested whether doxorubicin's actions could be rescued by SARM1$^{-/-}$ and hence a WD dependent mechanism (figure 32).

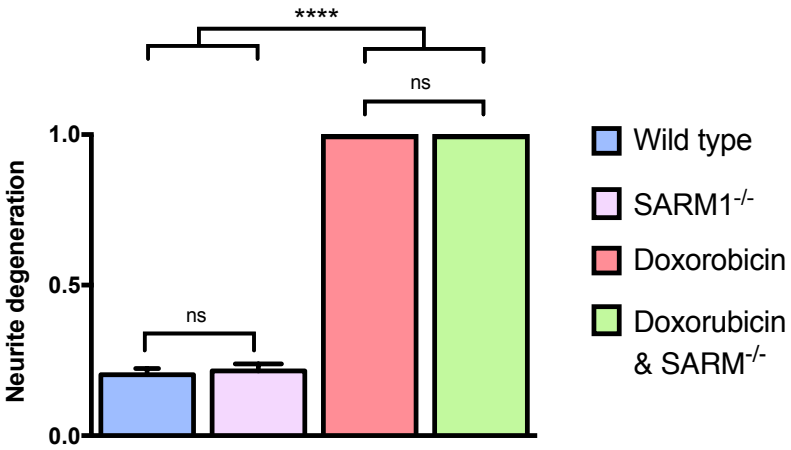

Figure 32. SARM1$^{-/-}$ does not protect against doxorubicin mediated toxicity

Wild type and SARM$^{-/-}$ superior cervical ganglion explants were treated with doxorubicin 0.5µM which caused complete neurite degeneration at 24 hours in both cases. This was not rescued by SARM1$^{-/-}$. n= 9 repeats. * = p≤ 0.05, ** = p≤ 0.01, *** = p≤ 0.001, **** = p≤ 0.0001, ns = non-significant (p>0.05). Error bars show SEM. Statistics: Student T test.

Treatment of SCGes with doxorubicin 0.5µM caused complete degeneration of neurites in wild type and SARM1$^{-/-}$ cultures. This suggest that doxorubicin mediated neuronal death occurs through a death pathway that is not SARM1 dependent and hence by definition is not WD. Although a depletion of NAD can trigger axon degeneration through the Wallerian pathway, as has been demonstrated with a NAMPT block by FK866, this would not occur within the 24 hour time frame seen in this case.

4. P7C3-A20 does not delay Wallerian degeneration

P7C3-A20 failed to delay Wallerian degeneration in superior cervical ganglion cells following transection

I assessed whether P7C3-A20 was capable of delaying WD in SCGe induced by sharp transection of neurites. The neurites were pre-treated with P7C3-A20 or DMSO control 1 hour prior to transection, or treated with P7C3-A20 at the time of cut. Imaging of neurite degeneration rates were then assessed 6 hours after transection (figure 33).

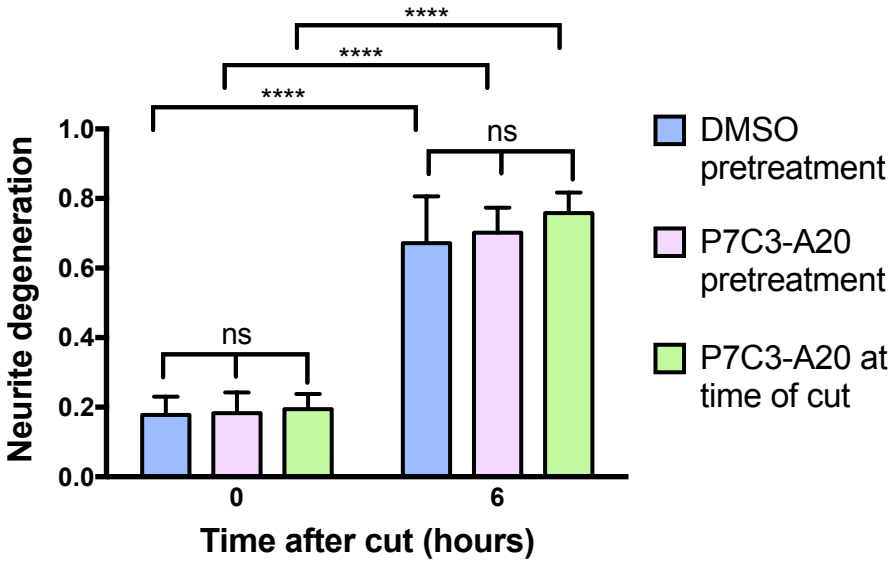

Image continued on next page

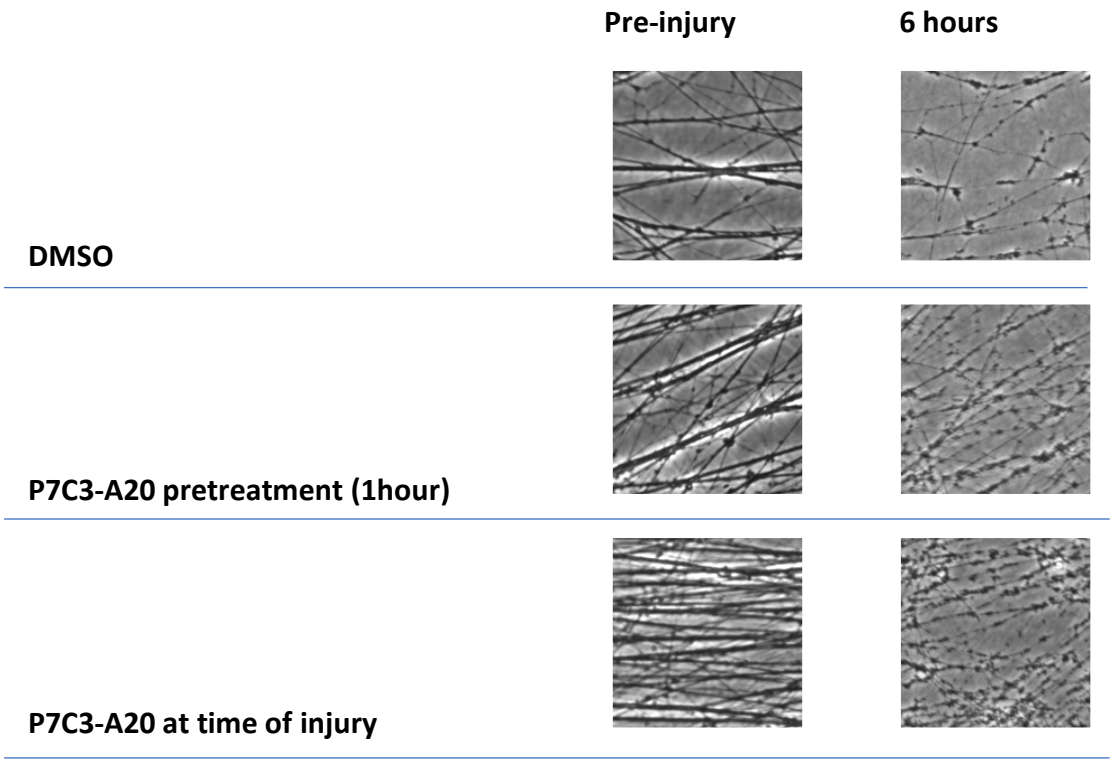

Figure 33. P7C3-A20 does not delay Wallerian degeneration in superior cervical ganglion cell cultures following transection

There was a comparable degree of degeneration at 6 hours post transection in P7C3-A20 and DMSO control pre-treated SCG cultures, and those treated with P7C3-A20 at the time of cut. Representative images show neurites pre-injury and 6 hours post injury. Shown are DMSO pretreatment (top), P7C3-A20 pretreatment (middle), and P7C3-A20 treatment given at time of injury (bottom). n= 8 repeats. * = p≤ 0.05, ** = p≤ 0.01, *** = p≤ 0.001, **** = p≤ 0.0001, ns = non-significant (p>0.05). Error bars show SEM. Statistics: Student T test.

SCGe treated or pre-treated with P7C3-A20 showed identical degeneration rates to DMSO controls treated SCGs at a 6 hour time point. This demonstrates that P7C3-A20 was incapable of delaying WD due to a transection in murine *in vitro* cultures from superior cervical ganglion cells.

P7C3-A20 failed to delay axon degeneration in superior cervical ganglion cells following stretch injury

In order to test if P7C3-A20 would affect the rate of degeneration following stretch injury it was administered to neurites 1 hour prior to stretch injury of the cultures. The stretch injury was administered using the stretch injury device described in chapter 4. All parameters of stretch were standardized with application of vertical deflection of 6mm, equivalent to a strain of ~20% at a strain rate of $7.5s^{-1}$ (figure 34).

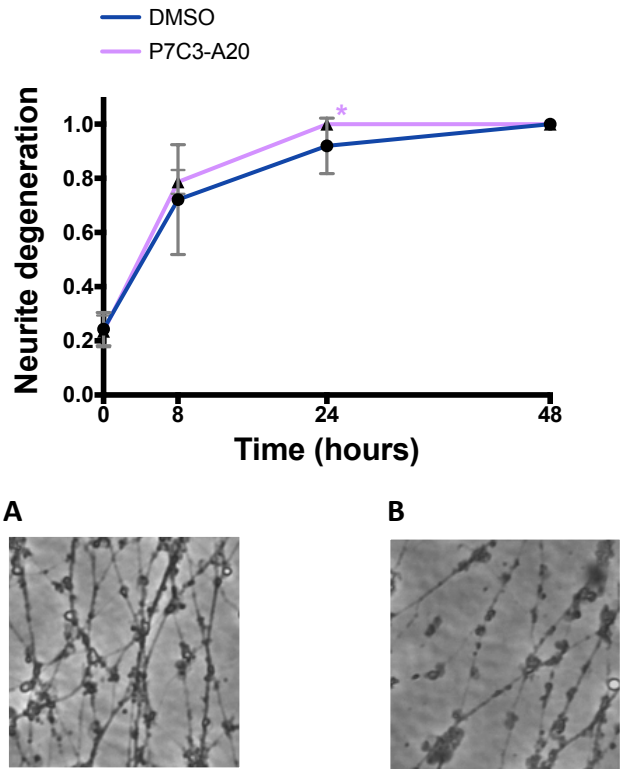

Figure 34. P7C3-A20 is associated with a small acceleration of neurite degeneration following stretch

One hour pre-treatment of wild type SCGe neurites with 100nM of the NAMPT activator P7C3-A20 was associated with a small mean increase in the rate of neurite degeneration in SCGe cultures at 24 hours compared to control SCGe treated with DMSO alone. Representative neurites are shown 8 hours post stretch in the following conditions, DMSO-control (A) and P7C3-A20 treated cultures (B). n = 9 repeats. * = p≤ 0.05, ** = p≤ 0.01, *** = p≤ 0.001, **** = p≤ 0.0001, ns = non-significant (p>0.05). Error bars show SD. Statistics: 1 way ANOVA.

Wild-type cultures pre-treated with P7C3-A20 at 100nM underwent neurite degeneration at a comparative rate to DMSO-control treated culture. There was a small statistically significant excess burden of premature neurite degeneration at 24 hours, with all conditions completely

degenerated by 48 hours. Although small, this difference may suggest that P7C3-A20 could have the potential to accelerate neurite degeneration, particularly in cases where NMN accumulation could be potentiated, for example in situations where NMNAT2 activity is reduced or an individual has low levels of expression.

P7C3-A20 failed to delay Wallerian degeneration induced by vincristine in primary cortical neurons

We have demonstrated that P7C3-A20 does not delay WD in SCGe cultures. However, it does not necessarily follow that this is the case for all neuronal subpopulations. Indeed, a partial rescue of doxorubicin-induced depletion in NAD by P7C3-A20 treatment was found in PCNd but not SCGe. Therefore, it is necessary to assess the effects of P7C3-A20 in cortical cultures if we wish a true representation of CNS effects in an *in vitro* murine model. In dissociated PCN cultures, neurite length and growth patterns make their physical transection difficult and unreliable without the use of more advance techniques like laser-transection. Also, assessment of neurite degeneration in such instances requires manual assessment as the automated Image J plugin requires a larger field to be effective. In order to overcome this WD was chemically induced with a 10nM dose of vincristine. Vincristine is a vinca alkaloid chemotherapeutic drug that causes a length dependent axon degeneration[384]. Vincristine induced axon degeneration through the WD pathways that can be delayed by WLD^{s} or $SARM1^{-/-}$ [133,385,386]. Hence, vincristine is an example of an exogenous pharmacological agent that can be used to trigger WD of an axon without the requirement for a physical injury. This is thought to occur through inhibition of axonal transport. Neurite degeneration induced by vincristine activates the WD pathway as evidenced by the capacity of WLD^{s} or $SARM1^{-/-}$ to delay degeneration[133,386]. PCNd were pretreated with either DMSO control or P7C3-A20 1 hour prior to vincristine treatment, or co-treated with P7C3-A20 and vincristine together. Neurite degeneration was then assessed 24 hours later (figure 35).

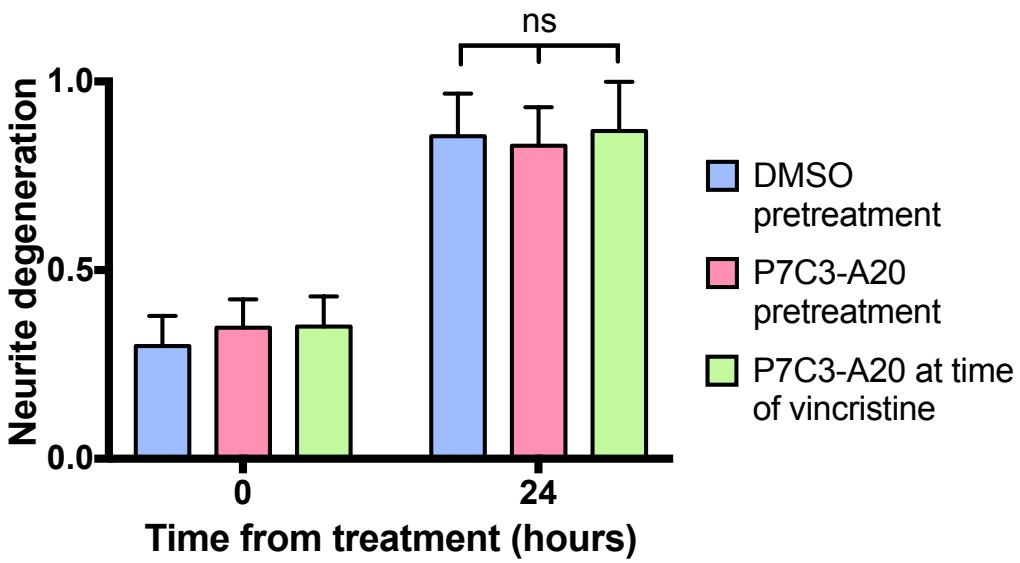

Figure 35. P7C3-A20 failed to prevent Wallerian degeneration initiated by vincristine

Dissociated primary cortical neurons were assessed for neurite degeneration 24 hours after vincristine administration in cultures pre-treated for one hour with P7C3-A20 or DMSO, and in cultures co-treated with vincristine and P7C3-A20. Representative images show neurites pre-vincristine treatment (left) and 24 hours post-vincristine (right). Shown are DMSO pretreatment (top), P7C3-A20 pretreatment (middle), and P7C3-A20 treatment given at time of vincristine dosing (bottom). n= 8 repeats. * = p≤ 0.05, ** = p≤ 0.01, *** = p≤ 0.001, **** = p≤ 0.0001, ns = non-significant (p>0.05). Error bars show SEM. Statistics: 2 way ANOVA.

In dispersed PCN cultures, neurite length and growth patterns make their physical transection unreliable, so WD was induced with a 10nM concentration of vincristine. Unlike WLD^{s} and $SARM1^{-/-}$, P7C3-A20 failed to prevent neurite degeneration due to vincristine regardless of dosage and timing[133,386].

Discussion

P7C3 and its active derivatives including P7C3-A20 have shown promise in various animal models of neurological disease, including TBI, chronic visual deficits, PD, and ALS[378–381]. P7C3 has also been suggested as a possible therapeutic agent for other neurodegenerative diseases including AD, and as a guardian of cognitive capacity in aging[335,374]. In order to progress from animal models to human trials it is important to have a thorough understanding of the mechanistic effects of a drug. The experiments outlined in this chapter were undertaken to further characterize the mechanism of P7C3-A20 action, and to explore the proposition that its effects are due to NAMPT activation leading to protection against Wallerian degeneration.

P7C3-A20 has previous been demonstrated to increase NAD levels in U2OS cells. However, we found its ability to maintain NAD in the face of doxorubicin administration was incomplete and was only partially effective in some cell types. Furthermore, no protection against Wallerian degeneration was found in any cell type, regardless of whether the injury was physical transection or by vincristine. The compound P7C3-A20 was found to cause a small excess burden of degeneration at 24 hours following stretch injury. This finding conflict with *in vivo* reports of P7C3-A20s neuroprotective effects, but it is consistent with FK866 findings that indicate an NMN dependent mechanism of WD axon degeneration in this model. The reasons for the differences in P7C3-A20 action *in vivo* and *in vitro* warrant further investigation.

Our findings did not support a proposed mechanism of P7C3-A20 as a NAMPT activator, and in particular we found no evidence that it could protect by modulating Wallerian degeneration. This suggests that the mechanism of action of P7C3-A20 is still unknown and needs further investigation. Its failure to protect against WD suggests that it might not be an appropriate agent to treat diseases that have a major WD component, for example, chemotherapy-induced and chronic inflammatory peripheral neuropathy, glaucoma and some forms of hereditary motor sensory neuropathy, unless other mechanistic effects are found with further research.

An additional unexpected finding was the concentration-related toxicity of P7C3-A20. It has previously been reported in rodent models to have a wide-therapeutic index[336]. In this study we found that there was marked concentration dependent toxicity in both SCG and PCN cell types. When considering the possible reasons for the unexpected degeneration seen with high-dose P7C3 we hypothesized that it might be due to triggering of the WD pathway by supra-physiological NAMPT activation leading to NMN accumulation. In normal circumstances NAMPT is the rate-limiting enzyme and excess NMN is harmlessly shuttled into NAD. However, potentially a large rise in NAMPT activation could overwhelm this pathway with endogenous NMN production, leading to high levels of NMN that have been implicated in triggering of WD. However, the failure of FK866 and CH828 to protect against degeneration suggest that an alternative mechanism must be the cause. Likewise, the failure of WLD^{s} and $SARM1^{-/-}$ mutations to protect against P7C3-A20 induced neurite degeneration suggests it is not due to NAMPT over-activation and is likely due to a mechanism independent of WD. This toxicity needs to be better understood, mechanistically in an *in vitro* setting, and in the design of any human clinical trials.

Summary

The anti-apoptotic, neuro-protective agent P7C3-A20 caused neurite degeneration at concentrations of 500nM or greater in SCGd, SCGe, and PCNd. At concentrations of 100nM P7C3-A20 was able to partially rescue doxorubicin induced NAD depletion in PNCd, but not in SCGe. P7C3-A20 failed to delay WD induced by transection in SCGe, or by vincristine in dissociated PNC. These findings are important in understanding the consequences of exposing neurons to various concentrations of P7C3-A20, and identifying the mechanisms by which the compound exerts its action. Additional investigation of the mechanistic action of P7C3-A20, and its potential toxicity, is required to build the necessary foundation for potential human studies.

Next steps

In order to address some of the limitation inherent in a pure neuronal *in vitro* culture systems, and allow to study the effects of a stretch injury on a mixed CNS cellular culture, we next pursued the development of an TBI stretch-injury model using organotypic hippocampal slice cultures.

Chapter 6

Development of an organotypic hippocampal slice model of stretch injury

Introduction

1. The requirement for an organotypic model of stretch injury

Animal and cellular models of disease are necessary due to practical experimental and ethical restrictions inherent in studying a pathology directly in humans. In human patients who experience a TBI we have the opportunity to undertake limited contemporaneous and retrospective data collection (table 13).

Category of data
Tissue (including tissue substrates for biomarkers)
Cerebrospinal fluid
Microdiasylate
Serum
Brain
Neuroimaging
Structural
Functional
Metabolic
Neurocritical care and general medical parameters
Physiological markers including neuromonitoring and biochemical markers of organ dysfunction
Psychology
Behavioural/functional measures
Neuropsychology
Biomechanical
Video recordings, personal accelerometers, vehicle impact monitoring systems
Post mortem
Tissue histology
Structural imaging

Table 13. Sources of experimental data relating to TBI in human subjects

However, in order to undertake interventional studies in humans, it is generally agreed that a degree of experimental work must already exists in cellular or animal models to suggest the intervention may have a favorable cost/benefit ratio, or at least that equipoise exists in this regard. These models also provide the experimental systems necessary for much of the basic science experimentation to elucidate mechanistic information, for example, surrounding secondary brain injury.

Chapter 4 explored the development, calibration and utilization of a primary neuronal stretch system. While this system has numerous advantages as discussed in the thesis introduction and chapter 4, it also has several limitations when compared to an *in vivo* system, not least an extremely simplified model that lacks non-neuronal cell types. Organotypic hippocampal slices (OHS) provide an intermediate between primary neuronal cultures and an *in vivo* system. They provide some of the benefits of both *in vivo* and *in vitro* system – these benefits, and a comparison to a pure neuronal culture system are outlined below (table 14).

	Pure neuronal cultures	Organotypic slice cultures
Advantages	Simple system with well-characterized responses including neurite degeneration	Contains multiple cell types including astrocytes and microglia
	Robust protocols with highly standardized cultures	Some preservation of tissue architecture and electrophysiological responses and neuronal networks
		Allows longer term culturing (6-8 weeks)
		Easily accessible culture supernatant
Disadvantages	Lacks non-neuronal cells	Variable imaging quality depending on slice thickness and membrane auto-florescence
	Cultures generally can only be used maximum of 1-2 weeks	Some variability in individual slices

Table 14. Advantages and disadvantages of primary neuronal culture and organotypic culture based systems

Both pure neuronal cultures and an OHS system also allow experimental manipulation of the extracellular environment, repeated live cell imaging/ multiple timepoint analysis, and access to the culture supernatant[387]

Organotypic hippocampal slice cell culture techniques have been used in one of my supervisor's laboratories (Professor Michael Coleman) by Dr Claire Harwell using an adapted 'interface method' based on the methods of De Simoni and Gogolla (figure 36)[323,324].

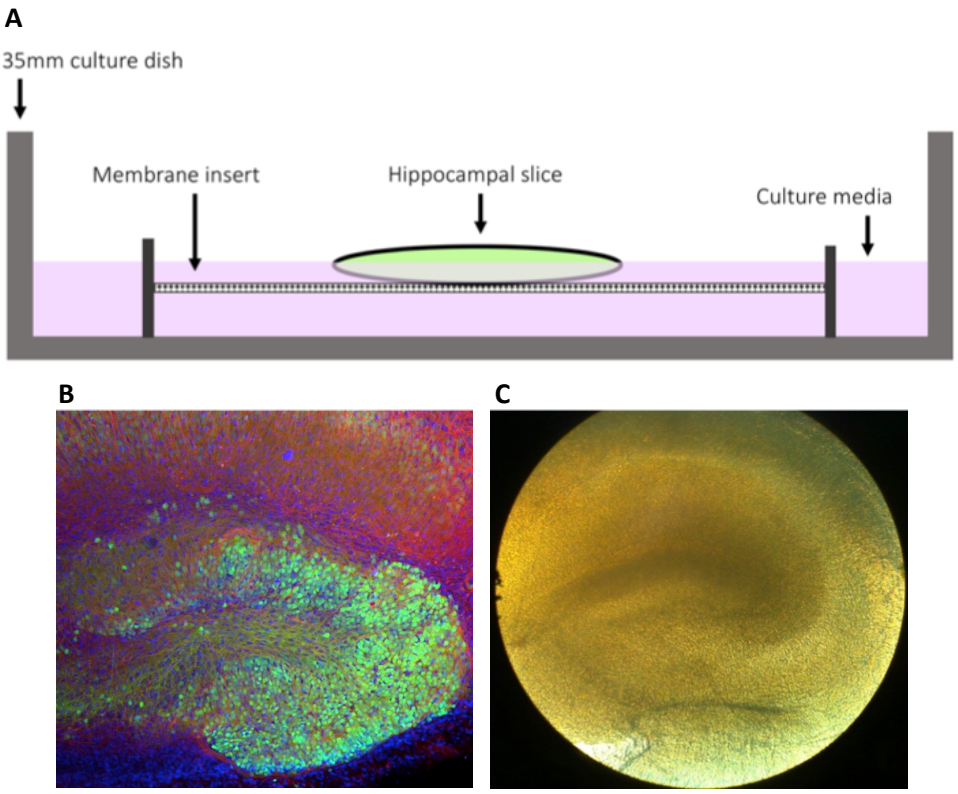

Figure 36. Interface organotypic hippocampal slice culture system

This schematic diagram shows the key components of the organotypic hippocampal slice culture interface method system, including a representation of how the brain slice is bathed in media that permeates the membrane insert allowing oxygenation from above and hydration and nutrition from media below (A). The next image shows calmodulin green staining that highlights the cells of the dentate gyrus within a 2 week old hippocampus (B)- t*this image was provided by Dr Claire Harwell, University of Cambridge*. At 6 weeks the hippocampal slice still maintains much of its existing architecture and remains reminiscent of early brightfield images from an acute 7 day old slice (C).

The development and usage of these cultures for physical injury experimentation had not been previously performed by our group. Although axonal stretch and organotypic slice stretch injury devices have been developed and employed in TBI research previously (see chapter 1 for details) none were in use at the University of Cambridge at the time of this thesis.

Aims

The decision to develop an OHS stretch model was based primarily upon the need for a model that could allow *in vitro* assessment of injury responses that depend upon, or are modulated, by a mixed cellular CNS population. Certain questions, particularly those relating to the interaction of inflammatory cytokines, amyloid and modulators of WD cannot be answered in a pure neuronal culture model.

Consequently, the aims of this chapter were to:

- Modify the stretch injury device developed in chapter 4 for use with OHS cultures
- Calibrate and validate the injury model in organotypic hippocampal slices
- Establish effects of stretch injury on amyloid responses and explore influence of inflammatory cytokines on markers of physical injury

Results

1. Establishing organotypic hippocampal slice cultures on a suitable substrate for injury

Cell culture membrane development

As with primary neuronal cultures, the ideal substrate for an OHS would be one that allows high levels of elasticity and a high elasticity limit with resistance to tearing, is thin, optically transparent, and it is resistant to tearing and thermal changes, and is semipermeable to gases. Unlike primary cortical cells an OHS cannot be submerged in media without rapid and widespread death. This is thought to be due to inadequate oxygenation. Given the suitability of silicone to fulfil these requirements, initial culture of OHS on a silicone membrane was attempted. However, they consistently demonstrated poor attachment and viability despite numerous modifications to improve culture conditions. These included, altering membrane coating (PLL, PDL, PO, Geltrex™, Matrigel™), variations of within-incubator rocker systems to improve oxygenation including orbital rocking, different age pups, and different membrane substrates including polyacrylamide/alginate hybrid gels developed in conjunction with the Oyen lab and based on the protocol of Yang *et al*[388]. Despite these adaptations consistent healthy OHS cultures were difficult to obtain. This is in contrast to when the interface method was used[323,324]. This involves culturing OHS on PTFE membranes. In this system, long-term viability of cultures up to 6 weeks or more can be successful generated. These membranes have a number of advantages over silicone for culturing including a porous surface for cellular adhesion and high permeability for gas exchange – this facilitates the formation of a thin meniscus of media over the OHS and hence ensures adequate hydration and maximizes gas exchange[323,324]. Therefore, given the inability to reliably culture OHS on alternative substrates the PTFE membranes were used.

Biopore membrane inserts (#PICM030, Merck) are constructed of 0.4µM PTFE. They are highly permeable to gas therefore it was necessary to place a thin, highly elastic, silicone membrane of 125µM thickness underneath the Millipore membrane immediately prior to stretch to prevent airflow through the membrane. This ensured any tissue damage was due to cellular stretch as opposed to the impulse of air. The maximal membrane deformation achieved with a driving pressure of 60 psi was 6mm. This occurred in a similar time frame to the silicone

membrane and it was therefore possible to estimate the degree of strain, and strain rate would be similar. An adjustment to the piston position aimed at increasing the vertical deformation, and hence strain, resulted in no further appreciable stretch. This was felt to be due to the PTFE membrane reaching its elastic limit – when greater forces were applied manually the membrane tended to yield further but only with irreversible deformation and then subsequent failure. No membrane failures were seen with either the silicone or Biopore membranes in over 200 deformations with a driving pressure of 60 psi or less.

2. Calibration for organotypic hippocampal slice membranes

Cellular death due to application of stretch impulse

Assessment of the effects of the stretch system on OHS cultures included PI staining to demonstrate the extent to which a calibrated stretch injury induced cellular death. This was initially performed in healthy wild-type OHS cultures to quantify stretch effects (figure 37).

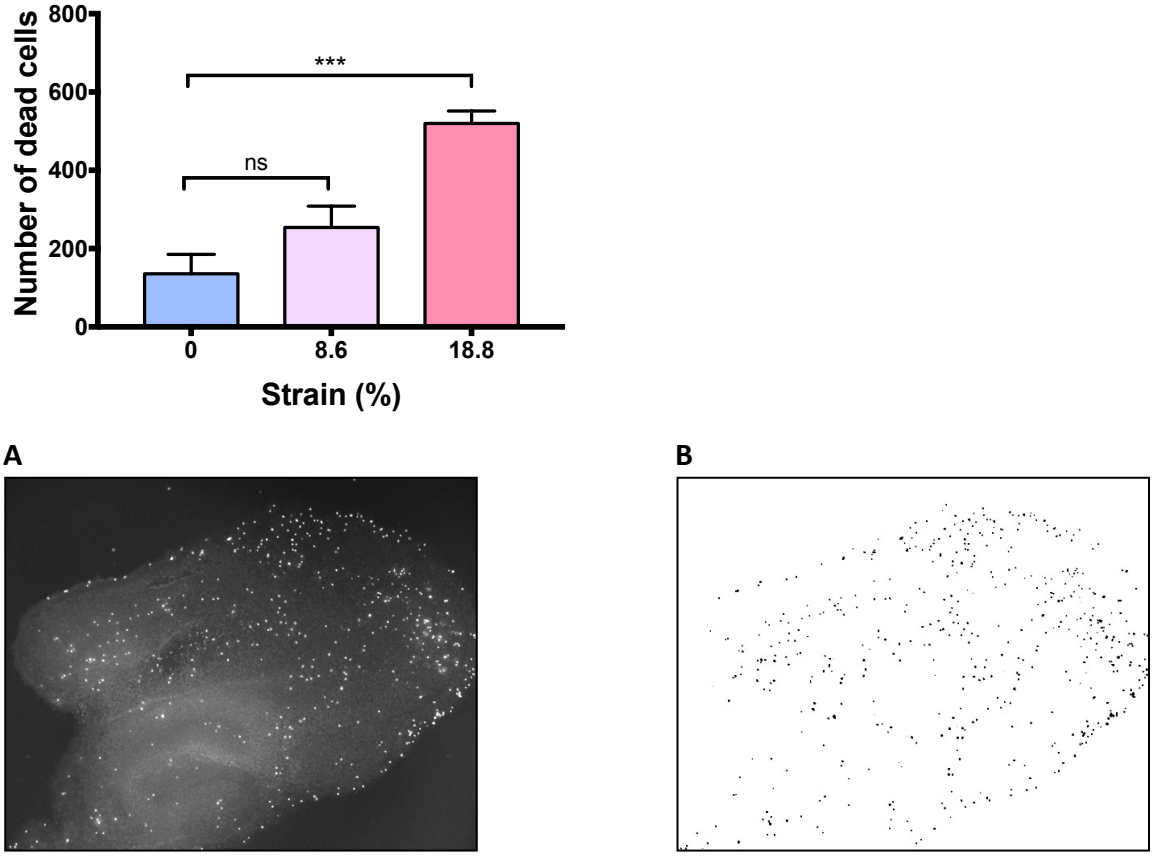

Figure 37. Stretch injury causes strain dependent cellular death

Stretch injury causes strain dependent cellular death in organotypic hippocampal slice cultures at 24 hours as assessed by PI staining. PI staining of injured organotypic hippocampal slices is shown (A) along with corresponding automated particle analysis by Image J (B). (n = 5 per condition. * = p≤ 0.05, ** = p≤ 0.01, *** = p≤ 0.001, **** = p≤ 0.0001, ns = non-significant (p>0.05). Error bars show SEM. Statistics: Student's T test.

A stretch injury with 8.6% strain did not produce a significant increase in cellular death, but at 18.8% strain there was a significant excess burden of cellular death at 24 hours.

Direct assessment of neurite injury with immunohistochemistry

Direct assessment of axonal damage following stretch injury in the OHS system was trialed with immunohistological staining for APP (figure 38).

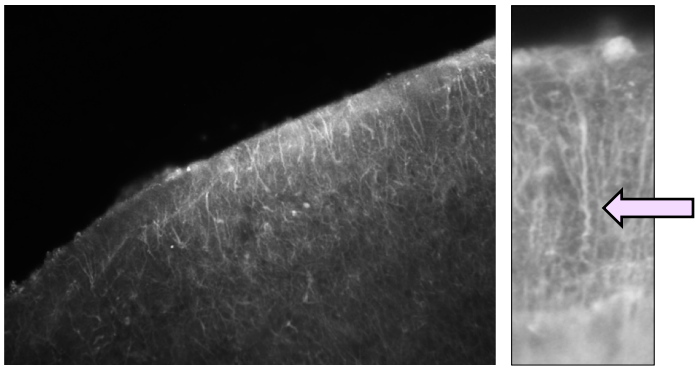

Figure 38. APP labelled apical neurites in a organotypic hippocampal slice showing undulations following stretch injury

Immunohistochemical straining with a mouse anti-APP antibody demonstrates apical neurites at the peripheral boundary of an organotypic hippocampal slice culture. An undulating neurite is highlighted following stretch injury (arrow).

Immunostaining with axonal markers– βIII tubulin and APP– resulted in widespread fluorescent signal of high intensity throughout the OHS despite protocol optimization. This did not allow individual axon resolution and hence meaningful analysis. This was the case throughout the main parenchyma of the OHS. At the periphery of the OHS apical neurites could sometimes be individually resolved including occasional undulations following stretch. However, fluorescent quantification in this region was also variable and did not appear to be a reliable method of assessing injury.

Transfection

In order to directly visualize individual neurons and quantify damage in their neurites following a stretch injury a number of live cell-labelling methods were used including magnetofection and BacMam baculovirus (Cell Lights) transfection (figure 39). Despite attempts to optimize protocols, including varying age at transfection and culture reagents, the transfection efficacy in neurons remained poor with inconsistencies in the transfection rate, neuronal subtype labelled, and anatomical location of labelled neurons. Transfection was also non-specific with high rates of glial cell labelling frequently seen. These barriers prevented

reliable quantification of axonal injury with this method. There are reports of successful gene-gun biolistic transfection but this technique was not available in our laboratory at the time of these experiments[389].

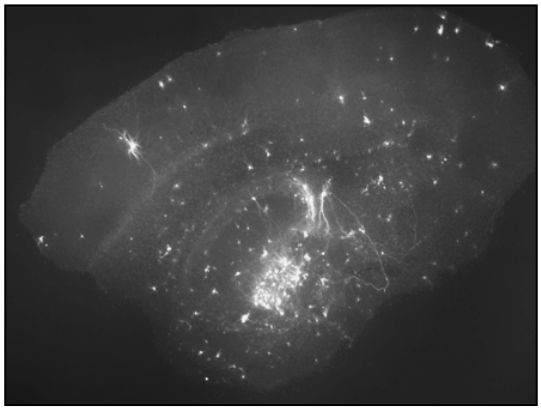

Figure 39. Transfection of organotypic hippocampal slices inconsistently labelled a mixture of cell types

Transfection of organotypic hippocampal slice cultures tended to label glial cells and occasional neurons in an inconsistent manner.

Neurofilament measurement

Neurofilaments are one of the primary cytoskeletal structural protein found in neurons. They consist of three polymeric proteins, neurofilament light (NFL, 68kDa), neurofilaments medium (NFM, 150kDa), and neurofilaments heavy (NFH, 200kDa). Each share similar rod domains but sidearms vary[390,391]. NFH has been used as a biomarker of axonal injury in traumatic brain injury, and various other neurodegenerative disorders including MS and ALS, usually measured by ELISA of CSF or serum[250,390,392–395]. In order to assess the extent of axonal injury induced by the stretch injury a NFH ELISA was used to assess levels in media supernatant of injured cultures. The use of ELISA for analysis of protein levels in OHS culture supernatant has been successfully undertaken for various proteins but published data examining NFH levels was lacking[396–398]. In this thesis the NFH levels were examined in wild-type control cultures, those treated with transection injury, stretch injury, or 10ng/ml of LPS treatment 24 hours following treatment/injury. In all examined conditions tested the NFH levels were found to be below the limit of detection regardless of condition. NFL is an intermediate filament that is structurally similar to NFH and has also been used as a potential biomarker in traumatic brain injury, to directly assess axon injury, and in several neurodegenerative diseases[272,399–404]. Its

sensitivity has been favorably compared to NFH for certain neurodegenerative conditions[392]. In order to establish if NFL could be assessed in an injury based OHS system ELISAs for NFL level were conducted in a range of condition including following traumatic axonal injury. However, again this was found to be below the limits of detection.

3. Assessment of stretch injury in an organotypic hippocampal system

The SARM1 loss-of-function mutation protects against cell death in an organotypic hippocampal slice culture following stretch injury

To probe whether WD was a mechanism underlying the injury phenotype seen following stretch in the OHS system we examined whether a slow WD mutation could protect against stretch induced cell death in a mixed-cellular murine *in vitro* system. Two week old OHS from wild-type and SARM1$^{-/-}$ mice were exposed to a stretch injury and then assessed with PI staining 24 hours and 7 days later (Figure 40).

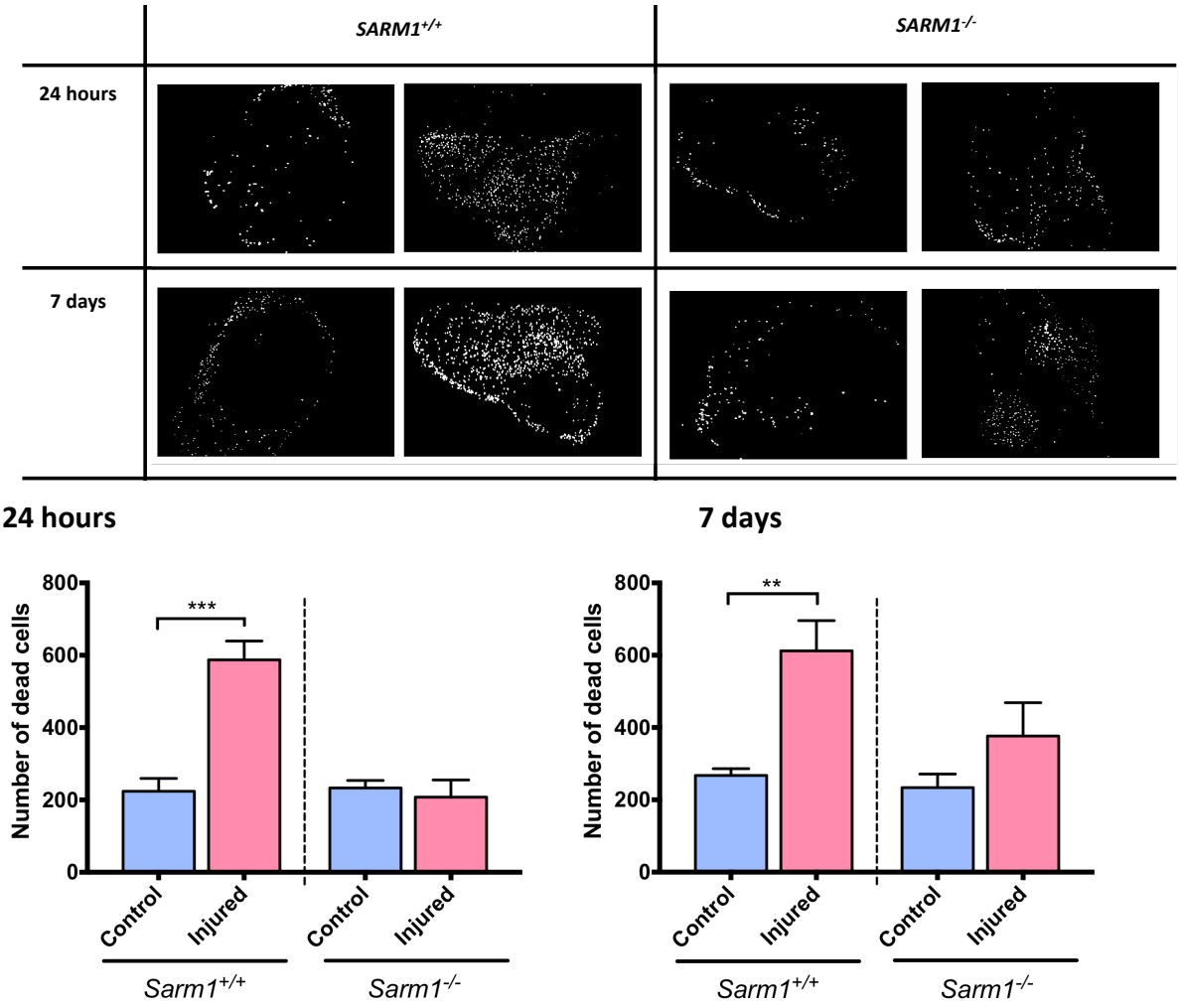

Figure 40. SARM1$^{-/-}$ protects against cell death in organotypic hippocampal slice culture following stretch injury

Organotypic hippocampal slice cultures derived from SARM1$^{-/-}$ mice showed significantly less cellular death than wild-type SARM1$^{+/+}$ derived cultures at 24 hours and 7 days post-stretch injury. Top panels show PI staining of OHS. n = 5 per condition. * = p≤ 0.05, ** = p≤ 0.01, *** = p≤ 0.001, **** = p≤ 0.0001, ns = non-significant (p>0.05). Error bars show SEM. Statistics: 2 way ANOVA.

OHS derived from SARM1$^{-/-}$ mice showed a significant protection against stretch induced cellular death at 24 hours and 7 days compared to wild type controls in a mixed cell population *in vitro* system. These findings suggest that in addition to its known axon-protective effects, SARM1$^{-/-}$ can reduce cellular death induced by a mechanical stretch injury in OHS containing mixed neuroglial cells.

Amyloid β quantification as a marker of stretch injury

TBI has been linked to several neurodegenerative disease including AD, PD, MND, and CTE[405–411]. The pathological hallmarks of AD are neurofibrillary tangles of tau protein and amyloid plaques. The exact relationship between these abnormal proteins, neuronal dysfunction, and clinical symptomatology is still being elucidated[412]. However, research suggests that soluble Aβ correlates with synaptic dysfunction, and clinical progression of the disease[413–416]. Axons, and axonal transport dysfunction, may provide a mechanistic convergence point for Aβ and tau in AD – possibly also explaining a mechanistic link between axonal damage seen in DAI and subsequent AD like processes[417]. Aβ originates from the transmembrane protein APP which is cleaved by one of two main routes, the α or β pathway (figure 41).

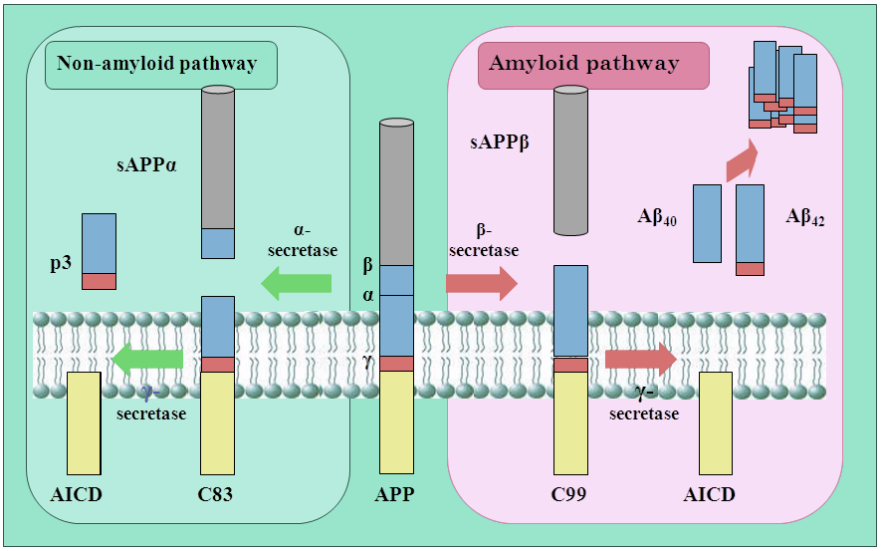

Figure 41. Processing of amyloid precursor protein and the amyloidogenic pathway

It has been hypothesised that there may be two alternative pathways available for processing of amyloid precursor protein. The physiological non-amyloidogenic pathway begins with α-secretase cleavage followed by processing of the resulting C83 fragment by γ-secretase creating a non-toxic amyloid intracellular domain (AICD) and a soluble fragment of amyloid precursor protein (sAPPα). In contrast, the amyloidogenic pathway initiates with β-secretase cleavage followed by processing of the resulting

C99 fragment by γ-secretase to create a toxic amyloid β peptides and a soluble fragment of amyloid precursor protein (sAPPβ). *Image taken from Babusikova et al 2013*[418].

The α pathway is considered the non-pathogenic non-amyloidogenic pathway, while the β is a pathogenic amyloidogenic pathway. In the amyloidogenic pathway cleavage by BACE1 produces an sAPPβ fragment and βAPP-CTF; the latter is subsequently acted on by γ-secretase to release Aβ from the AICD. Depending on the site of γ-secretase cleavage then this produces AICD and Aβ of either 40 ($Aβ_{1-40}$) or 42 ($Aβ_{1-42}$) amino acids[419–421]. $Aβ_{1-40}$ is the most abundant Aβ peptide in the brain but $Aβ_{1-42}$ has been suggested to be more toxic species. Increases in either peptide have been associated with AD[422,423,424]. There is mounting evidence that brain trauma can contribute to the development of AD and other related neurodegenerative diseases. However, the paucity of large prospective cohort trials, and overreliance on retrospective correlations, mean that such associations remain controversial[407,411,425–427]. PET imaging has demonstrated [11C]PiB binding in neocortical regions that correlates with post-mortem amyloid deposition in patients with TBI, but varies from amyloid distribution seen in AD[428,429]. Direct *in vivo* experimental evidence for TBI as a factor in Aβ processing includes increased expression of APP in a rat model of CCI, accumulation of $Aβ_{1-40}$ in APOε4 polymorphism mice, and aggregation and oligomerization of Aβ in AD model mice (x3 Tg) [430–432].

Validation of amyloid β ELISA in organotypic hippocampal slice supernatant

OHS have been used investigate synaptic dysfunction and measure human Aβ levels in supernatant derived from transgenic huAPP mice[396]. Numerous murine $Aβ_{1-40}$ and $Aβ_{1-42}$ ELISA kits are commercially available and have been assessed for specificity with APP-KO whole mouse brain homogenates[433]. However, the ability of these kits to detect murine Aβ in OHS supernatant has not been examined to our knowledge.

Confirmation of the ELISA kit specificity for Aβ has not previously been published. Therefore, this was investigated by using a BACE1 inhibitor to suppress $Aβ_{1-40}$ production, and assessing for associated changes in ELISA measurements (figure 42).

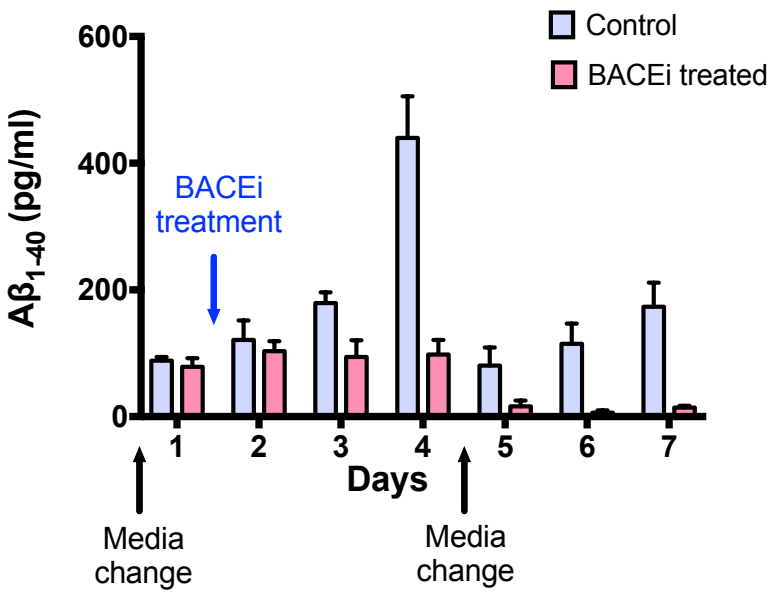

Figure 42. Amyloid-β$_{1-40}$ ELISA is specific as demonstrated by capacity of BACE1 inhibitor to halt production in organotypic hippocampal slice supernatant

After a single treatment with 5μM BACE1i all production of amyloid-β$_{1-40}$ ceased. This manifested as stable levels (~100pg/ml) on days 2-4, and negligible production (<20pg/ml) after a 100% media change (day 4-7). In contrast amyloid-β$_{1-40}$ levels gradually increased in control cultures peaking at day 4 before a 100% media change when they returned to baseline levels and again began to rise. The ability of the ELISA to report predicted amyloid-β$_{1-40}$ suppression with BACE1i suggests that it is a valid measurement tool. n = 3 repeats per condition.

At 14DIV a 100% media change was undertaken, 24 hours later (day 1) a baseline measurement of Aβ$_{1-40}$ was taken before treating the cultures with BACE1i. Levels of Aβ$_{1-40}$ were then measured for the next 3 days (day 2-4), following which a 100% media change was then performed to remove all existing Aβ$_{1-40}$ and the BACE1i from the culture media. Levels of Aβ$_{1-40}$ were then followed for a further 3 days (day 5-7). The ability of BACE1i to suppress Aβ production as measured by ELISA supports the assertion that it has a good degree of antibody specificity.

Suppression of amyloid β$_{1-40}$ with BACE1 inhibitor is not due to toxicity

In order to exclude the possibility that BACE1i was reducing Aβ$_{1-40}$ by causing cellular death the OHS were PI stained 3 days after BACE1i treatment (Figure 43).

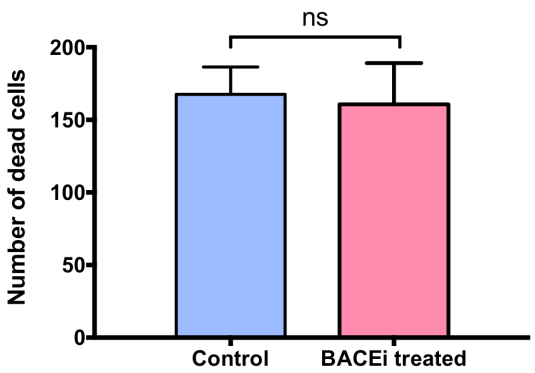

Figure 43. BACE1i did not cause cellular death in organotypic hippocampal slice cultures

Treatment of organotypic hippocampal slice cultures with 5µM of BACE1i for 3 days did not cause any cellular death as measured by propidium iodide. n = 9 repeats per condition. * = p≤ 0.05, ** = p≤ 0.01, *** = p≤ 0.001, **** = p≤ 0.0001, ns = non-significant (p>0.05). Error bars show SEM. Statistics: Student's T test.

This did not show any additional burden of death in BACE1i treated cultures, suggesting that the suppression of $A\beta_{1\text{-}40}$ seen with BACE1i is an authentic effect and the ELISA is specific for $A\beta_{1\text{-}40}$ measurements.

Stability of amyloid-$\beta_{1\text{-}40}$ levels in OHS cultures over time

A murine $A\beta_{1\text{-}40}$ ELISA kit (#KMB3481, Invitrogen) was used to assay $A\beta_{1\text{-}40}$ levels in the supernatant of 2 week old OHS over a 28 day period with 100% media changes at weekly intervals.

Levels remained consistently in the 500-600pg/ml range, suggesting that $A\beta_{1\text{-}40}$ is detectable in OHS slices using commercially available ELISA systems and that production remains consistent in OHS between 2 and 6 weeks of age (Figure 44).

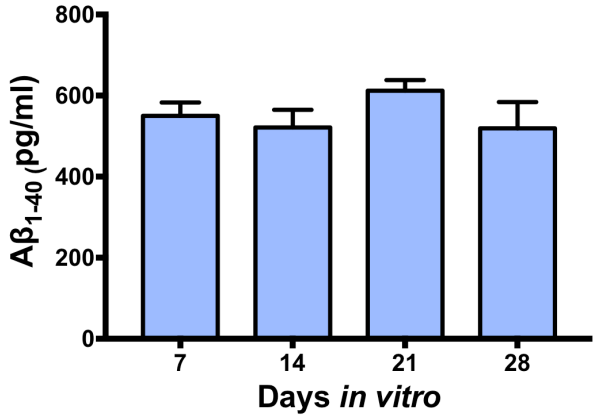

Figure 44. Amyloid-β$_{1-40}$ levels are detectable in organotypic hippocampal slice culture supernatant and levels are consistent over 4 weeks in vitro

The levels of amyloid-β_{1-40} were measured by ELISA immediately before a 100% media change at 7 day intervals. The concentrations of amyloid-β_{1-40} were consistently measurable in the 450-600pg/ml range. n = 3 repeats. * = p≤ 0.05, ** = p≤ 0.01, *** = p≤ 0.001, **** = p≤ 0.0001, ns = non-significant (p>0.05). Statistics: 1 way ANOVA.

Amyloid-β_{1-42} measurement in organotypic hippocampal slices exposed to a stretch injury

Increased $A\beta_{1-42}$ levels has been implicated in the pathogenesis of both sporadic and familial AD [415]. The hydrophobic nature of $A\beta_{1-42}$ may underlie its propensity to amyloidogenic formation. In order to explore the possibility that a stretch injury results in production of $A\beta_{1-42}$ the supernatant from healthy OHS with and without a stretch injury were analyzed (figure 45).

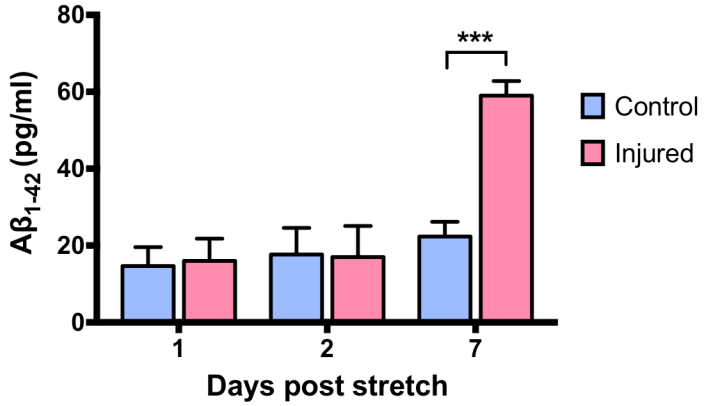

Figure 45. Aβ$_{1-42}$ levels in organotypic hippocampal slice culture supernatant are increased as a result of stretch injury

A complete culture medium change was undertaken immediately prior to a single stretch injury in a 2 week old organotypic hippocampal slice culture. Amyloid-β_{1-42} levels were then assessed by ELISA of culture supernatant at 1 day, 2 days and 7 days following the injury. Injured cultures showed a higher level of amyloid-β_{1-42} than in uninjured controls at 7 days. n = 3 repeats per condition. * = $p \leq 0.05$, ** = $p \leq 0.01$, *** = $p \leq 0.001$, **** = $p \leq 0.0001$, ns = non-significant ($p > 0.05$). Error bars show SEM. Statistics: Student's T test.

The ability of the OHS system to respond to injury with changes in Aβ levels opens the possibilities to probe the mechanisms of Aβ formation and toxicity, and therapeutic drug screening and investigation at *in vitro* level.

TBI, proinflammatory cytokines, and AD

TBI triggers an inflammatory cascade characterized by a complex profile of cytokines and chemokine production, including TNFα and IL-1β[144,434–436]. The neuroinflammation hypothesis postulates that an increased production of proinflammatory cytokines contributes to secondary brain injury and progressive neurodegeneration[437,438]. Inflammation and white matter degeneration has been shown to persist for many years after a single TBI, this has been linked to chronic microglial activation but the exact mechanism remains incompletely understood [9]. Many of the same neuroinflammatory cytokines produced by TBI have been linked to Alzheimer's disease[439,440]. The interaction between inflammatory cytokines and amyloid species has been the focus of considerable attention. Pro-inflammatory cytokines including TNFα and IL-1β levels correlate with AD, and polymorphisms are associated with the disease[441 442].

TNFα is a major proinflammatory cytokines that has neurotoxic effects on neuroglial cultures *in vitro*[443]. It has been suggested that TNFα has a dual role in TBI with both neurotoxic and neuroprotective effects predominating depending on timing and extent of TNFα activation[444]. Inhibition of TNF signalling has been shown to reduce amyloidogenic pathology in a mouse model of AD (3x Tg)[442,445].

IL-1β is an inflammatory cytokine expressed at low levels in healthy brain but upregulated in injury[446,447]. A lateral FPI rat model of TBI demonstrated upregulation of IL-1β mRNA transcription in response to injury[448]. IL-1β also has neurotoxic effects on neuroglial cultures

in vitro[443]. It increases loss of hippocampal neurons following TBI in a rat mode[449]. IL-1β has been suggested as a therapeutic target in TBI, and recombinant human IL-1 receptor antagonism (IL1-RA) has shown promise in a phase II RCT in severe TBI [450 451].

Effect of proinflammatory cytokines on $A\beta_{1-42}$ levels in stretch injured OHS

The effects of TNFα and IL-1β on $A\beta_{1-42}$ were investigated in the OHS culture system. $A\beta_{1-42}$ was measured 7 days after a 100% media change in 2 week old OHS in 4 different conditions; uninjured untreated, injured untreated, uninjured TNFα/IL-1β treated, and injured TNFα/IL-1β treated. TNFα/IL-1β treatments were added at the time of the baseline 100% media change, and cultures were stretch injured 1 hour after media changes (Figure 46 & 47).

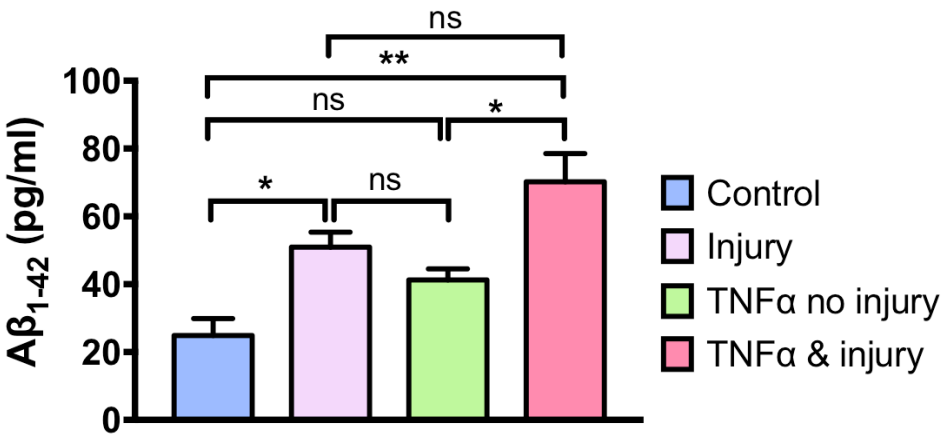

Figure 46. Tumour necrosis factor-α increases amyloid-β$_{1-42}$ in uninjured and stretch injured organotypic hippocampal culture supernatant

Amyloid-β_{1-42} levels were assessed by ELISA in organotypic supernatant 7 days post 100% media change in control OHS cultures, stretch injured cultures, and cultures treated with tumour necrosis factor-α 250pg/ml with or without a stretch injury 1 hour later. Tumour necrosis factor-α treated cultures showed a higher level of amyloid-β_{1-42} than in controls, and stretch injury further added to the amyloid-β_{1-42} levels. n = 3 per condition. * = p≤ 0.05, ** = p≤ 0.01, *** = p≤ 0.001, **** = p≤ 0.0001, ns = non-significant (p>0.05). Error bars show SEM. Statistics: 1 way ANOVA.

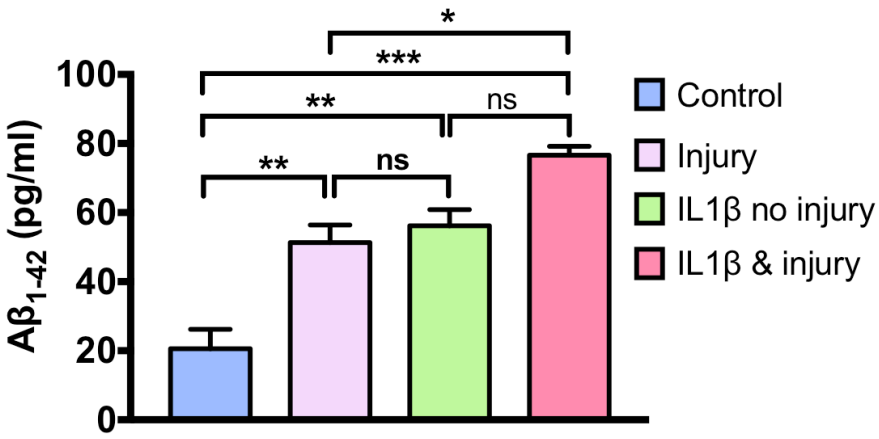

Figure 47. Interleukin-1β increases amyloid-β1-42 in uninjured and stretch injured organotypic hippocampal culture supernatant

Aβ1-42 levels were assessed by ELISA in OHS supernatant 7 days hours post 100% media change in control OHS cultures, stretch injured cultures, and cultures treated with IL-1β 25pg/ml with or without a stretch injury (1 hour after IL-1β treatment). IL-1β treated cultures showed increased levels of $A\beta_{1-42}$ to levels equivalent to stretch injured OHS. This effect was cumulative with stretch injury. (3 OHS per membrane, n = 3 repeats per condition, * = p≤ 0.05, ** = p≤ 0.01, *** = p≤ 0.001, **** = p≤ 0.0001, ns = non-significant (p>0.05). Error bars show SEM. Statistics: 1 way ANOVA).

The pro-inflammatory cytokines TNFα and IL-1β both independently increased $A\beta_{1-42}$ in OHS supernatant 7 days after addition. When TNFα was added to culture media 1 hour prior to a stretch injury, the resulting $A\beta_{1-42}$ level was greater than with either TNFα alone or with an isolated stretch injury. The mean $A\beta_{1-42}$ level was also greater for stretched cultures pre-treated with IL-1β but this did not reach significance.

Discussion

This chapter explored the development of a stretch based injury model using OHS, and the calibration and use of this system to explore the effects of stretch injury relating to neurodegenerative molecular (Aβ), proinflammatory cytokines (TNFα and IL1β), and transgenic modulators of WD (SARM1$^{-/-}$).

The development of this system will be particularly useful for understanding basic mechanisms of cellular response to a physical injury, particularly those that are not cell autonomous and result from neuron-glial interactions. It offers the potential for teste=ing direct drug administration, cellular environment manipulation, supernatant testing and repeat imaging across multiple time points.

The use of OHS stretch based systems has previously been documented by a limited number of groups including Geddes and Cargill, Morrison *et al*, and Di Pietro *et al*[64,77,80,92,310–313]. The use of an OHS injury system to explore neurodegenerative aspects of TBI in relation to WD is absent from the literature.

Culture modifications

The existing OHS stretch injury systems tend to culture OHS on silicone membranes. In our hands this resulted in high variability in slice health, and frequent poor viability. This is an issue that several authors refer to, and in effect limits most experimental approaches to the use of acute slices for TBI research[313,334,452]. One of the main benefits of an OHS– as seen with an optimized interface membrane method of preparation– is the opportunity to allow the slice cultures to 'recover' from the initial slicing insult and become fully organotypic. This takes around 7-10 days as evidenced by the slice losing its acute opacity, at this point markers of cell death such as PI staining are usually near absent[323]. The slice can then be cultured in a healthy state with minimal evidence of cell death up to around 6-8 weeks of age[323,324,396]. The primary benefit of culturing on silicone is the high elasticity of the material. However, it is impermeable to liquids and in most configurations is non-porous. This means that OHS cannot be cultured with silicone using the interface method of culture medium below the hippocampal slice. Instead the slices must be bathed in the media. OHS, unlike primary

cultures, have higher oxygen requirements and will rapidly degenerate if they remain submerged in media. This is the reason why OHS cultures on silicone required constant motion during incubation[452]. However, this constant motion leads to detachment of the OHS in many cases, and generally results in poor viability. Hence an alternative solutions was required. Numerous alternative culture substrates were trialed but all suffered limitations mainly relating to poor viability and inadequate adhesion. PTFE, the material that Millipore™ membrane inserts are made from, has the capacity to stretch and has some degree of elasticity. Although I did not formally establish the elastic limit of PTFE it did not appear to have the same degree of elastic recoil as silicone as evidenced by membrane failure under a manually applied stretch, something that was not noted with silicone membranes. In order for reliable experimentation to proceed the health of the OHS is paramount. Therefore, knowledge of the exact degree of elastic recoil was forgone in exchange for reliable OHS culture health. It should be noted that all membranes and the stretch system were standardized so comparisons between stretched and unstretched cultures, and different experimental conditions should still be comparable and internally valid. Indeed, publications on organotypic stretch do not generally present the elastic recoil of their substrates[92,313,334].

Challenges of validating axonal injury

Once the interface method was adapted for use with the stretch device is was necessary to calibrate the device and then quantify the injury. The quantification of an injury is more challenging in an organotypic culture system than a primary neuronal one. Whereas in the primary neuronal system we have a well-established readout of neurite degeneration, the same does not exist for OHS. Therefore, it was decided initially to examine the rates of cellular death in the OHS system. When examining the extent of cellular death post stretch there is no clear level that is unequivocally optimal. In the human condition different brain regions may undergo different degrees of neuronal loss in the acute phase. Thus, deciding how much cellular death is representative of the human condition, in an OHS, is an arbitrary decision. Pragmatically, it was felt that an injury that causes some degree of cellular death but not complete OHS death would be optimal as this would allow us to be sure that a significant injury had occurred, and have the opportunity to monitor cellular rescue and biochemical changes over time, without a terminal insult.

In chapter 4 we establish that a stretch injury of primary cortical neurons produced axonal injury as evidenced by degeneration measured with the neurite degeneration index, the same strategy cannot be applied to an OHS system as axons are not visible in an OHS under phase-contrast microscopy. On the basis of findings in SCGe we can hypothesize that the stretch injury damages axons in the OHS but we lack direct data on this point. Therefore, a range of other approaches were taken to establish evidence that supports or refutes axon-specific damage. It is notable that such quantification has generally been absent in other OHS models of TBI[92,313,334]. One of the primary benefits of an OHS system is the presence of native non-neuronal cells. Paradoxically, this presents a challenge to the issue of axon assessment. The density of cells is such that traditional staining techniques cannot resolve individual axons, and transection efficacy is generally poor as we have illustrated. A gene-gun approach may be more successful, other options might include the use of sparse labelling of axons with a viral vector or transgenic approaches. Due to the difficulties we encountered directly visualizing axons we attempted a biomarker assessment of axonal damage using ELISA assessment of neurofilaments for NFH and NFL. Both these showed low levels in all conditions that precluded use as a marker of axonal damage. Reasons for this may include limited neurofilament expression at the young developmental stage pups are used (P6-8), or a failure of neurofilament to be secreted into cell culture supernatant at sufficient quantities to be detected by the ELISA. NFH and NFL is expressed in the nervous systems of developmentally immature animals, however, detailed quantification of the extent of this expression is lacking and the levels may be low(see Gene Expression Database, www.informatics.jax.org accessed on 5.2.18)[453,454]

Looking for evidence of WD in the slice model

An alternative approach to determine that this OHS stretch injury model is subject to an axonal stretch is to examine for evidence of WD. We used a transgenic SARM1 knockout approach to determine if there was SARM1 dependent neuronal death in the slice cultures. As described, SARM1$^{-/-}$ is axon protective and has been shown to delay WD without affecting apoptosis, therefore it was not expected that SARM1$^{-/-}$ would be capable of influencing overall neuronal survival[455]. However, cultures derived from SARM1$^{-/-}$ animals and exposed to stretch injury showed a significantly lower level of cellular death at both 24 hours and 7 days compared to wild-types. This demonstrates that the stretch injury produced in our model system induces

WD and that this can be effectively rescued by a slow WD transgenic model. It also supports the hypothesis established in primary neuronal culture that modulating the WD pathway may alter neuronal outcomes following a stretch injury. These findings suggest that in addition to its known axon-protective effects, SARM1$^{-/-}$ can reduce cellular death induced by a mechanical stretch injury in OHS containing mixed neuroglial cells. SARM1$^{-/-}$ is generally considered to be an axon specific protection and so the exact mechanism of the neuroprotective effect in our system remains to be determined. One hypothesis is that injured neurons that would otherwise undergo WD have an extended period in which to recover due to the lack of WD initiation in SARM1$^{-/-}$ cultures. Whether this involves a direct SARM1$^{-/-}$ mediated protection of the cell body, a protection of the cell body secondary to axon preservation – for example due to maintenance of retrograde axonal transport– or another unrelated mechanism is still unknown. These findings support the further exploration of SARM1 inhibition, and other WD pathway modifiers, as a potential therapeutic intervention in brain injury.

Expanding markers of injury to include an exploration of amyloid β levels in response to stretch

A potential biomarker of axonal damage that links TAI to AD is Aβ, and particularly subspecies of Aβ that are less commonly found in normal healthy tissue such as long/fibrillary peptides like $A\beta_{1\text{-}42}$[429]. Disruption of axonal transport following stretch injury may provide an mechanistic explanation of the association between stretch and AD, mediated by Aβ and possibly the microtubule associated protein tau[417]. BACE1 is the major β secretase controlling production of Aβ from APP. Levels of BACE1 increase in TBI and have been shown to co-accumulate with APP in axonal injury, suggesting a pathogenic mechanism by which TAI can link to abnormal Aβ production and subsequent AD pathology [456,457]. Axonal injury might also lead to a direct leakage of Aβ into surrounding tissue, thereby linking axonal injury directly with Aβ levels[85].

We showed that OHS supernatant is capable of being used to detect and measure Aβ levels in the OHS system. Using a BACEi knock-down approach to Aβ we demonstrated our ELISA results were specific for Aβ detection. The $A\beta_{1\text{-}42}$ species is toxic subspecies that is hydrophobic and tends to accumulate in amyloid plaques in the human brain[458]. It is neurotoxic and leads to neuronal death and dysfunction[459,460]. We demonstrate that using our injury model levels

of $A\beta_{1-42}$ rise in response to a physical stretch injury. This supports the hypothesis that stretch injury can mediate Aβ accumulation and may be a pathogenic link between TBI and AD.

Inflammation in TBI

The contribution of certain aspects of inflammation to poor outcomes following TBI has been widely documented[461]. The interaction between TAI and inflammation, and between inflammation and amyloid β production is an active area of enquiry, with widespread Aβ deposits and axonal accumulation found in human brains early after injury and persisting in some cases for many years[461–466]. The stretch OHS system opens the opportunity to explore the molecular effects of stretch injury and associated molecular processes in a controlled system. This includes, but is not limited to, the further examination of the effects of stretch and inflammatory molecules, and their relationship to neurodegenerative proteinopathies and cellular responses.

Following a human TBI the most abundant soluble deposited Aβ peptide is the neurotoxic, aggregate prone form $A\beta_{1-42}$[467]. We examined the response of $A\beta_{1-42}$ levels to the addition of the proinflammatory cytokines TNFα and IL-1β, both with and without the addition of a stretch insult. The selection of representative cytokine doses for experimental use is a challenge. Even high doses of cytokines including TNFα and IL1-β– doses up to 100ng/ml (*data not shown*)– do not cause direct toxicity in primary neuronal cultures, with responses being mediated via non-neuronal components of brain tissue including microglia [468]. Supra-physiological doses may not be representative of pathophysiological mechanisms in humans, while insufficient doses may not demonstrate effects. The dose range used in this thesis were therefore selected based upon estimated pico-molar concentrations found in early stages of severe TBI and doses used in other *in vitro* experimental studies[434,469]. However, the relationship between dosing in a murine OHS system and how that equates to other *in vitro* models or the human condition have not been not clearly elucidated.

Pro-inflammatory cytokines including TNFα, IL-1β, interferon-γ, and IL-6 have been shown to stimulate γ-secretase activity and increase amyloidogenic APP processing to shift production towards toxic Aβ species[470,471]. In our OHS injury system TNFα and IL-1β both independently increased $A\beta_{1-42}$ in OHS supernatant 7 days after addition. When these cytokines were added

to culture media 1 hour prior to a stretch injury they also act in an additive manner to increase $A\beta_{1\text{-}42}$ levels to greater levels than if exposed to either a cytokine alone or an isolated stretch injury. These findings suggest that Aβ levels may be partially mediated in the stretch system by proinflammatory molecules, and demonstrate the versatility of the OHS stretch model to examine glial dependent neurodegenerative pathology. This system gives us the opportunity to investigate links between TAI, neuroinflammation, WD and neurodegenerative proteinopathies in a manner not possible with *in vivo* or primary neuronal culture systems.

Summary

This chapter explored the modification of an existing primary neuronal stretch system to accommodate OHS. A series of attempts to culture OHS on silicone substrates was made culminating in the use of the interface membrane method which was adapted to permit a stretch insult. The injury was quantified and calibrated to cause a small but significant degree of neuronal death. Attempts to assess axonal damage were undertaken by methods including immunohistochemistry, transfection and ELISA of neurofilament levels in supernatant. On the basis of findings in primary neuronal culture it was hypothesis that the cellular injury seen in this model would be partially accounted for by secondary injury mediated by WD. Cultures with a slow WD transgenic mutation, $SARM1^{-/-}$, demonstrated partial protection against stretch induced cellular death in this system confirming this finding. In order to explore the links between stretch injury and Aβ levels we first validated the ELISA purported to measure Aβ by looking to suppress production with a BACE1i. Once validated, the baseline level of Aβ was measured in OHS supernatant. The effects of stretch injury on Aβ were investigated and stretch injury was shown to cause a rise in Aβ levels. This route of enquiry was further developed by looking at the influence of key pro-inflammatory mediators, TNFα and IL-1β, on the survival of stretched and un-stretched cultures. Both were shown to independently increase cellular death in OHS, with stretch injury causing an additional burden of cellular death.

Next steps

The links between TAI induced WD, and Aβ are largely unexplored. Various avenues remain to explore these associations including TAI induced axonal transport impairment as a common mechanism involved in WD following TAI, and Aβ generation in neurodegenerative disease. In order to explore whether the Aβ rise we see in wild-type cultures was related to WD a next step would be to expose matched wild-type and SARM1$^{-/-}$ cultures to a standardized stretch injury and assessed $A\beta_{1-42}$ levels. It is plausible that axon degeneration due to WD could result in raised levels of Aβ which in turn is neurotoxic to cell bodies- hence, providing a potential explanation for how axon specific SARM1$^{-/-}$ might reduce overall neuronal death in the absence of direct cell body protection.

The association between stretch injury and synaptic degeneration could also be explored by assessing levels of the presynaptic marker protein synaptophysin in injured wild-type and SARM1$^{-/-}$ cultures, and uninjured controls. This would provide an important insight into the ability of WD modulators to protect against stretch induced synaptic loss.

In this thesis, we decided that in order to further explore the role of WD in TAI, and its association to neurodegeneration– we would pursue the development of a whole organism model of TBI. The following chapter outlines the development, validation and exploration of WD mechanisms in a *Drosophila* model of TBI.

Chapter 7

Highwire mutation partially rescues deficits resulting from high impact trauma in a *Drosophila Melanogaster* model

Introduction

1. The use of *Drosophila Melanogaster* as a model of traumatic brain injury

The nervous system of Drosophila Melanogaster

Drosophila Melanogaster is a model organism with a complex nervous system. The fly CNS is composed of the brain and the thoracic ganglion, a structure analogous to the spinal cord in mammals. Neurons account for 90% of the cells in the CNS, and glia the remaining 10%. The entire CNS contains around 200,000 to 300,000 neurons, *with* ~100,000 neurons in the brain. These neurons are structurally and functionally similar to human neurons including the same basic synaptic organization, mechanisms of vesicle release, and a similar range of ion channels and neurotransmitters including γ-aminobutyric acid (GABA), glutamate, acetylcholine, neuropeptides and other biogenic amines[472,473]. Likewise, the glia of flies are similar to their human counterparts. Variations include astrocytes, ensheathing glia, and cortex glia, each subserves comparable functions to their mammalian counterparts including formation of a blood-brain barrier and innate immunity[473,474].

The fly brain is encased in a rigid, hard, waxy exoskeleton called the cuticle. This protects the fly brain and constrains its shape. In-between the brain and the cuticle is a layer of hemolymph that bathes the brain in a manner analogous to cerebrospinal fluid in humans[298]. Like mammals, the fly brain has 2 hemispheres that joins to a central ganglion. The brain is divided into three lobes, the mammalian equivalent is in brackets– the protocerebrum (forebrain), the deutocerebrum (midbrain), and the tritocerebrum (hindbrain)[475,476]. The brain lobes are joined by fascicles of nerves. The brain parenchyma is divided into two histologically distinct regions, the neuronal cell cortex, composed of neuronal cell bodies, and the neuropil which is analogous to white matter in the human brain, and is composed of the axons and dendrites[473]. The fly brain is made up of many functionally distinct regions(figure 48).

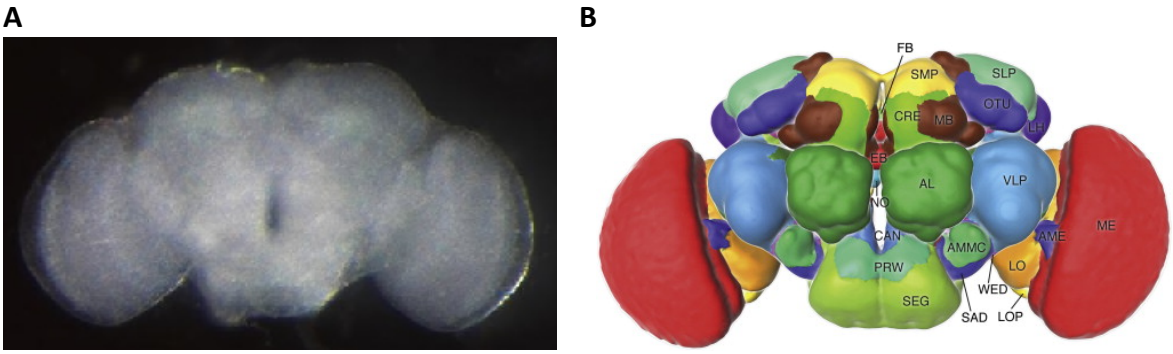

Figure 48. The Drosophila Melanogaster brain

The *Drosophila* brain has a complex anatomical structure composed of several functionally distinct regions. The figure on the left is a freshly dissected *Drosophila brain* (A), the figure on the right is a computer generated schematic in false colour that shows some of the major superficially located regions of the fly brain on an antero-posterior projection (B). Deep structures are not shown. AL, antennal lobe; AME, accessory medulla; AMMC, antenna-mechanosensory and motor center; CAN, cantle; CRE, crepine; EB, ellipsoid body; FB, fan-shaped body; LH, lateral horn; LO, lobula; LOP, lobula plate; MB, mushroom body; ME, medulla; NO, noduli; OTU, optic tubercle; PRW, prow; SAD, saddle; SLP, superior lateral protocerebrum; SMP, superior medial protocerebrum; SEG, subesophageal ganglion; VLP, ventrolateral protocerebrum; WED, wedge. *The right-hand figure including text is taken from Jennett et al*[477].

Drosophila Melanogaster as a model organism

Drosophila are a versatile model organism. Their short generation times, and the unique ease with which genetic modulations can be made, make them particularly suited to exploratory genetic studies, and determination of molecular pathways and development control mechanisms. Some of the many other advantages of this organism are summarized in table 15[293,478,479].

Benefits of *Drosophila* as a model organism
Short generation time (~10 days)
Rapid aging effects and short lifespan– allow assessment over whole lifespan
Economical
Few ethical concerns
Elaborate nervous system
Range of neuronal circuits
Whole organism model with range of complex behaviours (both innate and learned)
High degree of molecular similarity with mammals
Preservation (homologs) of many mammalian genes
Simple genetic manipulation and versatile tools include UAS/Gal4 system
Ability to maintain mutations in heterozygous state
MARCM system- allows expression of otherwise lethal mutations in subset of cells
Well established genetic screening protocols
Compact genome (1/30th size of humans)
Limited genetic redundancy
~75% of human disease genes conserved

Table 15. Drosophila Melanogaster as a model organism

There are several advantages to the use of *Drosophila Melanogaster* as a model organism- particularly relating to the simplicity and easy modification of their genome

Despite only having 4 chromosomes, *Drosophila* share substantial genetic code with humans including conservation of the majority of human disease causing genes, although most human gene families typically have a smaller number of fly orthologues.. Biologists have develop of a unique set of tools to genetically alter the fly, and this, combined with their complex behavioral patterns and elaborate nervous system have made them a premier model for neuroscience research. This has been particularly evident in the fields of circadian rhythms, cell proliferation, growth, learning and memory, and neurodegeneration, where they have contributed to major advances in understanding[293].

The more common animal models of TBI include the controlled-cortical impact (CCI) and fluid percussion injury (FPI) rodent models. These models are highly regulated by Home Office legislation due to the significant pain and distress they can cause to the animals[277,327]. Although they have provided important insights into the molecular and pathological processes involved in TBI, they have thus far failed to produce any successful translational therapies[11,12,480]. Large animal models including primate and pig models, have provided

further biomechanical information which is only possible in such large gyrencephalic brains[12]. However, there are even greater ethical restrictions in these models that limit the number animals that can be used and the procedures that can be carried out. Likewise, genetic manipulation is limited in large animals. Such restrictions do not exist for the use of *Drosophila*.

This combination of versatile genetic tools, sophisticated neurological system, behavioral assays, and ethical flexibility, make *Drosophila* a tractable and appealing organism for studying mechanistic aspects of TBI.

Models of TBI utilizing *Drosophila Melanogaster*

Drosophila have been used extensively to model neurodegenerative diseases such as AD and PD[481,482]. However, at the time of writing there are two published models of TBI in *Drosophila*. The first was described by Katzenberger *et al* in 2013[298]. This high impact trauma (HIT) device consists of loading flies in a polystyrene vial that is attached to a spring loaded device and released, causing a rapid acceleration then deceleration as the vial strikes a firm polyurethane foam pad. Therefore, the flies are subjected to a homogeneous impact force, but the orientation of the flies in the vial will introduce variability into the nature of the injury suffered. Severity of impact is adjustable. This model has been used to identify single-nucleotide polymorphisms regulating intestinal barrier dysfunction as an important determinant of outcome[298,299]. Barekat *et al* described a model of mild repetitive TBI using the Omni bead ruptor-24 homogenizer platform, a device that causes rapid oscillations of flies within a 2ml. The velocity of oscillations can be varied from a non-lethal level through to total lethality. In addition to demonstrating injury induced reduction of lifespan, the system showed activation of inflammatory and autophagic responses, Tau phosphorylation, and neuronal defects in sleep-related behavior[300].

The *Drosophila* models of TBI described have several limitations. These include a homogenous injury that includes a poorly defined polytrauma response, and the inherent limitations of a small animal model of trauma. They may also have limited suitability for certain experimental questions such as pharmacological treatments where drug dosing his difficult to accurately determine.

Drosophila Melanogaster and the Wallerian degeneration pathway

Drosophila can also be used to investigate molecular pathways. The WD pathway shows remarkable preservation in *Drosophila*, underlining the ancient nature of this cell-autonomous axonal death pathway. The key regulators of WD in the fly and mammalian systems are the same as far as we currently know[7]. Many of the key WD genes including dSARM (mammalian ortholog SARM1), *highwire,* and *axundead* were originally identified in *Drosophila*, and the fly continues to be the primary source by which new regulators of this pathway are now discovered[204,241,483].

The role of *highwire* in Wallerian degeneration

In order to investigate the effects of modulating WD on TBI there are a number of potential modulators/targets that could be explored, many of which have been described in earlier chapters, these include SARM1, WLD^{s}, WLD/DLK, highwire/PHR1, NAMPT, NMNAT, NMN and NAD. When considering potential therapeutic targets it may be preferable to choose one whose effect is mediated by a loss of function (LOF)/knockout as opposed to a gain of function (GOF). This is because LOF mediated effects are likely to be more amenable to drug targeting, as pharmacological inhibition of an existing substrate is often more biochemically straight-forward than overexpression.

The *highwire* gene

In 2000 an immunohistochemical screen with synaptotagmin and FAS II was undertaken to identify synaptic structural phenotypes. A collection of 230 viable EMS generated X chromosome mutant lines with walking deficits were screened. One of these, termed *highwire*, was identified with an expanded branching pattern of synaptic overgrowth in its NMJs. The location of the *highwire* mutation was mapped by complementation analysis and chromosomal/RNA *in situ* hybridization (figure 49)[218,223].

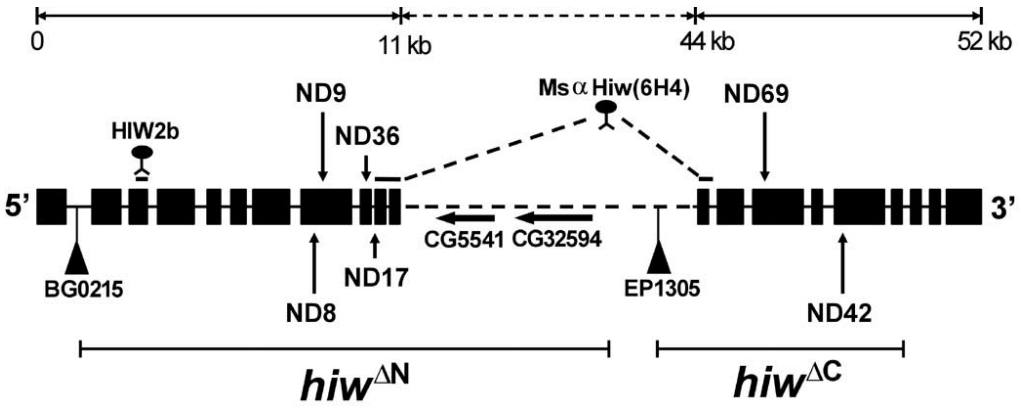

Figure 49. The highwire gene and key mutations

The *highwire* gene is encodes a large protein with E3 ubiquitin ligase activity that modulates levels of the dNMNAT enzyme. Black boxes indicate exons. Alleles ND8, ND9, ND42, and ND69 have nonsense mutation at amino acid 1930, 2001, 3173, and 3812, respectively. Molecular lesions of alleles ND17 and ND36 have not been identified by sequencing; however, they are proposed to be nonsense mutations at amino acid proximately 2700. The locations of two P-element alleles, BG0215 and EP1305, are indicated. These two P-elements were used to generate two deletion mutants, $hiw^{\Delta N}$ and $hiw^{\Delta C}$ by imprecise excision. *Image and text adapted from Wu et al*[223]

The *highwire* gene encodes a large 5233 amino acid protein with E3 ubiquitin ligase activity that modulates levels of dNMNAT[218,223–225]**.** *Highwire* LOF mutation profoundly delays WD in *Drosophila* axons following transection both *in vitro* and *in vivo.* The axon preservation persists for the whole life of the fly. This is as robust an effect as either $dSARM^{-/-}$ or WLD^{s} expression[223,224,226,227,484,485]. Delayed WD is also seen with mutations in the mammalian ortholog of *highwire*; *PHR1*[7,225,230]. *Highwire* can be constitutive expressed in *Drosophila* without any lethality or overt phenotype. *Highwire* has presynaptic regulatory activity that is required to control excess synaptic growth at the neuromuscular junction, but no CNS phenotype has been observed[218,223,228].

In contrast to *highwire,* dSARM LOF mutation is constitutively lethal in *Drosophila*. Although it can be studied in a subset of neural tissue using a MARCM approach this limitation makes it a less appealing target in *Drosophila.* WLD^{s} expression has a strong axon protective effect in the fly, comparable to that seen in mammalian systems [485]. However, it remains an aberrant GOF mutation and that limits its utility as a potential therapeutic target.

Given the role of *highwire* in dNMNAT depletion and subsequent axon degeneration, and the assessment that WD may contribute to the secondary brain injury seen in TBI, we hypothesised that flies with a null mutation in *highwire* (*hiw*$^{\Delta N}$) would show protection against the effects of TBI. It was decided to investigate the effects of a *highwire* LOF mutation because it is non-lethal and strongly delays WD through a well-characterized mechanism of action. The effects have also not been the subject of prior investigation in TBI.

Aims

This chapters aims to:

- Develop, calibrate and characterise a *Drosophila Melanogaster* model of traumatic impact
- Examine the effects of modulating Wallerian degeneration on the sequlae of traumatic inpact– including lifespan, behaviour, and neurodegeneration
- Explore the effects of Wallerian degeneration modulation on related pathologies

Results

1. Development and characterization of a *Drosophila* high-impact trauma device

Early death rates vary with the severity of injury

To model TBI in *Drosophila* we reproduced a version of the high impact trauma (HIT) device previously described[298]. This consists of a spring-loaded attachment that holds a polystyrene vial of flies, and inflicts a rapid acceleration-deceleration impact injury (figure 50).

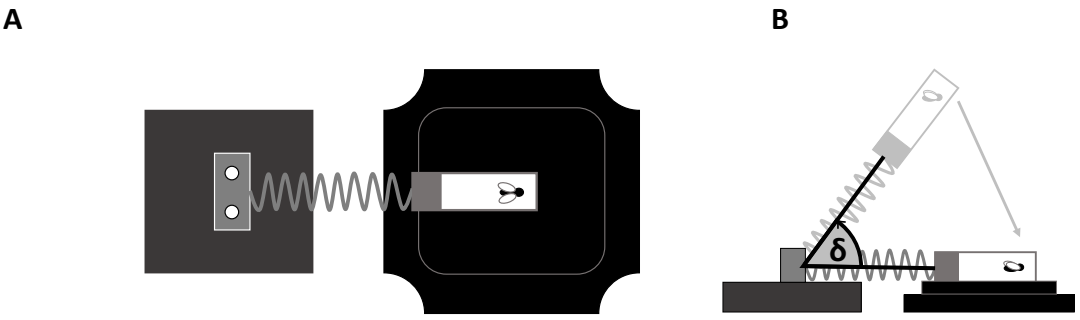

Figure 50. Schematic diagram of the high-impact trauma device demonstrating initial deflection angle adjustment

A top-down and lateral schematic of the high impact trauma device, this consists of a polystyrene vial attached to a spring– when released this creates a rapid acceleration-deceleration impact. Varying the angle of initial deflection (δ) alters the amount of stored energy and hence the restoring force upon release of the spring. When the released vial strikes the impact board the flies are subjected to a rapid deceleration force proportional to δ.

The initial deflection of the spring generates potential energy that upon release converts to kinetic energy and rapidly accelerates the vial and flies. When these strike the polyurethane foam pad there is a rapid deceleration and the flies strike the vial sides. After injury, vials were laid on their side and flies were given a 10 minutes to recover motility before being transferred to a glass vial containing standardised feed. All polystyrene vials were discarded after a single use. The rate of acceleration-deceleration impact, and hence the forces the flies experience, is dependent upon the angle of initial deflection of the device spring.

The severity of injury was calibrated in *hiw*$^{+/+}$ flies by assessing the death rates at 24 hours and 7 days following a single impact when the angle of initial deflection, and thus recoil force, was

adjusted. An angle of 90° produced an average death rate of 22% at 24 hours and 30% at 7 days post-injury in *hiw*$^{+/+}$ flies (figure 51).

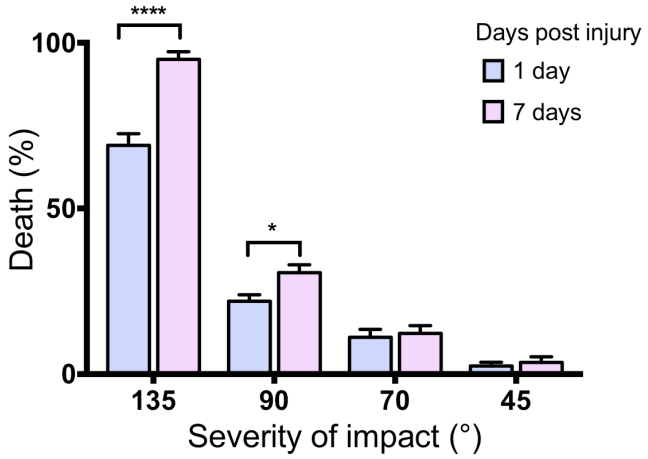

Figure 51. Rates of death following injury relate to the severity of a single impact as determined by the initial angle of impact device spring deformation

Percentage survival 1 day and 7 days post injury was assessed in relation to the severity of a single impact. Severity was altered by adjusting the degree of initial spring deformation calculated from the horizontal in the HIT. n = 9 vials of 20-35 flies per condition. * = p≤ 0.05, ** = p≤ 0.01, *** = p≤ 0.001, **** = p≤ 0.0001, ns = non-significant. Error bars show SEM. Statistics: 2 way ANOVA.

At 90° we never saw any signs of external injury to the flies, this is in contrast to higher angles, for example at 135° where evidence of appendicular and thoracic trauma were seen in around 50% of cases.

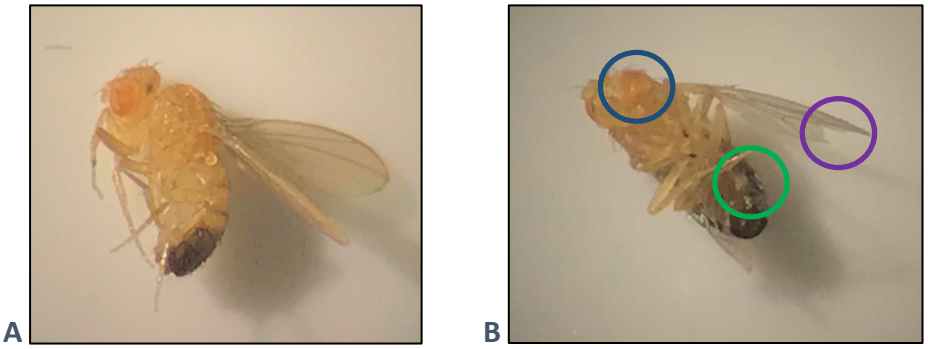

Figure 52. External injury is only evident with initial deflection angles above 90°

External injury was never seen with initial deflection angles below 90° however it was common in higher angles. Example of an incapacitated fly following 90° HIT with no signs of external injury (A) and a fly with wing (purple ring), abdominal (green ring) and ocular (blue ring) trauma after a 135° HIT.

Incapacitation rates vary with the severity of injury

The percentage incapacitation, defined as a period of at least 20 seconds during which the fly makes no apparent purposeful movements following a HIT, was assessed in *hiw*$^{+/+}$ flies at different initial angles of deflection (figure 53).

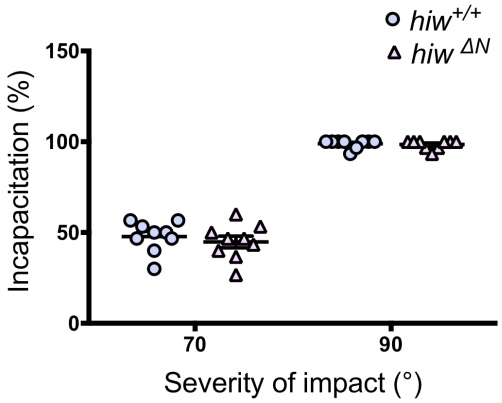

Figure 53. Incapacitation rates vary with force as determined by the angle of initial deflection but not genotype

Incapacitation rates were determined by subjecting flies to a single impact and assessing the percentage making no purposeful movement 20 seconds later. Each symbol represents the average incapacitation rate for one vial of flies following an impact at either 70° or 90° initial deflection. Rates of incapacitation are influenced by the initial deflection (70° v 90°, * $p \leq 0.0001$) but not the genotype. n = 9 vials of 20-35 flies per condition. * = $p \leq 0.05$, ** = $p \leq 0.01$, *** = $p \leq 0.001$, **** = $p \leq 0.0001$, ns = non-significant. Error bars show SEM. Statistics: 1 way ANOVA.

The angle of initial deflection determined the rate of incapacitation, with 70° deflection proportional to ~50% incapacitation, and 90° proportional to ~100%. HIT resulted in a high incapacitation rate that was comparable in both *hiw*$^{+/+}$ and *hiw*$^{\Delta N}$, with the majority recovering mobility within a few minutes.

Remaining experiments in this thesis were conducted at 90° unless otherwise stated. Given the high level of incapacitation and moderate rate of death at this angle, it was felt the most suitable to represent a severe injury, and also allow detection of treatment effects.

High impact trauma did not cause intestinal barrier failure

Intestinal barrier dysfunction (IBD) can be assessed in *Drosophila* by adding Brilliant Blue FCF dye (#80717, Sigma) to standard feed[299]. Following a single impact flies were fed standard

feed containing blue food dye. In the event of intestinal barrier dysfunction the dye would be expected to extend beyond the gut and proboscis, manifesting as a diffusely blue fly. We saw low rates of IBD (<2%) in flies 24 hours after exposure to a single high impact trauma regardless of genetic background (figure 54). The rates of IBD was not statistically different between injured and uninjured flies. This also supports the assertion that in our model HIT did not cause gross thoraco-abdominal trauma.

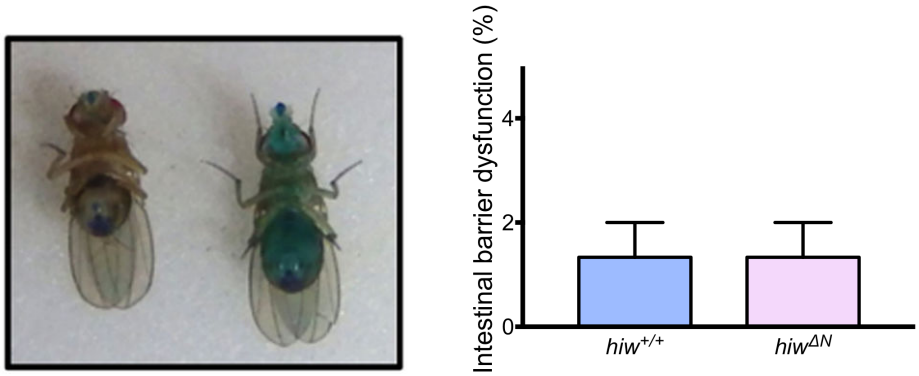

Figure 54. Rates of intestinal barrier dysfunction are low in hiw$^{+/+}$ and hiw$^{\Delta N}$ flies undergoing a single high impact trauma

When healthy uninjured flies are fed blue food dye it stays within their abdomens and proboscis, while in flies with disrupted intestinal barrier function the whole fly turns blue. We demonstrated that both *hiw*$^{+/+}$ and *hiw*$^{\Delta N}$ flies have equivalently low rates of intestinal barrier dysfunction after HIT. n= 9 repeats consisting of vials of 20-35 flies per condition. * = p≤ 0.05, ** = p≤ 0.01, *** = p≤ 0.001, **** = p≤ 0.0001, ns = non-significant. Error bars show SEM. Statistics: Student T test. *Image of flies from Barekat et al*[300].

2. Effect of *hiw*$^{\Delta N}$mutation on survival following high impact trauma

hiw$^{\Delta N}$mutation leads to an excess death at 24 hours but a reduction in long-term deaths over the entire lifespan in D*rosophila* exposed to a high impact trauma

To assess for variation in early death rates in different genotypes we exposed *hiw*$^{+/+}$ and *hiw*$^{\Delta N}$ flies to a single HIT. 24 hours later the percentage death was recorded (figure 55).

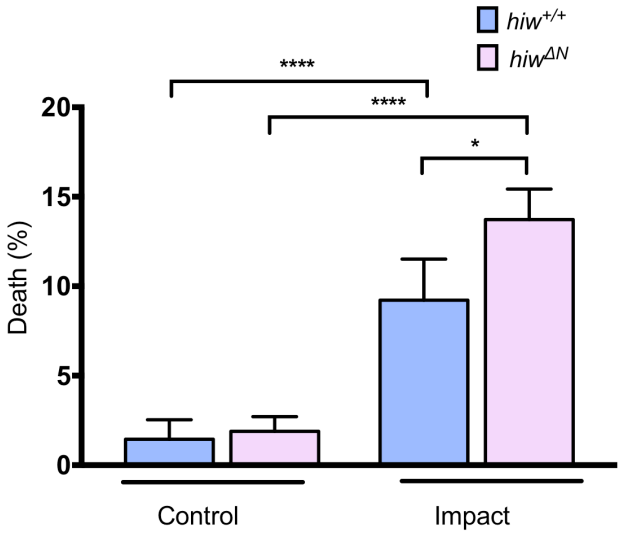

Figure 55. The percentage death in 24 hours following high impact trauma was greater in hiw$^{\Delta N}$ mutants compared to hiw$^{+/+}$ flies

All genotypes tested showed a significant increase in mortality 24 hours following a single severe TBI compared to matched controls. 24 hour mortality was greatest in the injured *hiw*$^{\Delta N}$ flies, which were significantly more likely to die than injured hiw+/+ flies. n = 9 vials of 20-35 flies per condition. * = p≤ 0.05, ** = p≤ 0.01, *** = p≤ 0.001, **** = p≤ 0.0001, ns = non-significant (p>0.05). Error bars show SEM. Statistics: 2 way ANOVA.

Flies with a *hiw*$^{\Delta N}$ mutation demonstrated a small early excess of deaths compared to wild type *hiw*$^{+/+}$ flies.

To determine if loss of highwire could protect against long-term effects of HIT we examined survival in animals that lived beyond the initial 24h post injury period. Flies alive 24 hours after HIT were monitored and the rates of death plotted with a survival curve until all flies had died (figure 56).

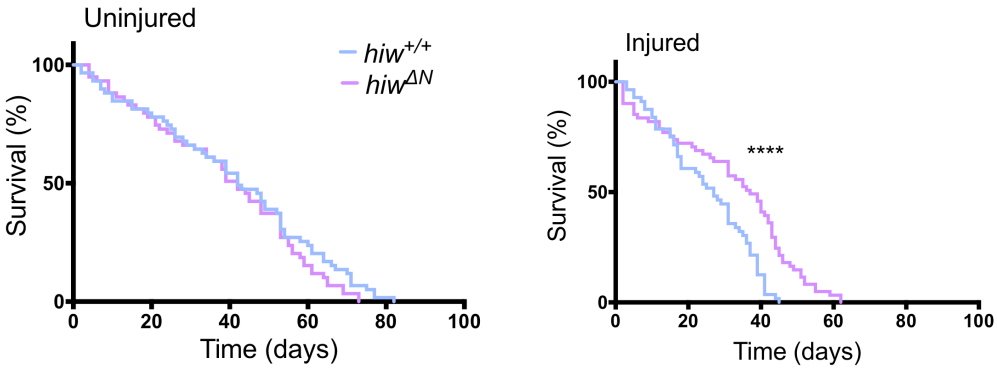

Figure 56. Rates of survival and total lifespan were greater in $hiw^{\Delta N}$ flies compared to $hiw^{+/+}$ following high impact trauma

$hiw^{\Delta N}$ and $hiw^{+/+}$ both showed an increase in mortality following a single HIT compared to matched controls. There was an additional significant burden in deaths in the $hiw^{+/+}$ flies compared to $hiw^{\Delta N}$. n = >60 flies per condition. * = p≤ 0.05, ** = p≤ 0.01, *** = p≤ 0.001, **** = p≤ 0.0001, ns = non-significant (p>0.05). Error bars show SEM. Statistics: log rank test.

We found that uninjured $hiw^{+/+}$ and $hiw^{\Delta N}$ demonstrated similar long-term survival, indicating no significant effect of the *highwire* null allele on baseline viability. Injury caused a significant reduction in long-term survival in both $hiw^{+/+}$ and $hiw^{\Delta N}$ animals compared to uninjured controls. However, $hiw^{\Delta N}$ animals demonstrated significantly increased survival following injury compared to hiw^{WT}, particularly from ~20 days post injury. Some of the delay in long-term death in the injured $hiw^{\Delta N}$ flies may be due to the early excess burden of death seen within the first 24 hours. However, the ~5% excess death seen in the first 24 hours post injury is insufficient to account for the marked difference in later death rates.

3. Effect of *hiw*$^{\Delta N}$mutation on functional measures following high impact trauma

High impact trauma causes functional deficits in climbing and flying behaviour that are rescued by *hiw*$^{\Delta N}$mutation

To determine if loss of *highwire* could rescue functional deficits induced by HIT we assessed the influence of HIT on complex motor pattern generation and execution in the form of climbing. This is a common measure of functional activity in *Drosophila* and is examined using a standardized rapid iterative negative geotaxis (RING) assay[325,326]. We examined the effects of HIT on RING in both *hiw*$^{+/+}$ and *hiw*$^{\Delta N}$ genotypes (figure 57).

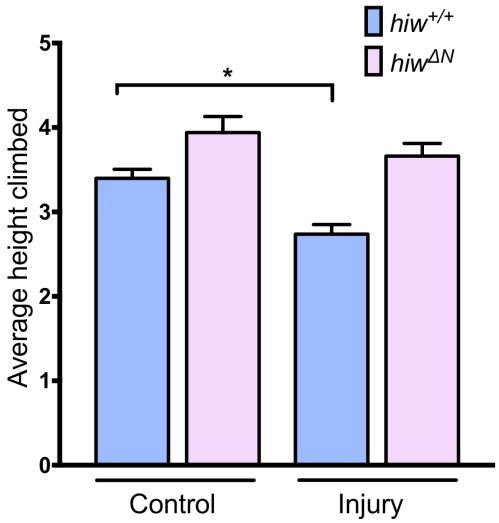

Figure 57. Rapid iterative negative geotaxis (RING) assay demonstrates a reduction in climbing ability that is attenuated in highwire mutants compared to controls

There was a significant reduction in climbing ability in injured versus uninjured *hiw*$^{+/+}$ flies at 45 days post injury. This response was attenuated in *hiw*$^{\Delta N}$ flies. n=6 vials of 25-35 flies per condition. * = p≤ 0.05, ** = p≤ 0.01, *** = p≤ 0.001, **** = p≤ 0.0001, ns = non-significant (p>0.05).Error bars show SEM. Statistics: 2 way ANOVA.

This experiment demonstrated a significant reduction in climbing ability after HIT in *hiw*$^{+/+}$ flies, which was attenuated at 45 days in those with a *hiw*$^{\Delta N}$ deletion. There was no significant baseline difference in climbing ability between *hiw*$^{+/+}$ flies and those with a *hiw*$^{\Delta N}$ deletion. In order to further validate these findings by testing another functional/behavioral measure of motor function we examined flying ability with HIT in different genotypes (figure 58).

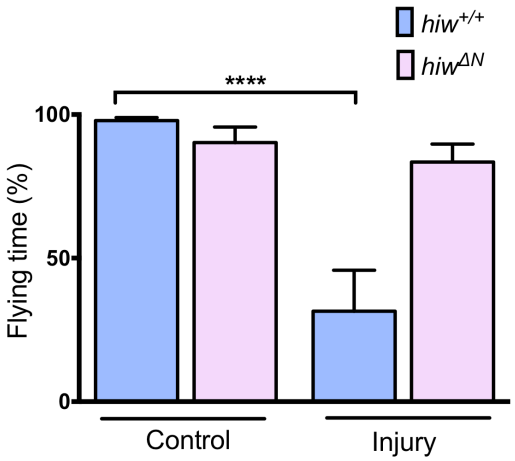

Figure 58. Flying time is significantly reduced following injury in hiw$^{+/+}$ flies but not in hiw$^{\Delta N}$ flies

At 7 days following injury *hiw*$^{+/+}$ show a significant reduction in the percentage of time they spend in flight. This deterioration in flying activity is rescued in the *hiw*$^{\Delta N}$ flies. There was a significant reduction in climbing ability in injured versus uninjured *hiw*$^{+/+}$ flies at 45 days post injury. This response was attenuated in *hiw*$^{\Delta N}$ flies. n= 12 per condition. * = p≤ 0.05, ** = p≤ 0.01, *** = p≤ 0.001, **** = p≤ 0.0001, ns = non-significant (p>0.05).Error bars show SEM. Statistics: 2 way ANOVA.

At 7 days following injury *hiw*$^{+/+}$ show a significant reduction in the percentage of time they spend in flight over a 30 second period when compared to controls of their own genotype. This deterioration in flying activity after injury is strikingly diminished in the *hiw*$^{\Delta N}$ flies. Flies that had lost the ability to fly after HIT still had wings that were overtly uninjured, make frequent spontaneous wing movements, and engage in wing grooming behavior, suggesting that the failure to fly even when provoked by a stimulus of air is not simply as a result of a peripheral wing injury. This is supported by the cases where short periods of flight are initiated but the flies seem unable to maintain for a prolonged duration.

4. Effect of *hiw*$^{\Delta N}$mutation on synaptic markers and nucleotide levels following high impact trauma

Loss of Highwire reduces synaptic protein loss following injury

The rescue of HIT induced premature mortality and climbing/flying deficits in *hiw*$^{\Delta N}$ flies invites further exploration. The most striking consequences of a LOF mutation in *highwire* flies, as previously described is the marked delay in WD and NMJ synaptic overgrowth. The synaptic overgrowth in *highwire* LOF mutations has only been described in the NMJ, and not centrally. However, axon protective phenotypes may also protect against synaptic loss, and synaptic loss may occur in TBI. Therefore, we hypothesized that HIT would cause synaptic loss, and that *hiw*$^{\Delta N}$ mutation would protect against this loss. This was investigated with antibodies against pre and post synaptic markers. We conducted Western blots analysis using the pan-neuronal marker Neuroglian (NGL), the presynaptic marker Bruchpilot (BRP), and the post synaptic maker Disc Large (DLG) at 24 hours and 7 days following injury (figure 59). All western blots are from pooled samples of 10 fly heads only. Full details of the WB process a is described in the Materials and Methods chapter (page 72).

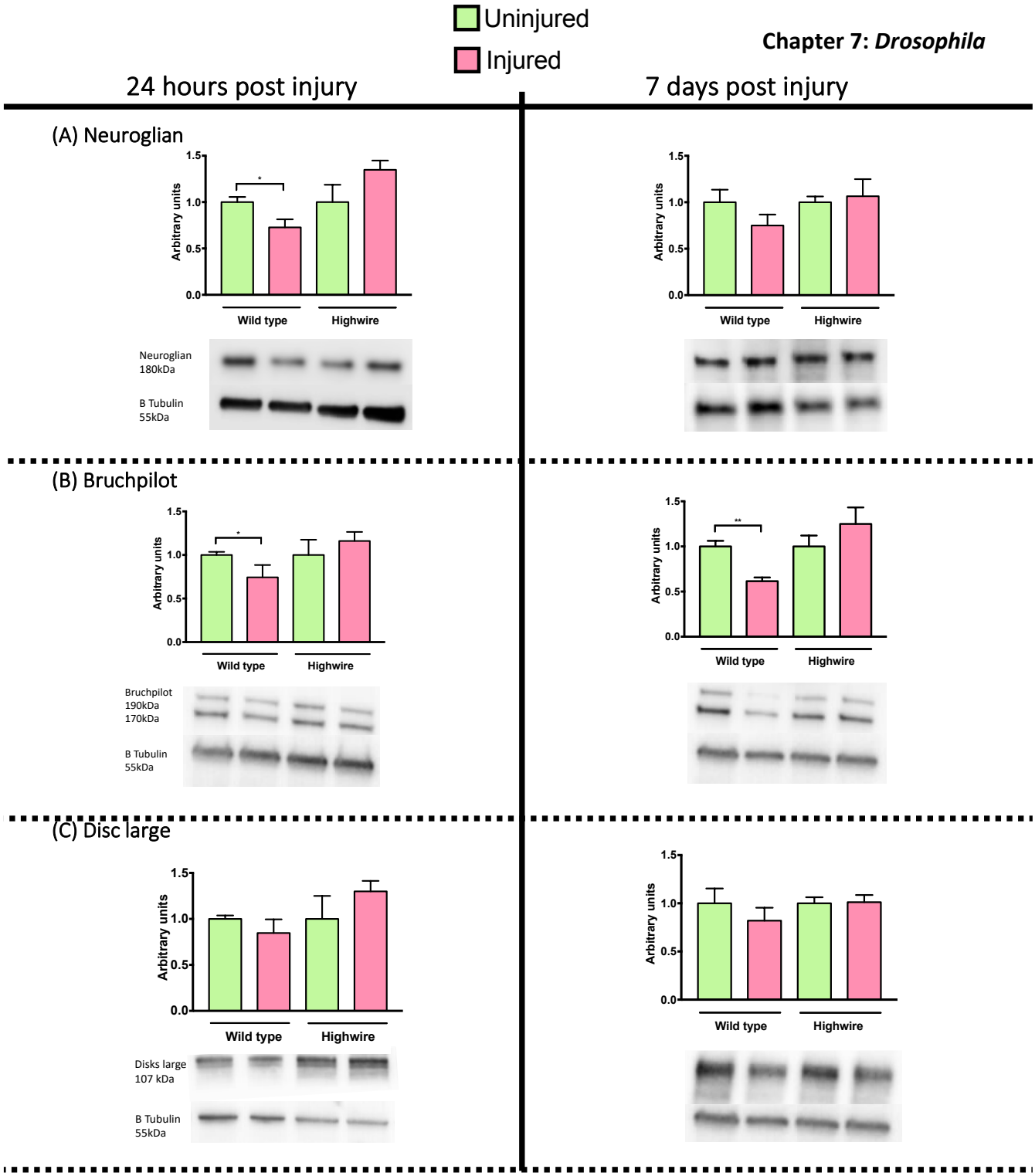

Figure 59. High impact trauma causes reduced levels of pan-neuronal and presynaptic markers that is rescued by highwire mutation

Western blot from pooled fly heads. At 24 hours following injury *hiw*$^{+/+}$ but not *hiw*$^{\Delta N}$ show a significant reduction in levels of the pan-neuronal marker neuroglian (NGL) and the presynaptic active zone marker bruchpilot (BRP). Levels of BRP fall further at 7 days in *hiw*$^{+/+}$, but the reduction in NGL no longer reaches significance. There is no change in the post-synaptic marker disc large (DLG) at any stage. n= 5 per condition. * = p≤ 0.05, ** = p≤ 0.01, *** = p≤ 0.001, **** = p≤ 0.0001, ns = non-significant (p>0.05).Error bars show SEM. Statistics: 2 way ANOVA.

NGL is a pan-neuronal marker, BRP a pre-synaptic marker of the active zone of synapses, and DLG is a post-synaptic marker. Western blot analysis demonstrated a significant fall in NGL and BRP following HIT at 24 hours. This was rescued by $hiw^{\Delta N}$ mutation. Similar reductions were seen at 7 days in $hiw^{+/+}$ but the reduction in NGL no longer reached significance. There were no significant changes in the post-synaptic marker DLG following HIT in $hiw^{+/+}$ or $hiw^{\Delta N}$ mutation, although there appeared to be a possible rise at 24 hours in $hiw^{\Delta N}$ mutants.

Exploring if HIT causes changes in NMN or NAD levels

The finding that HIT causes a reduction in presynaptic markers that can be rescued by $hiw^{\Delta N}$ opens the possibility that some aspects of the injury may be mediated by alterations in NMN or NAD levels. As previously described, reductions in dNMNAT levels distal to transections is a core aspect of the WD pathway and leads to an increase in NMN/NAD ratio. As *highwire* activity normally acts to deplete dNMNAT levels then $hiw^{\Delta N}$ might be hypothesised to maintain dNMNAT levels and hence delay a rise in NMN/NAD levels associated with WD following injury. It is unknown whether TBI alters levels of NMN/NAD, this can be tested by measurement using high performance liquid chromatography (HPLC). Therefore, to explore the mechanism of injury causing selective synaptic marker loss we examined total NMN and NAD levels in the heads of $hiw^{+/+}$ and $hiw^{\Delta N}$ mutation flies in an uninjured and post-HIT injured state (figure 60).

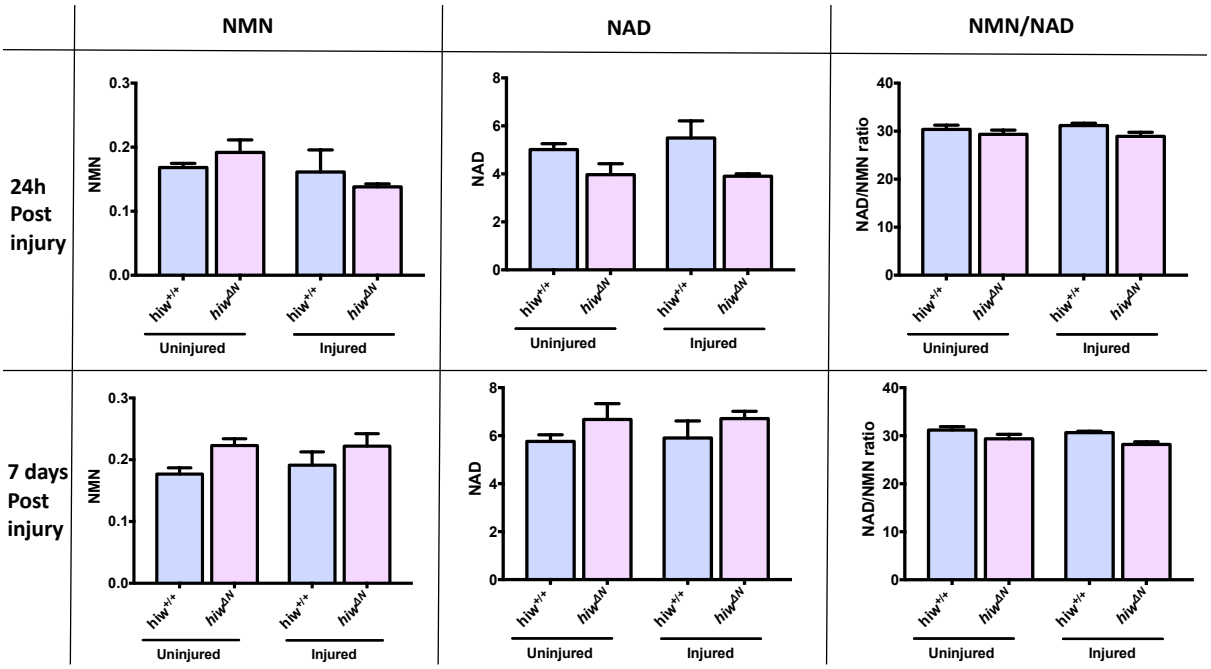

Figure 60. High impact trauma does not significantly alter NMN or NAD levels

There was no significant difference detected in NMN, NAD or NMN/NAD ratios in *hiw*$^{+/+}$ or *hiw*$^{\Delta N}$ flies that were 24 or 7 days post injury. n= 5 per condition. * = p≤ 0.05, ** = p≤ 0.01, *** = p≤ 0.001, **** = p≤ 0.0001, ns = non-significant (p>0.05).Error bars show SEM. Statistics: 2 way ANOVA.

No significant differences in NMN, NAD or NMN/NAD ratio were detected in any of the experimental conditions tested.

5. Effect of *hiw*$^{\Delta N}$mutation on neuronal cell loss following high impact trauma

HIT causes brain vacuolation independent of genotype

Brain vacuolation is a recognized marker of brain neurodegeneration in *Drosophila*[292,298,486,487]. In order to explore if HIT was causing brain neurodegeneration, and if the protective effects of *hiw*$^{\Delta N}$ were in part mediated by this process, we used haematoxylin and eosin (H&E) staining to assess for vacuolation at 28 days following injury (figure 61).

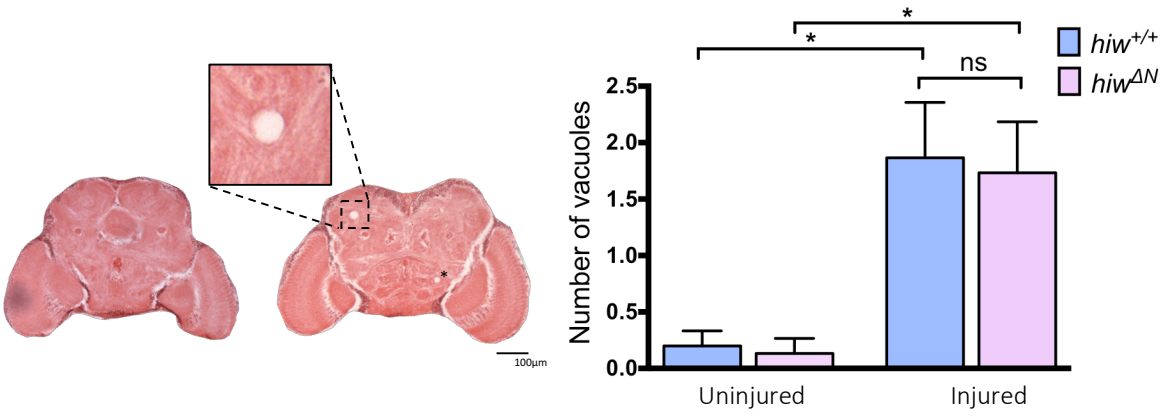

Figure 61. Injured flies develop greater vacuolation than controls independent of genotype

Representative hematoxylin and eosin stained brain sections from uninjured *hiw*$^{+/+}$ flies (left) and injured *hiw*$^{+/+}$ flies (right). The insert shows a close up of a typical vacuole. A further small vacuole is marked by an *. At 28 days following ssTBI the rates of vacuolation seen by hematoxylin and eosin staining in central brain regions was consistently greater in injured flies than uninjured flies. However, there was no significant difference based on genotype. n = 5 per condition. * = p≤ 0.05, ** = p≤ 0.01, *** = p≤ 0.001, **** = p≤ 0.0001, ns = non-significant (p>0.05).Error bars show SEM. Statistics: 2 way ANOVA.

H&E staining showed an increase in the rate of vacuolation following HIT compared to controls but this was the same regardless of genotype, with no statistical difference between injured *hiw*$^{+/+}$ and *hiw*$^{\Delta N}$ flies.

Flow cytometry of dissociated *Drosophila* brains shows necrosis but low levels of apoptosis after injury

In order to examine the mechanism of cellular loss in HIT– whole *Drosophila* brains were trypsinized and dissociated into a single cell solution from which cells were analysed with a flow cytometry using fluorescent stains for markers of apoptosis (annexin V) and necrosis (7AAD) (figure 62).

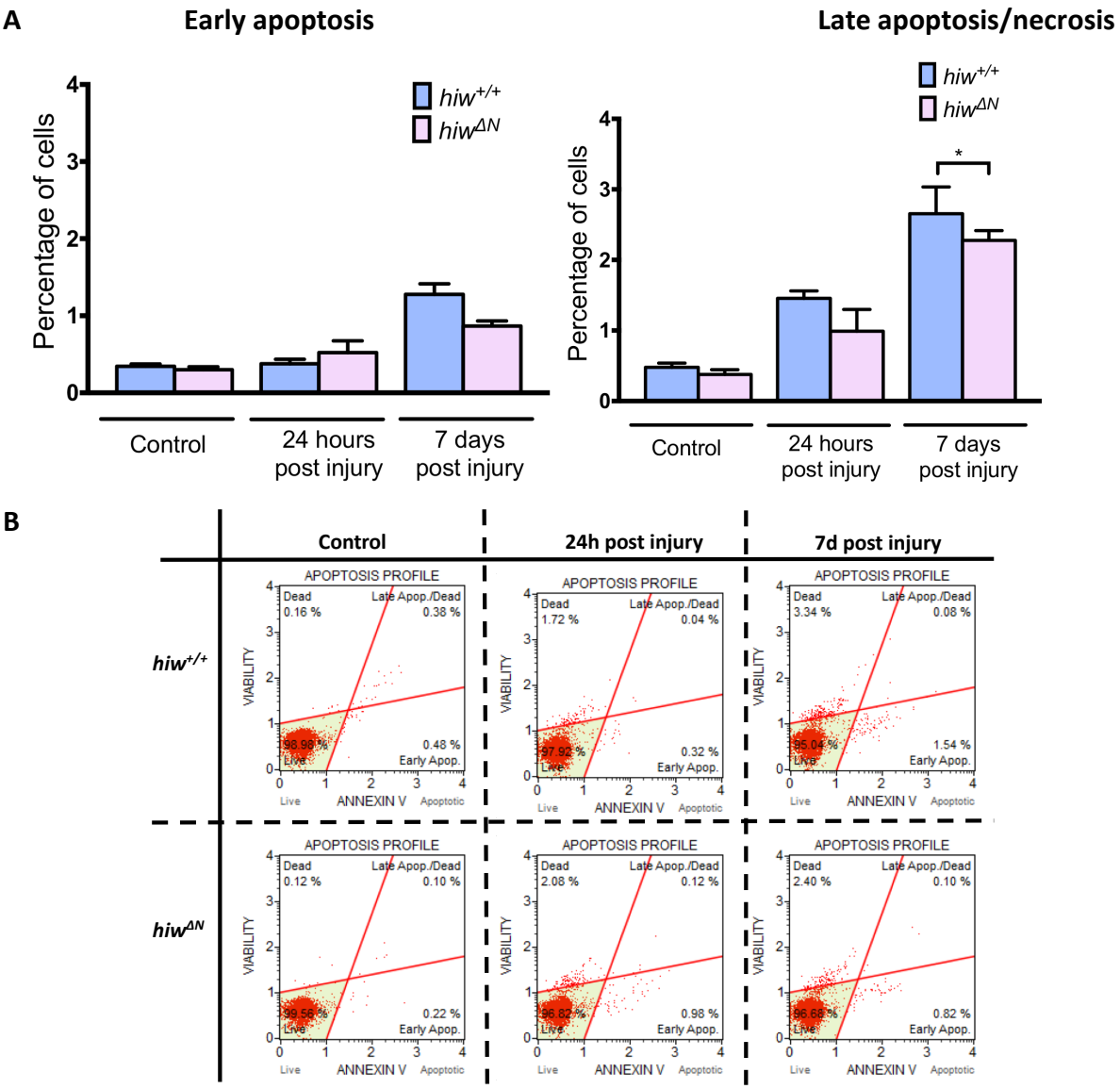

Figure 62. Flow cytometry of drosophila brains shows increased cellular death after HIT with a reduction in late apoptosis/necrosis in hiw$^{\Delta N}$ compared to hiw$^{+/+}$ flies at 7 days

(A) Rates of early apoptosis, and late apoptosis/death in uninjured controls, and injured fly brains 24 or 72 hours after HIT as assessed by flow cytometry. There is significantly less late apoptosis and death in *hiw*$^{\Delta N}$ compared to *hiw*$^{+/+}$ flies. (B) Representative flow cytometry data demonstrating the rates of dead and late apoptotic (grouped together for analysis) cells, and those demonstrating early apoptosis. n = 9 per condition. * = p≤ 0.05, ** = p≤ 0.01, *** = p≤ 0.001, **** = p≤ 0.0001, ns = non-significant (p>0.05).Error bars show SEM. Statistics: 2 way ANOVA.

Flow cytometry of dissociated fly brains demonstrated low-levels of baseline early apoptosis (Annexin V positive, 7 AAD negative) and late apoptosis/cell death (Annexin V positive and 7 AAD positive) in *hiw*$^{+/+}$ and *hiw*$^{\Delta N}$ uninjured controls (<0.5%).

Flow cytometry demonstrated a progressive increase in early apoptosis, and late apoptosis/cell death following injury at 24 hours and 7 days. There was significantly less late apoptosis/death in the *hiw*$^{\Delta N}$ flies at 7 days but the absolute difference was small (<0.5%).

High impact trauma causes a depletion of PPL1 cluster dopaminergic neurons that is attenuated by *hiw*$^{\Delta N}$ mutation

As there was no difference in the levels of vacuolation rates in *hiw*$^{+/+}$ and *hiw*$^{\Delta N}$ flies to explain the differences in lifespan and behavior, but flow cytometry suggested that there was a small additional burden of cellular death, this suggests that there may be a subpopulation of neurons vulnerable to injury. In order to test this hypothesis we examined a well-characterized subpopulation of neurons – the PPL1 cluster– that are associated climbing deficits when depleted, and are vulnerable in fly genetic models of Parkinson's disease, a condition that has been linked to TBI. The PPL1 neurons are a subgroup of dopaminergic neurons that stain positively for tyrosine hydroxylase antibody and are normally consistent in number. They cluster in the postero-lateral brain of the fly. We hypothesized that an injury might induce a reduction in the number of these cells, and this might underlie the deficits seen following a HIT, being one of the targets protected by *hiw*$^{\Delta N}$ mutation (figure 63).

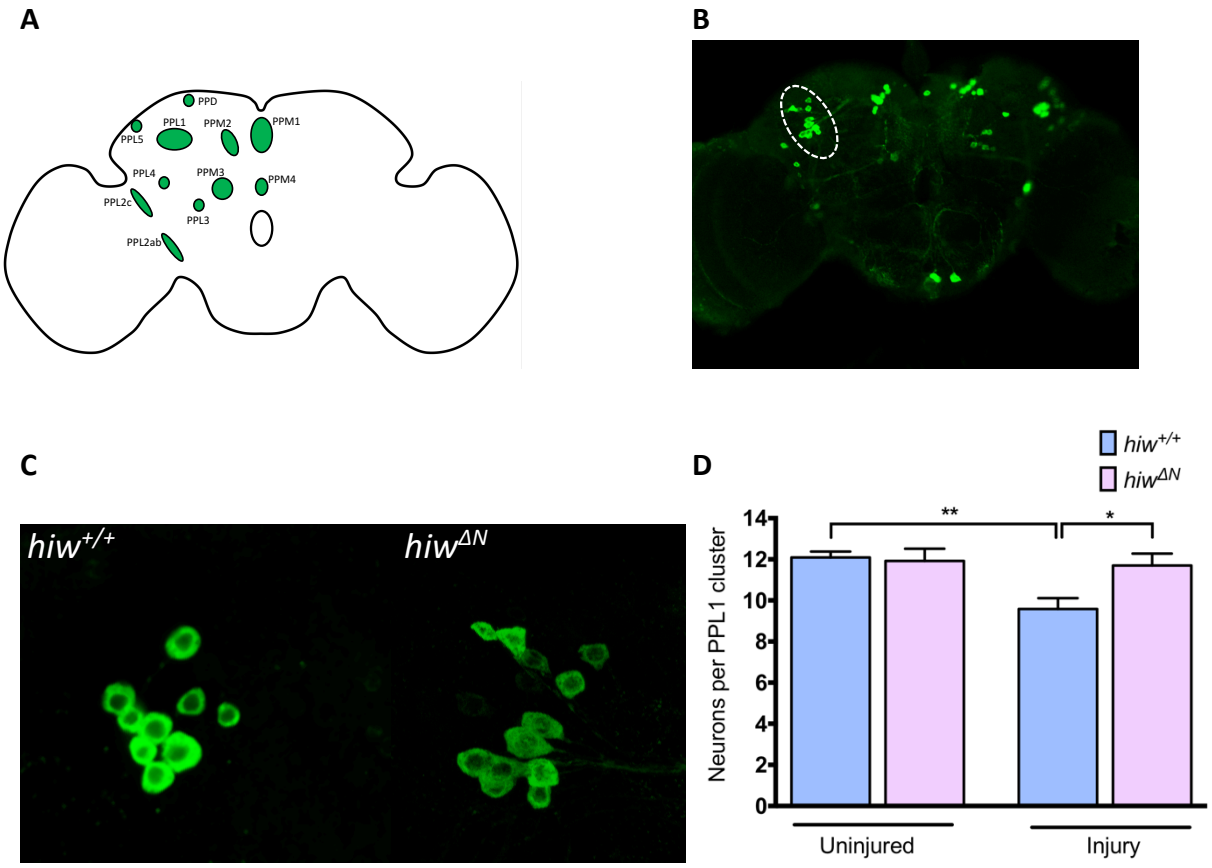

Figure 63. Injury causes a depletion of PPL1 cluster dopaminergic neurons that is attenuated by hiw$^{\Delta N}$ mutation

(A) Schematic image, and (B) TH stained whole brain mount showing the location of various dopaminergic neuronal clusters, including the PPL1 cluster. (C) Representative PPL1 dopaminergic neuronal clusters showing depleted neuron numbers in injured *hiw*$^{+/+}$ flies (9 neurons), and preserved numbers in injured *hiw*$^{\Delta N}$ flies (14 neurons). (D)The average number of PPL1 neurons is 12 in both *hiw*$^{+/+}$ and *hiw*$^{\Delta N}$ uninjured control flies. Following injury there is a significant reduction seen in the number of PPL1 neurons in *hiw*$^{+/+}$ but not *hiw*$^{\Delta N}$ flies. n = 10-12 clusters per condition. * = p≤ 0.05, ** = p≤ 0.01, *** = p≤ 0.001, **** = p≤ 0.0001, ns = non-significant (p>0.05).Error bars show SEM. Statistics: 2 way ANOVA.

Twenty-eight days following HIT a fall in the number of TH-positive PPL1 neurons was seen in *hiw*$^{+/+}$ flies, from ~12 to 10. This neuronal loss was wholly rescued in the *hiw*$^{\Delta N}$ flies where no reduction was seen.

6. Rotenone as a model of PPL1 neuronal loss

Rotenone has been used to model PPL1 neuronal loss but we found defects were indistinguishable from DMSO dosing

The ability of *hiw*$^{\Delta N}$ to rescue PPL1 dopaminergic loss following HIT opens up the intriguing possibility that it might also rescue PPL1 loss in other models with similar a mechanistic cause of cellular loss. Rotenone is a complex 1 inhibitor of the electron transport chain in mitochondria. Chronic exposure for 7 days in adult *Drosophila* has been used to model Parkinson's disease, with associated loss of locomotor function and selective dopaminergic neuron loss including of the PPL1 cluster[488]. Similar deficits in locomotion and dopaminergic neurons were seen in *Drosophila* larvae exposed to rotenone during development[489]. The mechanism of this selective dopaminergic loss has not been fully elucidated but has been attributed to reactive oxygen species and oxidative damage, associated with mitochondrial dysfunction[490,491].

Therefore, I planned to dose flies with rotenone to see if I could reproduce the locomotor deficits and PPL1 neuronal loss seen in the drosophila TBI model, and rescue the defects with *hiw*$^{\Delta N}$. This was with a view to exploring commonalities in mechanism between TBI and rotenone induced dopaminergic loss, and potentially expanding the therapeutic remit of the WD pathway/*highwire* mutation.

Rotenone comes as a powder that is insoluble in water (#8875, Sigma). It is prepared by dissolving in DMSO, chloroform, or 100% ethanol. The maximum solubility of rotenone in DMSO is 39.44mg/ml (100mM) but concentrations of 0.5mg/ml are recommended in some product information (source – Torcis and Sigma product information sheets). This was in keeping with my own findings where at concentrations above 125mM the rotenone remained particulate and did not fully dissolve. Rotenone can be dissolved in DMSO, chloroform or 100% ethanol but are all known to be toxic to *Drosophila*. with the toxicity limit for DMSO in larvae being reported as 0.5% of dietary concentration[492–497]. I dissolved rotenone in DMSO at the highest concentration possible before precipitation occurred (125mM) to minimise DMSO exposure. Experiments were performed by mixing the DMSO-drug combination into food (4-24 instant *Drosophila* Medium, Carolina Biological Supply, NC). Climbing ability and death

rates were assessed in *hiw*$^{+/+}$ flies at different rotenone concentrations with matched DMSO only controls (figure 64).

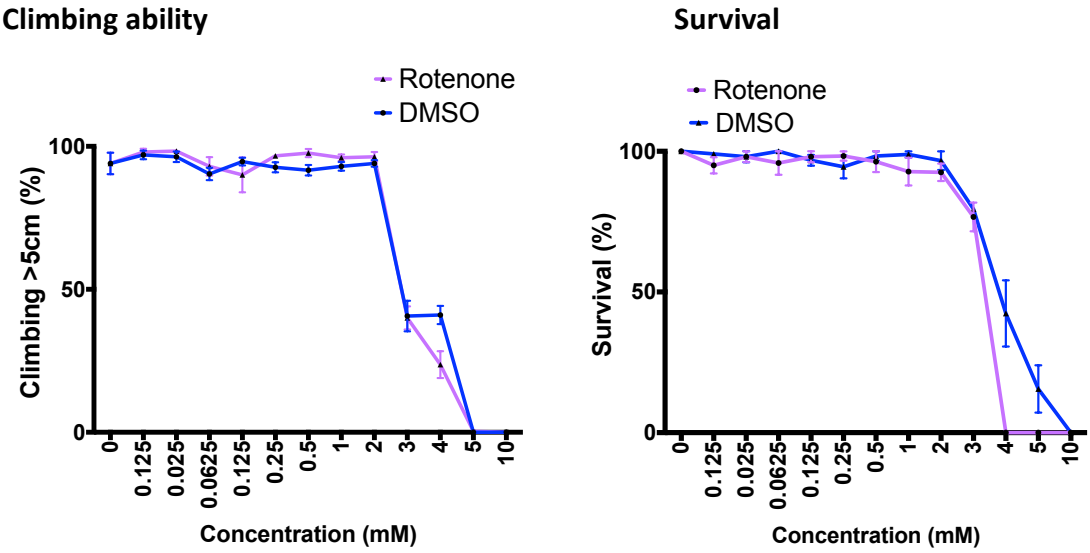

Figure 64. Effect of rotenone concentration and DMSO on climbing and survival

Effects of rotenone dissolved in DMSO, and equivalent volumes of DMSO without rotenone, on climbing ability and survival at 7 days after initiation of treatment. n= 3 repeats and 3 replicates per condition with 15-30 flies per vial.

1-4 day old *hiw*$^{+/+}$ flies were fed with freshly made feed with DMSO+/-rotenone solution each day. Monitoring drug ingestion can be challenging in Drosophila. In order to confirm that the flies were consuming a given drug, it was mixed with an inert blue food dye Brilliant Blue FCF (#80717, Sigma). When ingested this turned the abdomen of the fly unmistakably blue. While this confirms ingestion of the drug, quantification of the amount ingested is unknown, the assumption being made that ingestion is comparable in all flies/conditions. Flies that are desiccated by withholding all water die within 4 days without exception. Therefore, we can be sure that flies were consuming the drug in all cases. As rotenone is known to undergo light induced degradation, flies were stored in the dark throughout the experiment[498].

On the basis of this data, it appears that the toxic effects of DMSO and rotenone cannot be separated in adult flies in my hands, possibly due to low solubility of rotenone meaning that toxic volumes of DMSO are needed to dissolve the rotenone before effects are seen. Previous

reports state that fatal toxicity occurs when adult drosophila are exposed to 500µM of rotenone for 7 days in 55 to 95%+ of flies[490,499]. At these levels significant locomotor impairment and was also reported[488]. These rates of death were not seen in my experiments. I found that adult flies treated with rotenone in concentrations from 12.5µM up to 2mM for 7 days did not show excess death over those treated with DMSO. This trend continued when flies were followed for an additional 21 days (data not shown). The reason for this discrepancy may be related to unrecognised toxicity of the DMSO in some of the existing literature. To my knowledge, none of the publications exploring rotenone-toxicity in drosophila stated that they expose controls to matching levels of DMSO, or specify the volume of DMSO in which they dilute the rotenone. If rotenone is diluted at 0.5mg/ml (=1.25mM) as recommended by Sigma then to achieve a treatment dose of 500µM then food or sucrose feed would need to be 40% DMSO. With solutions of 16% DMSO I saw 100% death at 7 days. In the Leite *et al* paper rotenone is dissolved in 98% ethanol which is also given to their controls. In the ethanol exposed control flies they report ~15-20% mortality at 7 days, and state that this is comparable to the non-ethanol exposed controls, but they do not present this data they base this statement upon[499]. I did not dissolve rotenone in ethanol due to its well characterized toxic effects including a complete obliteration of negative geotaxis. The ethanol concentration that causes a 50% lethality was 0.65% ethanol vapour after 85 minutes exposure[478,495].

An alternative explanation for my failure to see toxic effects of rotenone at concentrations below that at which I saw DMSO related toxicity may be that the rotenone was degraded. It is a notoriously unstable compound. However, I repeated the experiment with fresh batches of rotenone (different lot numbers and suppliers, Abcam #143145 and Sigma #8875) on 2 different occasions without any change in results.

7. *hiw$^{\Delta N}$*mutation does not rescue functional deficits caused by a *PINK1^{B9}* mutation

PINK1^{B9} mutation causes climbing and flying deficits that are not rescued by *hiw$^{\Delta N}$* mutation

An alternative approach to investigate the role of *highwire* in dopaminergic cellular loss that is not dependent on drug administration is to use a genetic model. Drosophila PTEN-induced putative kinase 1 (*PINK1*) also known as CG4523 is a putative mitochondrial protein. Loss of function mutations in drosophila are viable and develop to adulthood but had reduced lifespans. They also have well characterised deficits including those seen in my model of TBI, specifically reductions in climbing and flying ability, and also PPL1 neuronal numbers [322]. As *highwire* and *PINK1* are both on the X chromosome it was necessary to utilize a recombination based approach with PCR confirmation to establish their knockout in the same flies. This recombination was undertaken by the Alex Whitworth lab on my behalf. We first examined if recombining *hiw*$^{\Delta N}$ with *PINK1^{B9}* would rescue the climbing or flying deficit 7 days after eclosion (figure 65).

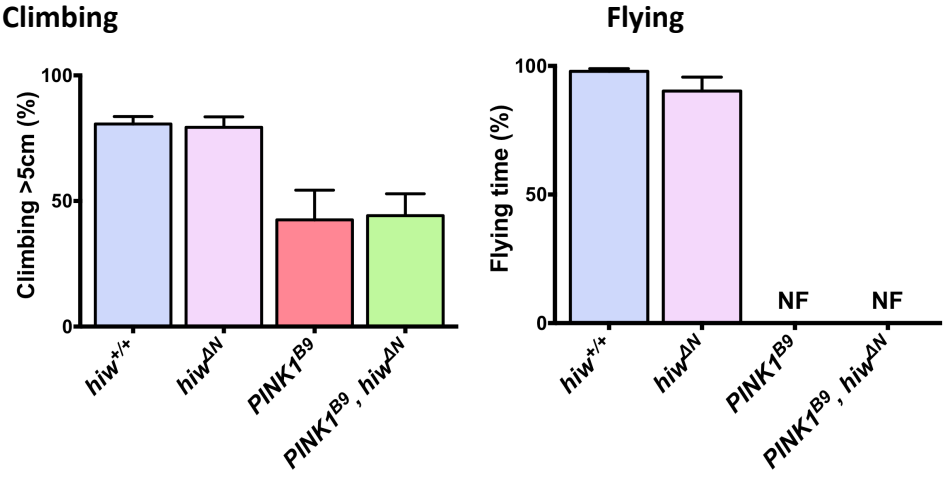

Figure 65. hiw$^{\Delta N}$ mutation does not rescue climbing or flying deficits due to PINK1^{B9} mutation

Climbing and flight at 7 days *in vivo* was the same in hiw$^{\Delta N}$ and hiw$^{\Delta N}$ flies. *PINK1^{B9}* flies climbed less, and flew for shorter duration than hiw$^{+/+}$ flies, this deficit was not rescued by *PINK1^{B9}*,hiw$^{\Delta N}$ recombination. NF = no flight. n = 3 repeats per condition for climbing and n = 9 repeats per condition for flying, both with 3 replicates. * = p≤ 0.05, ** = p≤ 0.01, *** = p≤ 0.001, **** = p≤ 0.0001, ns = non-significant (p>0.05). Error bars show SEM. Statistics: 1 way ANOVA.

We found that *hiw$^{\Delta N}$* was unable to rescue climbing or flying behaviour with indistinguishable activity between *PINK1^{B9}* flies and *PINK1^{B9}*,hiw$^{\Delta N}$ flies.

8. *hiw$^{\Delta N}$*mutation does rescue neuronal loss and death, but not male sterility caused by a *PINK1^{B9}* mutation

PINK1^{B9} mutation causes PPL1 neuronal loss that is rescued by *hiw$^{\Delta N}$* mutation

Although climbing and flying are partially mediated by selective dopaminergic loss, they are also dependent upon normal peripheral neuro-musculature. Therefore, failure of *hiw$^{\Delta N}$* to rescue these deficits does not necessarily mean that there it is failure to rescue dopaminergic neuron loss as this could still be the case despite motor deficits. In order to directly examine dopaminergic neurons for rescue we stained whole brain dissections with TH antibody (figure 66).

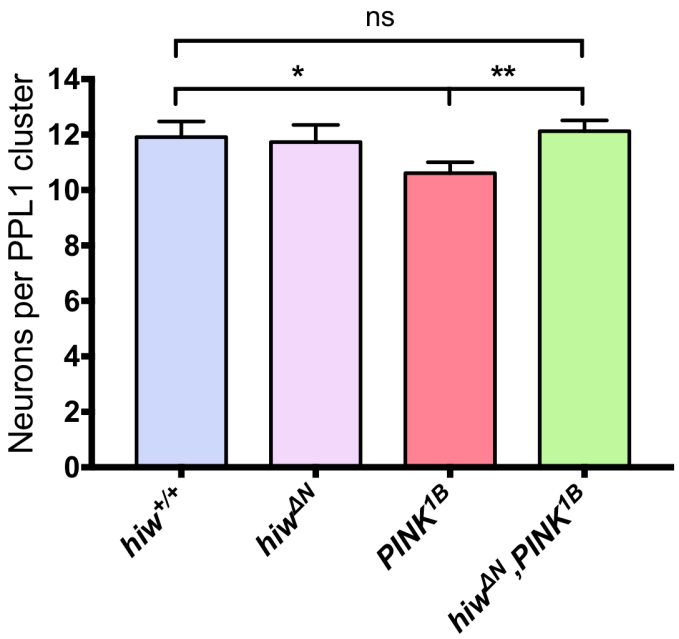

Figure 66. PINK1^{B9} mutation is associated with a reduction in PPL1 dopaminergic neurons, this is rescued by hiw$^{\Delta N}$ mutation

The mean number of PPL1 dopaminergic neurons in wild-type *hiw$^{+/+}$* and *hiw$^{\Delta N}$* flies is reliably ~12. In *PINK1^{B9}* flies this is significantly reduced to an average of 10.5. This is completely rescued by co-expression of a *highwire* LOF mutation in *PINK1^{B9},hiw$^{\Delta N}$* flies. n = 11-23 repeats per condition * = p≤ 0.05, ** = p≤ 0.01, *** = p≤ 0.001, **** = p≤ 0.0001, ns = non-significant (p>0.05).Error bars show SEM. Statistics: 1 way ANOVA

We found that *PINK1^{B9}* mutants had a small but significant mean reduction in neuronal number that was completely rescued by combination with a *hiw$^{\Delta N}$* mutation.

PINK1B9 mutation causes premature death that is rescued by hiwΔN mutation

A reduction in lifespan has been demonstrated in a number of *PINK1* studies[500–502]. In light of the PPL1 dopaminergic neuron rescue we explored whether combination with a *hiw$^{\Delta N}$* mutation was also able to rescue the lifespan survival deficit (figure 67).

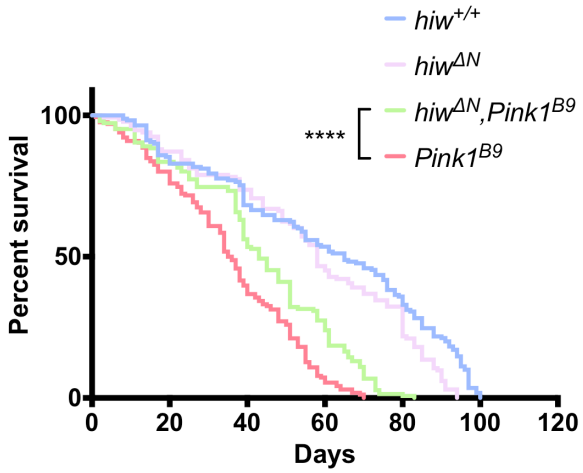

Figure 67. PINK1^{B9} mutation is associated premature death, this is rescued by hiw$^{\Delta N}$ mutation

The rate of death is accelerated in *PINK1^{B9}* flies. This is partially rescued by co-expression of a *highwire* LOF mutation in *PINK1^{B9},hiw$^{\Delta N}$* flies. n = 150+ flies per condition * = p≤ 0.05, ** = p≤ 0.01, *** = p≤ 0.001, **** = p≤ 0.0001, ns = non-significant (p>0.05).Error bars show SEM. Statistics: log rank test.

As previously reported, *PINK1^{B9}* flies experience premature death compared to wild-type *hiw$^{+/+}$* flies. We found that *PINK1^{B9}* had a significantly reduced lifespan with a median survival of 36 days, and maximum survival ~70 days. This compares to a median survival of 65 days and maximum survival of 90-100 days for wild-type flies. It is notable that this increased rate of mortality in *PINK1^{B9}* flies could be partially rescued by combination of with *hiw$^{\Delta N}$* mutation (*PINK1^{B9},hiw$^{\Delta N}$*). The *PINK1^{B9}, hiw$^{\Delta N}$* flies demonstrated a partial rescue of mortality, with a significantly slower rate of death compared to *PINK1^{B9}*. The median survival was 43 days and maximum lifespan was 85 days.

PINK1^{B9} mutation causes male sterility that is not rescued by *hiw$^{\Delta N}$* mutation

PINK1^{B9} mutant flies have an established male sterility, and female subfertility related to mitochondrial dysfunction and nebenkern malformation [501]. In order to establish if the

addition of a *hiw*$^{\Delta N}$ loss-of-function mutant was able to rescue male sterility four recently eclosed individual male flies were placed with four wild type virgin female flies (w^{1118}) in vials. Males were scored as sterile if the paired females failed to produce larval progeny by day 10. In eight separate trials all male *PINK1*^{B9},*hiw*$^{\Delta N}$ flies were found to be infertile, indicating a failure of this recombination to rescue fertility.

Summary

The *highwire* gene encodes a large 5233 amino acid protein with E3 ubiquitin ligase activity that modulates levels of dNMNAT[218,223–225]. LOF mutations in the *highwire* gene are associated with a strong delay in axon degeneration following transection both *in vitro* and *in vivo*[223,224,226,227]. We reproduced and characterised a fly model of TBI[298]. The WD pathway is also preserved across species, with evidence that the key molecular processes are conserved between mammals and flies [7,179,204,225,297]. Reflecting the known role of *highwire* in dNMNAT depletion and subsequent axon degeneration, and the assessment that WD may contribute to the secondary brain injury seen in TBI, we hypothesised that flies with a LOF mutation in *highwire* (*hiw$^{\Delta N}$*) would show protection against the effects of TBI. We found that *hiw$^{\Delta N}$* flies showed relative protection against long-term mortality, behavioural assays, cell death including dopaminergic neuron loss, and presynaptic marker depletion following HIT. These findings suggest that *highwire* is a potential therapeutic target in TBI. Given the dopaminergic cell loss seen after HIT, and the relationship between TBI and PD, it was hypothesized that *hiw$^{\Delta N}$* would protect against the dopaminergic depleting *PINK1* mutation. We demonstrated that this was the case, and that *hiw$^{\Delta N}$* mutation was able to completely rescue *PINK1* mutation related dopaminergic cell loss, and partially rescue premature death, but not flying and climbing assays. These findings suggest for the first time that *highwire* may be a novel potential therapeutic target in both TBI and PD.

Discussion

Developing and characterizing a model of TBI in Drosophila

To investigate the role of the *highwire* gene as a potential novel therapeutic target of TBI we utilised a *Drosophila* model of TBI, in which WD pathways show extensive conservation with mammalian species[7,179,204,225,297,298,300]. The initial results presented in this chapter were concerned with the development and characterisation of the *Drosophila* model of high impact trauma. While a similar device has been previously described, it was still necessary to establish this model in our hands and calibrate and further characterise its effects[298,299]. Key preliminary questions that must be considered are the degree to which the HIT is producing a brain injury, the pathophysiological nature of this injury, and if such an injury is an isolated cranial injury or combined with other extracranial injury. Such questions were posed in previous studies with a similar device and they concluded that TBI did occur but could not exclude the co-existence of extra-cranial injuries[298,299]. Traditional markers of brain injury including pathological examination, imaging findings, and biomarkers are not available in a *Drosophila* model–therefore determining that a TBI was occurring was based upon a combination of a mechanism consistent with a TBI, a TBI appropriate behavioural response to injury, health consequences including changes in mortality, and analysis of the fly brains for markers of neuronal injury.

The HIT model causes flies to hit the sides of the polystyrene vial so mechanistically this is in keeping with a closed head injury trauma capable of causing a brain injury. Previous studies have demonstrated this with high-speed video analysis[298]. Flies are also seen to undergo a period of incapacitation, defined by temporary loss of voluntary movement. During this period flies often remain immobile and lie prostate, as they recover they demonstrate twitching of limbs and initial movements that appear to lack purpose, before eventually righting themselves. After a further period of irregular and unsteady/ataxic movement, until they recover apparently normal motility. Temporary incapacitation suggests but does not prove a brain injury. The rates of incapacitation were reproducible and severity dependent. Likewise, the HIT model we presented showed a rate of death at 24 hours following injury that was severity dependent. The low rates of IBD in our model also suggests that there was an absence of gross thoraco-abdominal trauma. Other findings including brain specific markers of injury -

brain vacuolation, PPL1 neuronal loss, and increased cellular death, occurred following HIT. These all support the assertion that the HIT device causes a TBI. It seems likely that given the mechanism of injury there would be a proportion of extra-cranial injuries in the flies exposed to HIT. However, quantification of this was not undertaken in previous publications and we also did not establish the degree to which this contributed to outcomes in our model other than the demonstration that we did not see intestinal barrier dysfunction. At an initial spring deflection of 90°– the force determining angle used throughout this investigation– we rarely saw any evidence of overt extra-cranial damage as assessed visually, and those with such evidence did not survive beyond the initial 24 hour period. Therefore, we think that this HIT model is capable of causing a TBI that may or may not be associated with extracranial injury, but any such associated injury generally occurs at a severity insufficient to be recognised by visual inspection.

HIT causes several measurable defects in behavior, survival and neuronal responses

In keeping with prior publications of TBI in *Drosophila,* we demonstrated that HIT caused marked defects in climbing and flying in wild-type flies. These are complex functional activities that depend upon a variety of intact elements including leg or wing structural integrity, functional musculature, peripheral nerves, motor circuitry, and brain activity including the negative gravitaxis/flight initiation response[325,326]. The ability of climbing/flying assays to reduce these broad elements of a complex systems to a single numerical value make them attractive and widely used[503]. This pragmatic approach gives a utilitarian measure of overall functional activity. In our HIT model the injured flies that do not have flight activity still have healthy looking wings, make frequent spontaneous wing movements, and engage in wing grooming behavior, suggesting that the failure to fly even when provoked by a stimulus of air is not simply as a result of a peripheral wing injury. This is supported by the cases where short periods of flight are initiated but the flies seem unable to maintain for a prolonged duration. A reduction in specific neuronal clusters within the brain has been associated with impaired climbing ability[504–506]. Likewise, flight behavior has been shown to vary with the number of protocerebral anterior medial (PAM) dopaminergic neurons[504].However, despite the capacity of selective brain-specific single-pathway neuronal knockouts to impair climbing and flying behaviour, a deficiency in these activities in HIT exposed flies may be non-specific and in isolation cannot not localise the underlying aetiology/source of the deficit[503,504,507].

A further effect of HIT injury was excess mortality. Within the first 24 hours *hiw*$^{\Delta N}$ flies demonstrated a small excess (<5%) mortality compared to *hiw*$^{+/+}$ flies. The reason for this is unclear. A previous study by Katzenberger *et al* found that the 24 hour mortality in *Drosophila* varied significantly depending on genotype. The source of this variation was in part attributed to TBI induced IBD and associated leakage of glucose from across the intestinal barrier into the haemolymph. *Highwire* does not have any known intestinal barrier function. However, the *hiw*$^{\Delta N}$ is a constitutively expressed LOF mutation present in all cells of the fly, and although its primary effect is thought to be related to dNMNAT levels, we cannot exclude the possibility that it has additional functions that may be unrelated to the brain. Flies that survived more than 24 hours after HIT experienced a significant reduction in long-term survival. As with deaths within 24 hours, the exact cause of these later deaths in HIT exposed flies cannot be determined with certainty.

HIT caused a reduction in the levels of NGL– a pan-neuronal marker, and BRP– a pre-synaptic marker of the active zone of synapses, but not DLG– a post-synaptic marker, at 24 hours and 7 days following injury. This provides supporting evidence that HIT causes TBI. NGL is an intergral membrane glycoprotein expressed in neurons and glia. It is involved in cellular adhesion and synapse maintenance. Depletion of NGL following HIT is consistent with a reduction in synapse numbers[508].

This selective loss of presynaptic marker BRP is in keeping with the findings of several neurodegenerative diseases, including AD, and may represent a greater vulnerability of presynaptic terminals due to their greater distance from the cell body[396].

Further evidence that HIT causes brain injury, and a neurodegenerative process come from the finding that it induces vacuolation when fly brains were examined 28 days after injury. Brain vacuolation is a recognized marker of brain neurodegeneration in *Drosophila* and has been used previously to demonstrate the long-term neurodegenerative potential of a HIT injury[292,298,486,487].While the true aetiology of vacuolation is unknown it is commonly used as a marker of neurodegeneration and may be comparable to mammalian parenchymal volume loss, something that is well-described after TBI[9,298,481,509].

In keeping with the vacuolation seen following HIT, we also demonstrated increased rates of cellular death in *Drosophila* brains using a flow cytometry approach. Co-staining with Annexin V & 7-AAD allows the classification of cells into alive (Annexin V negative & 7AAD negative), early apoptosis (Annexin V positive & 7AAD negative), and late apoptosis/necrosis (Annexin V positive or negative & 7AAD positive). Differentiation of late apoptosis and death can be challenging by flow cytometry and easily influenced by gating, therefore results were classified into early apoptosis *or* late apoptosis/necrosis. Notably only a small proportion of the identified cellular death was due to early apoptosis and rates were below the level of significance at all time points. There was a small progressive increase in the rates of late apoptosis/necrosis at 24 h and 7 days after injury. This suggests most cellular loss is executed via non-apoptotic mechanisms of cellar death.

Parkinsonism is a recognised risk of brain trauma in human TBI, and this may be related to loss of dopaminergic neurons[505,510]. The PPL1 neurons are a well-characterised subpopulation of dopaminergic neurons which are involved in climbing and flying behaviour[504,506]. Dopaminergic neurons demonstrate selective vulnerability following brain injury across a range of animal models, and in various neurodegenerative conditions[294,505,506,510]. The number of neurons in the PPL1 cluster is remarkably consistent in wild-type flies, with an average of 12 neurons. Immunostaining for TH demonstrated a significant decrease in the number of neurons in the PPL1 cluster following injury in $hiw^{+/+}$ flies. This directly links TBI to dopaminergic cell loss in a model organism. Whether this neuronal loss was as a direct result of physical injury to the soma or axons, or due to a secondary injury process was not immediately apparent.

The effect of $hiw^{\Delta N}$ in rescuing the HIT phenotype

Given the role of *highwire* in dNMNAT depletion and subsequent axon degeneration, and the assessment that WD may contribute to the secondary brain injury seen in TBI, we hypothesised that flies with a null mutation in *highwire* ($hiw^{\Delta N}$) would show protection against the deleterious effects of TBI as caused by the *Drosophila* HIT device.

On initial characterisation of HIT injury there was no difference in incapacitation rates between $hiw^{\Delta N}$ and $hiw^{+/+}$ flies. This suggests that the immediate concussive effects of the TBI

are the same in *hiw*$^{\Delta N}$ flies as in *hiw*$^{+/+}$. Likewise, there was no difference in the rates of IBD after injury in wild-type or a LOF *highwire* mutant fly.

The *hiw*$^{\Delta N}$ loss of function mutation caused a striking rescue of climbing and flying activity after HIT. The mechanism by which this protection is executed is unclear. However, given the known axon-protective activity of *hiw*$^{\Delta N}$, and the dependence of *Drosophila* upon specific dopaminergic neuronal clusters (including PPL1 and PAM) for effective flight and climbing, we can hypothesize that the mechanism of *hiw*$^{\Delta N}$ protection is directly related to protection of these neuronal clusters[504,506]. Dopaminergic neurons demonstrate selective vulnerability following brain injury and in various neurodegenerative conditions [294,505,506,510]. HIT injury reduced PPL1 neuronal numbers in wild-type flies but that this deficit was completely rescued in *hiw*$^{\Delta N}$ flies, supporting our hypothesis that the protective phenotype seen with *hiw*$^{\Delta N}$ mutation is related to direct neuronal protection. Furthermore, although PPL1 neurons are known to be vulnerable to insults, it would be surprising if *hiw*$^{\Delta N}$ related axon protection did not occurs across a range of neuronal subtypes. Preservation of other dopaminergic neurons, and other neuronal subclasses, may have contributed to the protective effect.

The *hiw*$^{\Delta N}$ mutation was seen to reduce the rates of HIT induced death that occurred after 24 hours compared to wild-type animals, this is in keeping with longer-term protection against secondary brain injury processes. This was particularly the case after 20 days when survival curves began to markedly diverge. Given the assumed heterogeneity of the HIT injury, and the numerous secondary brain injury processes that may be co-occurring, it is challenging to determine with certainty how exactly *hiw*$^{\Delta N}$ mutation is causing the preservation of lifespan. For example, it is unclear whether this is a direct consequence of neuronal protection, a secondary effects of brain protection– e.g. through maintenance of behaviour necessary for prolonged lifespan, or through a separate unidentified mechanism of action. Determination of these mechanisms is unlikely to be possible or necessary in a *Drosophila* model, and instead can be further explored in larger animal models.

The reduction in NGL and BRP seen in wild-type flies exposed to HIT was rescued by *hiw*$^{\Delta N}$ mutation. This suggest that *hiw*$^{\Delta N}$ is able to protect synapses against HIT induced degradation.

The protection could be due to axonal protection as a result of delayed WD, alternatively dNMNAT has previously been demonstrated to stabilize BRP by a direct protein-protein interaction (Zang et al 2013). This may explain the protection seen with *hiw*$^{\Delta N}$ mutation – as it leads to maintenance of dNMNAT levels.

The failure of *hiw*$^{\Delta N}$ to protect against vacuolation 28 days following HIT indicates that it is incapable of completely attenuating a neurodegenerative phenotype, it also underlines the insensitivity of vacuolation in assessing neurodegeneration, given that improvements in functional measures, lifespan, and protection of neuronal subtypes were seen in the absence of any demonstrable change in vacuolation rates. Unlike vacuolation, the levels of late apoptosis/death were significantly lower in the *hiw*$^{\Delta N}$ flies compared to *hiw*$^{+/+}$ 7 days after injury, however the absolute difference was small (~0.5%). This finding again supports the assertion that *hiw*$^{\Delta N}$ is capable of directly attenuating brain injury after HIT.

What is the mechanism underlying hiw$^{\Delta N}$ protective effects against traumatic brain injury?

The *hiw*$^{\Delta N}$ mutation results in a complete loss-of-function of the *highwire* gene. We have presented several lines of evidence that demonstrate that *hiw*$^{\Delta N}$ is capable of attenuating the deleterious effects of HIT. This includes protection against premature reduction in lifespan, neuronal death and pre-synaptic loss, dopaminergic cell depletion, and behavioral consequences such as climbing and flying ability. It is important to consider how *hiw*$^{\Delta N}$ mutation could cause these beneficial effects.

There are two known mechanisms by which *hiw*$^{\Delta N}$ could mediate a protective effect following HIT– maintenance of dNMNAT resulting in delayed WD and/or chaperone like function.
Therefore, the mechanism underlying the protection seen with *hiw*$^{\Delta N}$ mutation is likely to be related to its dNMNAT maintaining activity. It is important to consider how maintenance of dNMNAT levels could be mediating injury responses. As previously described, the NMNAT enzymes are the final common step in NAD synthesis. They are found in all living organisms and are essential for life. There are 3 mammalian NMNAT genes, each with a specific tissue expression profiles and subcellular localization. In *Drosophila* there is a single dNMNAT gene with 7 tandem exons that sub-serve all of the functions of the 3 mammalian isoforms. dNMNAT undergoes alternative splicing, a post-transcriptional mechanism that produces

transcript diversity. dNMNAT alternative splicing functions as a molecular switch that regulates neuroprotective activity under stress. The final 3 exons can be spliced to generate one of two mRNA variants, RA or RB, each with an alternative protein isoform–PA/PC or PB/PD respectively. Under stress– including hypoxia, heat and proteotoxic– splicing occurs in neurons in favour of the RB variant and subsequently PB/PD protein isoform, this localizes to the cytoplasm where it demonstrates refolding activity and has a robust neuroprotective profile[173]. The neuroprotective capacity of dNMNAT in flies may be multifactoral. As in mammals, dNMNAT functions to convert NMN to NAD, this is necessary to avoid activation of the WD pathway in axons[7]. dNMNAT has a molecular structure similar to known chaperones and demonstrates chaperone-like functions in cellular cultures and in biochemical assays. This is separate to the NAD synthetic activity of dNMNAT as demonstrated by retained neuroprotective capacity with enzymatically inactivated forms of NMNAT[172,180,186]. An example of dNMNATs chaperone function is its interaction with BRP. BRP is a presynaptic marker of the active zone region of a synapse, it is homologous to ELKS/CAST/ERC in the human synapse[511]. Its function is to control calcium channel clustering, promote active zone assembly, and mediate vesicle based neurotransmitter release[512]. dNMNAT localizes to the peri-active zone and interacts with BRP by direct protein-protein interaction in an activity dependent manner, stabilizing it and protecting it from ubiquitin-proteasome-mediated degradation[513]. As *Drosophila* only have one NMNAT isoform we can hypothesize that depletion of dNMNAT would be lethal to the whole cell, unlike in mammalian cells where axonal knockdown of NMNAT2 is only lethal to the axon and not the soma[134]. This could have important consequences for any pathological process that depletes NMNAT, as an axonal injury might potentially result in whole cellular death[513]. This may explain the reduced cellular death seen with flow cytometry and TH staining of PPL1 in the *hiw*$^{\Delta N}$ mutants.

There are several approaches that could be taken to establish whether the protection against the deleterious effects of HIT seen with *hiw*$^{\Delta N}$ mutation were dNMNAT– and hence WD or chaperone activity– dependent. These would form future streams of investigation. Firstly, we would determine if HIT leads to a reduction in dNMNAT levels, and if *hiw*$^{\Delta N}$ mutation could rescue this enzyme depletion. It is currently unknown whether TBI alters levels of dNMNAT so a further important next step would be to directly assess the levels of dNMNAT in response to injury. It is challenging to directly measure dNMNAT levels. It can be probed with an

antibody but this is not commercially available and I was unable to acquire it during this thesis[224]. This antibody also has poor specificity, with numerous non-specific bands that make accurate analysis challenging. We attempted to gauge WD activity in the HIT fly by directly measuring NMN or NAD levels in whole fly heads after HIT. These might be expected to change in response to HIT if it was causing widespread variations in dNMNAT level or WD. However, we were unable to demonstrate any significant changes in NMN or NAD regardless of injury or *highwire* gene status. While this does not support delayed WD as the mechanism of neuroprotection in our model, it cannot definitively exclude it either – as changes could be masked by relative stability of NMN and NAD in other cell types. An alternative approach to assess dNMNAT levels is to use a HA-NMNAT tag that can then be probed with an anti-HA antibody. The HA-NMNAT tag can be selectively expressed in neuronal tissue using the Gal4-UAS system. This would allow assessment of dNMNAT levels following HIT and also establish if $hiw^{\Delta N}$ has protection against any such depletion. Alternatively, the replication of our findings with a WLD^{s} expressing fly would lend support to the hypothesis that protection is can be afforded by modulation within the WD pathway. Furthermore, dNMNAT-enzyme *Drosophila* would clarify whether the effects are due to the enzymatic activity of dNMNAT or due to non-enzymatic function such as chaperone activity. In a mammalian system reduction in NMNAT2 levels are normally seen in the distal compartment of an axon following transection as part of the WD pathway. However, the effects of a TAI on NMNAT level in the cell body has not been explored. These levels could conceivably be affected directly by the axonal injury, or as a secondary consequence of alterations other aspects of the injury environment including inflammatory signaling. The fact that *Drosophila* only have a single isoform of NMNAT is likely to mean that any reduction in levels would affect the axon and the cell body, and result in cellular death in both compartments.

Direct visualisation of axons in the fly brain following HIT– with the aim of confirming if WD occurred and was protected by $hiw^{\Delta N}$ would be an important experimental finding to clarify the mechanism of neuroprotection. Quantification of the extent of axonal injury in this model is important in order to correctly classify the brain injury and understand in greater detail how it relates to human pathology. We applied a range of techniques in an attempt to directly visualize dopaminergic cell axons and demonstrate axonal protection, but without success(see results)- this include TH-Gal4/UAS or a MARCM approaches that were both unable to facilitate

direct visualization of axonal pathology. An alternative approach would be to use a more specific Gal4/UAS to express GFP in a restricted subset of neurons. Ideally, we might choose to express GFP using a highly specific neuronal expression of GFP in the PPL1 neuronal cluster. This would facilitate direct assessment of axonal injury and degeneration following injury, and also permit a volumetric analysis of the synaptic arbors. This could be assessed in WT and *hiw*$^{\Delta N}$ mutants. However, there are currently no ideal Gal4 drivers of expression in the PPL1 cluster. Other options would be Gal4-NP6510 driver which when paired with a GFP-UAS would results in GFP expression only in a subset of around 15 dopaminergic PAM neurons per hemisphere. This highly selective expression profile might allow resolution of individual axons, in addition to the axonal arborization itself, and would be a logical next step.

The effect of highwire loss of function mutation on genetic model of Parkinson's disease

There are strong epidemiological links between TBI and development of Parkinsonism [411,505], [410]. These include evidence of injury induced dopaminergic neuronal loss or network dysfunction[510,514–517]. However, the underlying mechanism of dopaminergic system dysfunction in TBI, and its relationship to sporadic/pharmacologically induced Parkinsonism remains incompletely understood.

The ability of a mutation in the *highwire* gene to rescue dopaminergic cell loss after a HIT suggested that it may also be able to rescue dopaminergic cell loss due to other, potentially mechanistically related, disorders. We explored the effects of *hiw*$^{\Delta N}$ on two well- recognised *Drosophila* models of Parkinson's disease– rotenone exposure and *PINK1*^{B9} mutation. Unfortunately, I was unable to disentangle the effects of rotenone from the that of its solvent DMSO, a factor that has been poorly reported in previous publications of rotenone in *Drosophila.* Other toxins have been used to model Parkinson's disease, including paraquat, 1-methyl-4-phenyl-1-2-3-6-tetrahydropyridine (MPTP), and 6-hydroxydopamine (6-ODHA). The provide alternatives that could be used in future research.

PINK1^{B9} mutation is a loss of function mutant generated by Park *et al* 2006. Mutations in the human homolog of this gene cause an autosomal-recessive early-onset form of Parkinsonism. *PINK1*^{B9} mutants have impaired mitochondrial function and are a well-characterised genetic model of Parkinsonism in *Drosophila*. The phenotype is less severe than some other

Parkinson's mutations like *Parkin*, so in order to establish if any rescue was possible with $hiw^{\Delta N}$ mutation this seemed a logical initial choice[322,501]. In order to examine whether $hiw^{\Delta N}$ mutation could rescue the phenotypic effects of $PINK1^{B9}$ mutation we recombined $hiw^{\Delta N}$ and $PINK1^{B9}$ mutations on the X chromosome and screened the resulting offspring with PCR confirmation (undertaken by Alex Whitworth lab on our behalf). We found that $hiw^{\Delta N}$,$PINK1^{B9}$ flies did not show any evidence of rescuing flying or climbing behavior. This could be because the $PINK1^{B9}$ phenotype is mediated through an independent pathway or tissues unrelated to the action of $hiw^{\Delta N}$, or that the phenotype it produces is simply to too robust for a phenotypic rescue. Strikingly, we found that although $hiw^{\Delta N}$,$PINK1^{B9}$ recombination was unable to rescue climbing or flying activity, it did partially rescue lifespan, and completely rescued PPL1 dopaminergic neuron depletion. It is intriguing to consider how $hiw^{\Delta N}$ may have rescued $PINK1^{B9}$ induced dopaminergic cell loss. *PINK1* is a putative mitochondrial kinase that contains a mitochondrial targeting sequence and is thought to act by protecting the cell from stress-induced dysfunction and targeting dysfunctional mitochondria for degradation. In a healthy state mitochondria will import *PINK1* across their membrane where it is removed. In mitochondria with impaired membrane potential the accumulation of *PINK1* to the outer membrane recruits the E3 ubiquitin ligase *Parkin* which then degrades the damaged mitochondria via an autophagic response[322,501,502]. It would be interesting to examine whether *Parkin* mutation, which has similar effects to *PINK1* mutation on PPL1 neuronal depletion, would also be rescued by $hiw^{\Delta N502}$. The fact that *highwire* and *Parkin* are both E3 ubiquitin ligases could be co-incidental, or it could be that they have some degree of opposing function through intermediate molecular controls. Central to *PINK1* activity is its influence on mitochondrial function- loss of PINK1 activity has been demonstrated to lead to the accumulation of dysfunctional mitochondria[322,501,518]. Mitochondrial dysfunction has been linked to WD, and has been shown to induce SARM1 dependent axon degeneration, possibly as a consequence of ROS accumulation[455,519,520]. The ability of $hiw^{\Delta N}$ to prevent toxicity that accompanies loss of *PINK1* function might therefore suggest that this is a WD dependent process. This could be confirmed by examining whether other mediators of WD including WLD^{s} or SARM1 knockout can also rescue *PINK1* pathology. Therefore, increased dNMNAT levels seen in $hiw^{\Delta N}$ may be acting to oppose the downstream effects of mitochondrial dysfunction resulting from *PINK1* mutation.

Conclusion

The findings presented in this chapter provide support for the hypothesis that a *highwire* LOF mutation can protect against the deleterious effects of TBI and a genetic model of PD. This suggests that the mammalian orthologue of *highwire,* PHR1, may represents a novel and serviceable therapeutic target for these conditions.

Chapter 8

Discussion & Conclusion

Discussion

The failure of translation in traumatic brain injury

In recent years there has been a shift to describe TBI as a disease, this is based upon a cognizant attempt to try and organise TBI into a condition that has structured diagnosis and treatment[521]. While this structuring may have helped service organisation and general clinical management it is less helpful for framing the content of TBI research efforts. In actuality, TBI is in fact an event, initiated by an often-unpredictable primary biomechanical force that causes physical-anatomical injury, which then induces a cascade of molecular secondary brain injury events, and may indeed lead to a chronic disease-like state[11]. This conceptual division of TBI into a primary and secondary processes has several consequences for TBI research and care. Firstly, as the initial injury occurs in an unpredictable fashion, then widespread prophylactic neuroprotective therapy becomes impractical. Primary prevention largely centres around health and safety policy in terms of factors such as road traffic management, falls prevention, and personal protective equipment for high risk activities. Secondly, although a physical restoration of normal anatomy/physiology- in the form of surgery- is sometimes indicated for pathologies such as some haemorrhagic-compressive lesions, it is evident that some degree of a primary injury, particularly a widespread anatomical disruption of the brain parenchyma– particularly in essential regions such as the brainstem, may be so severe as to not be remediable by any surgical or medical therapy[11].

Improvements in surgery, anaesthesia, prehospital care, critical care, and medical care have impacted outcomes by rapidly normalising disrupted anatomy where possible, and identifying optimal ranges for physiological parameters including such as blood pressure, oxygenation, glycaemic levels, and temperature. Likewise, prevention of systemic complications including infections and thrombosis has saved lives[522–526]. For survivors, rehabilitation programmes and social care have doubtless affected quality of life measures[527,528]. However, in terms of pharmacological interventions to improve outcomes from TBI, we still lack any therapeutic agents. This is despite over 40 years of active research into the reduction of secondary brain injury mechanisms[529]. Several reasons have been postulated for this (figure 68).

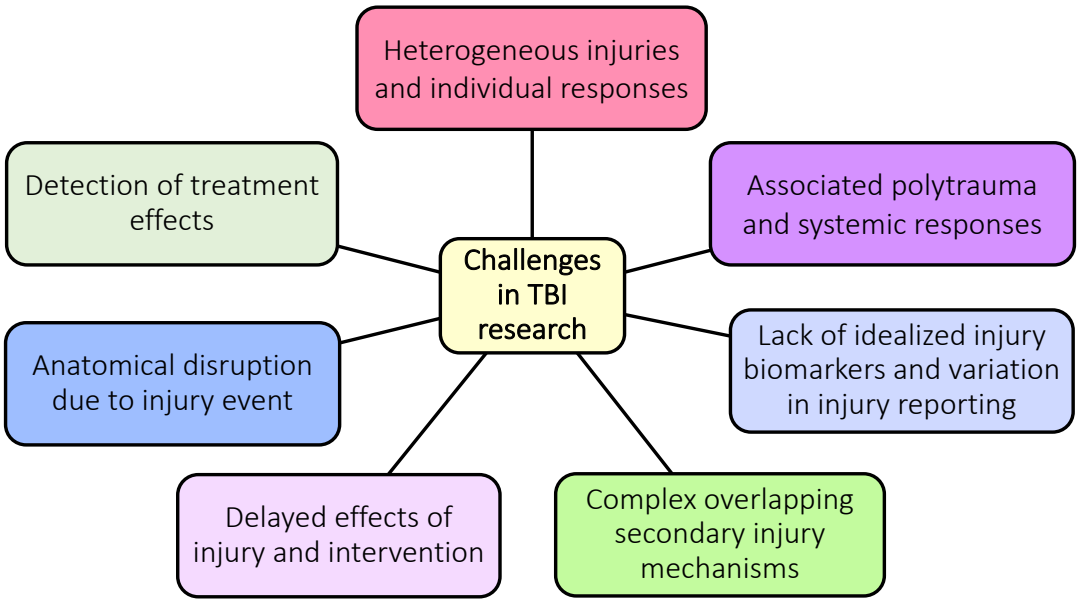

Figure 68. Challenges in research and translational therapeutics in traumatic brain injury

These include failure including delayed/mistiming of drug administration, over-reliance on small animal models, inaccurate classification systems, lack of standardized common data elements, and historical underinvestment in TBI research[19,21,529–531].

Other reasons for the failure of translation may include the specific mechanisms of secondary brain injury that have been targeted. Some aspects of secondary brain injury, for example WD, have been relatively unexplored, while others have received comparatively more attention. It may be that some secondary brain injury mechanisms are more complex or less therapeutically efficacious than others, or that a combined approach is necessary to achieve tangible benefit[6].

An additional confounding factor in establishing therapeutic efficacy may be the delay between a TBI occurring and the manifestation of its sequelae. While a reduction in mortality may be identifiable at an early stage after injury, other consequences of injury including cognitive dysfunction may not be apparent for months or even years[407,532]. This makes the correlation of injury, therapeutics, and any outcome vulnerable to numerous confounding influences.

The heterogeneity of TBI manifests not only in the initial injury but also in the responses of individuals to what are seemingly similar injuries. This diversity in response makes the detection of small and moderate treatment effects more difficult, and fact that has markedly limited high quality clinical trials. The reasons for the heterogeneity in outcomes is largely unknown but is likely to be due in part to genetic variability and molecular diversity in secondary brain injury pathways, and unrecognised differences in clinical care[533,534]. It may also be influenced by the association of TBI with a range of associated extracranial injuries[535]. In addition, systemic dysfunction often occurs in polytrauma and many severe head injuries have associated systemic dysfunction including sepsis, coagulopathy, hypoxia, hypotension, dysglycaemia, and the effect of general co-morbidities[523,536,537].

These legion confounders are further complicated by the challenge of trying to detect what are often small treatment effects. The wider the variability in the specified outcome of a therapy, then the more difficult it becomes to detect a treatment effect. For example, in order to assess the efficacy of a pharmacological agent in the management of early TBI it would be necessary to randomize 20,000 patients, to detect a 2% improvement in survival at $p<0.01$ for a cohort with placebo treated death rates of 15%[538]. This difficulty in detecting treatment effects is compounded by imperfect outcome measures that have limited sensitivity and may not give a true global representation of the patient's injury and their global response. Selecting the most appropriate outcome measure for a given therapy is a significant challenge. An ideal biomarker of TBI that is sensitive, and accurately represents the extent of injury or response to therapy remains a chief goal of TBI research [28,271,274,539,540].

When all these various confounding influences are considered it becomes more understandable why medical research has been unsuccessful in making significant improvements to TBI therapy, and why it is more challenging that a simple monogenetic disorder.

It is not pragmatic to attempt to address all the barriers to translational TBI research that we have discussed in a single body of work. However, by developing a variety of injury models and using diverse investigational techniques including pharmacological and genetic

approaches, we were able to tackle the role of a previously neglected secondary brain injury mechanism in TBI and assess its potential as a therapeutic target.

Choosing an optimal model based approach to traumatic brain injury research

An important point to consider when exploring TBI is the choice of which model is most appropriate for the question posed. In earlier chapters we considered the benefits of various TBI model systems including *in vitro* primary and mixed/organotypic culture systems, and *in vivo* models from *Drosophila* to large animal models using pigs and primates. Whenever posing a new research question we must re-evaluate the existing model systems in order to decide which is most appropriate for a given experiment so as to optimise methodology and ensure the validity of our results. In this thesis it was necessary to selectively use different model systems order to answer specific experimental questions. It is impossible to reproduce all aspects of a heterogenous condition like TBI with a single model and indeed one of the primary functions of a model is to provide simplification of a complex phenomenon[327]. Unfortunately, the literature is replete with examples of promising preclinical therapies that subsequently failed in clinical trials. This does not necessarily prove a failure of the preclinical models and many of these failures in translation may in fact be due to complex confounding systemic factors that could be incorporated into existing models[327]. There may be some research questions that are not amenable to interrogation with existing model systems, and in such cases we might need to develop a new model, but we should be wary about developing these without a clear indication of need. Wherever possible the use of existing models is not only pragmatic but may facilitate the interpretation of results and comparison between projects. Each of the currently existing model systems has its own particular benefits and limitations that make them more or less appropriate in answering specific experimental questions[12,13]. Broadly speaking- *in vitro* models are generally more appropriate for answering basic mechanistic questions, while more complex *in vivo* models can provide information about therapeutic responses that may have more validity in the human condition. The overarching aim of using TBI models is to enhance our understanding of human TBI in order to develop novel treatments, or optimise existing therapy. Where research centred on TBI interfaces with novel exploratory basic science such a definition may blur, but it is prudent to

sporadically return to this centre-point in order to ensure that endeavours remain focussed on the aim of improving clinical care.

Secondary brain injury and the nature of future potential therapies

When considering research and therapy development in TBI and DAI it is important to remain cognisant of our overall aims, and of what it is possible for research to achieve. As alluded to previously, the anatomical disruption inherent in some severe fatal brain injuries may be beyond the limits of therapeutic salvage. For less severe injuries the broadest aims can be codified as reduction of mortality and minimising levels of disability. On a therapeutic level this can be translated to preventing any avoidable neuronal cell loss. Although this is intuitively a reasonable goal, we do not currently have definitive evidence that neuronal loss is the substrate of clinical disability following TBI. Moew specifically, it has not been proven that reducing neuronal death after TBI translates to clinical improvement. Indeed, even if we are successful in maximising neuronal preservation it is also likely to be necessary to prevent axonal degeneration and synaptic dysfunction to see any favourable effects. Furthermore, for clinical benefit it may also be necessary to maintain connectivity even in the case of neuronal survival– emerging research suggests that network function may be important in outcomes of TBI independently or co-dependently with neuronal loss[541]. In addition to preventing neuronal loss due to early secondary brain injury mechanisms, there are longer term effects of the TBI that including toxic proteinopathies associated with neurodegenerative diseases such as AD, PD, and CTE. The termination of these deleterious processes or clearance of toxic proteins may be an further important goal in TBI research, and indeed may represent one of the major opportunities to influence clinical outcomes. The majority of basic science research relating to TBI is based around defining the biomechanics of injury, understanding mechanisms of secondary brain injury that underlie neuronal loss and degeneration, and finding therapeutic treatments to ameliorate these effects. A further branch of TBI research involves the optimisation of plasticity and functional recovery.

A further important question in TBI research is deciding whether to take a targeted approach or one without a-priori assumptions (non-hypothesis driven). If a targeted approach is taken then we must consider the secondary brain injury mechanism we wish to investigate from the numerous options available. The ideal mechanism might be considered as one that is novel,

well-understood, easy to target, has minimal detrimental effects on an organism when modulated, has *in vitro* or *in vivo* evidence to support its efficacy, and that has predictable and measurable effects. Modulation of WD is a novel target in TBI research that fulfils many of these criteria: It is a well-understood mechanism and offers a potentially drugable target, while modulators of WD including *SARM1, WLD^{s}*, *highwire,* and neuron conditional PHR1 mutation have generally failed to show overt detrimental effects on the organism. WD is an appealing mechanism to target because it is a relatively unexplored secondary brain injury mechanism that is primarily concerned with axonal preservation– but may also be important in neuronal survival and preservation of synaptic connectivity.

Building on the findings of this thesis and associated research, further studies might aim to leverage relevant mechanistic insights to develop pharmacological mediators of WD. Indeed, there are already patents in place covering the development and use of such drugs to treat a variety of neurodegenerative diseases. Potential pharmacological targets include; NMNAT2 preservation– including via *highwire* (or its mammalian homolog *PHR1*) inhibition, *SARM1* inhibition, NAD+ biosynthesis, and MAPK pathway inhibition[542]. Furthermore, there may be a role for genomic profiling of WD genes in the risk stratification/prognostication of TBI patients, for example, levels of NMNAT2 and *SARM1* expression may vary in the general population and contribute to the heterogeneity seen in outcomes from apparently similar TBIs. The WD pathway may also provide future biomarkers of DAI, with measurement of NMN/NAD ratio, NMNAT2 levels, or *SARM1* activation providing a quantitative measure of neuronal/axonal degeneration

Conclusion

This thesis has describe a multifaceted investigation into various aspects of the WD pathway's interaction with models of TAI. We first described the design, development and calibration an *in vitro* stretch system to allow interrogation of biological responses to mechanically induced axonal stretch injuries. The chapter contains details of the design and calibration of a stretch injury device including the calculation of strain and strain-rates with the system. This was followed by details of the optimization of primary neuronal culture methods on deformable silicone membranes. Optimal parameters were established for a subtransection level force, then the effects of stretch injury on neurite degeneration in wild-type cultures was presented including induction of length dependent neurite degeneration. A series of experiments were then performed to investigate the effects of various WD modulators on the axonal response to injury. This was in order to establish whether WD was responsible for the axonal degeneration seen, and therefore if it was a potential therapeutic target. Genetic and pharmacological approaches were used to induce WD protective or vulnerable phenotypes in *in vitro* primary neuronal cultures. The results demonstrated that rates of neurite degeneration could be altered by modulators of the WD pathway, but that a complete rescue was not achieved, and that the rate of degeneration/protection varied from that seen in transection models, suggesting that although the WD program was sufficient to cause neurite degeneration following stretch, other mechanisms are likely to be involved.

Subsequently we explored the effects of the purported NAMPT activator P7C3-A20 on TAI to establish if pharmacological manipulation of WD could be protective in a stretch injury model. The drug P7C3-A20 has be suggested as an agent that is neuroprotective and exerts its protective action through NAD synthetic action, a component of the WD pathway. We demonstrated that this compound was toxic even at low doses by a non-WD mechanism in SCG cell cultures. NAD synthetic activity varied by cell-type and partial rescue of doxorubicin induced NAD depletion was demonstrated in primary neuronal cultures. WD induction by neurite transection or vincristine was not delayed or rescued by P7C3-A20. This suggests that P7C3-A20 may have conditional neurotoxicity and its neuroprotective actions may be due to mechanisms outside the WD pathway.

A series of modifications were then made to the stretch injury system previously developed, in order to characterize the response of a mammalian organotypic hippocampal brain slice model to a stretch injury and explore interactions between WD and other neurodegenerative pathology *in vivo*. This was in order to facilitate the interrogation of WD in an *in* vitro system containing neurons and glia, and with some preservation of tissue architecture. The stretch injury was adapted for use with OHS cultures. OHS from a WD mutant ($SARM^{-/-}$) demonstrated protection against cellular death. More specific analysis of axonal injury including immunohistochemistry and neurofilaments measurements and were not conclusive. Amyloid β level measurement was optimized in OHS and demonstrated an injury related rises that links stretch injury to neurodegenerative disease.

Next we characterized an *in vivo* TBI model using *Drosophila Melanogaster*. The model was established and the response to the inflicted injury was characterized in terms of effect on lifespan and a range of behavioral measures. This demonstrated that the model is able to recapitulate the effects of a TBI in a versatile model organism, opening up the possibility to explore a plethora of genetic mutations in TAI. This initially included an exploration of the effects of a *highwire* genetic mutation that delays WLD after injury. This demonstrated a partial rescue of deficits in lifespan, behavior, and neuronal and synaptic loss. A subset of dopaminergic neurons (PPL1) was identified as being particularly vulnerable. As a result of identification of selective dopaminergic neuron vulnerability, and the recognized association between TAI and dopaminergic neuron loss and Parkinsonism, we then explore the ability of the *highwire* mutant to rescue the effects of pharmacological and genetic mitochondrial toxins associated with dopaminergic neuron degeneration. The mitochondrial toxin rotenone was used but low solubility precluded further investigation with this agent. A genetic approach was then taken with a mutant *PINK1* fly, this model of Parkinsonism has a strong phenotype including PPL1 dopaminergic cell loss. *PINK1* mediated lifespan reduction and dopaminergic cell loss was salvaged with the *highwire* mutation. This demonstrated an *in vivo* rescue of a genetic cause of Parkinsonism and represents a novel therapeutic target in Parkinsonism.

Together these results help establish WD as an important secondary injury mechanism in TBI, and provide evidence that modulation of the WD pathways can improve outcomes in various

model systems. This provides a foundation for future translational research into the fields of WD and TBI.

References

1. **Menon DK, Schwab K, Wright DW, Maas AI** (2010) Position statement: definition of traumatic brain injury. *Archives of Physical Medicine and Rehabilitation* (91): 1637-1640.
2. **Maas AI *et al*** (2015) Collaborative European NeuroTrauma Effectiveness Research in Traumatic Brain Injury (CENTER-TBI): A Prospective Longitudinal Observational Study. *Neurosurgery* (76): 67-80.
3. **Jing S, Ju Y, He Y, He M, Mao B** (2001) Clinical features of diffuse axonal injury. *Chin J Traumatol* (4): 204-207.
4. **Haacke EM *et al*** (2010) Common data elements in radiologic imaging of traumatic brain injury. *Journal of Magnetic Resonance Imaging* (32): 516-543.
5. **Adams JH *et al*** (1989) Diffuse axonal injury in head injury: definition, diagnosis and grading. *Histopathology* (15): 49-59.
6. **Hill CS, Coleman MP, Menon DK** (2016) Traumatic axonal injury: mechanisms and translational opportunities. *Trends in neurosciences* (39): 311-324.
7. **Conforti L, Gilley J, Coleman MP** (2014) Wallerian degeneration: an emerging axon death pathway linking injury and disease. *Nat Rev Neurosci* (15): 394-409.
8. **Wang J, Hamm RJ, Povlishock JT** (2011) Traumatic axonal injury in the optic nerve: evidence for axonal swelling, disconnection, dieback, and reorganization. *J Neurotrauma* (28): 1185-1198.
9. **Johnson VE *et al*** (2013) Inflammation and white matter degeneration persist for years after a single traumatic brain injury. *Brain* (136): 28-42.
10. **Büki A, Povlishock JT** (2006) All roads lead to disconnection? - Traumatic axonal injury revisited. *Acta Neurochir (Wien)* (148): 181-193.
11. **Smith DH, Hicks R, Povlishock JT** (2013) Therapy development for diffuse axonal injury. *J Neurotrauma* (30): 307-323.
12. **Morganti-Kossmann MC, Yan E, Bye N** (2010) Animal models of traumatic brain injury: is there an optimal model to reproduce human brain injury in the laboratory? *Injury* (41 Suppl 1): S10-3.
13. **Morrison B, Elkin BS, Dolle JP, Yarmush ML** (2011) In vitro models of traumatic brain injury. *Annu Rev Biomed Eng* (13): 91-126.
14. **Humphreys I, Wood RL, Phillips CJ, Macey S** (2013) The costs of traumatic brain injury: a literature review. *Clinicoecon Outcomes Res* (5): 281-287.
15. **Faul M, Xu L, Wald MM, Coronado V** (2010) Traumatic brain injury in the United States: emergency department visits, hospitalizations, and deaths. *Center for Disease Control and Prevention, Atlanta (GA)*
16. **Parsonage M** (2016) Report: Traumatic brain injury and offending, an economic analysis. *Centre for mental health* 1-35.
17. **Thornhill S *et al*** (2000) Disability in young people and adults one year after head injury: prospective cohort study. *BMJ* (320): 1631-1635.
18. **Becker-Barroso E** (2013) A rally for traumatic brain injury research. *Lancet Neurology* (12): 1127.
19. **Menon DK, Maas AI** (2015) Traumatic brain injury in 2014. Progress, failures and new approaches for TBI research. *Nat Rev Neurol* (11): 71-72.
20. **Teasdale G, Jennett B** (1974) Assessment of coma and impaired consciousness. A practical scale. *Lancet* (2): 81-84.
21. **Saatman KE *et al*** (2008) Classification of traumatic brain injury for targeted therapies. *J Neurotrauma* (25): 719-738.

22. **Abelson-Mitchell N** (2008) Epidemiology and prevention of head injuries: literature review. *J Clin Nurs* (17): 46-57.
23. **Stritch S** (1956) Diffuse degeneration of the cerebral white matter in severe dementia following head injury. *J Neurol Neurosurg Psychiatry* (19): 163-185.
24. **Tao J-j *et al*** (2015) Susceptibility weighted imaging in the evaluation of hemorrhagic diffuse axonal injury. *Neural regeneration research* (10): 1879.
25. **Arfanakis K *et al*** (2002) Diffusion tensor MR imaging in diffuse axonal injury. *AJNR Am J Neuroradiol* (23): 794-802.
26. **Newcombe VF *et al*** (2007) Analysis of acute traumatic axonal injury using diffusion tensor imaging. *Br J Neurosurg* (21): 340-348.
27. **Betz J, Zhuo J, Roy A, Shanmuganathan K, Gullapalli RP** (2012) Prognostic value of diffusion tensor imaging parameters in severe traumatic brain injury. *J Neurotrauma* (29): 1292-1305.
28. **Ly M, Ji S, Yassa MA** (2014) Diffusion MRI Biomarkers of White Matter Damage in Traumatic Brain Injury. editors. White Matter Injury in Stroke and CNS Disease. *Springer press* 91-106.
29. **Dennis EL, Babikian T, Giza CC, Thompson PM, Asarnow RF** (2017) Diffusion MRI in pediatric brain injury. *Child's Nervous System* (33): 1683-1692.
30. **Adams JH, Graham DI, Murray LS, Scott G** (1982) Diffuse axonal injury due to nonmissile head injury in humans: an analysis of 45 cases. *Ann Neurol* (12): 557-563.
31. **Gennarelli TA *et al*** (1982) Diffuse axonal injury and traumatic coma in the primate. *Ann Neurol* (12): 564-574.
32. **Gentleman S, Nash M, Sweeting C** (1993) B-Amyloid precursor protein (BAPP) as a marker for axonal injury after head injury. *Neurosci Lett* (160): 139-144.
33. **Graham DI, Smith C, Reichard R, Leclercq PD, Gentleman SM** (2004) Trials and tribulations of using beta-amyloid precursor protein immunohistochemistry to evaluate traumatic brain injury in adults. *Forensic Sci Int* (146): 89-96.
34. **Johnson VE, Stewart W, Smith DH** (2013) Axonal pathology in traumatic brain injury. *Experimental neurology* (246): 35-43.
35. **Cordey J** (2000) Introduction: Basic concept and definitions in mechanics. *Injury* SB19-SB13.
36. **LaPlaca MC, Simon CM, Prado GR, Cullen DK** (2007) CNS injury biomechanics and experimental models. *Progress in brain research* (161): 13-26.
37. **Franze K** (2013) The mechanical control of nervous system development. *Development* (140): 3069-3077.
38. **McLean AJ, Anderson RWG** (1997) Biomechanics of closed head injury. *Head injury London: Chapman & Hall* 25-37.
39. **Adams JH, Graham DI, Doyle D, Lawrence A, McLellan DR** (1984) Diffuse axonal injury in head injuries caused by a fall. *The Lancet* (324): 1420-1422.
40. **Levi L, Guilburd JN, Lemberger A, Soustiel JF, Feinsod M** (1990) Diffuse axonal injury: analysis of 100 patients with radiological signs. *Neurosurgery* (27): 429-432.
41. **Graham DI, Clark JC, Adams JH, Gennarelli TA** (1992) Diffuse axonal injury caused by assault. *Journal of clinical pathology* (45): 840-841.
42. **Imajo T** (1996) Diffuse axonal injury: its mechanism in an assault case. *The American journal of forensic medicine and pathology* (17): 324-326.

43. **Skandsen T *et al*** (2010) Prevalence and impact of diffuse axonal injury in patients with moderate and severe head injury: a cohort study of early magnetic resonance imaging findings and 1-year outcome. *Journal of neurosurgery* (113): 556-563.
44. **Vieira R *et al*** (2016) Diffuse axonal injury: epidemiology, Outcome and associated risk Factors. *Frontiers in neurology* (7):
45. **Georgoff P, Meghan S, Mirza K, Stein SC** (2010) Geographic variation in outcomes from severe traumatic brain injury. *World neurosurgery* (74): 331-345.
46. **Blumbergs PC, Jones NR, North JB** (1989) Diffuse axonal injury in head trauma. *Journal of Neurology, Neurosurgery & Psychiatry* (52): 838-841.
47. **Yoganandan N *et al*** (2009) Association of contact loading in diffuse axonal injuries from motor vehicle crashes. *Journal of Trauma and Acute Care Surgery* (66): 309-315.
48. **Tarriere C** (1983) Risk of head and neck injury if there is no direct head impact. (Head and Neck Injury Criteria: A Consensus Workshop, Washington, DC, March 26-27, 1981): 13.
49. **Meaney DF, Thibault LE, Gennarelli T** (1994) Rotational brain injury tolerance criteria as a function of vehicle crash parameters. *IRCOBI Lyon, France*
50. **McLean AJ** (1995) Brain injury without head impact. *Journal of neurotrauma* (12): 621-625.
51. **Kleiven S** (2013) Why most traumatic brain injuries are not caused by linear acceleration but skull fractures are. *Frontiers in bioengineering and biotechnology* (1):
52. **Vink R, Bullock MR** (2010) Traumatic brain injury: therapeutic challenges and new directions. *Neurotherapeutics* (7): 1-2.
53. **Vink R** (2017) Large animal models of traumatic brain injury. *Journal of Neuroscience Research*
54. **Pittella JEH, Gusmão SNDS** (2004) The conformation of the brain plays an important role in the distribution of diffuse axonal injury in fatal road traffic accident. *Arquivos de neuro-psiquiatria* (62): 406-412.
55. **Posti JP *et al*** (2016) The Levels of Glial Fibrillary Acidic Protein and Ubiquitin C-Terminal Hydrolase-L1 During the First Week After a Traumatic Brain Injury: Correlations With Clinical and Imaging Findings. *Neurosurgery*
56. **Tse KM, Lim SP, Tan VBC, Lee HP** (2014) A review of head injury and finite element head models. *Am J Eng Technol Soc* (1): 28-52.
57. **Miller LE, Urban JE, Stitzel JD** (2016) Development and validation of an atlas-based finite element brain model. *Biomechanics and modeling in mechanobiology* (15): 1201-1214.
58. **Zhang J, Yoganandan N, Pintar FA, Gennarelli TA** (2006) Role of translational and rotational accelerations on brain strain in lateral head impact. *Biomed Sci Instrum* (42): 501-506.
59. **Yoganandan N, Li J, Zhang J, Pintar FA, Gennarelli TA** (2008) Influence of angular acceleration–deceleration pulse shapes on regional brain strains. *Journal of biomechanics* (41): 2253-2262.
60. **Fijalkowski RJ, Yoganandan N, Zhang J, Pintar FA** (2009) A finite element model of region-specific response for mild diffuse brain injury. *Stapp car crash journal* (53): 193.
61. **Forero Rueda MA, Cui L, Gilchrist MD** (2011) Finite element modeling of equestrian helmet impacts exposes the need to address rotational kinematics in future helmet designs. *Computer methods in biomechanics and biomedical engineering* (14): 1021-1031.
62. **Garimella HT, Kraft RH** (2017) Modeling the mechanics of axonal fiber tracts using the embedded finite element method. *International journal for numerical methods in biomedical engineering* (33):

63. **Sullivan S *et al*** (2015) White matter tract-oriented deformation predicts traumatic axonal brain injury and reveals rotational direction-specific vulnerabilities. *Biomechanics and modeling in mechanobiology* (14): 877-896.
64. **Morrison B** (2003) A tissue level tolerance criterion for living brain developed with an in vitro model of traumatic mechanical loading.
65. **Post A, Hoshizaki TB** (2012) Mechanisms of brain impact injuries and their prediction: a review. *Trauma* (14): 327-349.
66. **Meaney DF, Smith DH** (2015) Cellular biomechanics of central nervous system injury. *Handb Clin Neurol* (127): 105-114.
67. **Gutierrez E *et al*** (2001) A new model for diffuse brain injury by rotational acceleration: I. Model, gross appearance, and astrocytosis. *Journal of neurotrauma* (18): 247-257.
68. **Wojnarowicz MW, Fisher AM, Minaeva O, Goldstein LE** (2017) Considerations for Experimental Animal Models of Concussion, Traumatic Brain Injury, and Chronic Traumatic Encephalopathy—These Matters Matter. *Frontiers in Neurology* (8):
69. **McElhaney JH, Roberts VL, Hilyard JF** (1976) Properties of human tissues and components: nervous tissues. *Handbook of human tolerance, Automobile Research Institute Inc, Tokyo, Japan* (143):
70. **Cullen DK, Vernekar VN, LaPlaca MC** (2011) Trauma-induced plasmalemma disruptions in three-dimensional neural cultures are dependent on strain modality and rate. *Journal of neurotrauma* (28): 2219-2233.
71. **LaPlaca MC, Prado GR** (2010) Neural mechanobiology and neuronal vulnerability to traumatic loading. *Journal of biomechanics* (43): 71-78.
72. **Cloots RJ, van Dommelen JA, Nyberg T, Kleiven S, Geers MG** (2011) Micromechanics of diffuse axonal injury: influence of axonal orientation and anisotropy. *Biomech Model Mechanobiol* (10): 413-422.
73. **LaPlaca MC, Cullen DK, McLoughlin JJ, Cargill RS** (2005) High rate shear strain of three-dimensional neural cell cultures: a new in vitro traumatic brain injury model. *J Biomech* (38): 1093-1105.
74. **Margulies SS, Thibault LE** (1992) A proposed tolerance criterion for diffuse axonal injury in man. *Journal of biomechanics* (25): 917-923.
75. **Bain AC, Meaney DF** (2000) Tissue-level thresholds for axonal damage in an experimental model of central nervous system white matter injury. *Journal of biomechanical engineering* (122): 615-622.
76. **Donnelly BR, Medige J** (1997) Shear properties of human brain tissue. *Journal of biomechanical engineering* (119): 423-432.
77. **Morrison B, Meaney DF, Margulies SS, McIntosh TK** (2000) Dynamic mechanical stretch of organotypic brain slice cultures induces differential genomic expression: relationship to mechanical parameters. *J Biomech Eng* (122): 224-230.
78. **Tang-Schomer MD, Patel AR, Baas PW, Smith DH** (2010) Mechanical breaking of microtubules in axons during dynamic stretch injury underlies delayed elasticity, microtubule disassembly, and axon degeneration. *FASEB J* (24): 1401-1410.
79. **Tang-Schomer MD, Johnson VE, Baas PW, Stewart W, Smith DH** (2012) Partial interruption of axonal transport due to microtubule breakage accounts for the formation of periodic varicosities after traumatic axonal injury. *Exp Neurol* (233): 364-372.
80. **Di Pietro V *et al*** (2013) Potentially neuroprotective gene modulation in an in vitro model of mild traumatic brain injury. *Mol Cell Biochem* (375): 185-198.

81. **Zou H, Schmiedeler JP** (2008) Predicting brain injury under impact with a strain measure from analytical models. *International Journal of Crashworthiness* (13): 337-348.
82. **Geddes-Klein DM, Schiffman KB, Meaney DF** (2006) Mechanisms and consequences of neuronal stretch injury in vitro differ with the model of trauma. *Journal of neurotrauma* (23): 193-204.
83. **Gennarelli TA *et al*** (1989) Axonal injury in the optic nerve: a model simulating diffuse axonal injury in the brain. *Journal of neurosurgery* (71): 244-253.
84. **Smith DH, Meaney D** (2000) Axonal damage in traumatic brain injury. *The neuroscientist* (6): 483-495.
85. **Smith DH, Meaney DF, Shull WH** (2003) Diffuse axonal injury in head trauma. *J Head Trauma Rehabil* (18): 307-316.
86. **Chung RS *et al*** (2005) Mild axonal stretch injury in vitro induces a progressive series of neurofilament alterations ultimately leading to delayed axotomy. *J Neurotrauma* (22): 1081-1091.
87. **Kelley BJ, Farkas O, Lifshitz J, Povlishock JT** (2006) Traumatic axonal injury in the perisomatic domain triggers ultrarapid secondary axotomy and Wallerian degeneration. *Exp Neurol* (198): 350-360.
88. **Greer JE, Hanell A, McGinn MJ, Povlishock JT** (2013) Mild traumatic brain injury in the mouse induces axotomy primarily within the axon initial segment. *Acta Neuropathol* (126): 59-74.
89. **Wolf JA, Stys PK, Lusardi T, Meaney D, Smith DH** (2001) Traumatic axonal injury induces calcium influx modulated by tetrodotoxin-sensitive sodium channels. *J Neurosci* (21): 1923-1930.
90. **Staal JA L *et al*** (2010) Initial calcium release from intracellular stores followed by calcium dysregulation is linked to secondary axotomy following transient axonal stretch injury. *J Neurochem* (112): 1147-1155.
91. **Pike BR *et al*** (2000) Stretch injury causes calpain and caspase-3 activation and necrotic and apoptotic cell death in septo-hippocampal cell cultures. *Journal of neurotrauma* (17): 283-298.
92. **Di Pietro V *et al*** (2010) Transcriptomics of traumatic brain injury: gene expression and molecular pathways of different grades of insult in a rat organotypic hippocampal culture model. *J Neurotrauma* (27): 349-359.
93. **Arundine M *et al*** (2003) Enhanced vulnerability to NMDA toxicity in sublethal traumatic neuronal injury in vitro. *Journal of neurotrauma* (20): 1377-1395.
94. **Magou GC, Pfister BJ, Berlin JR** (2015) Effect of acute stretch injury on action potential and network activity of rat neocortical neurons in culture. *Brain Res* 1-11
95. **Salvador E, Burek M, Förster CY** (2015) Stretch and/or oxygen glucose deprivation (OGD) in an in vitro traumatic brain injury (TBI) model induces calcium alteration and inflammatory cascade. *Front Cell Neurosci* (9): 323.
96. **Staal JA, Vickers JC** (2011) Selective vulnerability of non-myelinated axons to stretch injury in an in vitro co-culture system. *J Neurotrauma* (28): 841-847.
97. **Choo AM *et al*** (2013) Antagonism of purinergic signalling improves recovery from traumatic brain injury. *Brain* (136): 65-80.
98. **Arundine M, Aarts M, Lau A, Tymianski M** (2004) Vulnerability of central neurons to secondary insults after in vitro mechanical stretch. *Journal of Neuroscience* (24): 8106-8123.

99. **Ji J *et al*** (2012) Mitochondrial injury after mechanical stretch of cortical neurons in vitro: biomarkers of apoptosis and selective peroxidation of anionic phospholipids. *Journal of neurotrauma* (29): 776-788.
100. **Kleele T *et al*** (2014) An assay to image neuronal microtubule dynamics in mice. *Nat Commun* (5): 4827.
101. **Conde C, Caceres A** (2009) Microtubule assembly, organization and dynamics in axons and dendrites. *Nat Rev Neurosci* (10): 319-332.
102. **Xu K, Zhong G, Zhuang X** (2013) Actin, spectrin, and associated proteins form a periodic cytoskeletal structure in axons. *Science* (339): 452-456.
103. **Deckwerth TL, Johnson EM** (1994) Neurites can remain viable after destruction of the neuronal soma by programmed cell death (apoptosis). *Dev Biol* (165): 63-72.
104. **Adalbert R, Nógrádi A, Szabó A, Coleman MP** (2006) The slow Wallerian degeneration gene in vivo protects motor axons but not their cell bodies after avulsion and neonatal axotomy. *Eur J Neurosci* (24): 2163-2168.
105. **Conforti L, Adalbert R, Coleman MP** (2007) Neuronal death: where does the end begin? *Trends Neurosci* (30): 159-166.
106. **Simon DJ *et al*** (2016) Axon degeneration gated by retrograde activation of somatic Pro-apoptotic signaling. *Cell* (164): 1031-1045.
107. **Maxwell WL, Bartlett E, Morgan H** (2015) Wallerian Degeneration in the Optic Nerve Stretch-Injury Model of Traumatic Brain Injury: A Stereological Analysis. *J Neurotrauma* (32): 780-790.
108. **Pettus EH, Povlishock JT** (1996) Characterization of a distinct set of intra-axonal ultrastructural changes associated with traumatically induced alteration in axolemmal permeability. *Brain Res* (722): 1-11.
109. **Koch JC *et al*** (2010) Acute axonal degeneration in vivo is attenuated by inhibition of autophagy in a calcium-dependent manner. *Autophagy* (6): 658-659.
110. **Knöferle J *et al*** (2010) Mechanisms of acute axonal degeneration in the optic nerve in vivo. *Proc Natl Acad Sci U S A* (107): 6064-6069.
111. **Lingor P, Koch JC, Tönges L, Bähr M** (2012) Axonal degeneration as a therapeutic target in the CNS. *Cell Tissue Res* (349): 289-311.
112. **Kerschensteiner M, Schwab ME, Lichtman JW, Misgeld T** (2005) In vivo imaging of axonal degeneration and regeneration in the injured spinal cord. *Nat Med* (11): 572-577.
113. **Beirowski B *et al*** (2004) Quantitative and qualitative analysis of Wallerian degeneration using restricted axonal labelling in YFP-H mice. *J Neurosci Methods* (134): 23-35.
114. **Beirowski B *et al*** (2005) The progressive nature of Wallerian degeneration in wild-type and slow Wallerian degeneration (Wld S) nerves. *BMC neuroscience* (6): 6.
115. **Wang JT, Medress ZA, Barres BA** (2012) Axon degeneration: molecular mechanisms of a self-destruction pathway. *J Cell Biol* (196): 7-18.
116. **Gilliatt RW, Hjorth RJ** (1972) Nerve conduction during Wallerian degeneration in the baboon. *J Neurol Neurosurg Psychiatry* (35): 335-341.
117. **Chaudhry V, Cornblath DR** (1992) Wallerian degeneration in human nerves: serial electrophysiological studies. *Muscle Nerve* (15): 687-693.
118. **Waller A** (1850) Experiments on the Section of the Glossopharyngeal and Hypoglossal Nerves of the Frog, and Observations of the Alterations Produced Thereby in the Structure of Their Primitive Fibres. *Philosophical Transactions of the Royal Society of London* 423-429.

119. **Finn JT *et al*** (2000) Evidence that Wallerian degeneration and localized axon degeneration induced by local neurotrophin deprivation do not involve caspases. *J Neurosci* (20): 1333-1341.
120. **Vohra BP *et al*** (2010) Amyloid precursor protein cleavage-dependent and -independent axonal degeneration programs share a common nicotinamide mononucleotide adenylyltransferase 1-sensitive pathway. *J Neurosci* (30): 13729-13738.
121. **Simon DJ *et al*** (2012) A caspase cascade regulating developmental axon degeneration. *Journal of Neuroscience* (32): 17540-17553.
122. **Burne JF, Staple JK, Raff MC** (1996) Glial cells are increased proportionally in transgenic optic nerves with increased numbers of axons. *J Neurosci* (16): 2064-2073.
123. **Whitmore AV, Lindsten T, Raff MC, Thompson CB** (2003) The proapoptotic proteins Bax and Bak are not involved in Wallerian degeneration. *Cell Death Differ* (10): 260-261.
124. **Sun L *et al*** (2012) Mixed lineage kinase domain-like protein mediates necrosis signaling downstream of RIP3 kinase. *Cell* (148): 213-227.
125. **Yang J *et al*** (2015) Pathological axonal death through a MAPK cascade that triggers a local energy deficit. *Cell* (160): 161-176.
126. **Yoon S, Kovalenko A, Bogdanov K, Wallach D** (2017) MLKL, the protein that mediates necroptosis, also regulates endosomal trafficking and extracellular vesicle generation. *Immunity* (47): 51-65. e7.
127. **Glass JD, Schryer BL, Griffin JW** (1994) Calcium-mediated degeneration of the axonal cytoskeleton in the Ola mouse. *J Neurochem* (62): 2472-2475.
128. **George EB, Glass JD, Griffin JW** (1995) Axotomy-induced axonal degeneration is mediated by calcium influx through ion-specific channels. *J Neurosci* (15): 6445-6452.
129. **Stirling DP, Stys PK** (2010) Mechanisms of axonal injury: internodal nanocomplexes and calcium deregulation. *Trends Mol Med* (16): 160-170.
130. **Ma M** (2013) Role of calpains in the injury-induced dysfunction and degeneration of the mammalian axon. *Neurobiol Dis* (60): 61-79.
131. **Ma M *et al*** (2013) Calpains mediate axonal cytoskeleton disintegration during Wallerian degeneration. *Neurobiol Dis* (56): 34-46.
132. **Vargas ME, Yamagishi Y, Tessier-Lavigne M, Sagasti A** (2015) Live Imaging of Calcium Dynamics during Axon Degeneration Reveals Two Functionally Distinct Phases of Calcium Influx. *J Neurosci* (35): 15026-15038.
133. **Watanabe M, Tsukiyama T, Hatakeyama S** (2007) Protection of vincristine-induced neuropathy by Wld S expression and the independence of the activity of Nmnat1. *Neuroscience letters* (411): 228-232.
134. **Gilley J, Coleman MP** (2010) Endogenous Nmnat2 is an essential survival factor for maintenance of healthy axons. *PLoS Biol* (8): e1000300.
135. **Barrientos SA *et al*** (2011) Axonal degeneration is mediated by the mitochondrial permeability transition pore. *J Neurosci* (31): 966-978.
136. **Stoll G, Griffin JW, Li CY, Trapp BD** (1989) Wallerian degeneration in the peripheral nervous system: participation of both Schwann cells and macrophages in myelin degradation. *J Neurocytol* (18): 671-683.
137. **Gaudet AD, Popovich PG, Ramer MS** (2011) Wallerian degeneration: gaining perspective on inflammatory events after peripheral nerve injury. *J Neuroinflammation* (8): 110.
138. **Bignami A, Ralston HJ** (1969) The cellular reaction to Wallerian degeneration in the central nervous system of the cat. *Brain Res* (13): 444-461.

139. **Perry VH, Brown MC, Gordon S** (1987) The macrophage response to central and peripheral nerve injury. A possible role for macrophages in regeneration. *J Exp Med* (165): 1218-1223.
140. **George R, Griffin JW** (1994) Delayed macrophage responses and myelin clearance during Wallerian degeneration in the central nervous system: the dorsal radiculotomy model. *Exp Neurol* (129): 225-236.
141. **Vargas ME, Barres BA** (2007) Why is Wallerian degeneration in the CNS so slow? *Annu Rev Neurosci* (30): 153-179.
142. **Koshinaga *et al*** (2000) Rapid and widespread microglial activation induced by traumatic brain injury in rat brain slices. *J Neurotrauma* (17): 185-192.
143. **Wang G *et al*** (2013) Microglia/macrophage polarization dynamics in white matter after traumatic brain injury. *J Cereb Blood Flow Metab* (33): 1864-1874.
144. **Holmin S, Mathiesen T** (1999) Long-term intracerebral inflammatory response after experimental focal brain injury in rat. *Neuroreport* (10): 1889-1891.
145. **Loane DJ, Kumar A, Stoica BA, Cabatbat R, Faden AI** (2014) Progressive neurodegeneration after experimental brain trauma: association with chronic microglial activation. *J Neuropathol Exp Neurol* (73): 14-29.
146. **Ramlackhansingh AF *et al*** (2011) Inflammation after trauma: microglial activation and traumatic brain injury. *Ann Neurol* (70): 374-383.
147. **Elward K, Gasque P** (2003) “Eat me” and “don’t eat me” signals govern the innate immune response and tissue repair in the CNS: emphasis on the critical role of the complement system. *Mol Immunol* (40): 85-94.
148. **Sievers C, Platt N, Perry VH, Coleman MP, Conforti L** (2003) Neurites undergoing Wallerian degeneration show an apoptotic-like process with annexin V positive staining and loss of mitochondrial membrane potential. *Neuroscience Research* (46): 161-169.
149. **Brown GC, Neher JJ** (2014) Microglial phagocytosis of live neurons. *Nat Rev Neurosci* (15): 209-216.
150. **Perry VH, Holmes C** (2014) Microglial priming in neurodegenerative disease. *Nat Rev Neurol* (10): 217-224.
151. **Collins PB, Chaykin S** (1971) Comparative metabolism of nicotinamide and nicotinic acid in mice. *Biochem J* (125): 117P.
152. **Gross CJ, Henderson LM** (1983) Digestion and absorption of NAD by the small intestine of the rat. *J Nutr* (113): 412-420.
153. **Magni G *et al*** (2004) Enzymology of NAD+ homeostasis in man. *Cell Mol Life Sci* (61): 19-34.
154. **Hassa PO, Haenni SS, Elser M, Hottiger MO** (2006) Nuclear ADP-ribosylation reactions in mammalian cells: where are we today and where are we going. *Microbiology and Molecular Biology Reviews* (70): 789-829.
155. **Revollo JR, Grimm AA, Imai S** (2007) The regulation of nicotinamide adenine dinucleotide biosynthesis by Nampt/PBEF/visfatin in mammals. *Curr Opin Gastroenterol* (23): 164-170.
156. **Imai S** (2009) Nicotinamide phosphoribosyltransferase (Nampt): a link between NAD biology, metabolism, and diseases. *Curr Pharm Des* (15): 20-28.
157. **Imai S, Yoshino J** (2013) The importance of NAMPT/NAD/SIRT1 in the systemic regulation of metabolism and ageing. *Diabetes Obes Metab* (15 Suppl 3): 26-33.
158. **Imai S-i, Guarente L** (2014) NAD+ and sirtuins in aging and disease. *Trends in cell biology* (24): 464-471.

159. **Di Stefano M, Conforti L** (2013) Diversification of NAD biological role: the importance of location. *FEBS J* (280): 4711-4728.
160. **Mori V *et al*** (2014) Metabolic profiling of alternative NAD biosynthetic routes in mouse tissues. *PLoS One* (9): e113939.
161. **Di Stefano M *et al*** (2017) NMN deamidase delays Wallerian degeneration and rescues axonal defects caused by NMNAT2 deficiency in vivo. *Current Biology* (27): 784-794.
162. **Bogan KL, Brenner C** (2008) Nicotinic acid, nicotinamide, and nicotinamide riboside: a molecular evaluation of NAD+ precursor vitamins in human nutrition. *Annu Rev Nutr* (28): 115-130.
163. **de Figueiredo LF, Gossmann TI, Ziegler M, Schuster S** (2011) Pathway analysis of NAD+ metabolism. *Biochem J* (439): 341-348.
164. **Berger F, Ramírez-Hernández MH, Ziegler M** (2004) The new life of a centenarian: signalling functions of NAD (P). *Trends in biochemical sciences* (29): 111-118.
165. **Koch-Nolte F, Fischer S, Haag F, Ziegler M** (2011) Compartmentation of NAD+-dependent signalling. *FEBS letters* (585): 1651-1656.
166. **Verdin E** (2015) NAD+ in aging, metabolism, and neurodegeneration. *Science* (350): 1208-1213.
167. **Pollak N, Dölle C, Ziegler M** (2007) The power to reduce: pyridine nucleotides–small molecules with a multitude of functions. *Biochemical Journal* (402): 205-218.
168. **Berger F, Lau C, Dahlmann M, Ziegler M** (2005) Subcellular compartmentation and differential catalytic properties of the three human nicotinamide mononucleotide adenylyltransferase isoforms. *Journal of Biological Chemistry* (280): 36334-36341.
169. **Magni G *et al*** (2004) Structure and function of nicotinamide mononucleotide adenylyltransferase. *Curr Med Chem* (11): 873-885.
170. **Berger F, Lau C, Dahlmann M, Ziegler M** (2005) Subcellular compartmentation and differential catalytic properties of the three human nicotinamide mononucleotide adenylyltransferase isoforms. *J Biol Chem* (280): 36334-36341.
171. **Lau C *et al*** (2010) Isoform-specific targeting and interaction domains in human nicotinamide mononucleotide adenylyltransferases. *Journal of Biological Chemistry* (285): 18868-18876.
172. **Zhai RG *et al*** (2006) Drosophila NMNAT maintains neural integrity independent of its NAD synthesis activity. *PLoS Biol* (4): e416.
173. **Ruan K, Zhu Y, Li C, Brazill JM, Zhai RG** (2015) Alternative splicing of Drosophila Nmnat functions as a switch to enhance neuroprotection under stress. *Nature communications* (6):
174. **Di Stefano M *et al*** (2015) A rise in NAD precursor nicotinamide mononucleotide (NMN) after injury promotes axon degeneration. *Cell Death Differ* (22): 731-742.
175. **Milde S, Fox AN, Freeman MR, Coleman MP** (2013) Deletions within its subcellular targeting domain enhance the axon protective capacity of Nmnat2 in vivo. *Scientific reports* (3):
176. **Milde S, Gilley J, Coleman MP** (2013) Subcellular localization determines the stability and axon protective capacity of axon survival factor Nmnat2. *PLoS Biol* (11): e1001539.
177. **Milde S, Coleman MP** (2014) Identification of palmitoyltransferase and thioesterase enzymes that control the subcellular localization of axon survival factor nicotinamide mononucleotide adenylyltransferase 2 (NMNAT2). *Journal of Biological Chemistry* (289): 32858-32870.
178. **Gilley J, Adalbert R, Yu G, Coleman MP** (2013) Rescue of peripheral and CNS axon defects in mice lacking NMNAT2. *The Journal of Neuroscience* (33): 13410-13424.

179. **Gilley J, Orsomando G, Nascimento-Ferreira I, Coleman MP** (2015) Absence of SARM1 Rescues Development and Survival of NMNAT2-Deficient Axons. *Cell Rep* (10): 1974-1981.
180. **Zhai RG *et al*** (2008) NAD synthase NMNAT acts as a chaperone to protect against neurodegeneration. *Nature* (452): 887-891.
181. **Ljungberg MC *et al*** (2011) CREB-activity and nmnat2 transcription are down-regulated prior to neurodegeneration, while NMNAT2 over-expression is neuroprotective, in a mouse model of human tauopathy. *Human molecular genetics* (21): 251-267.
182. **Ali YO, Li-Kroeger D, Bellen HJ, Zhai RG, Lu HC** (2013) NMNATs, evolutionarily conserved neuronal maintenance factors. *Trends Neurosci* (36): 632-640.
183. **Kitay BM, McCormack R, Wang Y, Tsoulfas P, Zhai RG** (2013) Mislocalization of neuronal mitochondria reveals regulation of Wallerian degeneration and NMNAT/WLDS-mediated axon protection independent of axonal mitochondria. *Human molecular genetics* (22): 1601-1614.
184. **Ali YO, McCormack R, Darr A, Zhai RG** (2011) Nicotinamide mononucleotide adenylyltransferase is a stress response protein regulated by the heat shock factor/hypoxia-inducible factor 1α pathway. *Journal of Biological Chemistry* (286): 19089-19099.
185. **Lavado-Roldán A, Fernández-Chacón R** (2016) Two for the Price of One: A Neuroprotective Chaperone Kit within NAD Synthase Protein NMNAT2. *PLoS Biol* (14): e1002522.
186. **Brazill JM, Li C, Zhu Y, Zhai RG** (2017) NMNAT: It's an NAD+ synthase… It's a chaperone… It's a neuroprotector. *Current Opinion in Genetics & Development* (44): 156-162.
187. **Ali YO *et al*** (2016) NMNAT2: HSP90 complex mediates Proteostasis in Proteinopathies. *PLoS Biol* (14): e1002472.
188. **Yang J *et al*** (2013) Regulation of axon degeneration after injury and in development by the endogenous calpain inhibitor calpastatin. *Neuron* (80): 1175-1189.
189. **den Hollander AI, Roepman R, Koenekoop RK, Cremers FPM** (2008) Leber congenital amaurosis: genes, proteins and disease mechanisms. *Progress in retinal and eye research* (27): 391-419.
190. **Perrault I *et al*** (2012) Mutations in NMNAT1 cause Leber congenital amaurosis with early-onset severe macular and optic atrophy. *Nature genetics* (44): 975-977.
191. **Koenekoop RK *et al*** (2012) Mutations in NMNAT1 cause Leber congenital amaurosis and identify a new disease pathway for retinal degeneration. *Nature genetics* (44): 1035-1039.
192. **Falk MJ *et al*** (2012) NMNAT1 mutations cause Leber congenital amaurosis. *Nature genetics* (44): 1040-1045.
193. **Chiang P-W *et al*** (2012) Exome sequencing identifies NMNAT1 mutations as a cause of Leber congenital amaurosis. *Nature genetics* (44): 972-974.
194. **Ali YO, Bradley G, Lu H-C** (2017) Screening with an NMNAT2-MSD platform identifies small molecules that modulate NMNAT2 levels in cortical neurons. *Scientific Reports* (7):
195. **Fang EF *et al*** (2017) NAD+ in Aging: Molecular Mechanisms and Translational Implications. *Trends in Molecular Medicine*
196. **Hodges A *et al*** (2006) Regional and cellular gene expression changes in human Huntington's disease brain. *Human molecular genetics* (15): 965-977.
197. **Lesnick TG *et al*** (2007) A genomic pathway approach to a complex disease: axon guidance and Parkinson disease. *PLoS genetics* (3): e98.
198. **Liang WS *et al*** (2008) Alzheimer's disease is associated with reduced expression of energy metabolism genes in posterior cingulate neurons. *Proceedings of the National Academy of Sciences* (105): 4441-4446.

199. **Milde S, Gilley J, Coleman MP** (2013) Axonal trafficking of NMNAT2 and its roles in axon growth and survival in vivo. *Bioarchitecture* (3): 133-140.
200. **Wang J *et al*** (2005) A local mechanism mediates NAD-dependent protection of axon degeneration. *J Cell Biol* (170): 349-355.
201. **Godzik K, Coleman M** (2014) The Axon-Protective WLD Protein Partially Rescues Mitochondrial Respiration and Glycolysis After Axonal Injury. *J Mol Neurosci* (55): 865-871.
202. **Shen H, Hyrc KL, Goldberg MP** (2013) Maintaining energy homeostasis is an essential component of Wld(S)-mediated axon protection. *Neurobiol Dis* (59): 69-79.
203. **Gerdts J, Brace EJ, Sasaki Y, DiAntonio A, Milbrandt J** (2015) SARM1 activation triggers axon degeneration locally via NAD^+ destruction. *Science* (348): 453-457.
204. **Osterloh JM *et al*** (2012) dSarm/Sarm1 is required for activation of an injury-induced axon death pathway. *Science* (337): 481-484.
205. **Loreto A, Di Stefano M, Gering M, Conforti L** (2015) Wallerian Degeneration Is Executed by an NMN-SARM1-Dependent Late Ca(2+) Influx but Only Modestly Influenced by Mitochondria. *Cell Rep* (13): 2539-2552.
206. **Vérièpe J, Fossouo L, Parker JA** (2015) Neurodegeneration in C. elegans models of ALS requires TIR-1/Sarm1 immune pathway activation in neurons. *Nature communications* (6): 7319.
207. **Sasaki Y, Nakagawa T, Mao X, DiAntonio A, Milbrandt J** (2016) NMNAT1 inhibits axon degeneration via blockade of SARM1-mediated NAD+ depletion. *Elife* (5): e19749.
208. **Gerdts J, Summers DW, Milbrandt J, DiAntonio A** (2016) Axon Self-Destruction: New Links among SARM1, MAPKs, and NAD+ Metabolism. *Neuron* (89): 449-460.
209. **Essuman K A *et al*** (2017) The SARM1 Toll/Interleukin-1 receptor domain possesses intrinsic NAD+ cleavage activity that promotes pathological axonal degeneration. *Neuron* (93): 1334-1343. e5.
210. **Gilley J, Ribchester RR, Coleman MP** (2017) Sarm1 Deletion, but Not Wld S, Confers Lifelong Rescue in a Mouse Model of Severe Axonopathy. *Cell reports* (21): 10-16.
211. **Coleman MP *et al*** (1998) An 85-kb tandem triplication in the slow Wallerian degeneration (Wlds) mouse. *Proc Natl Acad Sci U S A* (95): 9985-9990.
212. **Mack TGA *et al*** (2001) Wallerian degeneration of injured axons and synapses is delayed by a Ube4b/Nmnat chimeric gene. *Nature neuroscience* (4): 1199-1206.
213. **Fernando FS, Conforti L, Tosi S, Smith AD, Coleman MP** (2002) Human homologue of a gene mutated in the slow Wallerian degeneration (C57BL/Wld(s)) mouse. *Gene* (284): 23-29.
214. **Avery MA, Sheehan AE, Kerr KS, Wang J, Freeman MR** (2009) WldS requires Nmnat1 enzymatic activity and N16–VCP interactions to suppress Wallerian degeneration. *The Journal of cell biology* (184): 501-513.
215. **Sasaki Y, Vohra BPS, Baloh RH, Milbrandt J** (2009) Transgenic mice expressing the Nmnat1 protein manifest robust delay in axonal degeneration in vivo. *Journal of Neuroscience* (29): 6526-6534.
216. **Yahata N, Yuasa S, Araki T** (2009) Nicotinamide mononucleotide adenylyltransferase expression in mitochondrial matrix delays Wallerian degeneration. *Journal of Neuroscience* (29): 6276-6284.
217. **Guo Q, Xie J, Dang CV, Liu ET, Bishop JM** (1998) Identification of a large Myc-binding protein that contains RCC1-like repeats. *Proceedings of the National Academy of Sciences* (95): 9172-9177.

218. **Wan HI *et al*** (2000) Highwire regulates synaptic growth in Drosophila. *Neuron* (26): 313-329.
219. **McCabe BD *et al*** (2004) Highwire regulates presynaptic BMP signaling essential for synaptic growth. *Neuron* (41): 891-905.
220. **Murthy V *et al*** (2004) Pam and its ortholog highwire interact with and may negatively regulate the TSC1· TSC2 complex. *Journal of Biological Chemistry* (279): 1351-1358.
221. **Pierre SC, Häusler J, Birod K, Geisslinger G, Scholich K** (2004) PAM mediates sustained inhibition of cAMP signaling by sphingosine-1-phosphate. *The EMBO journal* (23): 3031-3040.
222. **Le Guyader S, Maier J, Jesuthasan S** (2005) Esrom, an ortholog of PAM (protein associated with c-myc), regulates pteridine synthesis in the zebrafish. *Developmental biology* (277): 378-386.
223. **Wu C, Waikar YP, Collins CS, DiAntonio A** (2005) Highwire function at the Drosophila neuromuscular junction: spatial, structural, and temporal requirements. *The Journal of Neuroscience* (25): 9557-9566.
224. **Xiong X *et al*** (2012) The Highwire ubiquitin ligase promotes axonal degeneration by tuning levels of Nmnat protein. *PLoS Biol* (10): 1-18.
225. **Grill B, Murphey RK, Borgen MA** (2016) The PHR proteins: intracellular signaling hubs in neuronal development and axon degeneration. *Neural development* (11): 8.
226. **Neukomm LJ, Burdett TC, Gonzalez MA, Züchner S, Freeman MR** (2014) Rapid in vivo forward genetic approach for identifying axon death genes in Drosophila. *Proc Natl Acad Sci U S A* (111): 9965-9970.
227. **Neukomm LJ, Freeman MR** (2014) Diverse cellular and molecular modes of axon degeneration. *Trends Cell Biol* (24): 515-523.
228. **Collins CA, Wairkar YP, Johnson SL, DiAntonio A** (2006) Highwire restrains synaptic growth by attenuating a MAP kinase signal. *Neuron* (51): 57-69.
229. **Shin JE, DiAntonio A** (2011) Highwire regulates guidance of sister axons in the Drosophila mushroom body. *Journal of Neuroscience* (31): 17689-17700.
230. **Babetto E, Beirowski B, Russler EV, Milbrandt J, DiAntonio A** (2013) The Phr1 ubiquitin ligase promotes injury-induced axon self-destruction. *Cell reports* (3): 1422-1429.
231. **Cargnello M, Roux PP** (2011) Activation and function of the MAPKs and their substrates, the MAPK-activated protein kinases. *Microbiology and molecular biology reviews* (75): 50-83.
232. **Wu C, Daniels RW, DiAntonio A** (2007) DFsn collaborates with Highwire to down-regulate the Wallenda/DLK kinase and restrain synaptic terminal growth. *Neural development* (2): 16.
233. **Xiong X, Wang X, Ewanek R, Bhat P, DiAntonio A *et al*** (2010) Protein turnover of the Wallenda/DLK kinase regulates a retrograde response to axonal injury. *The Journal of cell biology* (191): 211-223.
234. **Xiong X, Collins CA** (2012) A conditioning lesion protects axons from degeneration via the Wallenda/DLK MAP kinase signaling cascade. *Journal of Neuroscience* (32): 610-615.
235. **Nakata K *et al*** (2005) Regulation of a DLK-1 and p38 MAP kinase pathway by the ubiquitin ligase RPM-1 is required for presynaptic development. *Cell* (120): 407-420.
236. **Tedeschi A, Bradke F** (2013) The DLK signalling pathway—a double-edged sword in neural development and regeneration. *EMBO reports* (14): 605-614.
237. **Miller BR *et al*** (2009) A dual leucine kinase-dependent axon self-destruction program promotes Wallerian degeneration. *Nat Neurosci* (12): 387-389.

238. **Walker LJ *et al*** (2017) MAPK signaling promotes axonal degeneration by speeding the turnover of the axonal maintenance factor NMNAT2. *Elife* (6): e22540.
239. **Shin JE *et al*** (2012) SCG10 is a JNK target in the axonal degeneration pathway. *Proceedings of the National Academy of Sciences* (109): E3696-E3705.
240. **Shin JE, Geisler S, DiAntonio A** (2014) Dynamic regulation of SCG10 in regenerating axons after injury. *Experimental neurology* (252): 1-11.
241. **Neukomm LJ *et al*** (2017) Axon Death Pathways Converge on Axundead to Promote Functional and Structural Axon Disassembly. *Neuron* (95): 78-91.
242. **Gerdts J, Sasaki Y, Vohra B, Marasa J, Milbrandt J** (2011) Image-based screening identifies novel roles for IκB kinase and glycogen synthase kinase 3 in axonal degeneration. *Journal of Biological Chemistry* (286): 28011-28018.
243. **Wakatsuki S, Saitoh F, Araki T** (2011) ZNRF1 promotes Wallerian degeneration by degrading AKT to induce GSK3B-dependent CRMP2 phosphorylation. *Nature cell biology* (13): 1415-1423.
244. **Ikegami K, Kato S, Koike T** (2004) N-alpha-p-tosyl-L-lysine chloromethyl ketone (TLCK) suppresses neuritic degeneration caused by different experimental paradigms including in vitro Wallerian degeneration. *Brain research* (1030): 81-93.
245. **Zhai Q *et al*** (2003) Involvement of the ubiquitin-proteasome system in the early stages of wallerian degeneration. *Neuron* (39): 217-225.
246. **Coleman MP, Freeman MR** (2010) Wallerian degeneration, wld(s), and nmnat. *Annu Rev Neurosci* (33): 245-267.
247. **Maxwell WL, Watt C, Graham DI, Gennarelli TA** (1993) Ultrastructural evidence of axonal shearing as a result of lateral acceleration of the head in non-human primates. *Acta neuropathologica* (86): 136-144.
248. **Povlishock JT, Christman CW** (1995) The pathobiology of traumatically induced axonal injury in animals and humans: a review of current thoughts. *Journal of neurotrauma* (12): 555-564.
249. **Smith DH, Wolf JA, Lusardi TA, Lee VM, Meaney DF** (1999) High tolerance and delayed elastic response of cultured axons to dynamic stretch injury. *J Neurosci* (19): 4263-4269.
250. **Christman CW, Grady MS, Walker SA, Holloway KL, Povlishock JT** (1994) Ultrastructural studies of diffuse axonal injury in humans. *J Neurotrauma* (11): 173-186.
251. **Erturk A, Hellal F, Enes J, Bradke F** (2007) Disorganized microtubules underlie the formation of retraction bulbs and the failure of axonal regeneration. *J Neurosci* (27): 9169-9180.
252. **Mittal P** (2015) Diffuse Axonal Injury: Pathological and Clinical Aspects. *Forensic Res Criminol Int J* (1): 1-5.
253. **Maxwell WL, Bartlett E, Morgan H** (2015) Wallerian degeneration in the optic nerve stretch-injury model of traumatic brain injury: a stereological analysis. *Journal of neurotrauma* (32): 780-790.
254. **Milde S, Adalbert R, Elaman MH, Coleman MP** (2015) Axonal transport declines with age in two distinct phases separated by a period of relative stability. *Neurobiology of aging* (36): 971-981.
255. **Hung COY, Coleman MP** (2016) KIF1A mediates axonal transport of BACE1 and identification of independently moving cargoes in living SCG neurons. *Traffic* (17): 1155-1167.
256. **Fang Y, Soares L, Teng X, Geary M, Bonini NM** (2012) A novel Drosophila model of nerve injury reveals an essential role of Nmnat in maintaining axonal integrity. *Current Biology* (22): 590-595.

257. **Wang JT, Barres BA** (2012) Axon degeneration: where the Wlds things are. *Curr Biol* (22): 221-3.
258. **Avery MA *et al*** (2012) WldS prevents axon degeneration through increased mitochondrial flux and enhanced mitochondrial Ca2+ buffering. *Curr Biol* (22): 596-600.
259. **O'Donnell KC, Vargas ME, Sagasti A** (2013) WldS and PGC-1α regulate mitochondrial transport and oxidation state after axonal injury. *Journal of Neuroscience* (33): 14778-14790.
260. **Kanamori A, Catrinescu MM, Belisle JM, Costantino S, Levin LA** (2012) Retrograde and Wallerian axonal degeneration occur synchronously after retinal ganglion cell axotomy. *Am J Pathol* (181): 62-73.
261. **Hu Y *et al*** (2012) Differential effects of unfolded protein response pathways on axon injury-induced death of retinal ganglion cells. *Neuron* (73): 445-452.
262. **Rishal I, Fainzilber M** (2014) Axon-soma communication in neuronal injury. *Nat Rev Neurosci* (15): 32-42.
263. **Öztürk G *et al*** (2013) Two distinct types of dying back axonal degeneration in vitro. *Neuropathol Appl Neurobiol* (39): 362-376.
264. **Cavanagh JB** (1979) The 'dying back' process. A common denominator in many naturally occurring and toxic neuropathies. *Arch Pathol Lab Med* (103): 659-664.
265. **Oda K, Yamazaki K, Miura H, Shibasaki H, Kikuchi T** (1992) Dying back type axonal degeneration of sensory nerve terminals in muscle spindles of the gracile axonal dystrophy (GAD) mutant mouse. *Neuropathol Appl Neurobiol* (18): 265-281.
266. **Willison HJ, Winer JB** (2003) Clinical evaluation and investigation of neuropathy. *J Neurol Neurosurg Psychiatry* (74 Suppl 2): ii3-ii8.
267. **Magnifico S *et al*** (2013) NAD+ acts on mitochondrial SirT3 to prevent axonal caspase activation and axonal degeneration. *FASEB J* (27): 4712-4722.
268. **Gao X, Deng P, Xu ZC, Chen J** (2011) Moderate traumatic brain injury causes acute dendritic and synaptic degeneration in the hippocampal dentate gyrus. *PLoS One* (6): e24566.
269. **Cunnane ME, Moonis G, Shull WH** (2003) MRI findings of Wallerian degeneration after diffuse axonal injury: case report and review of literature. *European Journal of Radiology Extra* (47): 1-4.
270. **Chen YJ *et al*** (2017) Wallerian Degeneration Beyond the Corticospinal Tracts: Conventional and Advanced MRI Findings. *Journal of Neuroimaging* (27): 272-280.
271. **Zetterberg H, Smith DH, Blennow K** (2013) Biomarkers of mild traumatic brain injury in cerebrospinal fluid and blood. *Nature Reviews Neurology* (9): 201-210.
272. **Gatson JW *et al*** (2014) Detection of neurofilament-H in serum as a diagnostic tool to predict injury severity in patients who have suffered mild traumatic brain injury. *J Neurosurg* (121): 1232-1238.
273. **Kobeissy FH *et al*** (2015) Degradation of βII-Spectrin Protein by Calpain-2 and Caspase-3 Under Neurotoxic and Traumatic Brain Injury Conditions. *Mol Neurobiol* (52): 696-709.
274. **Carpenter KL *et al*** (2015) Systemic, local, and imaging biomarkers of brain injury: more needed, and better use of those already established? *Front Neurol* (6): 26.
275. **Fox GB, Faden AI** (1998) Traumatic brain injury causes delayed motor and cognitive impairment in a mutant mouse strain known to exhibit delayed Wallerian degeneration. *J Neurosci Res* (53): 718-727.
276. **Henninger N *et al*** (2016) Attenuated traumatic axonal injury and improved functional outcome after traumatic brain injury in mice lacking Sarm1. *Brain* 1-12.
277. **Xiong Y, Mahmood A, Chopp M** (2013) Animal models of traumatic brain injury. *Nat Rev Neurosci* (14): 128-142.

278. **Ganetzky B, Wassarman DA** (2016) Non-mammalian Animal Models Offer New Perspectives on the Treatment of TBI. *Current Physical Medicine and Rehabilitation Reports* (4): 1-4.
279. **Gama JHP** (1835) Traité des plaies de tête et de l'encéphalite, principalement de celle qui leur est consécutive: ouvrage dans lequel sont discutées plusieurs questions relatives aux fonctions du système nerveux en général. Paris.
280. **Holbourn AHS** (1943) Mechanics of head injuries. *The Lancet* (242): 438-441.
281. **Holbourn AHS** (1945) The mechanics of brain injuries. *British medical bulletin* (3): 147-149.
282. **Pudenz RH, Shelden CH** (1946) The lucite calvarium—a method for direct observation of the brain: II. Cranial trauma and brain movement. *Journal of neurosurgery* (3): 487-505.
283. **Ommaya AK** (1968) Mechanical properties of tissues of the nervous system. *Journal of Biomechanics* (1): 127-138
284. **Adams JH, Mitchell DE, Graham DI, Doyle D** (1977) Diffuse brain damage of immediate impact type. Its relationship to 'primary brain-stem damage' in head injury. *Brain: a journal of neurology* (100): 489-502.
285. **Adams JH, Jennett B, McLellan DR, Murray LS, Graham DI** (1999) The neuropathology of the vegetative state after head injury. *J Clin Pathol* (52): 804-806.
286. **Lighthall JW, Dixon CE, Anderson TE** (1989) Experimental models of brain injury. *Journal of neurotrauma* (6): 83-97.
287. **Meaney DF *et al*** (1995) Biomechanical analysis of experimental diffuse axonal injury. *Journal of neurotrauma* (12): 689-694.
288. **Feeney DM, Boyeson MG, Linn RT, Murray HM, Dail WG** (1981) Responses to cortical injury: I. Methodology and local effects of contusions in the rat. *Brain research* (211): 67-77.
289. **McIntosh TK *et al*** (1989) Traumatic brain injury in the rat: characterization of a lateral fluid-percussion model. *Neuroscience* (28): 233-244.
290. **Dixon CE, Clifton GL, Lighthall JW, Yaghmai AA, Hayes RL** (1991) A controlled cortical impact model of traumatic brain injury in the rat. *Journal of neuroscience methods* (39): 253-262.
291. **Perez-Polo JR *et al*** (2015) A rodent model of mild traumatic brain blast injury. *Journal of neuroscience research* (93): 549-561.
292. **Lessing D, Bonini NM** (2009) Maintaining the brain: insight into human neurodegeneration from Drosophila melanogaster mutants. *Nature Reviews Genetics* 359-370
293. **Bellen HJ, Tong C, Tsuda H** (2010) 100 years of Drosophila research and its impact on vertebrate neuroscience: a history lesson for the future. *Nature Reviews Neuroscience* (11): 514-522.
294. **Hirth F** (2010) Drosophila melanogaster in the study of human neurodegeneration. *CNS & Neurological Disorders-Drug Targets* (9): 504-523.
295. **Pandey UB, Nichols CD** (2011) Human disease models in Drosophila melanogaster and the role of the fly in therapeutic drug discovery. *Pharmacological reviews* (63): 411-436.
296. **Rooney TM, Freeman MR** (2014) Drosophila models of neuronal injury. *ILAR Journal* (54): 291-295.
297. **Fang Y, Bonini NM** (2012) Axon degeneration and regeneration: insights from Drosophila models of nerve injury. *Annual review of cell and developmental* (28):575-597
298. **Katzenberger RJ *et al*** (2013) A Drosophila model of closed head traumatic brain injury. *Proceedings of the National Academy of Sciences* (110): E4152-E4159.

299. **Katzenberger RJ *et al*** (2015) Death following traumatic brain injury in Drosophila is associated with intestinal barrier dysfunction. *Elife* (4): e04790.
300. **Barekat A *et al*** (2016) Using Drosophila as an integrated model to study mild repetitive traumatic brain injury. *Scientific reports* (6): 1-14
301. **Sherman SA *et al*** (2016) Stretch Injury of Human Induced Pluripotent Stem Cell Derived Neurons in a 96 Well Format. *Scientific reports* (6): 1-12.
302. **Meaney DF, Smith DH** (2011) Biomechanics of concussion. *Clinics in sports medicine* (30): 19-31.
303. **Ellis EF, McKinney JS, Willoughby KA, Liang S, Povlishock JT** (1995) A new model for rapid stretch-induced injury of cells in culture: characterization of the model using astrocytes. *Journal of neurotrauma* (12): 325-339.
304. **Johnson et al** (2008) Validation of an improved injury device for in vitro study of neural cell deformation. *Biomedical sciences* 1-6.
305. **Staal JA, Dickson TC, Chung RS, Vickers JC** (2007) Cyclosporin-A treatment attenuates delayed cytoskeletal alterations and secondary axotomy following mild axonal stretch injury. *Dev Neurobiol* (67): 1831-1842.
306. **Iwata A *et al*** (2004) Traumatic axonal injury induces proteolytic cleavage of the voltage-gated sodium channels modulated by tetrodotoxin and protease inhibitors. *Journal of Neuroscience* (24): 4605-4613.
307. **Lusardi TA, Wolf JA, Putt ME, Smith DH, Meaney DF** (2004) Effect of acute calcium influx after mechanical stretch injury in vitro on the viability of hippocampal neurons. *Journal of neurotrauma* (21): 61-72.
308. **Lusardi TA, Rangan J, Sun D, Smith DH, Meaney DF** (2004) A device to study the initiation and propagation of calcium transients in cultured neurons after mechanical stretch. *Annals of biomedical engineering* (32): 1546-1559.
309. **Yuen TJ, Browne KD, Iwata A, Smith DH** (2009) Sodium channelopathy induced by mild axonal trauma worsens outcome after a repeat injury. *Journal of neuroscience research* (87): 3620-3625.
310. **Geddes DM, Cargill RS** (2001) An in vitro model of neural trauma: device characterization and calcium response to mechanical stretch. *Journal of biomechanical engineering* (123): 247-255.
311. **Geddes DM, Cargill RS, LaPlaca MC** (2003) Mechanical stretch to neurons results in a strain rate and magnitude-dependent increase in plasma membrane permeability. *Journal of neurotrauma* (20): 1039-1049.
312. **Morrison B, Meaney DF, McIntosh TK** (1998) Mechanical characterization of an in vitro device designed to quantitatively injure living brain tissue. *Annals of biomedical engineering* (26): 381-390.
313. **Morrison B, Cater HL, Benham CD, Sundstrom LE** (2006) An in vitro model of traumatic brain injury utilising two-dimensional stretch of organotypic hippocampal slice cultures. *J Neurosci Methods* (150): 192-201.
314. **Dolle JP, Morrison B, Schloss RS, Yarmush ML** (2013) An organotypic uniaxial strain model using microfluidics. *Lab Chip* (13): 432-442.
315. **Pfister BJ, Weihs TP, Betenbaugh M, Bao G** (2003) An in vitro uniaxial stretch model for axonal injury. *Annals of biomedical engineering* (31): 589-598.
316. **Magou GC *et al*** (2011) Engineering a high throughput axon injury system. *Journal of neurotrauma* (28): 2203-2218.

317. **Tang-Schomer MD *et al*** (2014) Bioengineered functional brain-like cortical tissue. *Proceedings of the National Academy of Sciences* (111): 13811-13816.
318. **Lancaster MA, Knoblich JA** (2014) Organogenesis in a dish: modeling development and disease using organoid technologies. *Science* (345): 1247125.
319. **Bar-Kochba E, Scimone MT, Estrada JB, Franck C** (2016) Strain and rate-dependent neuronal injury in a 3D in vitro compression model of traumatic brain injury. *Scientific reports* (6): 1-11
320. **Mayer PR *et al*** (2010) Expression, localization, and biochemical characterization of nicotinamide mononucleotide adenylyltransferase 2. *Journal of Biological Chemistry* (285): 40387-40396.
321. **Chishti MA *et al*** (2001) Early-onset amyloid deposition and cognitive deficits in transgenic mice expressing a double mutant form of amyloid precursor protein 695. *J Biol Chem* (276): 21562-21570.
322. **Park J *al*** (2006) Mitochondrial dysfunction in Drosophila PINK1 mutants is complemented by parkin. *Nature* (441): 1157-1161.
323. **De Simoni A, Yu LM** (2006) Preparation of organotypic hippocampal slice cultures: interface method. *Nat Protoc* (1): 1439-1445.
324. **Gogolla N, Galimberti I, DePaola V, Caroni P** (2006) Preparation of organotypic hippocampal slice cultures for long-term live imaging. *Nat Protoc* (1): 1165-1171.
325. **Gargano JW et al** (2005) Rapid iterative negative geotaxis (RING): a new method for assessing age-related locomotor decline in Drosophila. *Experimental gerontology* (45) 125-130.
326. **Nichols CD, Becnel J, Pandey UB** (2012) Methods to assay Drosophila behaviour. *JoVE* (61):1-5.
327. **Morales DM *et al*** (2005) Experimental models of traumatic brain injury: do we really need to build a better mousetrap? *Neuroscience* (136): 971-989.
328. **Werner C, Engelhard K** (2007) Pathophysiology of traumatic brain injury. *Br J Anaesth* (99): 4-9.
329. **Stein MD, Feather CB, Napolitano LM** (2016) Traumatic Brain Injury Advances. *Advances in Trauma, An Issue of Critical Care Clinics* (33): 1-13.
330. **Proctor JL, Scutella D, Pan Y, Vaughan J, Rosenthal RE *et al*** (2015) Hyperoxic resuscitation improves survival but worsens neurologic outcome in a rat polytrauma model of traumatic brain injury plus hemorrhagic shock. *Journal of Trauma and Acute Care Surgery* (79): S101-S109.
331. **Agar A, Yip SS, Hill MA, Coroneo MT** (2000) Pressure related apoptosis in neuronal cell lines. *Journal of neuroscience research* (60): 495-503.
332. **Stubbe M, Nissen M, Schroeder J, Gimsa J** (2015) The effect of hyperbaric air on the electric activity of neuronal in vitro networks. *Biosensors and Bioelectronics* (73): 153-159.
333. **Statler KD *et al*** (2001) The simple model versus the super model: translating experimental traumatic brain injury research to the bedside. *Journal of neurotrauma* (18): 1195-1206.
334. **Cater HL *et al*** (2007) Stretch-induced injury in organotypic hippocampal slice cultures reproduces in vivo post-traumatic neurodegeneration: role of glutamate receptors and voltage-dependent calcium channels. *J Neurochem* (101): 434-447.
335. **Pieper AA, McKnight SL, Ready JM** (2014) P7C3 and an unbiased approach to drug discovery for neurodegenerative diseases. *Chem Soc Rev* (43): 6716-6726.

336. **Wang G, Han T, Nijhawan D, Theodoropoulos P, Naidoo J *et al*** (2014) P7C3 neuroprotective chemicals function by activating the rate-limiting enzyme in NAD salvage. *Cell* (158): 1324-1334.
337. **Yin TC, Britt JK, De Jesús-Cortés H, Lu Y, Genova RM *et al*** (2014) P7C3 neuroprotective chemicals block axonal degeneration and preserve function after traumatic brain injury. *Cell Rep* (8): 1731-1740.
338. **Cornelius DJ, Monroe CM** (1985) The unique properties of silicone and fluorosilicone elastomers. *Polymer Engineering & Science* (25): 467-473.
339. **Honig MG, Hume RI** (1986) Fluorescent carbocyanine dyes allow living neurons of identified origin to be studied in long-term cultures. *J Cell Biol* (103): 171-187.
340. **Cheng C, Trzcinski O, Doering LC** (2014) Fluorescent labeling of dendritic spines in cell cultures with the carbocyanine dye "DiI". *Frontiers in neuroanatomy* (8): 1-8
341. **Hanell A, Greer JE, McGinn MJ, Povlishock JT** (2015) Traumatic brain injury-induced axonal phenotypes react differently to treatment. *Acta Neuropathol* (129): 317-332.
342. **Cengiz N, Öztürk G, Erdoğan E, Him A, Oğuz EK** (2012) Consequences of neurite transection in vitro. *Journal of neurotrauma* (29): 2465-2474.
343. **Chazotte B** (2011) Labeling mitochondria with MitoTracker dyes. *Cold Spring Harbor Protocols* (2011): pdb. prot5648.
344. **Ellenbroek B, Youn J** (2016) Rodent models in neuroscience research: is it a rat race. *Disease models & mechanisms* (9): 1079-1087.
345. **Holen K, Saltz LB, Hollywood E, Burk K, Hanauske A-R** (2008) The pharmacokinetics, toxicities, and biologic effects of FK866, a nicotinamide adenine dinucleotide biosynthesis inhibitor. *Investigational new drugs* (26): 45-51.
346. **Hasmann M, Schemainda I** (2003) FK866, a highly specific noncompetitive inhibitor of nicotinamide phosphoribosyltransferase, represents a novel mechanism for induction of tumor cell apoptosis. *Cancer research* (63): 7436-7442.
347. **Moore Z *et al*** (2015) NAMPT inhibition sensitizes pancreatic adenocarcinoma cells to tumor-selective, PAR-independent metabolic catastrophe and cell death induced by β-lapachone. *Cell death & disease* (6): e1599; 1-10
348. **Barraud M *et al*** (2016) A pancreatic ductal adenocarcinoma subpopulation is sensitive to FK866, an inhibitor of NAMPT. *Oncotarget* (7): 53783-53786
349. **Esposito E *et al*** (2012) The NAMPT inhibitor FK866 reverts the damage in spinal cord injury. *Journal of neuroinflammation* (9): 66; 1-11
350. **Matsuda A *et al*** (2014) FK866, a Visfatin Inhibitor, Protects Against Acute Lung Injury After Intestinal Ischemia–Reperfusion in Mice via NF-κB Pathway. *Annals of surgery* (259): 1007-1017.
351. **Hu Q *et al*** (2017) Hyperbaric Oxygen Reduces Infarction Volume and Hemorrhagic Transformation Through ATP/NAD+/Sirt1 Pathway in Hyperglycemic Middle Cerebral Artery Occlusion Rats. *Stroke* (48): 1655-1664.
352. **Wang P *et al*** (2011) Nicotinamide phosphoribosyltransferase protects against ischemic stroke through SIRT1-dependent adenosine monophosphate–activated kinase pathway. *Annals of neurology* (69): 360-374.
353. **Chen C-X *et al*** (2017) NAMPT inhibitor protects ischemic neuronal injury in rat brain via anti-neuroinflammation. *Neuroscience*. (291):230-240
354. **Zhang X-Q *et al*** (2015) NAMPT inhibitor and metabolite protect mouse brain from cryoinjury through distinct mechanisms. *Neuroscience* (291): 230-240.

355. **Lunn ER, Perry VH, Brown MC, Rosen H, Gordon S** (1989) Absence of Wallerian Degeneration does not Hinder Regeneration in Peripheral Nerve. *Eur J Neurosci* (1): 27-33.
356. **Sasaki Y, Milbrandt J** (2010) Axonal degeneration is blocked by nicotinamide mononucleotide adenylyltransferase (Nmnat) protein transduction into transected axons. *Journal of Biological Chemistry* (285): 41211-41215.
357. **Lorber B, Tassoni A, Bull ND, Moschos MM, Martin KR** (2012) Retinal ganglion cell survival and axon regeneration in Wld S transgenic rats after optic nerve crush and lens injury. *BMC neuroscience* (13): 56.
358. **Mukherjee P, Woods TA, Moore RA, Peterson KE** (2013) Activation of the innate signaling molecule MAVS by bunyavirus infection upregulates the adaptor protein SARM1, leading to neuronal death. *Immunity* (38): 705-716.
359. **Thibault LE** (1993) Brain injury from the macro to the micro level and back again: what have we learned to date. *Proceedings of the International Research Council on the Biomechanics of Injury conference 21*: 3-25.
360. **Ahmed SM *et al*** (2002) NMDA receptor activation contributes to a portion of the decreased mitochondrial membrane potential and elevated intracellular free calcium in strain-injured neurons. *Journal of neurotrauma* (19): 1619-1629.
361. **Dechant G** (2002) Chat in the trophic web: NGF activates Ret by inter-RTK signaling. *Neuron* (33): 156-158.
362. **Biswas SC, Shi Y, Sproul A, Greene LA** (2007) Pro-apoptotic Bim induction in response to nerve growth factor deprivation requires simultaneous activation of three different death signaling pathways. *Journal of Biological Chemistry* (282): 29368-29374.
363. **Amendola J, Boumedine N, Sangiardi M, El Far O** (2015) Optimization of neuronal cultures from rat superior cervical ganglia for dual patch recording. *Scientific reports* (5): 1-10
364. **Jackson M, Tourtellotte W** (2014) Neuron culture from mouse superior cervical ganglion. *Bio-protocol* (4): 1-7
365. **Hao L, Xu Z, Sun H, Luo W, Yan Y *et al*** (2017) Direct induction of functional neuronal cells from fibroblast-like cells derived from adult human retina. *Stem cell research* (23): 61-72.
366. **Prior R, Van Helleputte L, Benoy V, Van Den Bosch L** (2017) Defective axonal transport: A common pathological mechanism in inherited and acquired peripheral neuropathies. *Neurobiology of Disease* (105): 300-320
367. **Wang X, Schwarz TL** (2009) Imaging axonal transport of mitochondria. *Methods in enzymology* (457): 319-333.
368. **Hicks AN *et al*** (2012) Nicotinamide mononucleotide adenylyltransferase 2 (Nmnat2) regulates axon integrity in the mouse embryo. *PLoS One* (7): e47869; 1-10
369. **Wang B, Harrison W, Overbeek PA, Zheng H** (2011) Transposon mutagenesis with coat color genotyping identifies an essential role for Skor2 in sonic hedgehog signaling and cerebellum development. *Development* (138): 4487-4497.
370. **Nikolaev A, McLaughlin T, O'Leary DDM, Tessier-Lavigne M** (2009) APP binds DR6 to trigger axon pruning and neuron death via distinct caspases. *Nature* (457): 981-989.
371. **Schoenmann *et al*** (2010) Axonal degeneration is regulated by the apoptotic machinery or a NAD+-sensitive pathway in insects and mammals. *Journal of Neuroscience* (30): 6375-6386.
372. **Cusack CL, Swahari V, Henley WH, Ramsey JM, Deshmukh M** (2013) Distinct pathways mediate axon degeneration during apoptosis and axon-specific pruning. *Nature communications* (4): 1876.

373. **Unsain N, Higgins JM, Parker KN, Johnstone AD, Barker PA** (2013) XIAP regulates caspase activity in degenerating axons. *Cell reports* (4): 751-763.
374. **Pieper AA *et al*** (2010) Discovery of a proneurogenic, neuroprotective chemical. *Cell* (142): 39-51.
375. **Sabbagh MN, Shill HA** (2010) Latrepirdine, a potential novel treatment for Alzheimer's disease and Huntington's chorea. *Current Opinion in Investigational Drugs* (11): 80.
376. **Jones R, 2010** (2010) Dimebon disappointment. *Alzheimer's research and therapy* (2): 1-3.
377. **Sweetlove M** (2012) Phase III CONCERT trial of latrepirdine. *Pharmaceutical medicine* (26): 113-115.
378. **Dutca LM *et al*** (2014) Early detection of subclinical visual damage after blast-mediated TBI enables prevention of chronic visual deficit by treatment with P7C3-S243. *Invest Ophthalmol Vis Sci* (55): 8330-8341.
379. **Blaya MO, Bramlett HM, Naidoo J, Pieper AA, Dietrich WD** (2014) Neuroprotective efficacy of a proneurogenic compound after traumatic brain injury. *J Neurotrauma* (31): 476-486.
380. **De Jesús-Cortés H *et al*** (2012) Neuroprotective efficacy of aminopropyl carbazoles in a mouse model of Parkinson disease. *Proceedings of the National Academy of Sciences* (109): 17010-17015.
381. **Tesla R *et al*** (2012) Neuroprotective efficacy of aminopropyl carbazoles in a mouse model of amyotrophic lateral sclerosis. *Proceedings of the National Academy of Sciences* (109): 17016-17021.
382. **Carvalho C *et al*** (2009) Doxorubicin: the good, the bad and the ugly effect. *Current medicinal chemistry* (16): 3267-3285.
383. **Thorn CF *et al*** (2011) Doxorubicin pathways: pharmacodynamics and adverse effects. *Pharmacogenetics and genomics* (21): 440-406
384. **Wang M-S, Wu Y, Culver DG, Glass JD** (2000) Pathogenesis of axonal degeneration: parallels between Wallerian degeneration and vincristine neuropathy. *Journal of Neuropathology & Experimental Neurology* (59): 599-606.
385. **Araki T, Sasaki Y, Milbrandt J** (2004) Increased nuclear NAD biosynthesis and SIRT1 activation prevent axonal degeneration. *Science* (305): 1010-1013.
386. **Gerdts J, Summers DW, Sasaki Y, DiAntonio A, Milbrandt J** (2013) Sarm1-mediated axon degeneration requires both SAM and TIR interactions. *J Neurosci* (33): 13569-13580.
387. **Holopainen IE** (2005) Organotypic hippocampal slice cultures: a model system to study basic cellular and molecular mechanisms of neuronal cell death, neuroprotection, and synaptic plasticity. *Neurochemical research* (30): 1521-1528.
388. **Yang CH, Wang MX, Haider H, Yang JH, Sun J-Y *et al*** (2013) Strengthening alginate/polyacrylamide hydrogels using various multivalent cations. *ACS applied materials & interfaces* (5): 10418-10422.
389. **Woods G, Zito K** (2008) Preparation of gene gun bullets and biolistic transfection of neurons in slice culture *JoVE* (12): 675; 1-4
390. **Chen XH *et al*** (1999) Evolution of neurofilament subtype accumulation in axons following diffuse brain injury in the pig. *J Neuropathol Exp Neurol* (58): 588-596.
391. **Yuan A, Rao MV, Nixon RA** (2012) Neurofilaments at a glance. *Journal of cell science* (125): 3257-3263.
392. **Kuhle J *et al*** (2013) A comparative study of CSF neurofilament light and heavy chain protein in MS. *Multiple Sclerosis Journal* (19): 1597-1603.

393. **Lu C-H *et al*** (2012) Plasma neurofilament heavy chain levels correlate to markers of late stage disease progression and treatment response in SOD1G93A mice that model ALS. *PLoS One* (7): e40998; 1-13

394. **Xu Z, Henderson RD, David M, McCombe PA** (2016) Neurofilaments as biomarkers for amyotrophic lateral sclerosis: a systematic review and meta-analysis. *PloS one* (11): e0164625; 1-18

395. **Gendron TF *et al*** (2017) Phosphorylated neurofilament heavy chain: A biomarker of survival for C9ORF72-associated amyotrophic lateral sclerosis. *Annals of neurology* 82 (1): 139-146

396. **Harwell CS, Coleman MP** (2016) Synaptophysin depletion and intraneuronal Aβ in organotypic hippocampal slice cultures from huAPP transgenic mice. *Molecular neurodegeneration* (11): 44; 1-16

397. **Lutz JA, Carter M, Fields L, Barron S, Littleton JM** (2015) The dietary flavonoid rhamnetin inhibits both inflammation and excitotoxicity during ethanol withdrawal in rat organotypic hippocampal slice cultures. *Alcoholism: Clinical and Experimental Research* (39): 2345-2353.

398. **Croft CL, Wade MA, Kurbatskaya K, Mastrandreas P, Hughes MM *et al*** (2017) Membrane association and release of wild-type and pathological tau from organotypic brain slice cultures. *Cell death & disease* (8): e2671.

399. **Gaiottino J *et al*** (2013) Increased neurofilament light chain blood levels in neurodegenerative neurological diseases. *PLoS One* (8): e75091.

400. **Scherling CS *et al*** (2014) Cerebrospinal fluid neurofilament concentration reflects disease severity in frontotemporal degeneration. *Annals of neurology* (75): 116-126.

401. **Neselius S, Brisby H, Granholm F, Zetterberg H, Blennow K** (2015) Monitoring concussion in a knocked-out boxer by CSF biomarker analysis. *Knee Surg Sports Traumatol Arthrosc* (23): 2536-2539.

402. **Bacioglu M *et al*** (2016) Neurofilament light chain in blood and CSF as marker of disease progression in mouse models and in neurodegenerative diseases. *Neuron* (91): 56-66.

403. **Shahim P, Gren M, Liman V, Andreasson U, Norgren N *et al*** (2016) Serum neurofilament light protein predicts clinical outcome in traumatic brain injury. *Scientific reports* (6): 36791; 1-9.

404. **Zetterberg H** (2016) Neurofilament Light: A Dynamic Cross-Disease Fluid Biomarker for Neurodegeneration. *Neuron* (91): 1-3.

405. **McKee AC *et al*** (2010) TDP-43 proteinopathy and motor neuron disease in chronic traumatic encephalopathy. *J Neuropathol Exp Neurol* (69): 918-929.

406. **Sivanandam TM, Thakur MK** (2012) Traumatic brain injury: a risk factor for Alzheimer's disease. *Neurosci Biobehav Rev* (36): 1376-1381.

407. **Smith DH, Johnson VE, Stewart W** (2013) Chronic neuropathologies of single and repetitive TBI: substrates of dementia? *Nat Rev Neurol* (9): 211-221.

408. **Stein TD, Alvarez VE, McKee AC** (2014) Chronic traumatic encephalopathy: a spectrum of neuropathological changes following repetitive brain trauma in athletes and military personnel. *Alzheimers Res Ther* (6): 4; 1-11.

409. **Daneshvar DH, Goldstein LE, Kiernan PT, Stein TD, McKee AC** (2015) Post-traumatic neurodegeneration and chronic traumatic encephalopathy. *Mol Cell Neurosci* (66): 81-90.

410. **Gardner RC *et al*** (2015) Traumatic brain injury in later life increases risk for Parkinson disease. *Annals of neurology* (77): 987-995.

411. **Crane PK JB *et al*** (2016) Association of traumatic brain injury with late-life neurodegenerative conditions and neuropathologic findings. *JAMA neurology* (73): 1062-1069.
412. **Herrup K** (2015) The case for rejecting the amyloid cascade hypothesis. *Nat Neurosci* (18): 794-799.
413. **Terry RD *et al*** (1991) Physical basis of cognitive alterations in Alzheimer's disease: synapse loss is the major correlate of cognitive impairment. *Annals of neurology* (30): 572-580.
414. **Engelborghs S, De PPD** (1997) The neurochemistry of Alzheimer's disease. *Acta neurologica belgica* (97): 67-84.
415. **Lue L-F *et al*** (1999) Soluble amyloid β peptide concentration as a predictor of synaptic change in Alzheimer's disease. *The American journal of pathology* (155): 853-862.
416. **Masliah E *et al*** (2001) β-Amyloid peptides enhance α-synuclein accumulation and neuronal deficits in a transgenic mouse model linking Alzheimer's disease and Parkinson's disease. *Proceedings of the National Academy of Sciences* (98): 12245-12250.
417. **Adalbert R, Gilley J, Coleman MP** (2007) Abeta, tau and ApoE4 in Alzheimer's disease: the axonal connection. *Trends Mol Med* (13): 135-142.
418. **Babusikova E, Evinova A, Hatok J, Dobrota D, Jurecekova J** (2013) Oxidative changes and possible effects of polymorphism of antioxidant enzymes in neurodegenerative disease. editors. Neurodegenerative Diseases. *InTech*.
419. **Chow VW, Mattson MP, Wong PC, Gleichmann M** (2010) An overview of APP processing enzymes and products. *Neuromolecular medicine* (12): 1-12.
420. **Jonsson T *et al*** (2012) A mutation in APP protects against Alzheimer's disease and age-related cognitive decline. *Nature* (488): 96-99.
421. **Xu T-H *et al*** (2016) Alzheimer's disease-associated mutations increase amyloid precursor protein resistance to γ-secretase cleavage and the Aβ42/Aβ40 ratio. *Cell discovery* (2): 16026; 1-14
422. **Verma M, Vats A, Taneja V** (2015) Toxic species in amyloid disorders: Oligomers or mature fibrils. *Annals of Indian Academy of Neurology* (18): 138.
423. **Sengupta U, Nilson AN, Kayed R** (2016) The role of amyloid-β oligomers in toxicity, propagation, and immunotherapy. *EBioMedicine* (6): 42-49.
424. **Kuperstein I *et al*** (2010) Neurotoxicity of Alzheimer's disease Aβ peptides is induced by small changes in the Aβ 42 to Aβ 40 ratio. *The EMBO journal* (29): 3408-3420.
425. **Blennow K, Hardy J, Zetterberg H** (2012) The neuropathology and neurobiology of traumatic brain injury. *Neuron* (76): 886-899.
426. **Julien J *et al*** (2017) Association of traumatic brain injury and Alzheimer disease onset: A systematic review. *Annals of Physical and Rehabilitation Medicine*
427. **Weiner MW, Crane PK, Montine TJ, Bennett DA, Veitch DP** (2017) Traumatic brain injury may not increase the risk of Alzheimer disease. *Neurology* (89): 1923-1925.
428. **Hong YT *et al*** (2014) Amyloid imaging with carbon 11-labeled Pittsburgh compound B for traumatic brain injury. *JAMA Neurol* (71): 23-31.
429. **Tsitsopoulos PP, Marklund N** (2013) Amyloid-β Peptides and Tau Protein as Biomarkers in Cerebrospinal and Interstitial Fluid Following Traumatic Brain Injury: A Review of Experimental and Clinical Studies. *Front Neurol* (4): 79.
430. **Tran HT, LaFerla FM, Holtzman DM, Brody DL** (2011) Controlled cortical impact traumatic brain injury in 3xTg-AD mice causes acute intra-axonal amyloid-β accumulation and

independently accelerates the development of tau abnormalities. *Journal of Neuroscience* (31): 9513-9525.

431. **Washington PM, Burns MP** (2016) The Effect of the APOE4 Gene on Accumulation of Aβ 40 After Brain Injury Cannot Be Reversed by Increasing apoE4 Protein. *Journal of Neuropathology & Experimental Neurology* (75): 770-778.

432. **Washington PM, Morffy N, Parsadanian M, Zapple DN, Burns MP** (2014) Experimental traumatic brain injury induces rapid aggregation and oligomerization of amyloid-beta in an Alzheimer's disease mouse model. *J Neurotrauma* (31): 125-134.

433. **Teich AF, Patel M, Arancio O** (2013) A reliable way to detect endogenous murine β-amyloid. *PloS one* (8): e55647.

434. **Helmy A, Carpenter KLH, Menon DK, Pickard JD, Hutchinson PJA** (2010) The cytokine response to human traumatic brain injury: temporal profiles and evidence for cerebral parenchymal production. *Journal of Cerebral Blood Flow & Metabolism* (31): 658-670.

435. **Helmy A, Antoniades CA, Guilfoyle MR, Carpenter KLH, Hutchinson PJ** (2012) Principal component analysis of the cytokine and chemokine response to human traumatic brain injury. *PloS one* (7): e39677.

436. **Lin Y, Wen L** (2013) Inflammatory response following diffuse axonal injury. *Int J Med Sci* (10): 515-521.

437. **Perry RT, Collins JS, Wiener H, Acton R, Go RC** (2001) The role of TNF and its receptors in Alzheimer's disease. *Neurobiol Aging* (22): 873-883.

438. **Bachstetter AD *et al*** (2016) MW151 Inhibited IL-1β Levels after Traumatic Brain Injury with No Effect on Microglia Physiological Responses. *PLoS One* (11): e0149451.

439. **Swardfager W *et al*** (2010) A meta-analysis of cytokines in Alzheimer's disease. *Biol Psychiatry* (68): 930-941.

440. **Djordjevic J, Golam Sabbir M, C Albensi B** (2016) Traumatic brain injury as a risk factor for Alzheimer's disease: is inflammatory signaling a key player. *Current Alzheimer Research* (13): 730-738.

441. **Nicoll JAR *et al*** (2000) Association of interleukin-1 gene polymorphisms with Alzheimer's disease. *Annals of neurology* (47): 365.

442. **Zheng C, Zhou X-W, Wang J-Z** (2016) The dual roles of cytokines in Alzheimer's disease: update on interleukins, TNF-α, TGF-β and IFN-γ. *Translational neurodegeneration* (5): 7.

443. **Jeohn GH, Kong LY, Wilson B, Hudson P, Hong JS** (1998) Synergistic neurotoxic effects of combined treatments with cytokines in murine primary mixed neuron/glia cultures. *J Neuroimmunol* (85): 1-10.

444. **Shohami E, Ginis I, Hallenbeck JM** (1999) Dual role of tumor necrosis factor alpha in brain injury. *Cytokine Growth Factor Rev* (10): 119-130.

445. **McAlpine FE *et al*** (2009) Inhibition of soluble TNF signaling in a mouse model of Alzheimer's disease prevents pre-plaque amyloid-associated neuropathology. *Neurobiology of disease* (34): 163-177.

446. **Allan SM, Tyrrell PJ, Rothwell NJ** (2005) Interleukin-1 and neuronal injury. *Nature Reviews Immunology* (5): 629-640.

447. **Simi A, Tsakiri N, Wang P, Rothwell NJ** (2007) Interleukin-1 and inflammatory neurodegeneration. *Biochem Soc Trans* (35): 1122-1126.

448. **Fan L *et al*** (1995) Experimental brain injury induces expression of interleukin-1β mRNA in the rat brain. *Molecular Brain Research* (30): 125-130.

449. **Lu K-T, Wang Y-W, Yang J-T, Yang Y-L, Chen H-I** (2005) Effect of interleukin-1 on traumatic brain injury–induced damage to hippocampal neurons. *Journal of neurotrauma* (22): 885-895.
450. **Helmy A *et al*** (2014) Recombinant human interleukin-1 receptor antagonist in severe traumatic brain injury: a phase II randomized control trial. *J Cereb Blood Flow Metab* (34): 845-851.
451. **Murray KN, Parry-Jones AR, Allan SM** (2015) Interleukin-1 and acute brain injury. *Frontiers in cellular neuroscience* (9):
452. **Gähwiler BH** (1981) Organotypic monolayer cultures of nervous tissue. *Journal of neuroscience methods* (4): 329-342.
453. **Trojanowski JQ, Walkenstein N, Lee VM** (1986) Expression of neurofilament subunits in neurons of the central and peripheral nervous system: an immunohistochemical study with monoclonal antibodies. *Journal of Neuroscience* (6): 650-660.
454. **Pernas-Alonso R *et al*** (1996) Early upregulation of medium neurofilament gene expression in developing spinal cord of the wobbler mouse mutant. *Molecular brain research* (38): 267-275.
455. **Summers DW, DiAntonio A, Milbrandt J** (2014) Mitochondrial dysfunction induces Sarm1-dependent cell death in sensory neurons. *J Neurosci* (34): 9338-9350.
456. **Chen X-H *et al*** (2004) Long-term accumulation of amyloid-β, β-secretase, presenilin-1, and caspase-3 in damaged axons following brain trauma. *The American journal of pathology* (165): 357-371.
457. **Loane DJ *et al*** (2009) Amyloid precursor protein secretases as therapeutic targets for traumatic brain injury. *Nature medicine* (15): 377.
458. **Brody DL *et al*** (2008) Amyloid-beta dynamics correlate with neurological status in the injured human brain. *Science* (321): 1221-1224.
459. **Walsh DM *et al*** (2002) Naturally secreted oligomers of amyloid β protein potently inhibit hippocampal long-term potentiation in vivo. *Nature* (416): 535.
460. **Mattson MP** (2004) Pathways towards and away from Alzheimer's disease. *Nature* (430): 631.
461. **Breunig JJ, Guillot-Sestier MV, Town T** (2013) Brain injury, neuroinflammation and Alzheimer's disease. *Front Aging Neurosci* (5): 26.
462. **Johnson VE, Stewart W, Smith DH** (2010) Traumatic brain injury and amyloid-beta pathology: a link to Alzheimer's disease? *Nat Rev Neurosci* (11): 361-370.
463. **Johnson VE, Stewart W, Smith DH** (2012) Widespread tau and amyloid-beta pathology many years after a single traumatic brain injury in humans. *Brain Pathol* (22): 142-149.
464. **Mannix RC, Whalen MJ** (2012) Traumatic brain injury, microglia, and Beta amyloid. *Int J Alzheimers Dis* (2012): 608732.
465. **Collins JM, King AE, Woodhouse A, Kirkcaldie MTK, Vickers JC** (2015) The effect of focal brain injury on beta-amyloid plaque deposition, inflammation and synapses in the APP/PS1 mouse model of Alzheimer's disease. *Experimental neurology* (267): 219-229.
466. **Kokiko-Cochran O *et al*** (2016) Altered neuroinflammation and behavior after traumatic brain injury in a mouse model of Alzheimer's disease. *Journal of neurotrauma* (33): 625-640.
467. **DeKosky ST *et al*** (2007) Association of increased cortical soluble Aβ42 levels with diffuse plaques after severe brain injury in humans. *Archives of neurology* (64): 541-544.
468. **Neniskyte U, Vilalta A, letters GCB-FEBS, 2014** Tumour necrosis factor alpha-induced neuronal loss is mediated by microglial phagocytosis. *Elsevier*

469. **Helmy A, De Simoni MG, Guilfoyle MR, Carpenter KL, Hutchinson PJ** (2011) Cytokines and innate inflammation in the pathogenesis of human traumatic brain injury. *Prog Neurobiol* (95): 352-372.
470. **Lüth H-J, Holzer M, Gärtner U, Staufenbiel M, Arendt T** (2001) Expression of endothelial and inducible NOS-isoforms is increased in Alzheimer's disease, in APP23 transgenic mice and after experimental brain lesion in rat: evidence for an induction by amyloid pathology. *Brain research* (913): 57-67.
471. **Liao Y-F, Wang B-J, Cheng H-T, Kuo L-H, Wolfe MS** (2004) Tumor necrosis factor-α, interleukin-1β, and interferon-γ stimulate γ-secretase-mediated cleavage of amyloid precursor protein through a JNK-dependent MAPK pathway. *Journal of Biological Chemistry* (279): 49523-49532.
472. **Littleton JT, Ganetzky B** (2000) Ion channels and synaptic organization: analysis of the Drosophila genome. *Neuron* (26): 35-43.
473. **Freeman MR** (2015) Drosophila Central Nervous System Glia. *Cold Spring Harb Perspect Biol* (7):
474. **DeSalvo MK, Mayer N, Mayer F, Bainton RJ** (2011) Physiologic and anatomic characterization of the brain surface glia barrier of Drosophila. *Glia* (59): 1322-1340.
475. **Reichert H** (2005) A tripartite organization of the urbilaterian brain: developmental genetic evidence from Drosophila. *Brain Res Bull* (66): 491-494.
476. **Schlegel P, Costa M, Jefferis GS** (2017) Learning from connectomics on the fly. *Curr Opin Insect Sci* (24): 96-105.
477. **Jenett A *et al*** (2012) A GAL4-driver line resource for Drosophila neurobiology. *Cell reports* (2): 991-1001.
478. **Guarnieri DJ, Heberlein U** (2003) Drosophila melanogaster, a genetic model system for alcohol research. *International review of neurobiology* (54): 199-228.
479. **Guo M** (2012) Drosophila as a model to study mitochondrial dysfunction in Parkinson's disease. *Cold Spring Harbor perspectives in medicine* (2): a009944.
480. **Marklund N, Hillered L** (2011) Animal modeling of traumatic brain injury in preclinical drug development: where do we go from here. *Br J Pharmacol* (164): 1207-1229.
481. **Jeibmann A, Paulus W** (2009) Drosophila melanogaster as a model organism of brain diseases. *Int J Mol Sci* (10): 407-440.
482. **Prüßing K, Voigt A, Schulz JB** (2013) Drosophila melanogaster as a model organism for Alzheimer's disease. *Mol Neurodegener* (8): 35.
483. **Chang Q, Balice-Gordon RJ** (2000) Highwire, rpm-1, and futsch: balancing synaptic growth and stability. *Neuron* (26): 287-290.
484. **Hoopfer ED *et al*** (2006) Wlds protection distinguishes axon degeneration following injury from naturally occurring developmental pruning. *Neuron* (50): 883-895.
485. **MacDonald JM *et al*** (2006) The Drosophila cell corpse engulfment receptor Draper mediates glial clearance of severed axons. *Neuron* (50): 869-881.
486. **Kretzschmar D et al** (1997) The swiss cheese mutant causes glial hyperwrapping and brain degeneration in Drosophila. *J Neurosci.* 17(19): 7425-7432
487. **Mutsuddi M, Nambu JR** (1998) Neural disease: Drosophila degenerates for a good cause. *Current biology* 8(22): 809-811
488. **Coulom H, Birman S** (2004) Chronic exposure to rotenone models sporadic Parkinson's disease in Drosophila melanogaster. *Journal of Neuroscience* (24): 10993-10998.

489. **Varga SJ, Qi C, Podolsky E, Lee D** (2014) A new Drosophila model to study the interaction between genetic and environmental factors in Parkinson' s disease. *Brain research* (1583): 277-286.
490. **Hosamani R, Ramesh SR** (2010) Attenuation of rotenone-induced mitochondrial oxidative damage and neurotoxicty in Drosophila melanogaster supplemented with creatine. *Neurochemical research* (35): 1402-1412.
491. **Whitworth AJ, Wes PD, Pallanck LJ** (2006) Drosophila models pioneer a new approach to drug discovery for Parkinson's disease. *Drug discovery today* (11): 119-126.
492. **Mollet P, Graf U, Würgler FE** (1974) Toxicity and mutagenicity of dimethyl sulfoxide in two strains of Drosophila melanogaster. *Archiv fur Genetik* (47): 184.
493. **Gamo S, Ogaki M, Nakashima-Tanaka E** (1979) Inheritance of chloroform resistance in Drosophila melanogaster. *The Japanese journal of genetics* (54): 229-234.
494. **Ranganathan S, Davis DG, Hood RD** (1987) Developmental toxicity of ethanol in Drosophila melanogaster. *Teratology* (36): 45-49.
495. **Scholz H, Ramond J, Singh CM, Heberlein U** (2000) Functional ethanol tolerance in Drosophila. *Neuron* (28): 261-271.
496. **Nazir A, Mukhopadhyay I, Saxena DK, Chowdhuri DK** (2003) Evaluation of the no observed adverse effect level of solvent dimethyl sulfoxide in Drosophila melanogaster. *Toxicology mechanisms and methods* (13): 147-152.
497. **Cvetković VJ *et al*** (2015) Toxicity of dimethyl sulfoxide against Drosophila melanogaster. *Biologica Nyssana* (6):
498. **Cavoski I, Caboni P, Sarais G, Cabras P, Miano T** (2007) Photodegradation of rotenone in soils under environmental conditions. *Journal of agricultural and food chemistry* (55): 7069-7074.
499. **Leite GDO *et al*** (2017) Protective effect of (-)-α-Bisabolol on rotenone-induced toxicity in Drosophila melanogaster. *Canadian Journal of Physiology and Pharmacology*
500. **Yang Y *et al*** (2006) Mitochondrial pathology and muscle and dopaminergic neuron degeneration caused by inactivation of Drosophila Pink1 is rescued by Parkin. *Proceedings of the National Academy of Sciences* (103): 10793-10798.
501. **Clark IE *et al*** (2006) Drosophila pink1 is required for mitochondrial function and interacts genetically with parkin. *Nature* (441): 1162-1166.
502. **Shiba-Fukushima K, Inoshita T, Hattori N, Imai Y** (2014) PINK1-mediated phosphorylation of Parkin boosts Parkin activity in Drosophila. *PLoS genetics* (10): e1004391.
503. **Mohr SE** (2018) First in Fly: Drosophila Research and Biological Discovery. *Harvard University Press*.
504. **Agrawal T, Hasan G** (2015) Maturation of a central brain flight circuit in Drosophila requires Fz2/Ca^{2+} signaling. *Elife* (4): e07046.
505. **Impellizzeri D *et al*** (2016) Traumatic Brain Injury Leads to Development of Parkinson's Disease Related Pathology in Mice. *Front Neurosci* (10): 458.
506. **Whitworth AJ *et al*** (2005) Increased glutathione S-transferase activity rescues dopaminergic neuron loss in a Drosophila model of Parkinson's disease. *Proceedings of the National Academy of Sciences* (102): 8024-8029.
507. **Riemensperger T *et al*** (2013) A single dopamine pathway underlies progressive locomotor deficits in a Drosophila model of Parkinson disease. *Cell reports* (5): 952-960.
508. **Godenschwege TA, Kristiansen LV, Uthaman SB, Hortsch M, Murphey RK** (2006) A conserved role for Drosophila Neuroglian and human L1-CAM in central-synapse formation. *Current biology* (16): 12-23.

509. **Sunderhaus ER, Kretzschmar D** (2016) Mass Histology to Quantify Neurodegeneration in Drosophila. *Journal of visualized experiments: JoVE*

510. **Hutson CB *et al*** (2011) Traumatic brain injury in adult rats causes progressive nigrostriatal dopaminergic cell loss and enhanced vulnerability to the pesticide paraquat. *Journal of neurotrauma* (28): 1783-1801.

511. **Wagh DA *et al*** (2006) Bruchpilot, a protein with homology to ELKS/CAST, is required for structural integrity and function of synaptic active zones in Drosophila. *Neuron* (49): 833-844.

512. **Kittel RJ *et al*** (2006) Bruchpilot promotes active zone assembly, Ca2+ channel clustering, and vesicle release. *Science* (312): 1051-1054.

513. **Zang S, Ali YO, Ruan K, Zhai RG** (2013) Nicotinamide mononucleotide adenylyltransferase maintains active zone structure by stabilizing Bruchpilot. *EMBO reports* (14): 87-94.

514. **Chen Y-H *et al*** (2017) Impact of traumatic brain injury on dopaminergic transmission. *Cell transplantation* 26(7):1156-1168.

515. **Jenkins PO *et al*** (2016) Disruption to the dopaminergic system after traumatic brain injury. *ABN*.

516. **Wang F, Franco R, Skotak M, Hu G, Chandra N** (2014) Mechanical stretch exacerbates the cell death in SH-SY5Y cells exposed to paraquat: mitochondrial dysfunction and oxidative stress. *Neurotoxicology* (41): 54-63.

517. **Shimada R, Abe K, Furutani R, Kibayashi K** (2014) Changes in dopamine transporter expression in the midbrain following traumatic brain injury: an immunohistochemical and in situ hybridization study in a mouse model. *Neurological research* (36): 239-246.

518. **Celardo I *et al*** (2016) Mitofusin-mediated ER stress triggers neurodegeneration in pink1/parkin models of Parkinson's disease. *Cell death & disease* (7): e2271.

519. **Press C, Milbrandt J** (2008) Nmnat delays axonal degeneration caused by mitochondrial and oxidative stress. *J Neurosci* (28): 4861-4871.

520. **Tokunaga S, Araki T** (2012) Wallerian degeneration slow mouse neurons are protected against cell death caused by mechanisms involving mitochondrial electron transport dysfunction. *J Neurosci Res* (90): 664-671.

521. **Masel BE, DeWitt DS** (2010) Traumatic brain injury: a disease process, not an event. *Journal of neurotrauma* (27): 1529-1540.

522. **Helmy A, Vizcaychipi M, Gupta AK** (2007) Traumatic brain injury: intensive care management. *British Journal of Anaesthesia* (99): 32-42.

523. **Lim HB, Smith M** (2007) Systemic complications after head injury: a clinical review. *Anaesthesia* (62): 474-482.

524. **Haddad SH, Arabi YM** (2012) Critical care management of severe traumatic brain injury in adults. *Scandinavian journal of trauma, resuscitation and emergency medicine* (20): 12.

525. **Glassner S *et al*** (2013) Prevention of venous thrombotic events in brain injury: review of current practices. *Rambam Maimonides medical journal* (4):

526. **Abdel-Aziz H, Dunham CM, Malik RJ, Hileman BM** (2015) Timing for deep vein thrombosis chemoprophylaxis in traumatic brain injury: an evidence-based review. *Critical Care* (19): 96.

527. **Barnes MP** (1999) Rehabilitation after traumatic brain injury. *British medical bulletin* (55): 927-943.

528. **Holloway M, Fyson R** (2015) Acquired brain injury, social work and the challenges of personalisation. *The British Journal of Social Work* (46): 1301-1317.

529. **Maas AIR, Roozenbeek B, Manley GT** (2010) Clinical trials in traumatic brain injury: past experience and current developments. *Neurotherapeutics* (7): 115-126.
530. **Maas AI *et al*** (2010) Common data elements for traumatic brain injury: recommendations from the interagency working group on demographics and clinical assessment. *Arch Phys Med Rehabil* (91): 1641-1649.
531. **Maas AI *et al*** (2011) Standardizing data collection in traumatic brain injury. *J Neurotrauma* (28): 177-187.
532. **Ling H, Hardy J, Zetterberg H** (2015) Neurological consequences of traumatic brain injuries in sports. *Molecular and Cellular Neuroscience* (66): 114-122.
533. **Bulstrode H *et al*** (2014) Mitochondrial DNA and traumatic brain injury. *Ann Neurol* (75): 186-195.
534. **Greene NH, Kernic MA, Vavilala MS, Rivara FP** (2018) Variation in Adult Traumatic Brain Injury Outcomes in the United States. *The Journal of head trauma rehabilitation* (33): E1-E8.
535. **Groswasser Z, Cohen M, Blankstein E** (1990) Polytrauma associated with traumatic brain injury: incidence, nature and impact on rehabilitation outcome. *Brain Injury* (4): 161-166.
536. **Gaddam SSK, Buell T, Robertson CS** (2015) Systemic manifestations of traumatic brain injury. editors. Handbook of clinical neurology 127. Elsevier. pp. 205-218.
537. **McDonald SJ, Sun M, Agoston DV, Shultz SR** (2016) The effect of concomitant peripheral injury on traumatic brain injury pathobiology and outcome. *Journal of neuroinflammation* (13): 90.
538. **Roberts I *et al*** (2004) Effect of intravenous corticosteroids on death within 14 days in 10008 adults with clinically significant head injury (MRC CRASH trial): randomised placebo-controlled trial. *Lancet* (364): 1321-1328.
539. **Pineda JA, Wang KK, Hayes RL** (2004) Biomarkers of proteolytic damage following traumatic brain injury. *Brain Pathol* (14): 202-209.
540. **Li J, Li XY, Feng DF, Pan DC** (2010) Biomarkers associated with diffuse traumatic axonal injury: exploring pathogenesis, early diagnosis, and prognosis. *J Trauma* (69): 1610-1618.
541. **Sharp DJ, Scott G, Leech R** (2014) Network dysfunction after traumatic brain injury. *Nat Rev Neurol* (10): 156-166.
542. **Gerdts J, Summers DW, Milbrandt J, DiAntonio A** (2016) Axon self-destruction: new links among SARM1, MAPKs, and NAD+ metabolism. *Neuron* (89): 449-460.